THE NITRIDING OF IRON-NICKEL-NIOBIUM ALLOYS

A dissertation submitted for the degree of

Doctor of Philosophy

of the University of Newcastle upon Tyne

by

Jack Richard Handley

Department of Metallurgy

University of Newcastle upon Tyne

June 1974

PREFACE

This dissertation describes original work which has not been submitted for a degree at any other University.

The investigations were carried out in the Department of Metallurgy of the University of Newcastle upon Tyne during the period October, 1970 to September, 1973 under the supervision of Professor K.H. Jack and Dr. J.H. Driver.

The main part of the thesis describes a study of precipitation in nitrided austenitic iron-nickel-niobium alloys and the mechanical properties of the nitrided alloys and is part of a wider investigation being carried out at Newcastle on the effect of substitutional alloying elements on the behaviour of interstial solutes in iron. Subsidiary topics on the nitriding of iron-nickel alloys and on precipitation in iron-nickel-niobium alloys are discussed in the two appendices.

G.P. Meadley

ACKNOWLEDGEMENTS

I wish to thank Professor K.H. Jack and Dr. J.H. Driver for advice, encouragement and general supervision of the work.

I also wish to thank Professor Jack for providing facilities in the Crystallography Laboratory of the Department of Metallurgy at the University of Newcastle upon Tyne.

I also wish to express gratitude to the Science Research Council for the award of a maintenance grant.

I wish to thank my colleagues in the Department of Metallurgy of the University of Newcastle upon Tyne for their help and advice.

I wish to thank Mrs. A. Rule for typing the script.

To Pat.

June, 1974

ABSTRACT

A modulated structure is formed in nitrided Fe:35Ni:Nb alloys at 500 to 750°C in NH_3:H_2 gas mixtures when the niobium and nitrogen concentration exceed critical values associated with a metastable zone solvus. The modulated structure is formed by substitutional-interstitial solute-atom clusters on {100} matrix planes and it overages to give a fine dispersion of homogeneous precipitates of γ-NbN. The initial spheroidal particles of γ-NbN coarsen at 800°C by forming octahedra with their faces parallel to the {111} matrix planes. After prolonged ageing these niobium nitride octahedra transform to platelets parallel to the {100} matrix planes. The interfacial surface energy of γ-NbN is determined as approximately 600 ergs/cm^2.

Stacking fault precipitation of γ-NbN in nitrided Fe-35Ni:Nb alloys occurs when the niobium concentration exceeds the nitrogen concentration.

The dislocation-particle interaction of γ-NbN in nitrided Fe:35Ni:Nb alloys occurs by the Orawan mechanism.

The nitriding kinetics are dependent upon nitrogen-atom diffusion in Fe:35Ni.

CONTENTS

INTRODUCTION

Previous work at Newcastle on nitrided ferritic Fe-Cr, Fe-Nb, Fe-V, and Fe-W alloys (Mortimer, 1971; Spiers, 1969; Roberts, 1970; Pope, 1972 and Stephenson, 1974) has shown that a high hardness is developed at 450 to 650°C during nitriding in ammonia-hydrogen gas mixtures. This high hardness is attributed to the formation of mixed substitutional-interstitial solute-atom clusters (Guiner-Preston zones) during "constant activity ageing" in NH_3:H_2 at 450 to 650°C at nitrogen potentials which exceed critical values associated with a metastable zone solvus.

Following these observations it was thought that mixed substitutional-interstitial solute-atom clusters might also be formed in face-centred cubic alloys. For this reason investigations were carried out on nitrided austenitic Fe:M_n and Fe:Mn:V alloys (Hayes, 1972), on Fe:35Ni:V alloys (Driver et al, 1974) and on nitrided austenitic Fe:35Ni:Nb described in the present work. The investigations on nitrided austenitic Fe:Mn:V and Fe:35Ni:V alloys (Hayes, 1972; Driver et al, 1974) showed that mixed substitutional-interstitial solute-atom clusters are formed and are associated with an electron

microstucture and X-ray and electron diffraction effects similar to those observed in spinodal decomposition of Cu:Ni:Fe alloys (Butler and Thomas, 1970; Daniel and Lipson, 1943). They also showed that the modulated stucture overages to give the equilibrium phase VN.

Any examination of the quaternary Fe-Ni-Nb-N system requires knowledge of the relevant portions of the six binary systems Fe-N, Fe-Nb, Fe-Ni, Nb-N, Nb-Ni and Ni-N, and of the iron-rich ternary systems Fe-Nb-N, Fe-Ni-N and Fe-Ni-Nb. Consequently, a limited study was undertaken in order to provide background information for the main topic.

In an attempt to determine the mechanism of strengthening in nitrided austenite a preliminary study was made of the dislocation-particle interaction in Fe:35Ni:Nb:N alloys.

Chapter I

PREVIOUS INVESTIGATIONS

I.1 Iron-nitrogen alloys

Figure I.1 shows the variation of nitrogen solubility in iron at one atmosphere of nitrogen compiled from the data of Fast and Verrijp (1955) for body centred cubic α-Fe; Sieverts et al (1938) for b.c.c. δ-Fe; Sieverts et al (1938), Darken et al (1951), Corney and Turkdogan (1955) for face centred cubic γ-Fe, and Pehlke and Elliot (1960) for liquid iron.

In the iron-nitrogen system shown in Figure I.2 there are five major phases formed with increasing nitrogen potentials; α-nitrogen ferrite, γ-nitrogen austenite, γ'-Fe_4N, ε-Fe_3N and ζ-Fe_2N, and two additional phases, α'-nitrogen martensite formed by transformation of γ, and α''-$Fe_{16}N_2$ obtained by tempering α'. Table I.1 (after Jack, 1951a) summarises the composition ranges, crystal structures and unit-cell dimensions of these phases. Of the five major phases formed in nitrided iron only α, γ, γ' and ε are of immediate interest to this study.

Fig. I.1

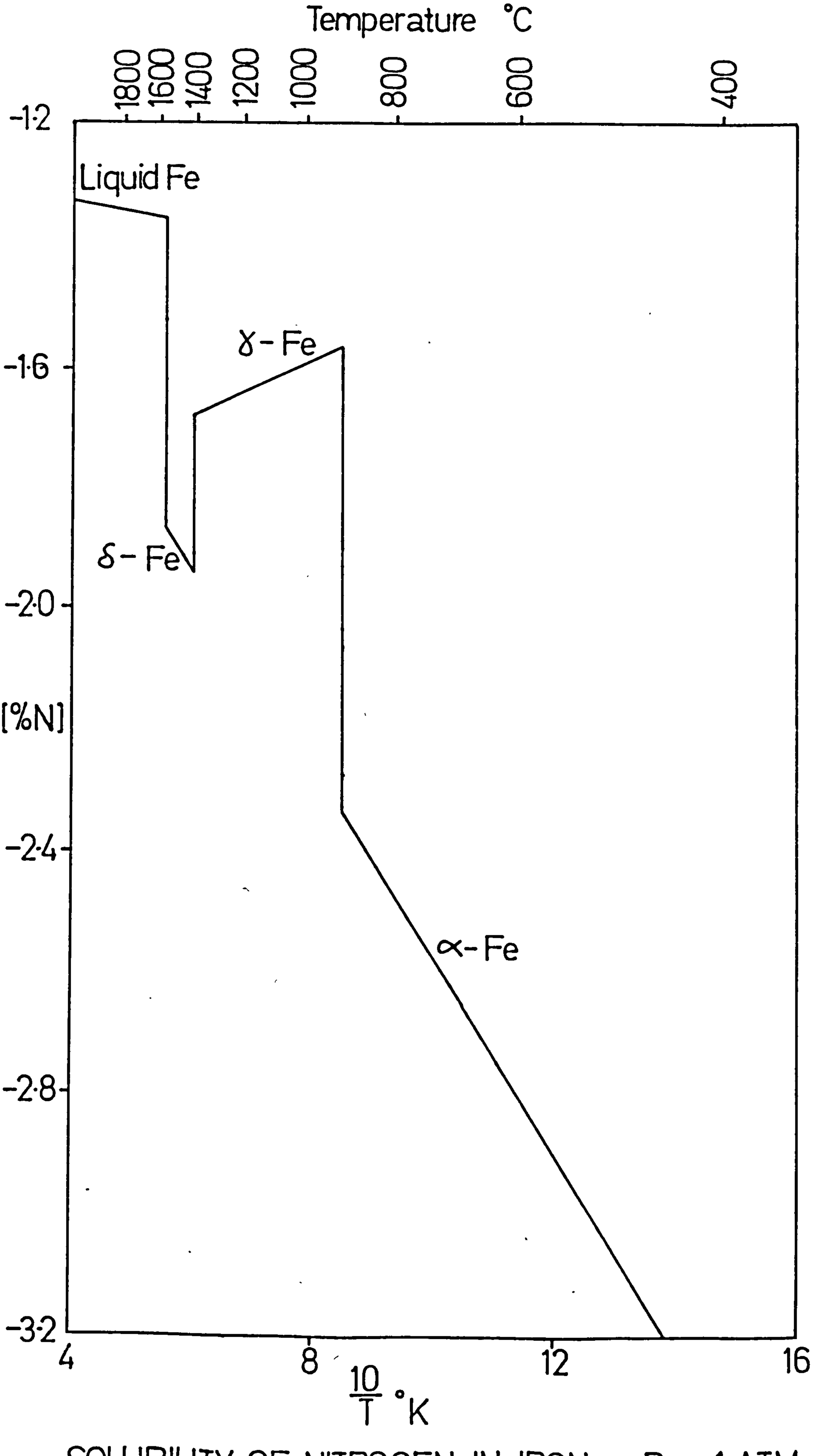

SOLUBILITY OF NITROGEN IN IRON P_{N_2} = 1 ATM.

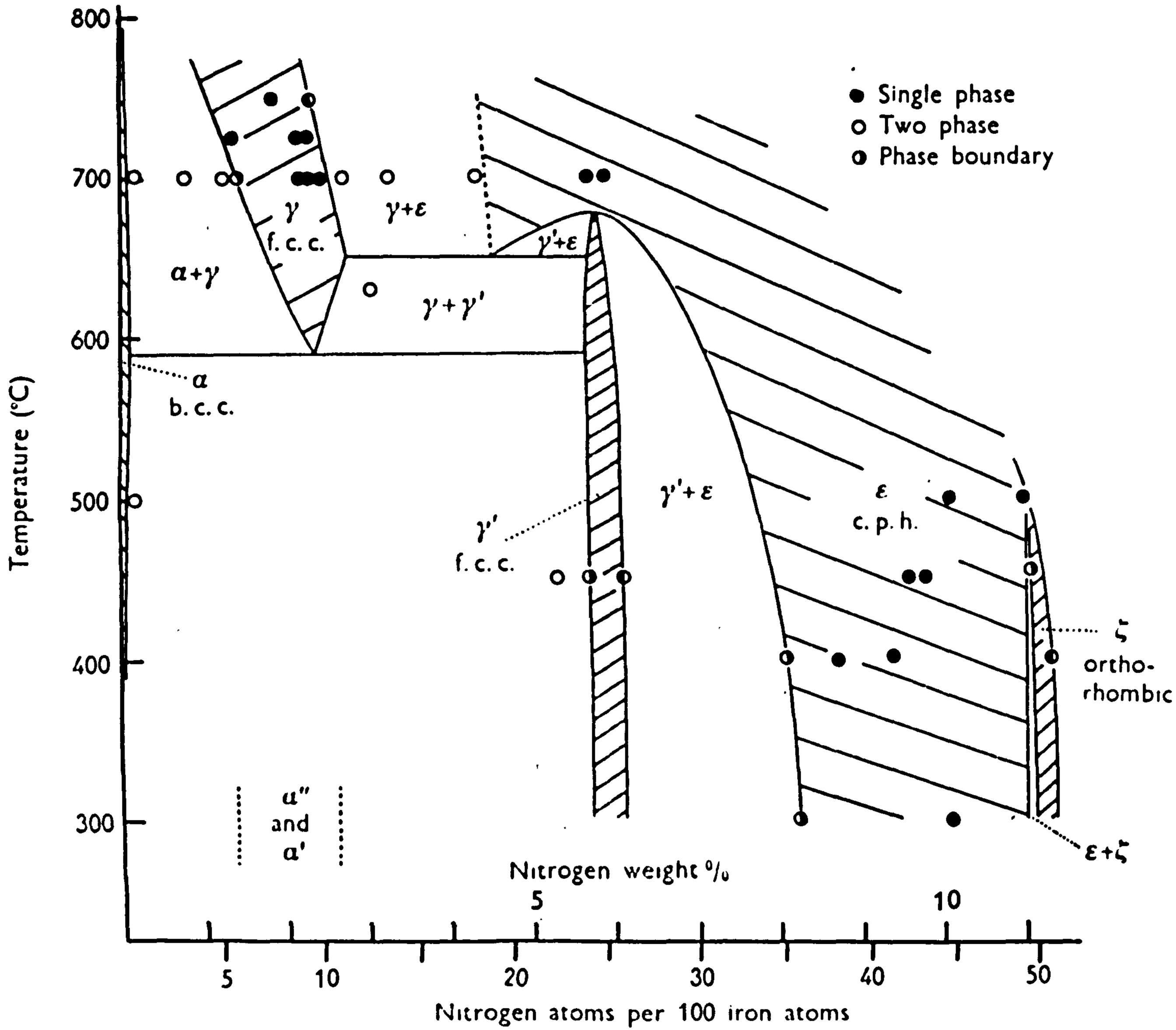

Fig.I.2 THE IRON-NITROGEN DIAGRAM. (JACK K.H. 1951)

Table I.1

Unit-cell dimensions and composition limits of iron-nitrogen phases and iron-nickel-nitrogen phases

phase symbol	crystal structure	composition limits	unit-cell dimensions	composition	references
α	b.c.c.	0 - 0.1wt.%N; i.e. $Fe-FeN_{0.01}$	a,2.866 Å a,2.869 Å	Fe 0.1wt.%N	Wriedt and Zwell (1962)
γ	f.c.c.	0 - 2.8wt.%N; i.e. $Fe-FeN_{0.12}$	a,3.615 Å a,3.654 Å a,3.571 Å a,3.645 Å	1.5wt.%N 2.8wt.%N Fe 2.4wt.%N	Paranjpe et al (1950) Jack (1951a)
γ'	cubic	5.29 - 5.7wt.%N; i.e. $FeN_{0.23}-FeN_{0.24}$ 5.75 - 6.10wt.%N; i.e. $FeN_{0.24}-FeN_{0.26}$	a,3.791 Å a,3.801 Å a,3.787 Å a,3.795 Å	5.29wt.%N 5.71wt.%N 5.75wt.%N 6.10wt.%N	Paranjpe et al (1950) Jack (1948)
ε	c.p. hexagonal (dimensions for pseudo-cell)	5.70 - 11.0wt.%N; i.e. $FeN_{0.24}-FeN_{0.49}$	a,2.660; c,4.344 Å a,2.764; c,4.420 Å a,2.657; c,4.380 Å a,2.770; c,4.432 Å	5.70wt.%N 11.0wt.%N 7.30wt.%N 11.0wt.%N	Jack (1948) Paranjpe et al (1950)

Table I.1 continued

phase symbol	crystal structure	composition limits	unit-cell dimensions	composition	references
ε	orthorhombic (dimensions for pseudo-cell)	11.1 - 11.3wt.%N; i.e. $FeN_{0.50}$-$FeN_{0.51}$	a,2.762; b,4.830 c,4.416 Å	11.3wt.%N	Jack (1948)
α'	b.c. tetragonal	as -austenite	a,2.851; c,3.071 Å	2.30wt.%N	Jack (1951a)
α''	tetragonal	3.1wt.%N; i.e. $FeN_{0.13}$	a,5.72; c,6.29 Å	3.1wt.%N	Jack (1951b)
Ni_3N	hexagonal		a,2.668; c,4.312 Å		Jack (1950)
$(Fe,Ni)_4N$	cubic	Fe_4N - $Fe_{1.05}Ni_{2.95}N_{1.2}$	a,3.797 - 3.755 Å		Arnott and Wold (1960)

Nitrogen-austenite (γ) has a random distribution of nitrogen atoms among the octahedral interstices (Figure I.3) and is isostructural with carbon austenite but has a wider range of homogeneity which exists down to the eutectoid at 590°C. The maximum solubility of nitrogen is 2.8wt% in austenite and 0.1wt% in ferrite.

γ'-Fe_4N has a face centred cubic arrangement of iron atoms (Figure I.3) with an ordered arrangement of nitrogen atoms occupying one in four of the octahedral interstics. ε -Fe_3N has a range of composition from about Fe_4N to Fe_2N and has a close-packed hexagonal metal-atom arrangement. Orthorhombic ζ -Fe_2N is a distorted modification of ε formed by a change in the nitrogen-atom ordering. The transition of ε to ζ causes an anistropic distortion of the iron lattice produced by re-ordering of nitrogen atoms. The relationship between the orthorhombic ζ unit-cell dimensions a_ζ, b_ζ and c_ζ, and the hexagonal unit-cell dimensions a_ε and c_ε are:

$$a_\zeta \approx 3a_\varepsilon \; ; \quad b_\zeta \approx 2a_\varepsilon \; ; \quad c_\zeta \approx c_\varepsilon$$

Body-centred tetragonal nitrogen martensite is formed on quenching from nitrogen austenite and is isostructural with carbon martensite. On ageing of the supersaturated ferrite and martensite, precipitation of

γ

nitrogen
austenite

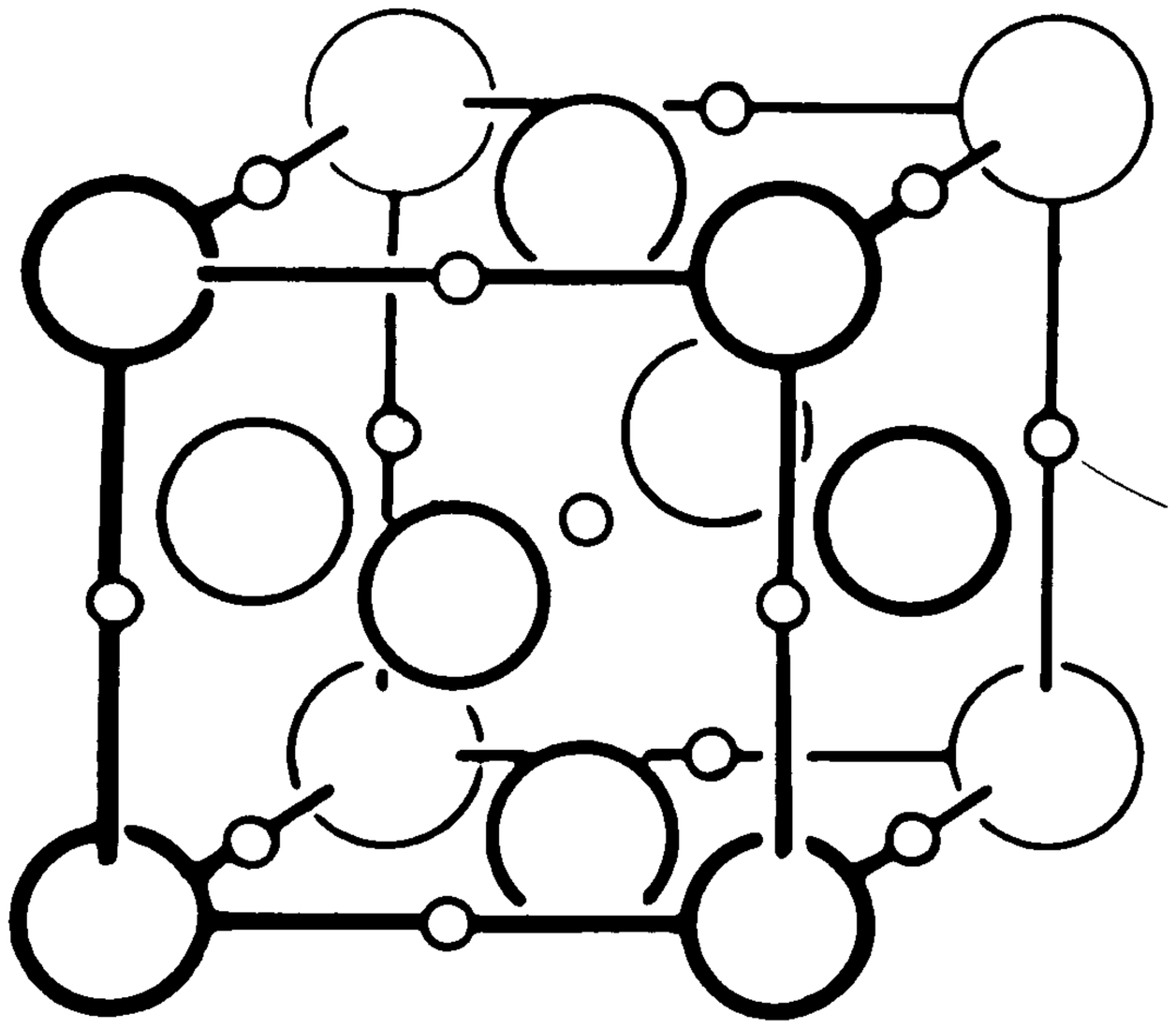

γ′

Fe_4N

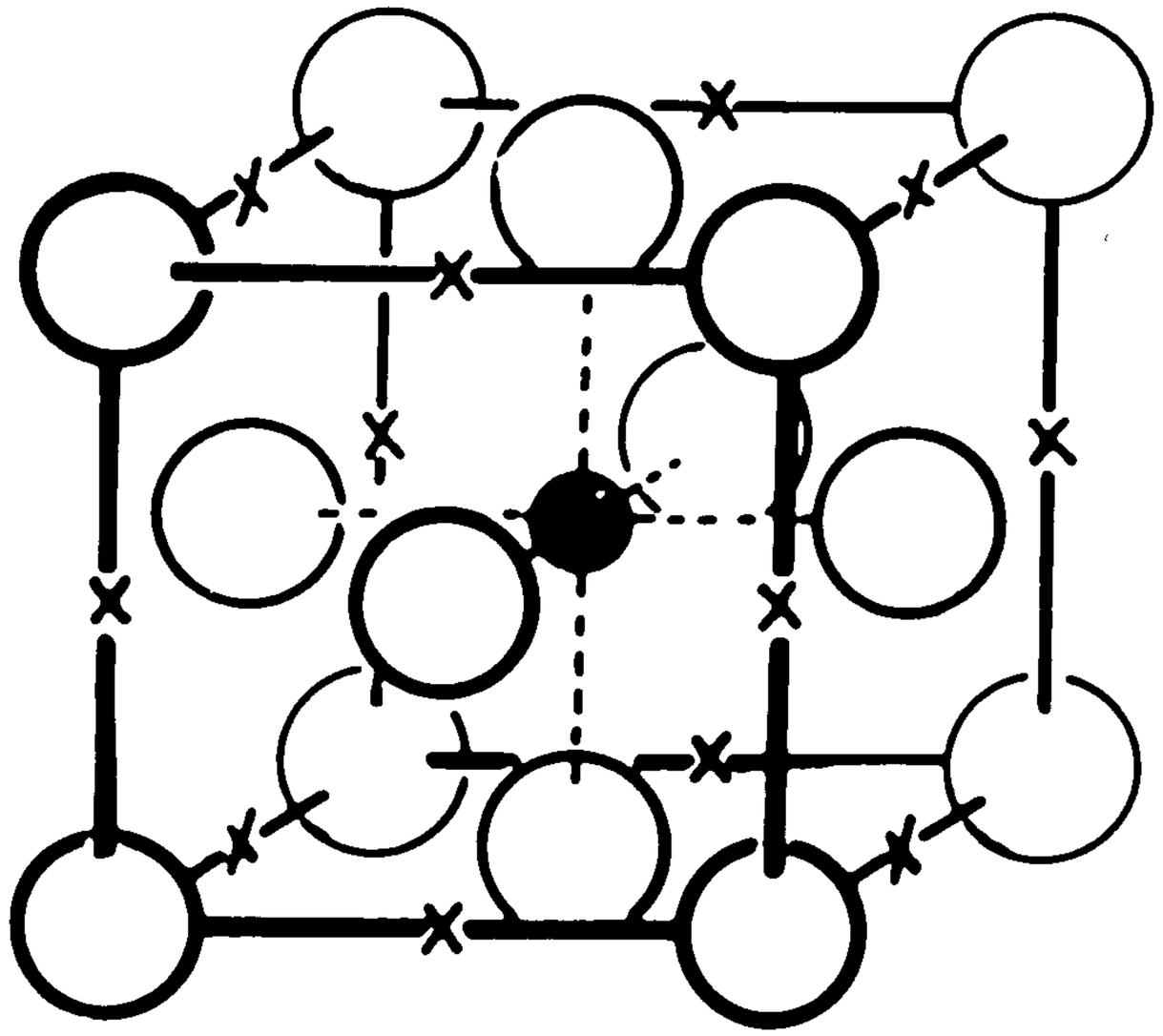

Fig.I.3

○ Fe atoms

× unoccupied interstices

o octahedral interstices
1 in 10 randomly filled

● N atom

the intermediate precipitate α'' $Fe_{16}N_2$ occurs (Jack, 1951b).

I.2 Iron-nickel alloys

As the nickel concentration in iron is increased the stability of austenite increases and the austenite to ferrite transition temperature is lowered (Figure I.4). At nickel contents greater than 30 at% γ is stable under most conditions. Above 63 at% Ni an ordered phase $FeNi_3$ is formed below a temperature of 500°C.

I.3 Iron-nickel-nitrogen alloys

Nickel markedly reduces the solubility of nitrogen in ferrite (Imai et al, 1968) and in austenite (Wriedt and Gonzalez, 1961; Heckler and Peterson, 1969; Atkinson and Bodsworth, 1970). Three phases are found in iron-nickel-nitrogen alloys; γ'-$(Fe,Ni)_4N$ (Hahn and Muhlberg, 1949; Weiner and Berger, 1955; Arnott and Wold, 1960); hexagonal Ni_3N (Arnott and Wold, 1960; Rienacher and Hohl, 1960) and ε Fe_3N (Atkinson and Bodsworth, 1970). γ'-$(Fe,Ni)_4N$ has a wide range of nickel contents from 0 to 80 at% Ni, but Ni_3N which is unstable above 500 to 550°C has only a slight solubility of iron (Arnott and Wold, 1960). The range of homogeneity, crystal structure

Fig. I.4

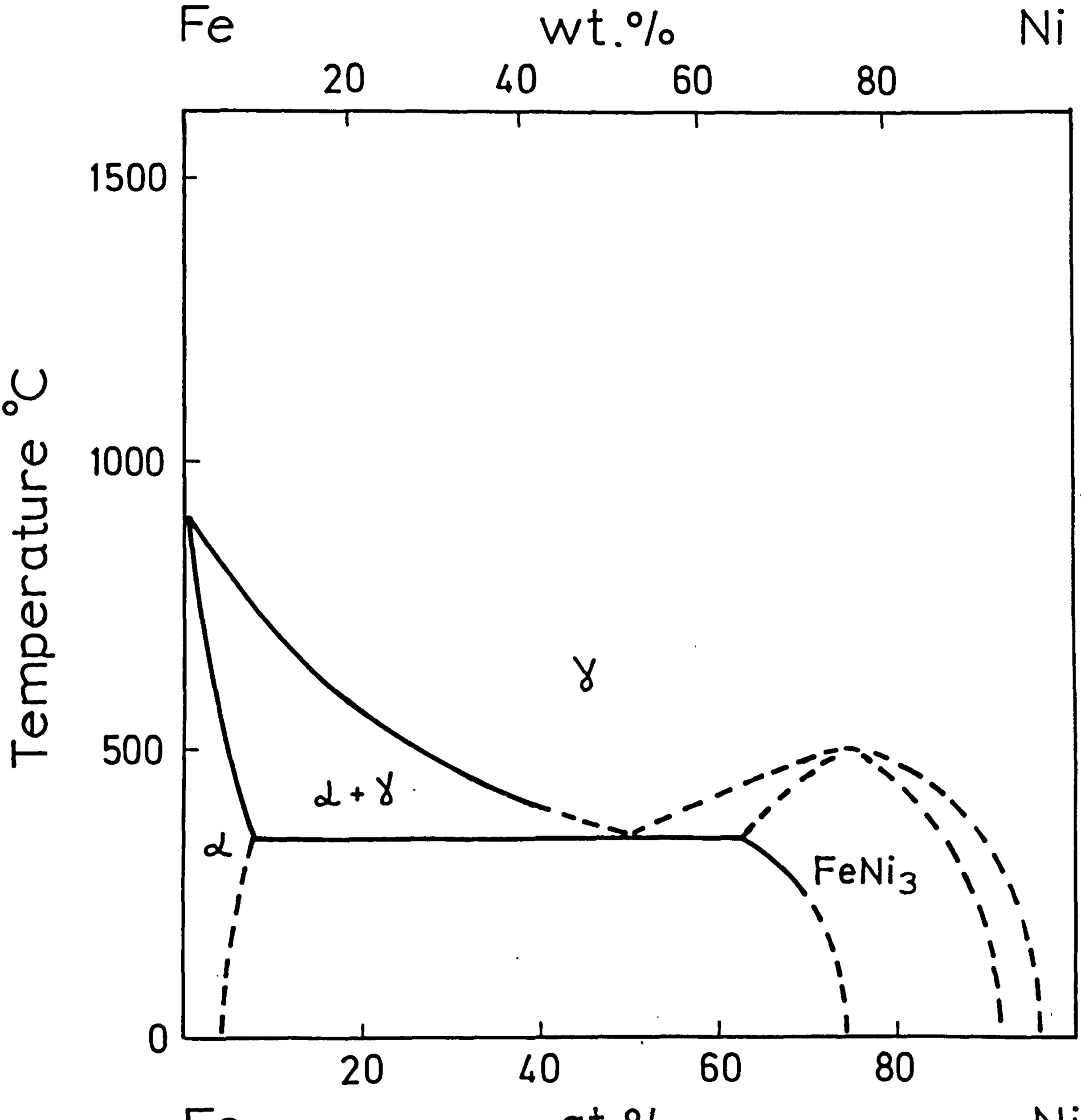

The Iron - Nickel equilibrium diagram after Shunk (1969).

and unit-cell dimensions are tabulated in Table I.1.

I.4 The niobium-nitrogen system

The phase diagram due to Elliot (1965) has been modified to incorporate the more recent results recorded in Shunk (1969) and of Roberts (1970) and Taylor and Doyle (1966) and is illustrated in Figure I.5. Table I.2 gives the structure, composition ranges and unit-cell dimensions of the main phases reported by Brauer and Jander (1952) in the niobium-nitrogen system.

Taylor and Doyle (1966) confirmed earlier work by Gerhardt, Fromm and Jakob (1964) and by Cost and Wert (1963) that the nitrogen solubility in niobium varied with temperature as shown in Figure I.5. Taylor and Doyle attributed the previously reported variations of nitrogen solubility in niobium to oxygen pick-up at high temperatures and pressures.

The close-packed hexagonal β (Nb_2N) has a range of homogeneity (Table I.2) and may accommodate some oxygen (Roberts 1970). NbN is reported to exist as four structures (γ, γ', δ and ϵ as shown in Table I.2) after Brauer and Jander (1952) and Schönberg (1954). Roberts (1970) showed that γ', δ and ϵ are oxynitrides whose compositions lie within the ternary Nb-N-O system

Fig. I.5

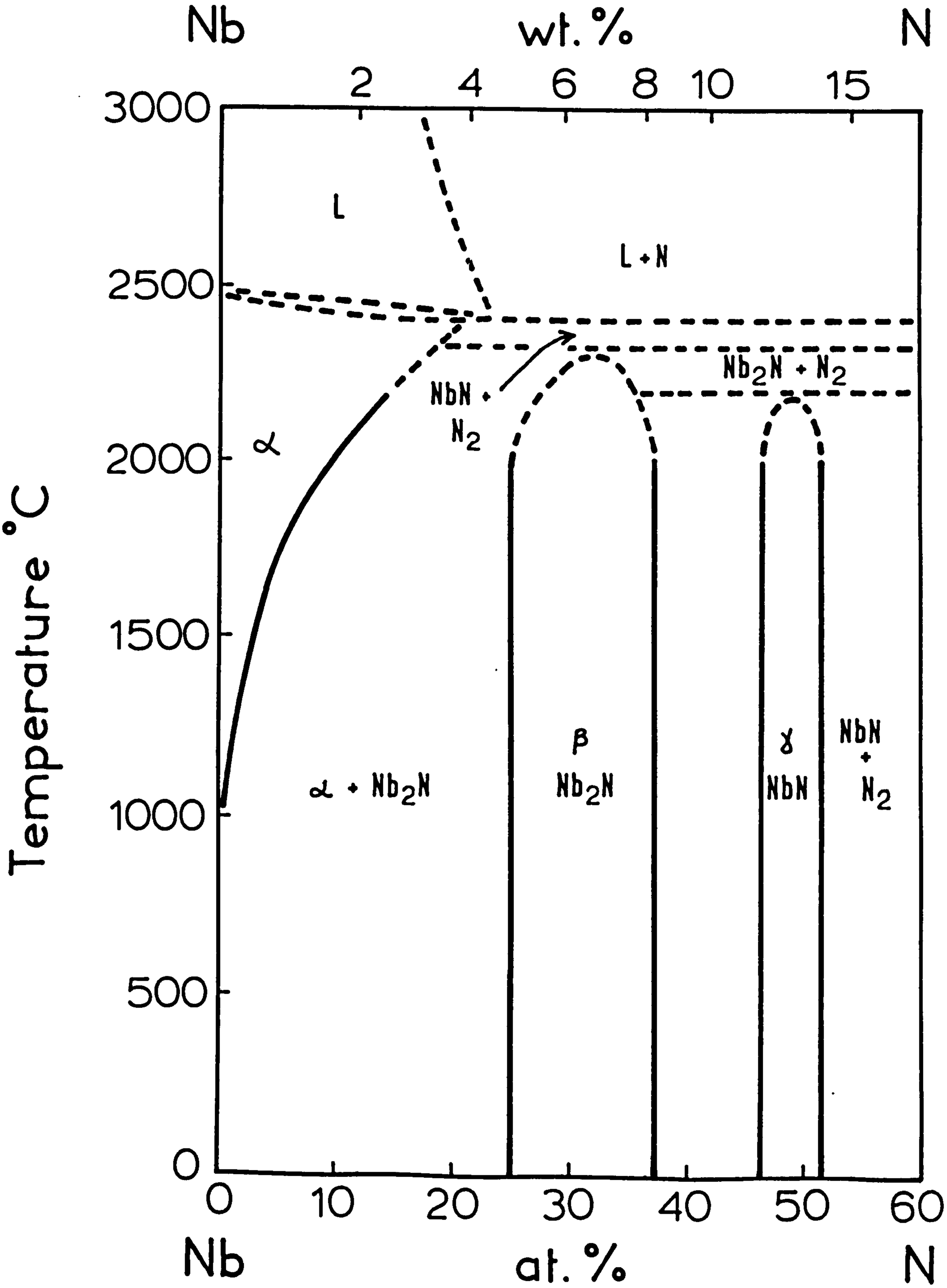

Niobium-Nitrogen equilibrium diagram after Elliot (1965), Shunk (1969), Taylor & Doyle (1967) and Roberts (1970).

Table I.2

Phases characterized by Brauer and Jander (1952) in the niobium-nitrogen system

phase symbol	crystal structure	approximate composition limits	unit-cell dimensions
α	b.c.c.	$Nb - Nb_{0.01}$	$\underline{a}$, 3.300 Å for pure Nb
β	c.p. hexagonal	$NbN_{0.4}$ to $NbN_{0.5}$	$\underline{a}$, 3.052; $\underline{c}$, 4.956 Å
			$\underline{a}$, 3.056; $\underline{c}$, 4.997 Å
γ'	f.c. tetragonal	$NbN_{0.79}$	$\underline{a}$, 4.385; $\underline{c}$, 4.316 Å
γ	f.c.c.	$NbN_{0.87}$ to $NbN_{0.94}$	$\underline{a}$, 4.380 Å
			$\underline{a}$, 4.389 Å
δ	c.p. hexagonal	$NbN_{0.95}$	$\underline{a}$, 2.968; $\underline{c}$, 5.535 Å
ε	hexagonal (AABB)	$NbN_{1.00}$	$\underline{a}$, 2.950; $\underline{c}$, 11.252 Å

illustrated in Figure I.6 and concluded that previous equilibrium diagrams by Schönberg (1964), Brauer and Esselborn (1961) and by Guard, Savage and Swarthout (1967) were from pseudo-binary sections of the Nb-N-O system. Thus, small quantities of oxygen have a pronounced effect on the phases formed in the Nb-N-O system.

I.5 The Fe-Nb, Ni-Nb and Fe-Ni-Nb systems

The phase diagram for the austenitic iron-rich portion of the Fe-Nb system is shown in Figure I.7a (Elliot, 1965), and has been modified to include later results given by Shunk (1969).

The maximum solubility of niobium in austenite found by Peters and Fisher (1948) is 0.6at%Nb at 1200°C. At higher concentrations of niobium in austenite the hexagonal Laves phase Fe_2Nb is formed with unit-cell dimensions: a, 4.829; c, 7.877 Å; c/a, 1.632 (Speich, 1962).

The phase diagram for the nickel-rich portion of the nickel-niobium system is shown in Figure I.7b (Duerden and Hume-Rothery, 1966). The maximum solubility of niobium in nickel is 16.8at%Nb at 1250°C. At higher niobium contents Ni_3Nb is formed with an orthorhombic structure of unit-cell dimension a, 5.11; b, 4.25; c, 4.54 Å (Pylaeoa, Gladshevskii and Kripyakevich, 1958).

Fig. I.6

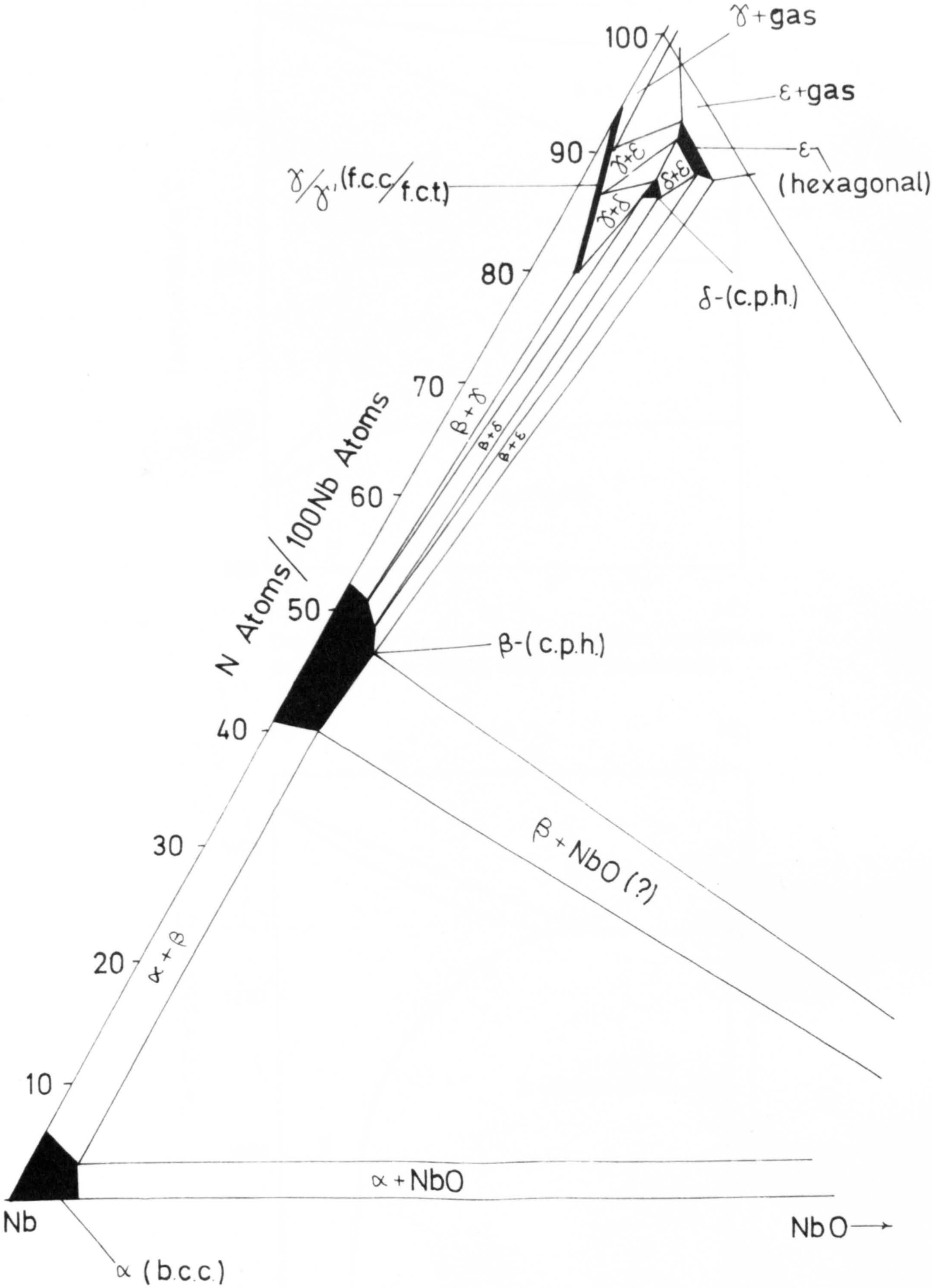

PROPOSED TERNARY DIAGRAM FOR THE Nb-N-O SYSTEM. [SCHEMATIC]

Fig. I.7

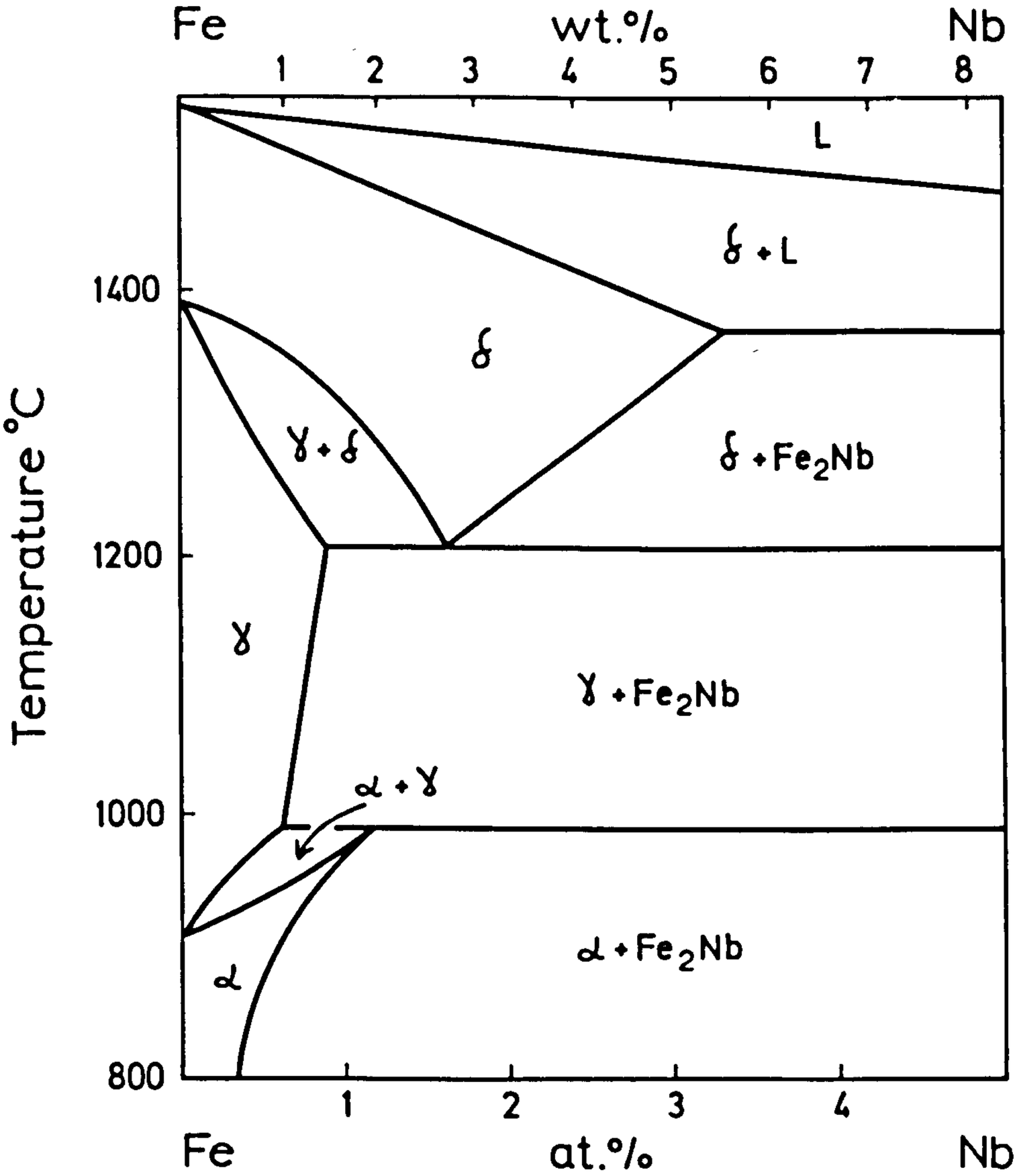

The Iron rich side of the Iron-Niobium equilibrium diagram after Elliot(1965) and Shunk(1969).

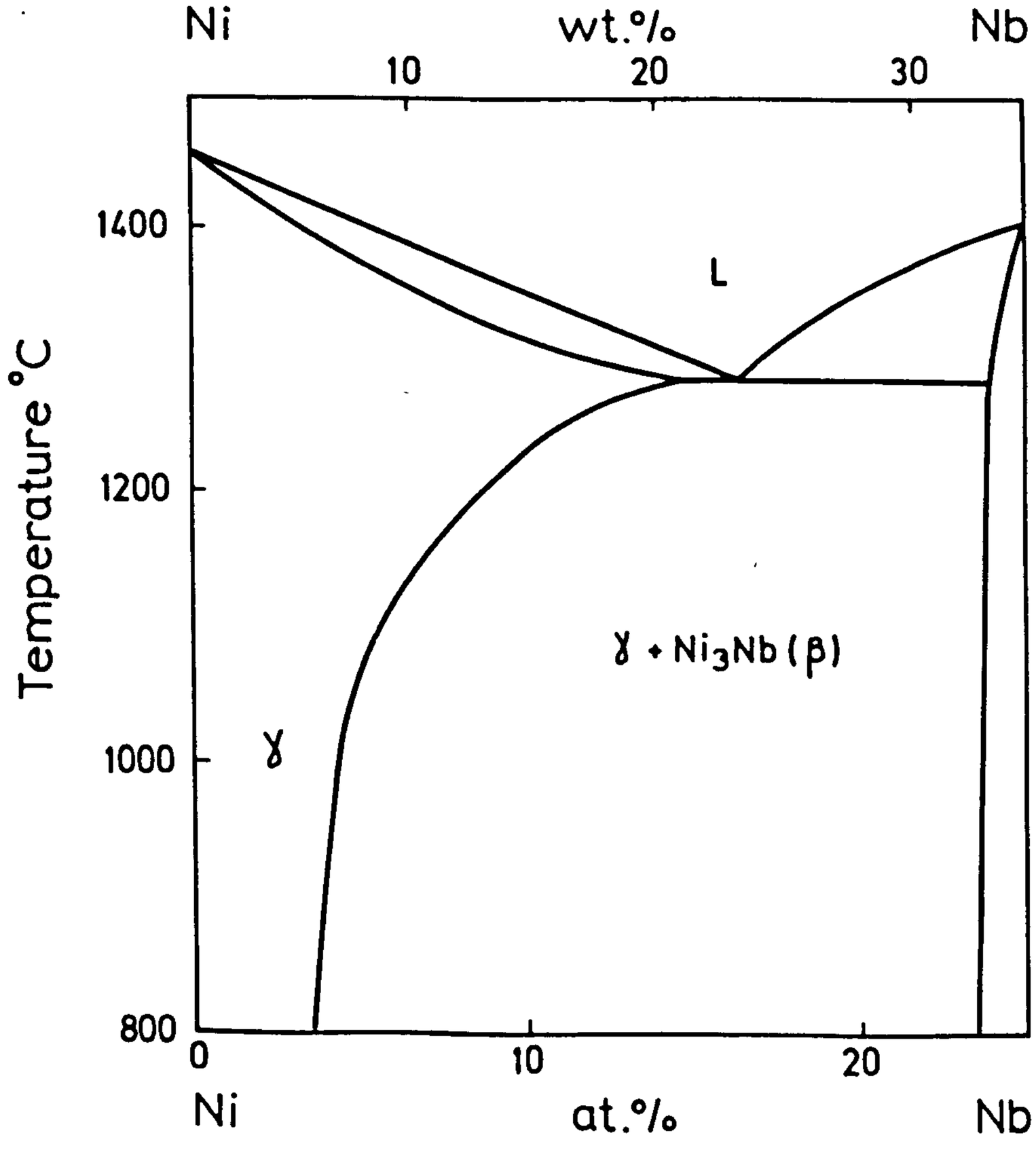

The Nickel rich side of the Nickel-Niobium equilibrium diagram after Duerden and Hume-Rothery (1966).

The effect of nickel additions to iron-niobium alloys is to increase the solubility of niobium in austenite (Leith and Chaturvedi, 1971) and to promote the formation of Ni_3Nb, (Praed and Borland, 1969; Leith and Chaturvedi, 1971) at the expense of the Laves phase Fe_2Nb.

I.6 The Fe-Nb-N and Fe-Cr-Ni-Nb-N systems

Roberts (1970) found eight different phases in ferritic Fe-Nb alloys nitrided at temperatures above 500°C under the conditions shown in Figure I.8: λ_1 -$FeNb_4N_4$, λ_2 -$FeNb_2N_2$, δ -NbN(O), ε -NbN(O), γ-NbN, austenite, Fe_4N, and α'-martensite.

λ_1-$FeNb_4N_4$ exists over a small range of homogeneity and has a hexagonal structure with unit-cell dimensions a, 5.192; c, 10.36 Å; c/a 1.977, and is isostructural with λ_1 formed in Ni-Nb-N alloys. The structure of λ_2-$FeNb_2N_2$ is undetermined and exists over a small range of homogeneity. δ -NbN(O) transforms to ε -NbN(O) after prolonged nitriding at temperatures above 700°C in NH_3:H_2 gas mixtures.

Mixed substitutional-interstitial solute-atom clusters (Guinier-Preston zones) are formed isothermally in Fe-Nb alloys during "constant activity ageing" in NH_3:H_2 at 400-650°C (Roberts 1970).

Fig. I.8

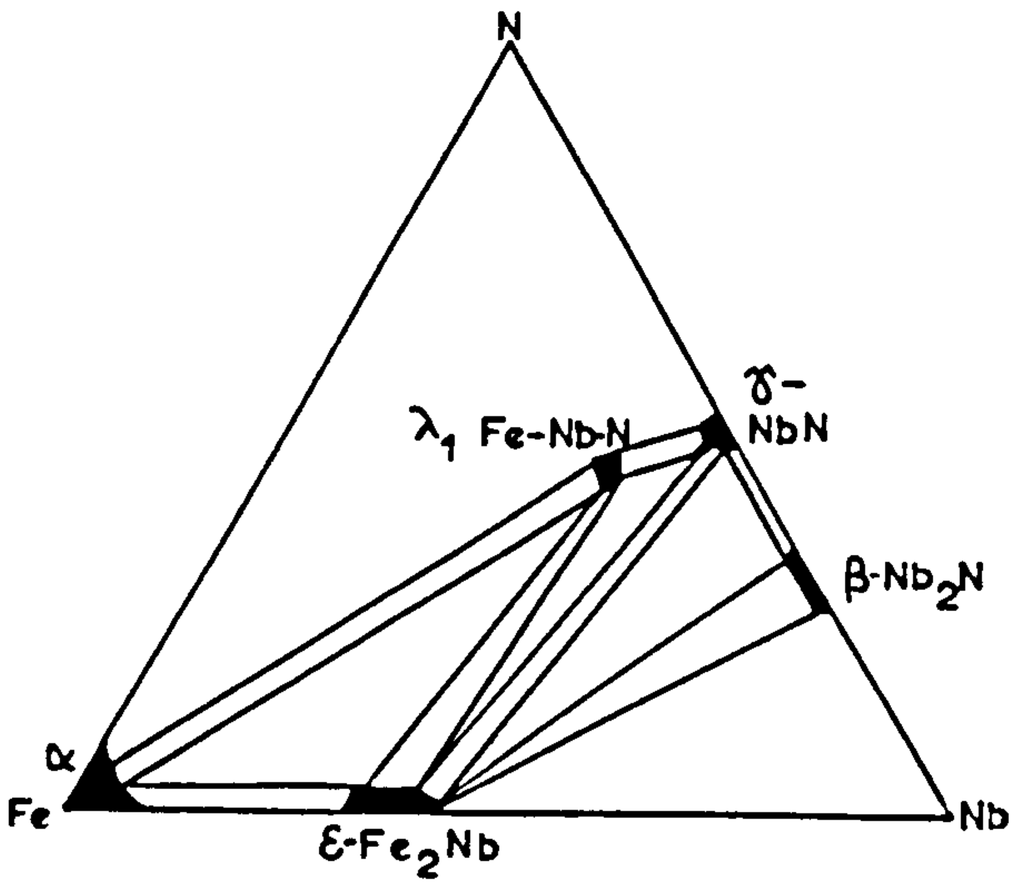

1. NH_3-H_2 [high pNH_3].

pN_2~ 5,000 Atm.

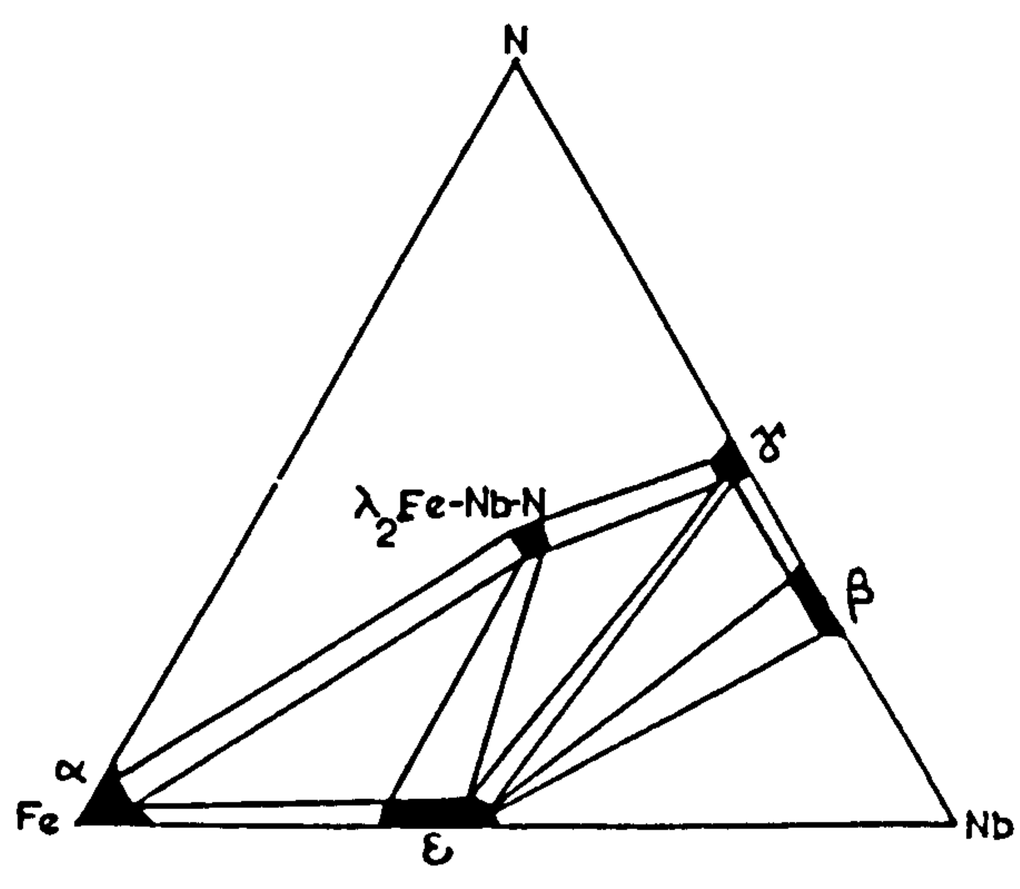

2. NH_3-H_2 [low pNH_3].

pN_2~2,500 Atm.

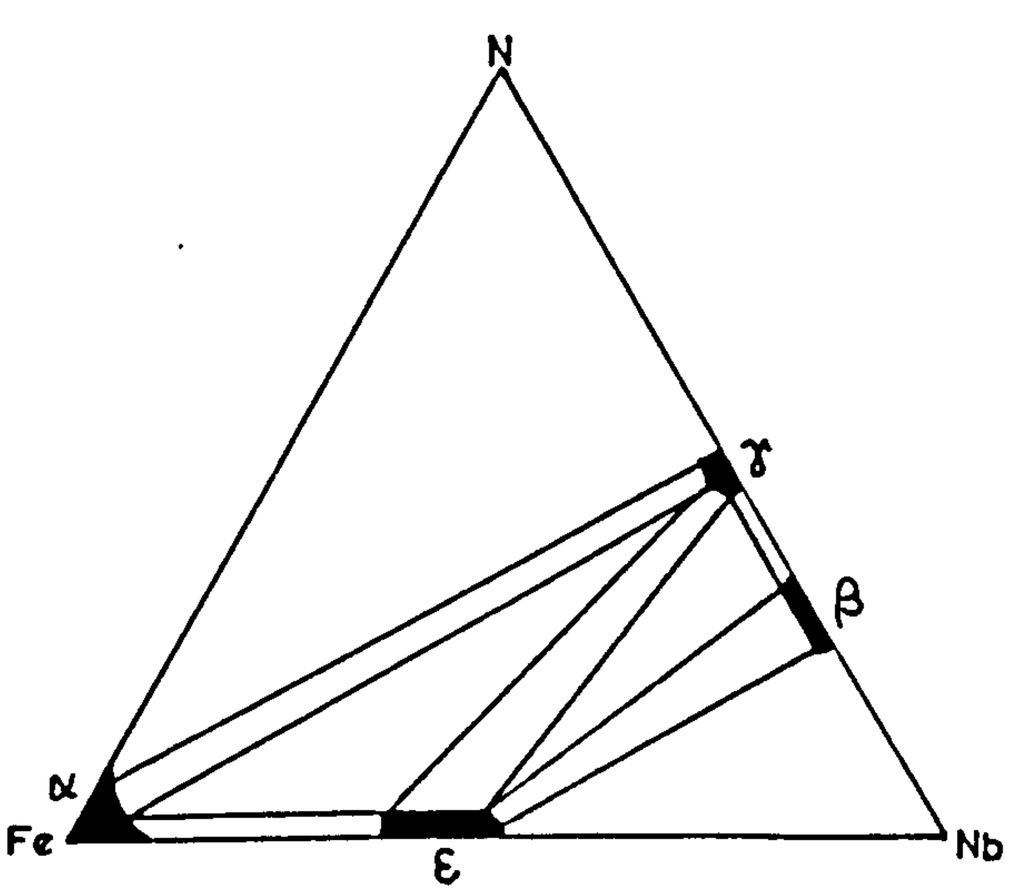

3. N_2-H_2 & P. Nitriding.

pN_2. 0·1–50 Atm.

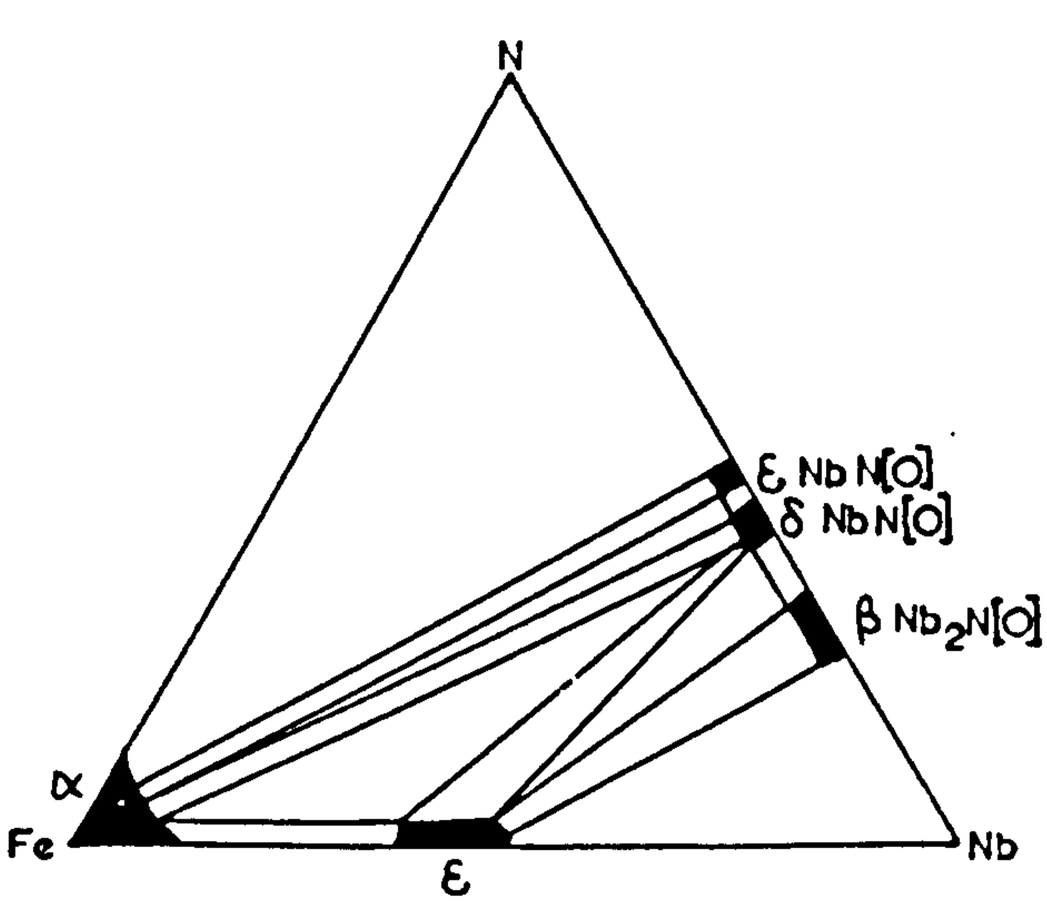

4. As 3 with O_2 present.

PROPOSED TERNARY DIAGRAMS FOR Fe-Nb-N

ALLOYS AT VARIOUS NITROGEN PRESSURES.

G.P. zones are metastable and so have a higher solubility than the equilibrium precipitate (Jack, 1972). The high supersaturation, which is the driving force to form zones, can therefore only be obtained conventionally by cooling to low temperatures, and here the solute-atom diffusivity is too small to allow clustering unless there is also an abnormally high concentration of quenched in vacancies. These conditions are not met in b.c.c. metals and so, although they have been looked for, G.P. zones have not previously been found in dilute iron alloys.

The high supersaturations relative to the zone solvus which can be introduced and maintained even at high temperatures by constant activity ageing in NH_3:H_2 allows the isothermal formation of substitutional-interstitial solute-atom clusters e.g. G.P. zones and moreover in much greater densities than can be obtained in any zone formation by a quench aged procedure. Once the G,P. zones are formed they persist for several hours over-ageing at temperatures approaching 700°C (Jack, 1972).

The sequence of precipitation in nitrided Fe-Nb alloys at 400 to 650°C goes through similar stages to those found in G.P. zone formation in aluminium alloys:

(i) coherent disc shaped G.P. zones on {100} planes;

(ii) semi-coherent disc-shaped intermediate precipitates on {100} planes with a body-centred tetragonal

structure of the $Fe_{16}N_2$ α'' type containing some substitutional niobium atoms at 600-800°C;

(iii) after prolonged ageing at 600-800°C transformation of ferrite to austenite occurs with the precipitation of γ-NbN (Roberts, 1970). Electron micrographs of the G.P. zones are similar to the tweed microstructure observed in Cu-Be alloys with pronounced streaking in the $\langle 100 \rangle_\alpha$ directions (Speirs et al 1970).

In austenite Fe-Cr-Ni-Nb low nitrogen alloys solution treated at 1300°C, water quenched and aged at 600-800°C Borland (1969) and Borland and Honeycombe (1970) detected four precipitated phases: γ-NbN, $(Fe,Cr,Ni,Nb)_6N$, Laves phase Fe_2Nb, and Z-phase $Cr_2Nb_2N_2$. M_6N has a complex cubic structure with a lattice parameter of 11.31 Å and a structure similar to the η-carbide Cr_3Nb_3C. Z-phase $Cr_2Nb_2N_2$ has a tetragonal structure of unit-cell dimensions $\underline{a}$, 3.108; $\underline{c}$, 5.887 Å; $\underline{c}/\underline{a}$, 1.894 (Jack and Jack, 1972).

Precipitation of γ-NbN in austenitic Fe-Cr-Ni-Nb-N alloys occurred on dislocations, in association with stacking faults, in the matrix, and at grain boundaries. After prolonged ageing stacking fault precipitation of γ-NbN transforms to sheets of M_6N. Stacking fault precipitation of γ-NbN occurs on $\{111\}$ planes by a

mechanism generally accepted to be proposed by Silcock and Tunstall (1964) for niobium carbide precipitation in austenitic stainless steels.

The Laves phase was observed in very low nitrogen alloys and probably contained chromium.

I.6 Summary of previous work

A literature survey on nitrided austenitic alloys failed to find any information on either the nitriding of Fe-Ni-Nb alloys or precipitation in Fe-Ni-Nb-N alloys.

Previous work of the greatest relevance to the present investigation of nitride precipitation in Fe-35Ni-Nb alloys is work by Roberts (1970) and by Borland (1969).

Borland (1969) reported stacking fault precipitation of γ-NbN in austenitic Fe-Cr-Ni-Nb low N alloys at temperatures between 600 and 800°C.

Roberts (1970) found substitutional-interstitial solute-atom clusters are found at 400-600°C in nitrided Fe-Nb-N alloys when the nitrogen potential exceeds the G.P. zone solvus. The G.P. zones overaged to give an intermediate α''-$Fe_{16}N_2$ precipitate and, after prolonged ageing, niobium nitrides. His work on the niobium-nitrogen system and the iron-niobium-nitrogen system has

shown that small amounts of impurities, e.g. oxygen and carbon can affect the structure of the nitrided phases.

Work of a lesser importance to this study is by Arnott and Wold (1960) and by Atkinson and Bodsworth (1970) on the Fe-Ni-N system, and by Pread and Borland (1969) on the Fe-Ni-Nb system.

In Fe-Ni-N alloys nitrided at temperatures between 500 and 800°C the formation of nickel-containing γ'-Fe_4N and ϵ-Fe_3N may occur (Arnott and Wold 1960; Atkinson and Bodsworth (1970).

Precipitation of orthorhombic Ni_3Nb and the hexagonal Laves phase Fe_2Nb may occur in the unnitrided alloys (Pread and Borland, 1969).

Chapter II

EXPERIMENTAL METHODS

II.1 Preparation of alloys

The iron-nickel-niobium alloys were supplied by Firth Brown Co. Ltd., Sheffield, and had a nominal composition of Fe:35wt%Ni: 0.0, 0.5, 1.0 and 2.0 wt%Nb. Alloys of other nickel contents were prepared by argon arc melting small sections of the master alloys together with either pure iron, or nickel, or iron-niobium alloys supplied by the British Iron and Steel Research Association. The alloy buttons were melted at least three times and then annealed in evacuated silica capsules for 24hrs at 1200°C to ensure homogeneity. Analysis of the master alloys was carried out by the Consett Works of the British Steel Corporation and are given in Table II.1. All alloys referred to in the text are in wt% unless stated otherwise.

X-ray samples were prepared from 0.5mm diameter wire from cold rolled and drawn sections cut from the original hot extruded master alloys, and from the annealed alloy buttons.

Table II.1

Alloy No.	Nominal composition		Analysis			
	wt%Ni	wt%Nb	wt%Ni	wt%Nb	wt%V	wt%C
BV 1732	35	-	35.6	-	-	0.010
BV 1766	35	0.5	35.4	0.43	0.028	0.010
BV 1767	35	1.0	35.4	0.87	-	0.010
BV 1768	35	2.0	35.4	1.98	-	0.010
8	8	-	7.80			
18a	8	-	8.11			
12	12	-	12.01			
18b	18	-	18.49			
25	25	-	24.85			
40	40	-	40.93			
47.5	47.5	-	47.09			
7	12	1.0				
8	18	1.0				
9	25	1.0				
10	12	2.0				
11	18	2.0				
12	25	2.0				

Optical and electron microspecimens were prepared from 1.0 to 0.15mm strip which had been similarly rolled down.

All samples were electropolished at 20 volts in 68 vol% acetic acid, 16 vol% perchloric acid and 16 vol% 2-dibutoxyethanol solution at $0^{o}C$ prior to annealing and nitriding. Samples of Fe:35Ni, and Fe:35Ni: 0.5, 1.0 and 2.0Nb were annealed for 0.5h at 950, 1050, 1150 and $1200^{o}C$ respectively in evacuated silica capsules to give approximately the same grain size of 0.1mm unless stated otherwise.

II.2 Ammonia-hydrogen nitriding

Specimens were nitrided in ammonia-hydrogen gas mixtures of varying proportions at temperatures between 500 and $800^{o}C$. For the nitriding reaction the equilibrium constant K at any temperature is:

$$NH_{3(g)} \rightleftharpoons \underline{N} + \tfrac{3}{2} H_{2(g)}$$

$$K = \frac{a_N \, p_{(H_2)}^{\frac{3}{2}}}{p_{(NH_3)}} \qquad \ldots\ldots \text{II.1}$$

where a_N is the activity of nitrogen in solid solution in iron and p_{H_2} and p_{NH_3} are the partial

pressures of hydrogen and ammonia. The nitriding potentials of ammonia-hydrogen gas mixtures in the Fe-N system have been determined by Lehrer (1930) and Paranjpe et al (1950); see Figure II.1a.

As the nitrogen activity in iron is increased at 700°C three phases are formed α, γ and ε-Fe_3N. As the nitrogen concentration is increased from zero the activity a_N increases from zero to a value $a_N^{\alpha max}$ at the limit of nitrogen solubility in ferrite. Further increase in the nitrogen concentration will promote the transformation of ferrite to austenite and with increasing nitrogen concentration the proportion of ferrite will decrease until it disappears. Only after complete transformation of ferrite will the nitrogen activity in austenite increase with increasing nitrogen content. Once the limit of nitrogen solubility $a_N^{\gamma max}$ is reached ε Fe_3N is formed where the activity $a_N^{\gamma max}$ equals $a_N^{\varepsilon min}$ and any increase in the nitrogen concentration will promote the transformation of γ to ε-Fe_3N. Since a_N is proportional to

$$p_{(NH_3)}/p_{(H_2)}^{3/2}$$

an ammonia-hydrogen gas mixture of a given composition will be in equilibrium with a fixed nitrogen composition in iron at a given temperature. In practice the maintenance of a constant NH_3/H_2 ratio in the nitriding

Fig. II.1

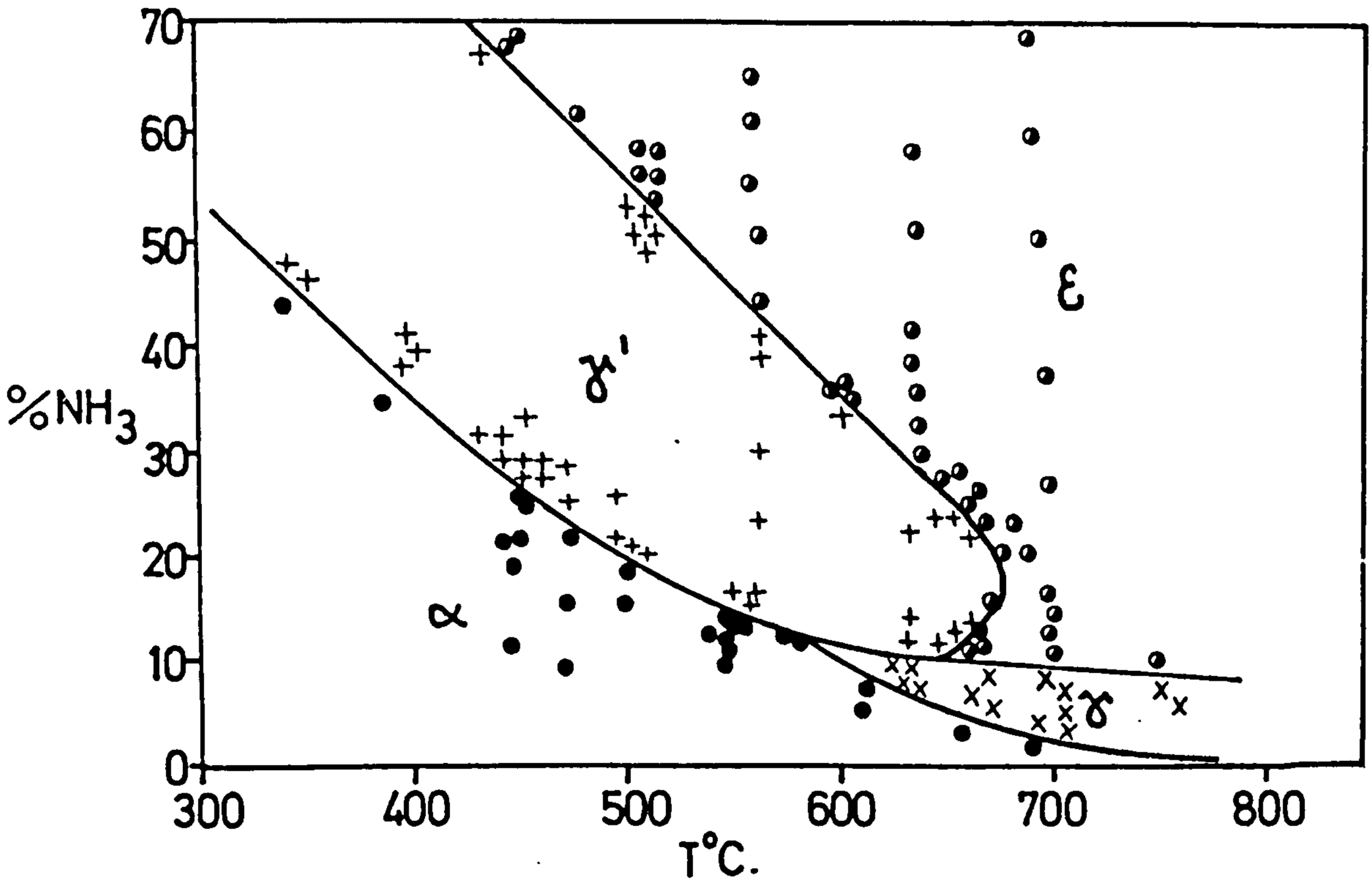

EQUILIBRIUM BETWEEN NH_3-H_2 MIXTURES [1 ATM.] AND SOLID PHASES OF THE IRON-NITROGEN SYSTEM [AFTER LEHRER (1930)].

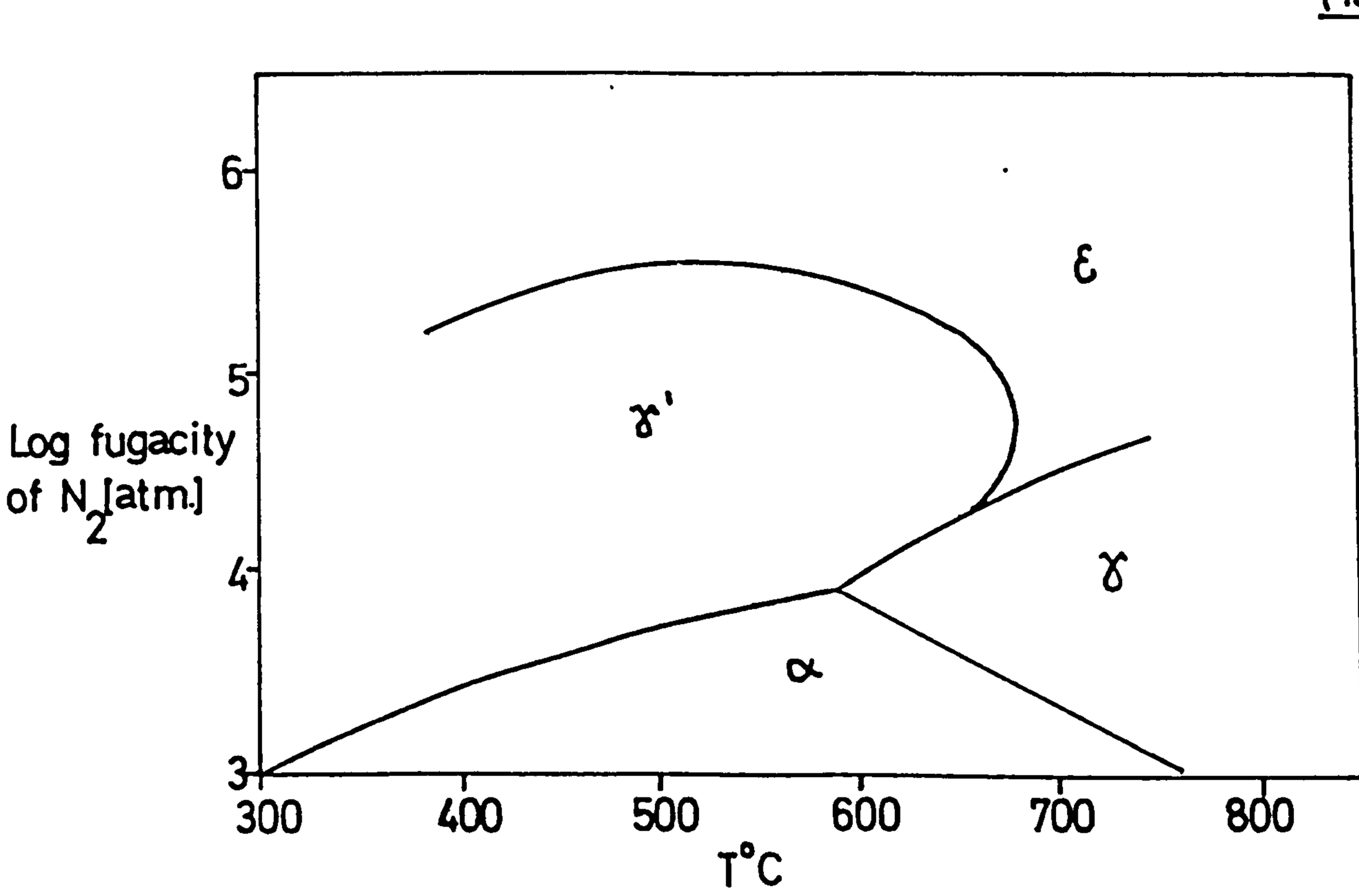

FUGACITY-TEMPERATURE DIAGRAM FOR THE IRON-NITROGEN SYSTEM USING DATA FROM THE PREVIOUS FIGURE.

gas mixture is complicated by the cracking of ammonia and this is dependent upon the flow rate, temperature and surface area (Coffman, 1932). The cracking is minimised by using high flow rates (200cc/min) over a small surface area ($2cm^2$) and at 700^oC is effectively zero. Figure II.1b shows the fugacity-temperature diagram for ammonia-hydrogen nitriding of iron alloys.

II.3 Nitriding apparatus

Specimens were nitrided in a vertical furnace (see Figure II.2) with an internal recrystallised alumina reaction tube (25mm internal diameter) heated by silicon carbide elements up to temperatures of 1200^oC to give a hot zone of 10cm in length. The temperature was maintained to $\pm 3^oC$ by means of a Cambridge controller and measured by a Pt-Pt:13%Rh thermocouple in the reaction zone.

The cylinder gases (hydrogen, ammonia and nitrogen or argon) were purified to remove traces of oxygen, carbon dioxide and water vapour (see Figure II.3) and their flow rates measured with capillary flowmeters (see Figure II.4) which had been calibrated by a bubble displacement technique. The gas pressure in the system was maintained above atmospheric pressure by 30 to 40mm

Fig. II.2

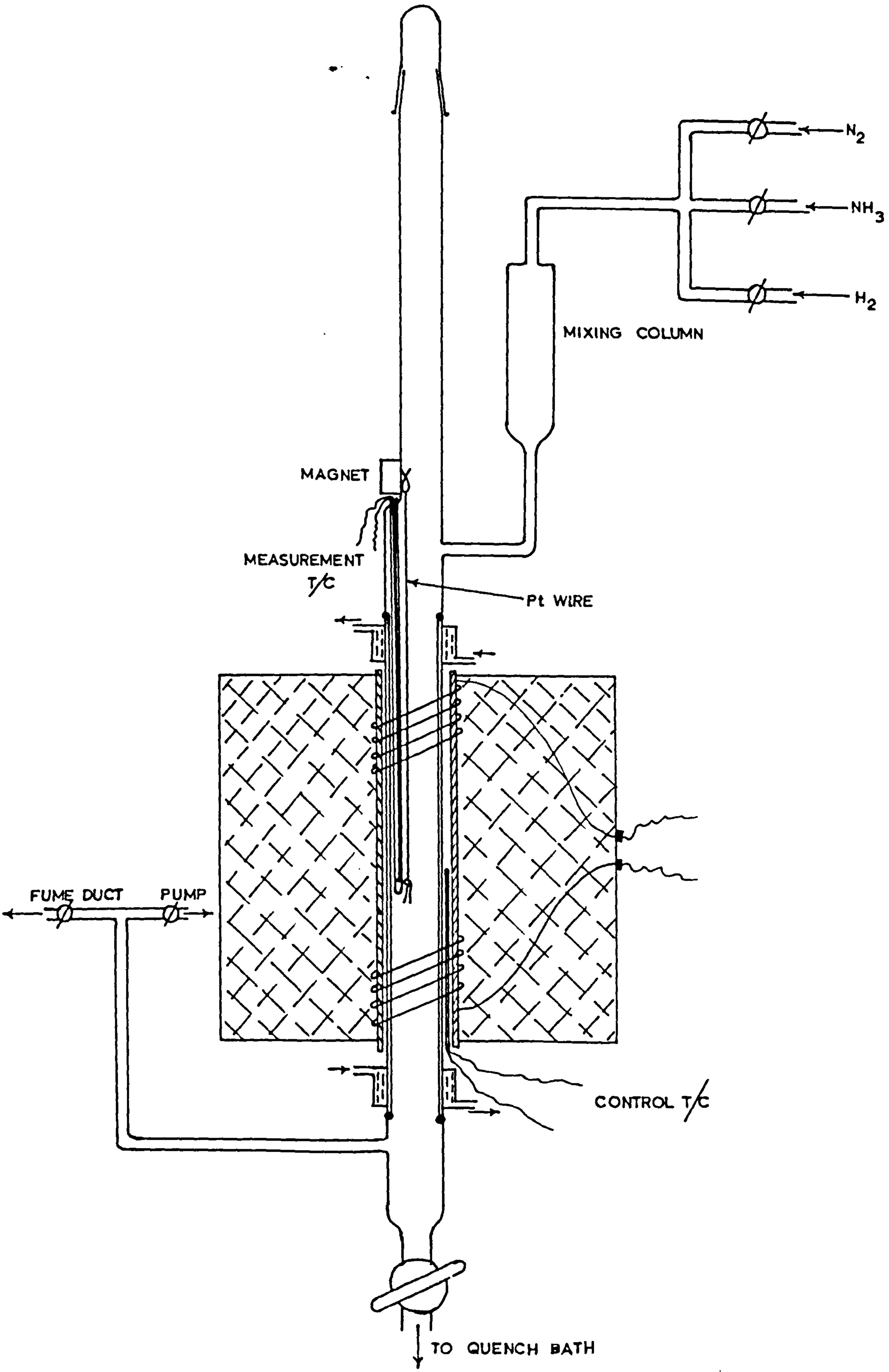

THE VERTICAL NH_3-H_2 AND N_2-H_2 EQUILIBRATION APPARATUS.

Fig. II.3

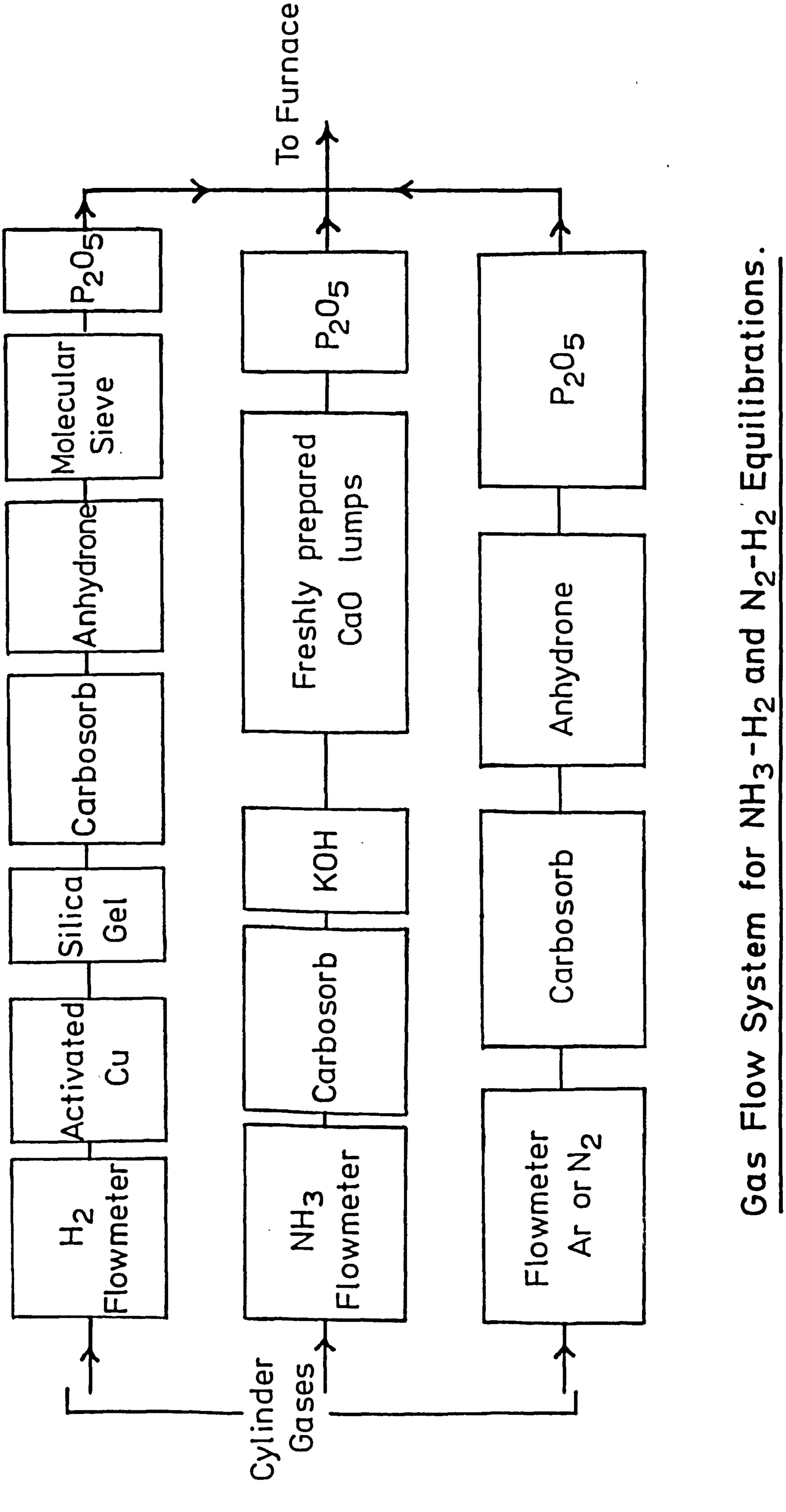
To Furnace
P_2O_5
Molecular Sieve
Anhydrone
Carbosorb
Silica Gel
Activated Cu
H_2 Flowmeter
P_2O_5
Freshly prepared CaO lumps
KOH
Carbosorb
NH_3 Flowmeter
P_2O_5
Anhydrone
Carbosorb
Flowmeter Ar or N_2
Cylinder Gases
Gas Flow System for NH_3-H_2 and N_2-H_2 Equilibrations.

Fig. II.4

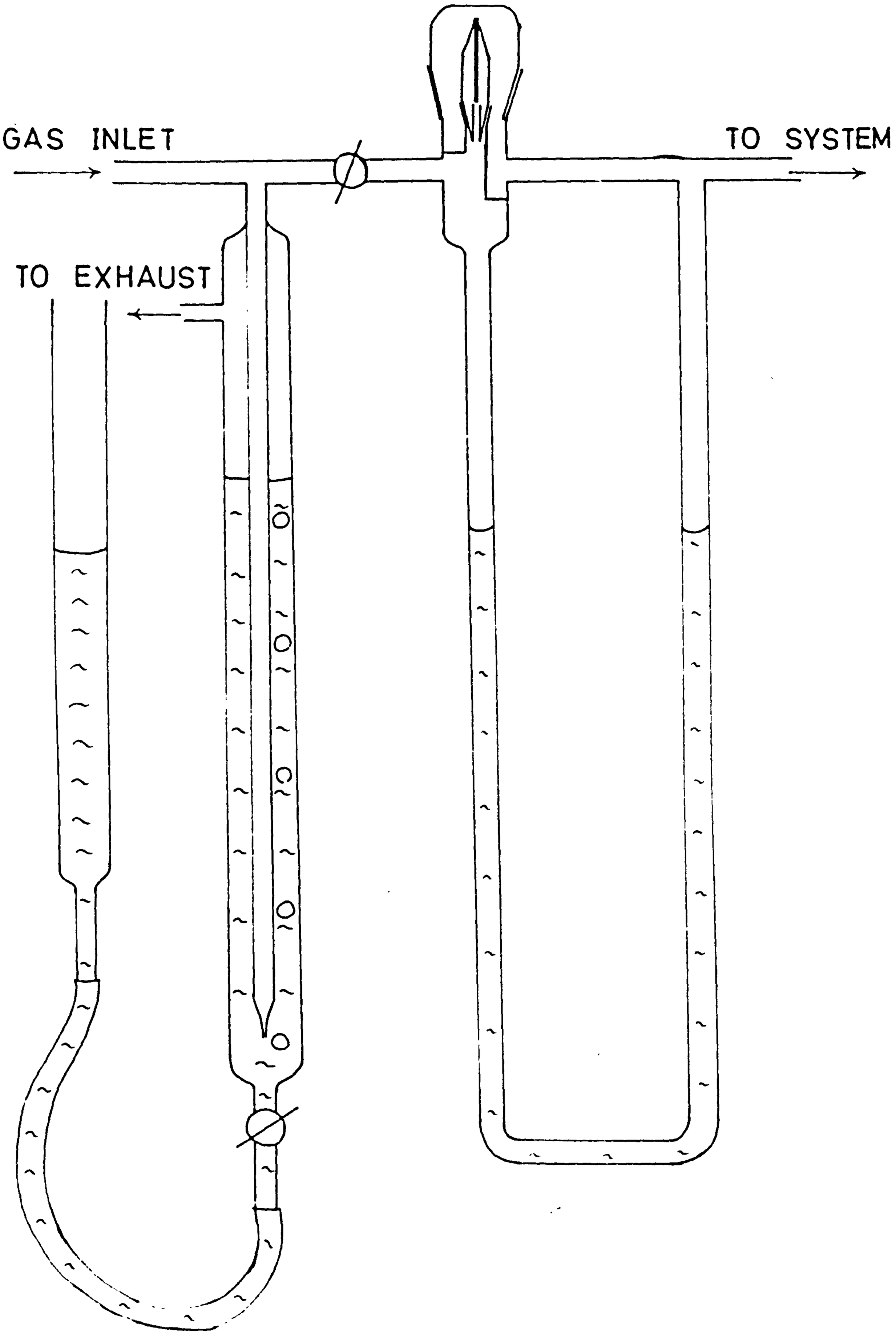

A CAPILLARY FLOWMETER [SCHEMATIC].

of oil. A phosphorus pentoxide boat and potash tower were used after the exit bubbler to prevent back diffusion of moisture.

The specimens were suspended on an alumina hook and the furnace tube evacuated to 10^{-1} torr by a rotary pump. Purified nitrogen was bled into the furnace tube till it reached atmospheric pressure, and the furnace flushed out for 0.5h with hydrogen prior to nitriding. The specimens were lowered into the hot zone in the appropriate NH_3:H_2 gas mixture at a linear flow rate of 40cm/min. After nitriding the specimens were raised out of the hot zone and cooled in hydrogen.

II.4 X-ray examination

X-ray diffraction patterns of the nitrided specimens were obtained using monochromatic X-radiation reflected from a lithium fluoride single crystal. Powder photographs were taken on 9cm and 19cm Unicam cameras using $FeK\alpha$, $CoK\alpha$ and $CrK\alpha$ radiation. Lattice parameter measurements were made on 19cm cameras and determined from the results by using a Nelson and Riley (1945) extrapolation.

II.5 Metallographic examination

Specimens were mounted in bakelite and polished on successive silicon carbide papers down to 600 grade, and finally polished on diamond wheels from 15 to 0.25μm. The specimens were then electroetched at 2 volts in 10:90 HCl:ethanol and examined on a Reichert projection microscope.

II.6 Hardness testing

Metallographic specimens were hardness tested on a Reichert diamond microhardness tester using 50 and 20g loads.

II.7 Electron microspecimen examination

Due to the difficulties encountered by polished nitrided specimens in the conventional electropolishing solutions used on the pure annealed alloys (see section II.1; mainly due to grain boundary perforation) the following technique was adopted. Each specimen was initially polished in a solution of 14vol% perchloric acid, 30vol% acetic acid, 30vol% formic acid, 12vol% 2-dibutoxyethanol and 14vol% diethyl phthalate at 40 volts with a current density of 0.25-0.3 amps/cm^2 at -30°C;

and finally polished in 14vol% perchloric acid, 56vol% acetic acid, 4vol% formic acid, 13vol% 2-dibutoxyethanol and 13vol% diethyl phthalate at 30 volts and a current density of 0.25 amps/cm^2 at 0^oC using a stainless steel cathode. Thin foils were stored under ethanol before examination in a Philips EM300 or a JEM100U electron microscope at 100 KV.

II.8 Mechanical testing

Mechanical testing was carried out on tensile specimens with gauge length of 10 and 25mm, thicknesses of 0.15, 0.30, 0.50 and 1.25mm, and widths of 5 and 12.5mm. Tensile tests were carried out on an Instron type III4 testing machine at a nominal strain rate of 1.33 and 1.65×10^{-3} sec^{-1} for gauge lengths of 25 and 10mm respectively. Mean values of 0.2% proof stress, tensile stress, work hardening rate and elongation were determined from at least two specimens for each treatment.

II.9 Chemical analysis

Nitrogen analysis was carried out using a standard semi-micro Kjeldahl apparatus with colorimetric determination of distilled ammonia using Nessler's

reagent and with ammonium chloride as a standard. The nitrogen content of the alloy was followed by weight changes of one gram samples to give an accuracy of $\pm$ 0.01wt%.

The extent of ammonia cracking was determined from 500cc samples, collected in a dried vessel, of inlet and outlet NH_3:H_2 gas mixtures. The gas sample was then expelled from the collecting vessel through a diffuser by argon into a known volume of N/10 HC1. This solution was then back titrated by adding a known volume of N/10 NaOH and titrated by adding N/10 HC1 using a screened methyl red - methylene blue indicator. The reproducibility was $\pm$ 0.2vol% NH_3.

Chapter III

SCOPE OF THE PRESENT INVESTIGATION

Previous investigations at Newcastle have shown that mixed interstial-substitutional solute-atom clusters (Guinier-Preston zones) are formed in nitrided ferritic Fe-Mo, Fe-Nb and Fe-V alloys (Spiers, 1969; Roberts, 1970; Pope, 1972) at 400-650°C at nitrogen potentials which exceed the G.P. zone solvus. Similar observations of mixed interstitial-substitutional solute-atom clusters have been made in nitrided Fe-Mn-V and Fe-35Ni-V alloys (Hayes, 1972; Driver, Sinclair and Jack, 1974) at nitrogen potentials which exceed the modulated structure solvus.

It was proposed to study the structure and mechanical properties of austenitic Fe-35Ni-Nb alloys nitrided in NH_3:H_2 at 500-800°C:

(i) to determine whether mixed interstitial-substitutional solute-atom clusters are formed in these alloys during constant activity ageing in NH_3:H_2;

(ii) to investigate the conditions under which niobium nitrides are formed during nitriding;

(iii) to determine the hardening mechanisms and relate

them to existing dislocation particle interaction theories;

and (iv) to investigate the nitrogen solubility and nitriding kinetics of Fe-35Ni-Nb alloys in NH_3:$_2$ at 500-800°C.

In order to characterise the structures of nitrided Fe-35Ni-Nb alloys a limited study has also been made of the Fe-Ni-N and Fe-Ni-Nb systems to determine the nature of any phases that maybe precipitated in the nitriding temperature range, 500-800°C.

The techniques used in this investigation involved electron and optical microscopy, X-ray diffraction and tensile testing. In addition, the application of thermodynamic principles and theories for dislocation-particle interactions were necessary for the interpretation of results.

Chapter IV

THE STRUCTURE OF NITRIDED Fe:35Ni:Nb ALLOYS

IV.1 Introduction

Previous work by Roberts (1970) on the nitriding of ferritic Fe-Nb alloys in ammonia-hydrogen gas mixtures has shown that δ- and ϵ-NbN(O) are formed at 700-800°C. Roberts (1970) also found that mixed interstitial-substitutional solute-atom clusters (Guinier-Preston zones) are formed in Fe-Nb alloys nitrided in $NH_3:H_2$ at temperatures below 650°C providing the nitriding potential exceeds the G.P. zone solvus and is less than that required to precipitate iron nitrides. The disc shaped G.P. zones are formed on {100} planes. They overage to form a semicoherent intermediate precipitate of the $Fe_{16}N_2$ type, and after ageing at higher temperatures the intermediate precipitate transforms to needles of γ-NbN.

Recent work at Newcastle by Driver, Sinclair and Jack (1974) on the nitriding of Fe:35Ni:V alloys at 500-800°C in $NH_3:H_2$ has shown that interstitial-substitutional solute-atom interaction at 500-750°C results in the formation of a modulated structure which

is similar in many aspects to spinodal decomposition in Cu:Ni:Fe alloys. The modulated structure is formed in nitrided Fe:35Ni:V alloys when:

(i) both the nitrogen and vanadium activities exceed a nucleation "solvus", and outside this solvus homogeneous precipitation of VN occurs in a periodic array in austenite;

(ii) the nitriding temperature is below a critical value of about 780°C; above this temperature homogeneous precipitation of VN occurs;

(iii) the equilibrium precipitate (VN) has a similar crystal structure to the matrix; and

(iv) the nitride exhibits a large free energy of formation in austenite.

Stacking fault precipitation of γ-NbN occurs in austenitic Fe:Cr:Ni:Nb low-nitrogen alloys during ageing at 600 to 800°C (Borland and Honeycombe, 1970) on {111} planes by a mechanism generally accepted to be that proposed by Silcock and Tunstall (1964) for niobium carbide precipitation in austenitic stainless steels. After prolonged ageing, the stacking fault precipitates of γ-NbN transform to sheets of M_6N.

IV.2 Experimental

Fe:35Ni:0-2Nb alloys were prepared as 0.15mm strip

and annealed for 2hrs at 1200°C. X-ray specimens of Fe:35Ni:0.0, 0.5, 1.0 and 2.0Nb alloys were prepared as wires and annealed for 0.5hr at 950, 1050, 1150 and 1200°C respectively. The specimens were "constant activity" aged in various $NH_3:H_2$ gas mixtures at temperatures of 500 to 800°C.

IV.3 Results

The following structures are formed in Fe:35Ni:Nb alloys nitrided in $NH_3:H_2$ at temperatures between 500 and 800°C as shown in Figure IV.1:

(i) a modulated structure is formed in Fe:35Ni:1 and 2Nb alloys at 500-750°C, and at nitrogen potentials greater than 5:95 $NH_3:H_2$ at 600°C;

(ii) homogeneous precipitation of γ-NbN occurs at 800°C, and in a periodic array at temperatures less than 800°C in Fe:35Ni:0.5 Nb alloys and in Fe:35Ni:1 and 2Nb alloys outside the modulated structure solvus and as the modulated structure overages;

(iii) stacking fault precipitation of γ-NbN occurs in advance of the homogeneous precipitated layer at temperatures of 650 to 750°C in all $NH_3:H_2$ gas mixtures.

The above conditions of temperature and nitrogen

Fig. IV.1

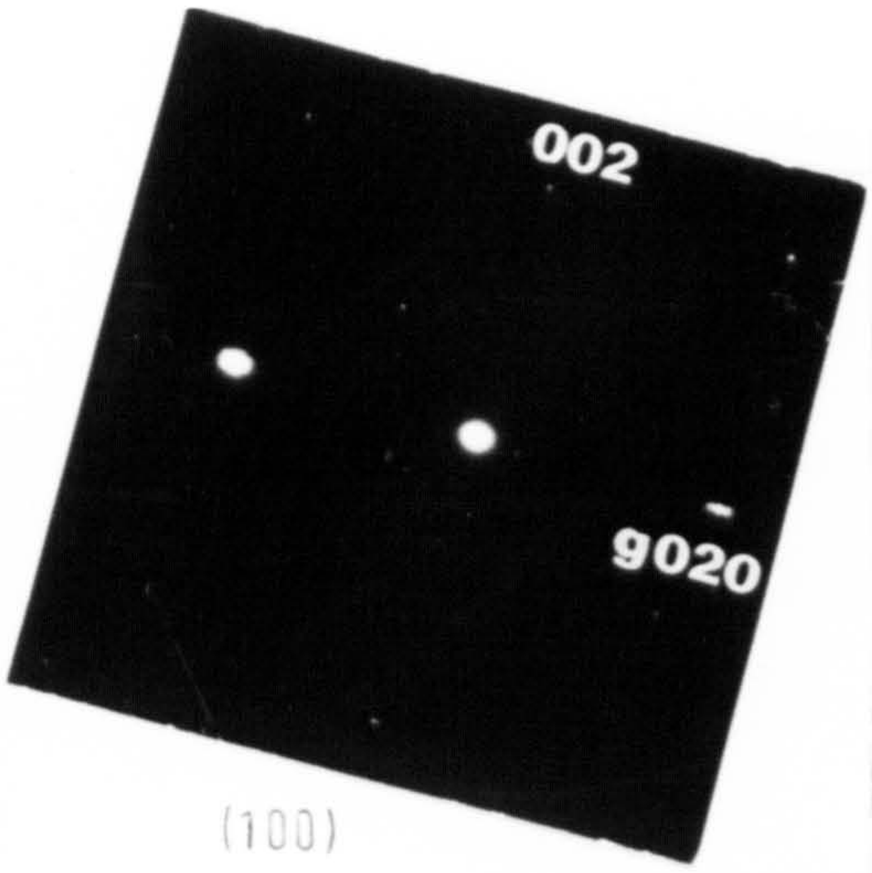

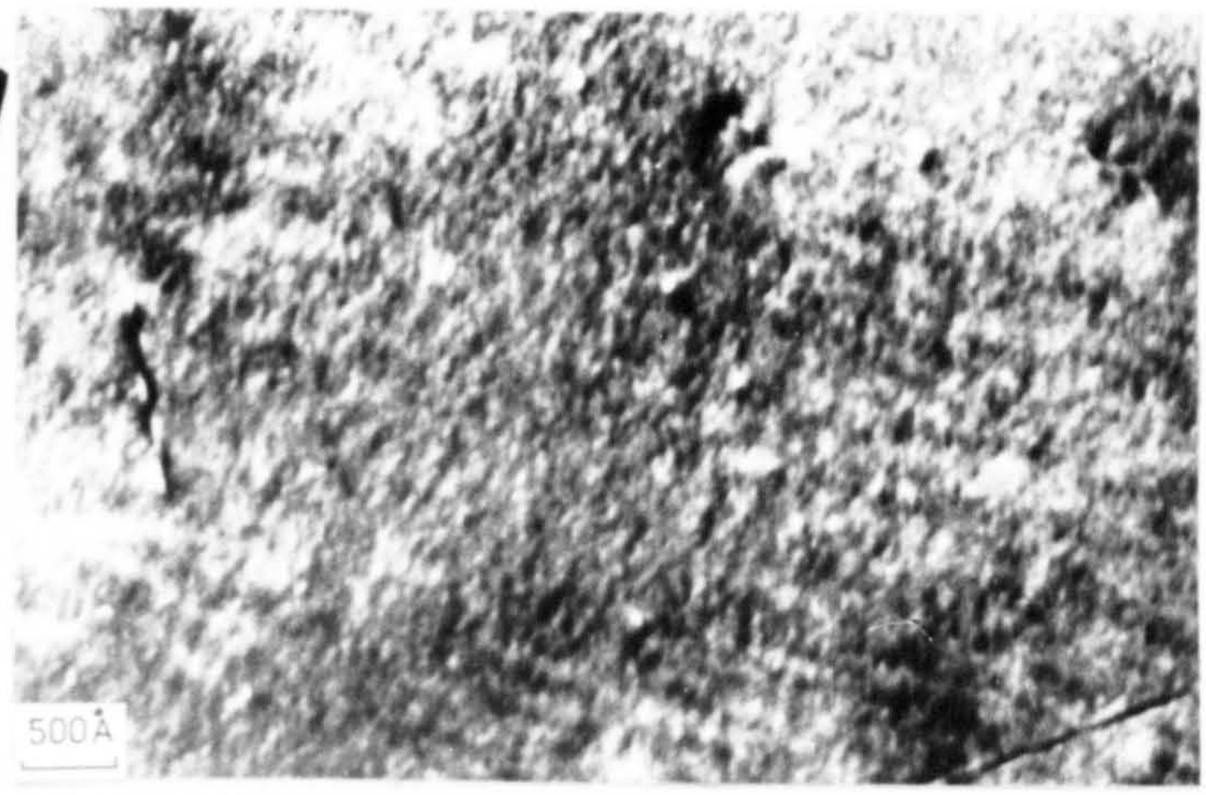

MODULATED STRUCTURE FORMED IN Fe:35Ni:2Nb

NITRIDED FOR 235hrs AT 550°C IN 21:79NH_3:H_2

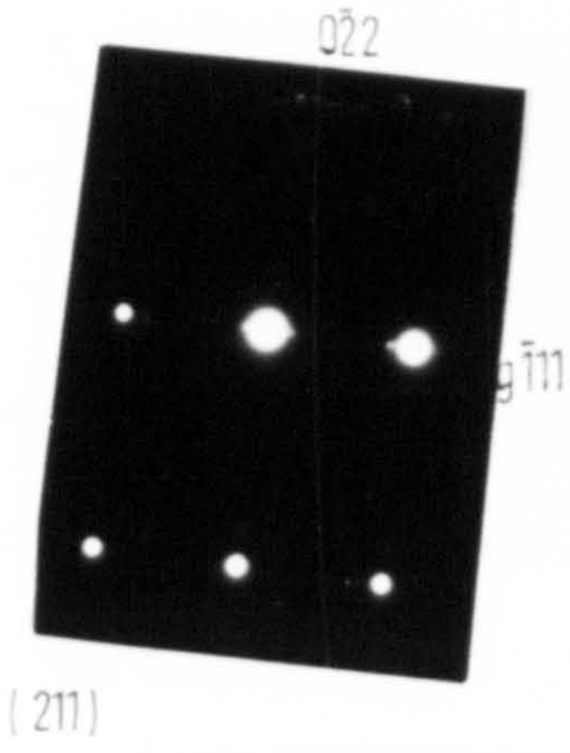

STACKING FAULT PRECIPITATION OF γNbN IN Fe:35Ni:0.5Nb

NITRIDED FOR 17hrs AT 700°C IN 2:98NH_3:H_2

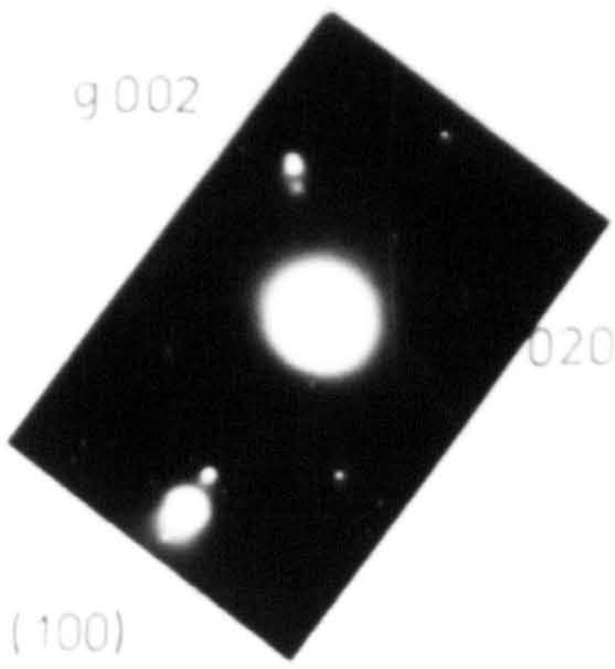

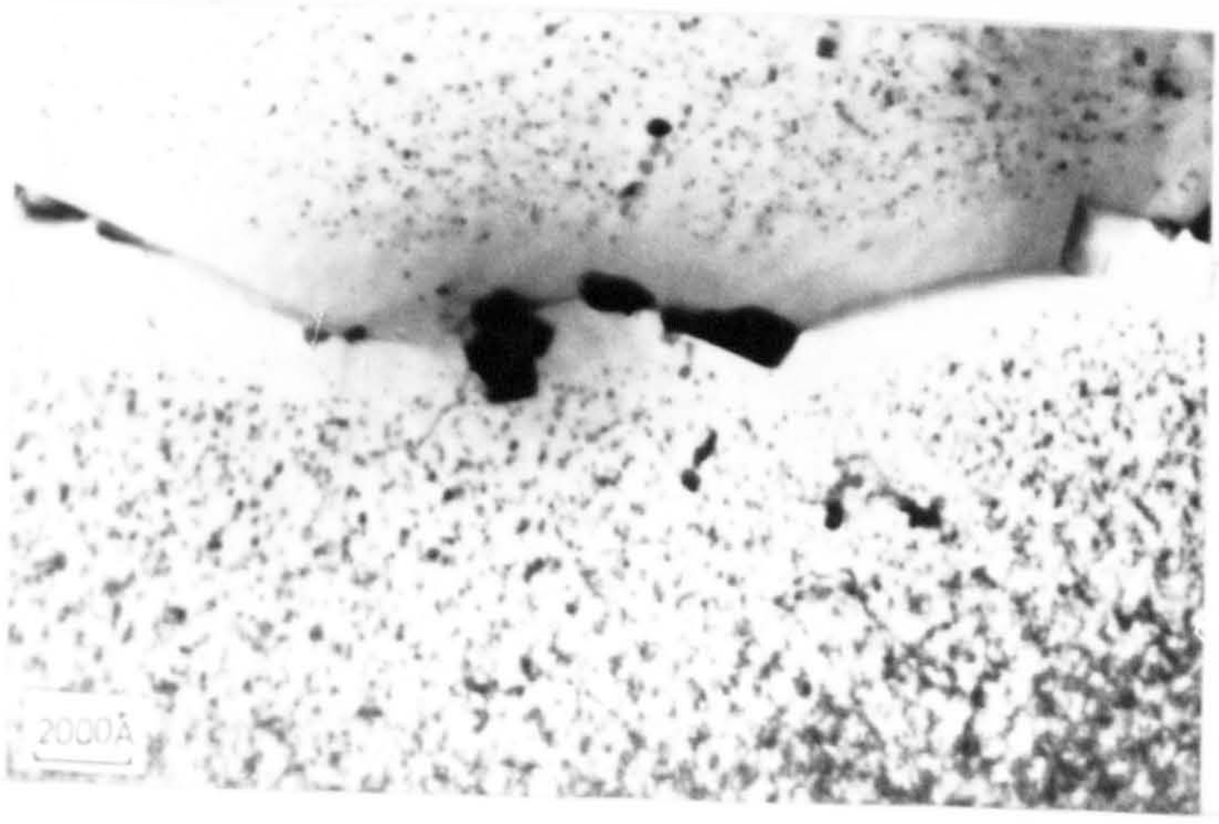

HOMOGENEOUS PRECIPITATION OF γNbN IN Fe:35Ni:0.5Nb

NITRIDED FOR 33hrs AT 800°C IN 1:99NH_3:H_2

ELECTRON MICOSTRUCTURES OF NITRIDED Fe:35Ni:Nb ALLOYS AT 550 - 800°C

potential are not known precisely because considerable overlap occurs between the occurrence of different structures in different specimens and in different regions of the same specimen.

IV.3.1 Modulated structures.

Thin foil electron microscopic examination of Fe:35Ni:1 and 2Nb alloys nitrided in $NH_3:H_2$ at 550 and 600°C revealed a fine wavy structure modulated in ⟨100⟩ matrix directions with a similar morphology to that observed by Butler and Thomas (1970) in the early stages of spinodal decomposition of Cu:Ni:Fe alloys (Figure IV.2 and IV.3). The modulation structure produced characteristic "side-band" reflections on both sides of each Bragg reflection in X-ray photographs (Figures IV.4 to IV.7) and diffuse satellite reflections in ⟨100⟩ directions about the matrix spots in electron diffraction patterns (Figure IV.8).

The modulation wavelength λ is determined from X-ray photographs and electron diffraction patterns by using the relationship derived by Daniel and Lipson (1943):

$$\lambda = \frac{h\ a\ \tan\ \theta}{(h^2 + k^2 + l^2)d\theta} \qquad \ldots\ \text{IV.1}$$

Fig. IV.2

(a) Fe:35Ni:2.0Nb

(b) Fe:35Ni:2.0Nb

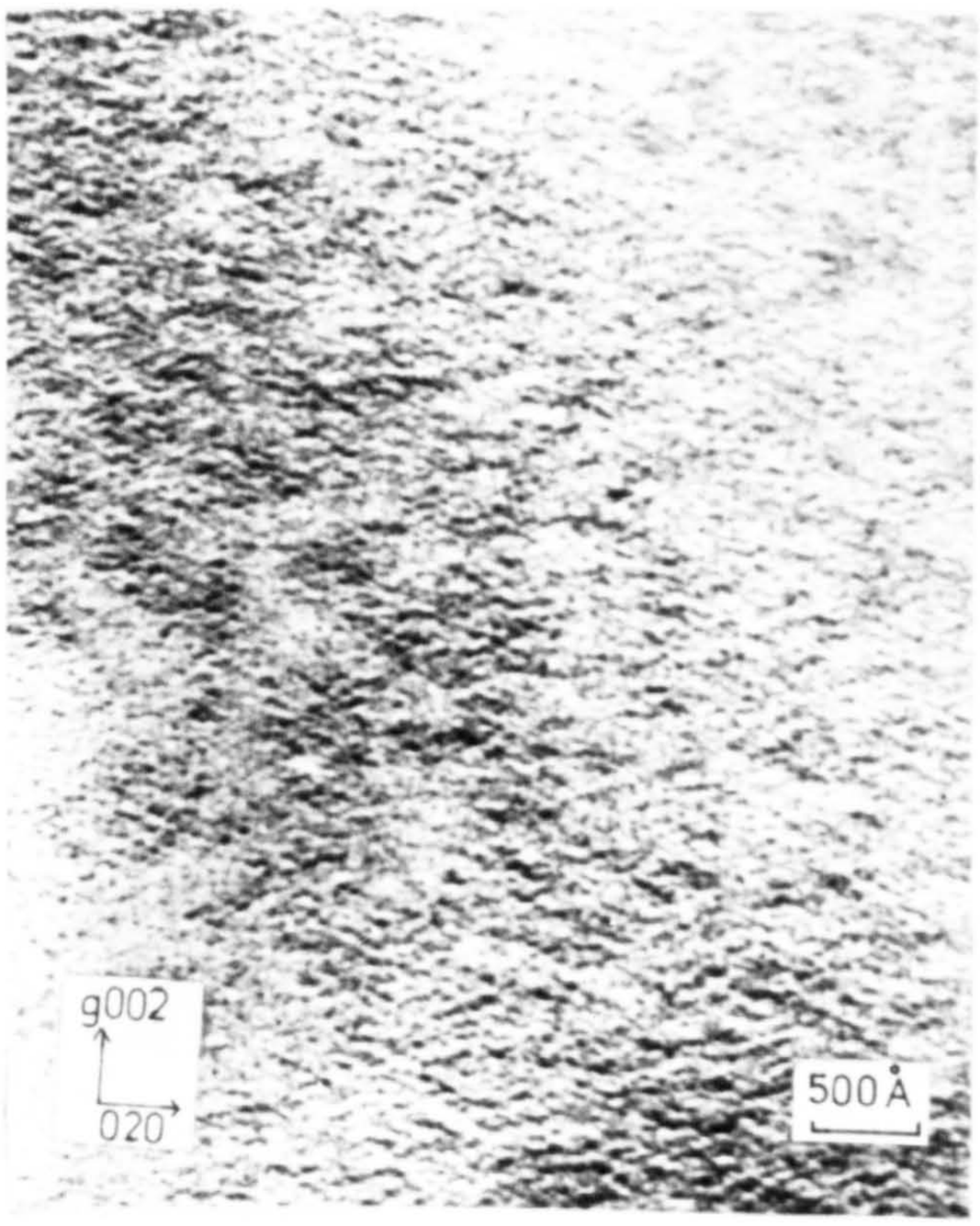

(c) Fe:35Ni:1.0Nb

(d) Fe:35Ni:0.5Nb

ELECTRON MICROGRAPHS OF Fe:35Ni:Nb NITRIDED AT 550°C IN 20NH_3:80H_2 FOR a 235hrs AND b, c, & d 333hrs

Fig. IV.3

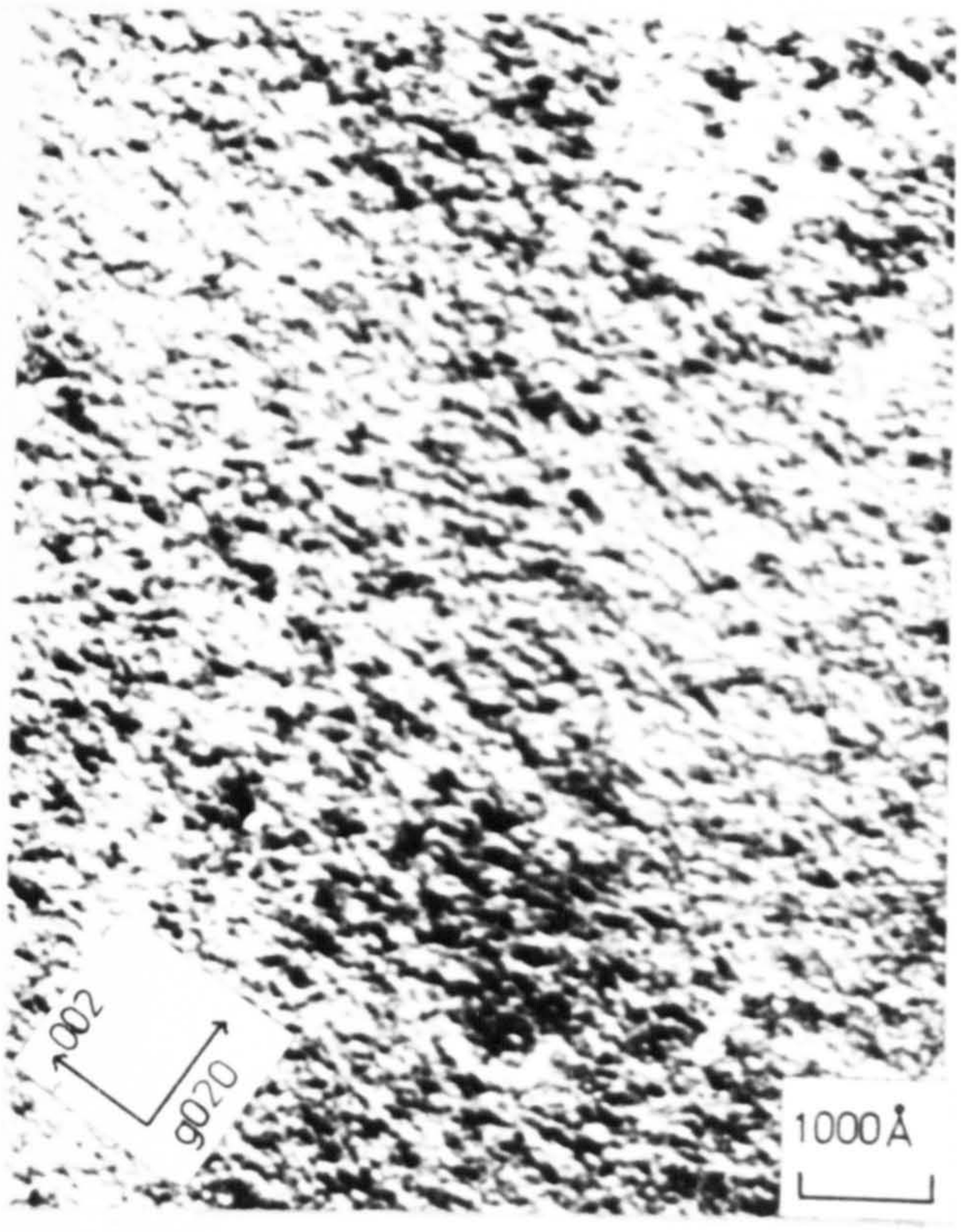

(a) 119 hrs in 5:95 $NH_3:H_2$

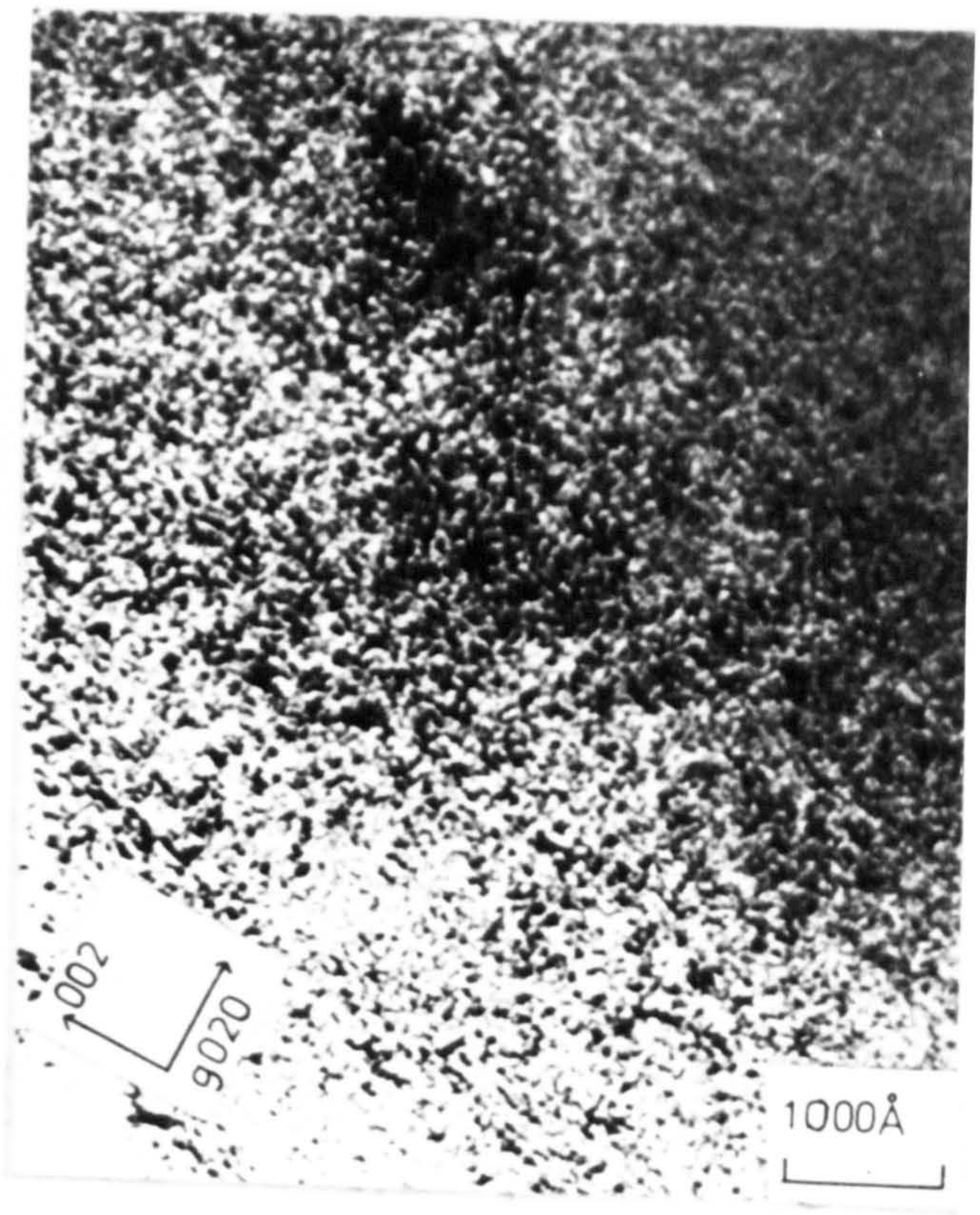

(b) 64.5 hrs in 10:90 $NH_3:H_2$

(c) 41 hrs in 15:85 $NH_3:H_2$

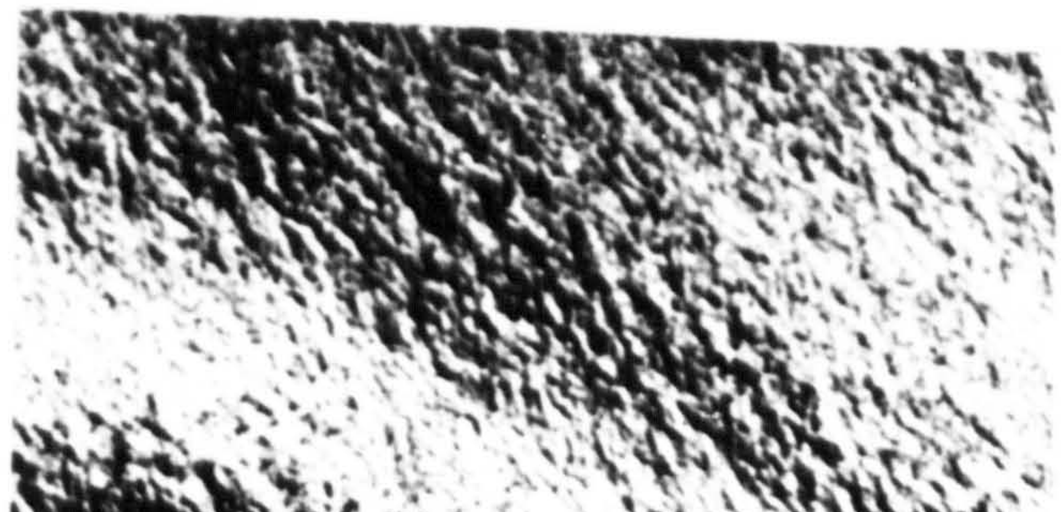

(d) 16.5 hrs 20:80 $NH_3:H_2$

ELECTRON MICROGRAPHS OF Fe:35Ni:2Nb NITRIDED IN VARIOUS $NH_3:H_2$ GAS MIXTURES AT 600°C

Fig. IV.4

118 hrs

IN 30:70NH_3:H_2 AT 500°C

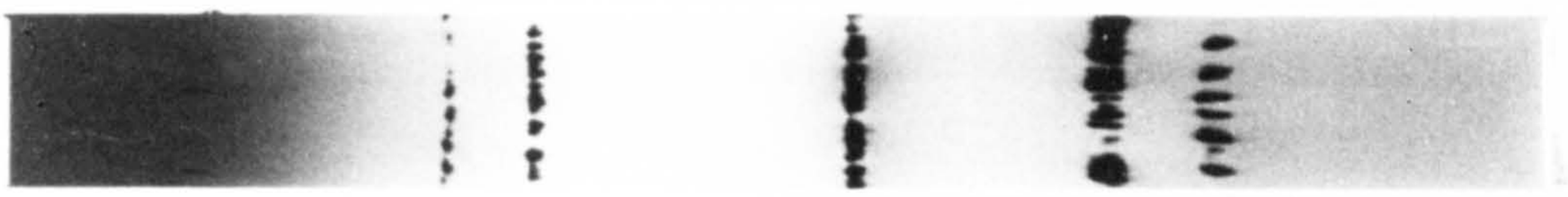

14 hrs

67.5 hrs

125 hrs

IN 21:79NH_3:H_2 AT 550°C

X-RAY PHOTOGRAPHS (FeKα) OF

NITRIDED Fe:35Ni:2Nb AT 500 & 550°C

Fig. IV.6

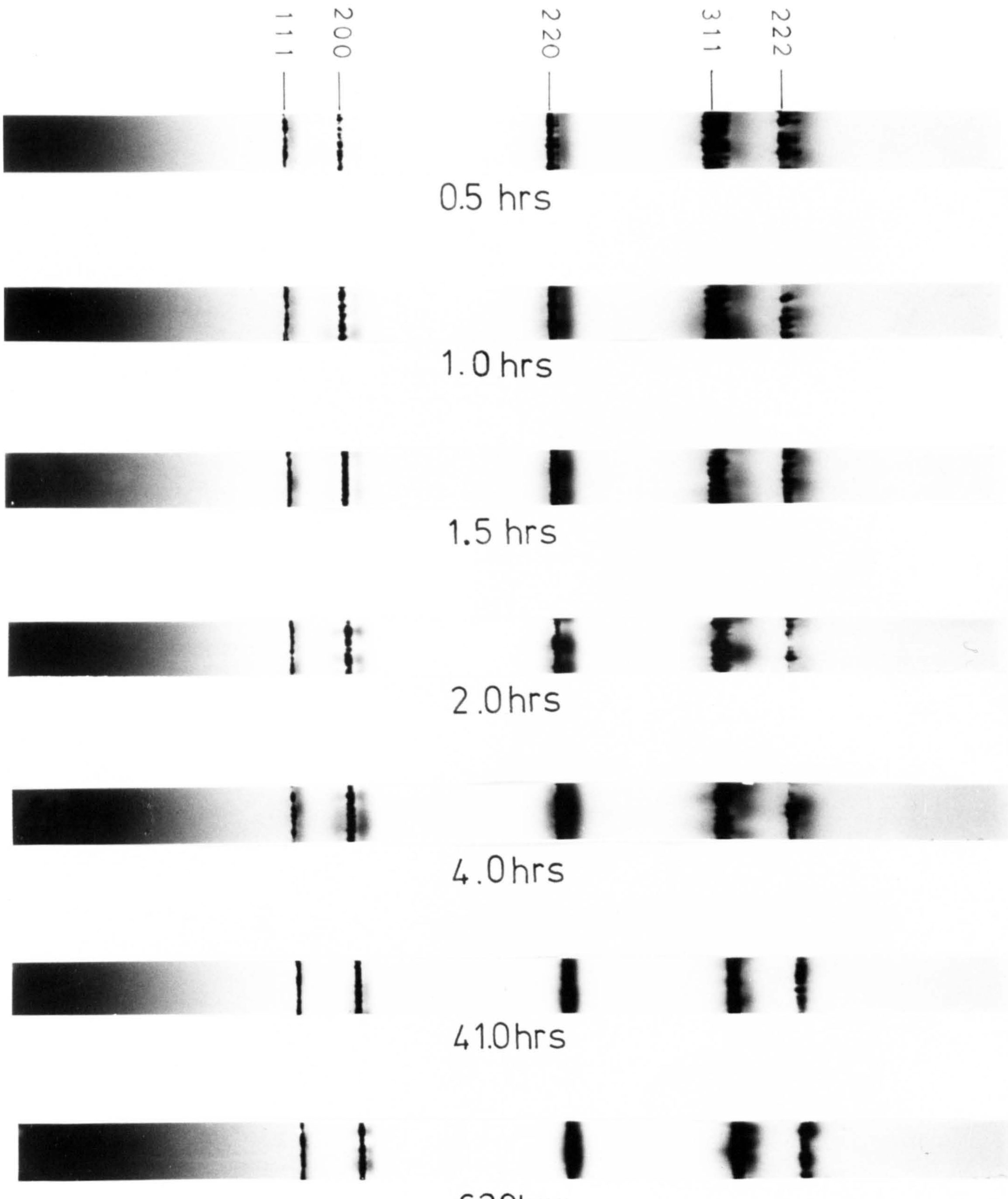

X-RAY PHOTOGRAPHS (Fe K α 2 days exp.) OF MODULATED Fe-35Ni-2Nb ALLOY NITRIDED IN 11:89 NH_3:H_2 AT 650°C

Fig. IV.7

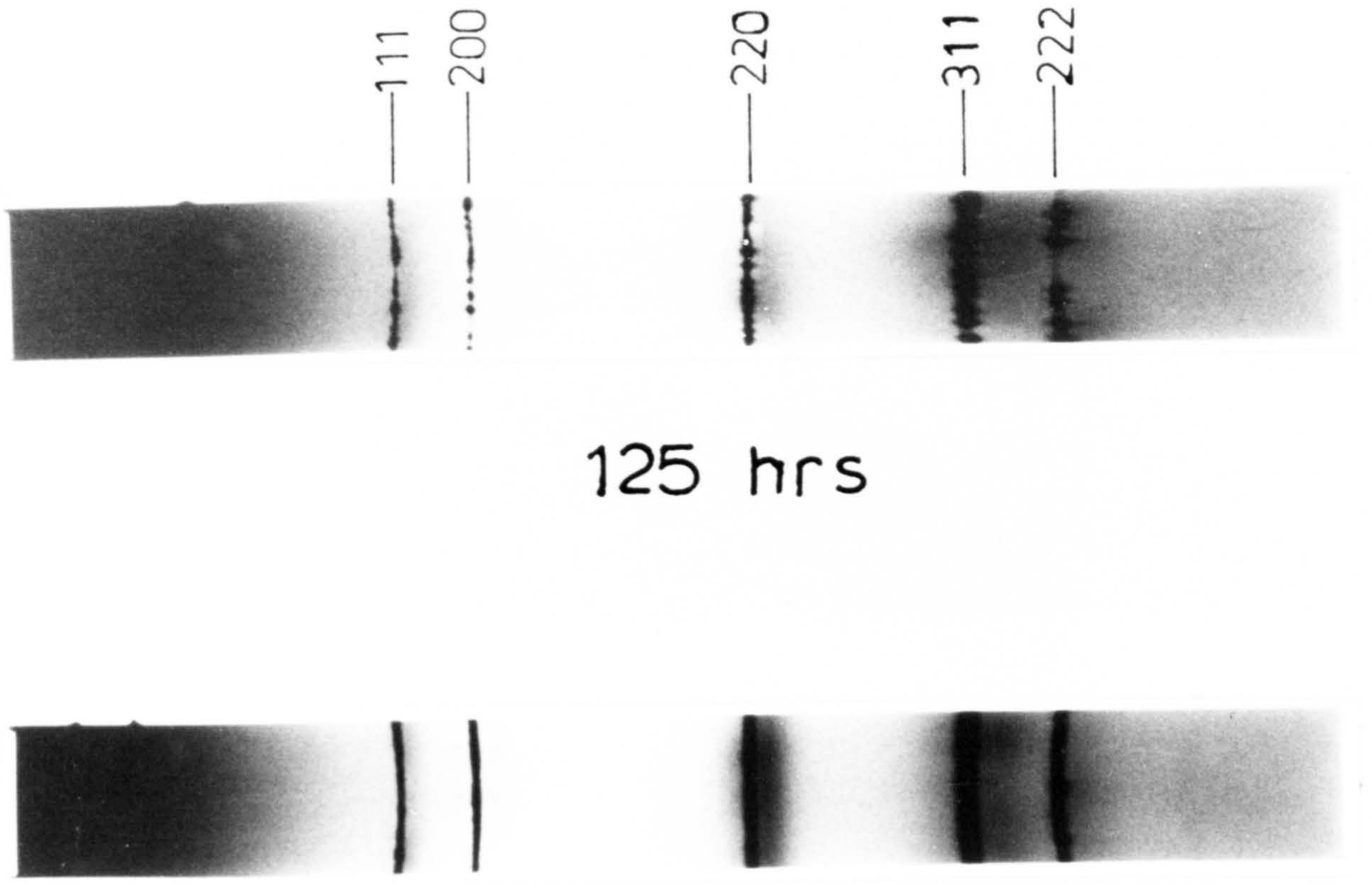

125 hrs

235 hrs

IN 21:79 $NH_3:H_2$ AT 550°C

6 hrs

IN 11:89 $NH_3:H_2$ AT 650°C

X-RAY PHOTOGRAPHS (Fe K α) OF

NITRIDED Fe:35Ni:1Nb AT 550 & 650°C

Fig. IV.8

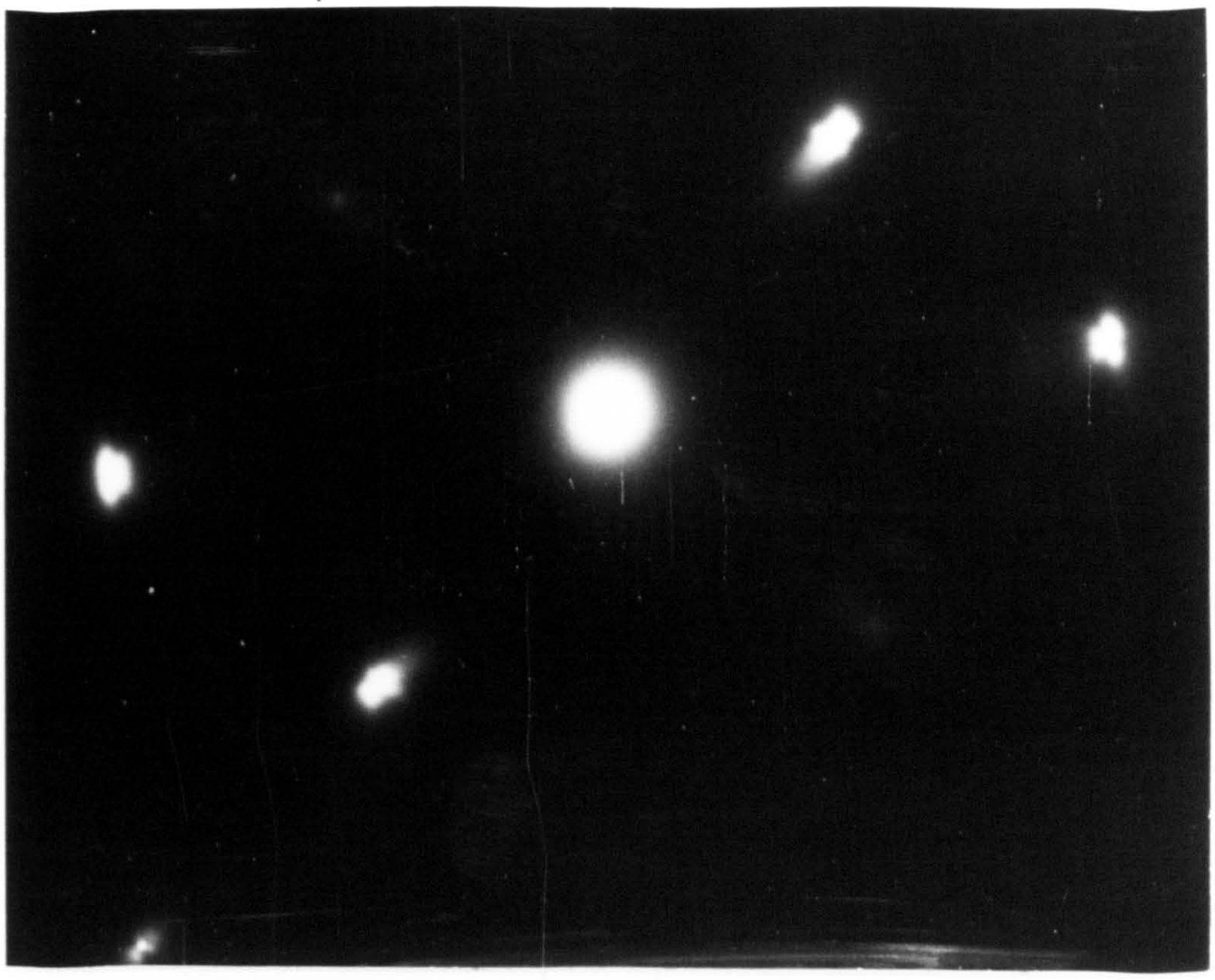

Fe:35Ni:2Nb nitrided for 92hrs 600°C in 15:85 NH_3:H_2

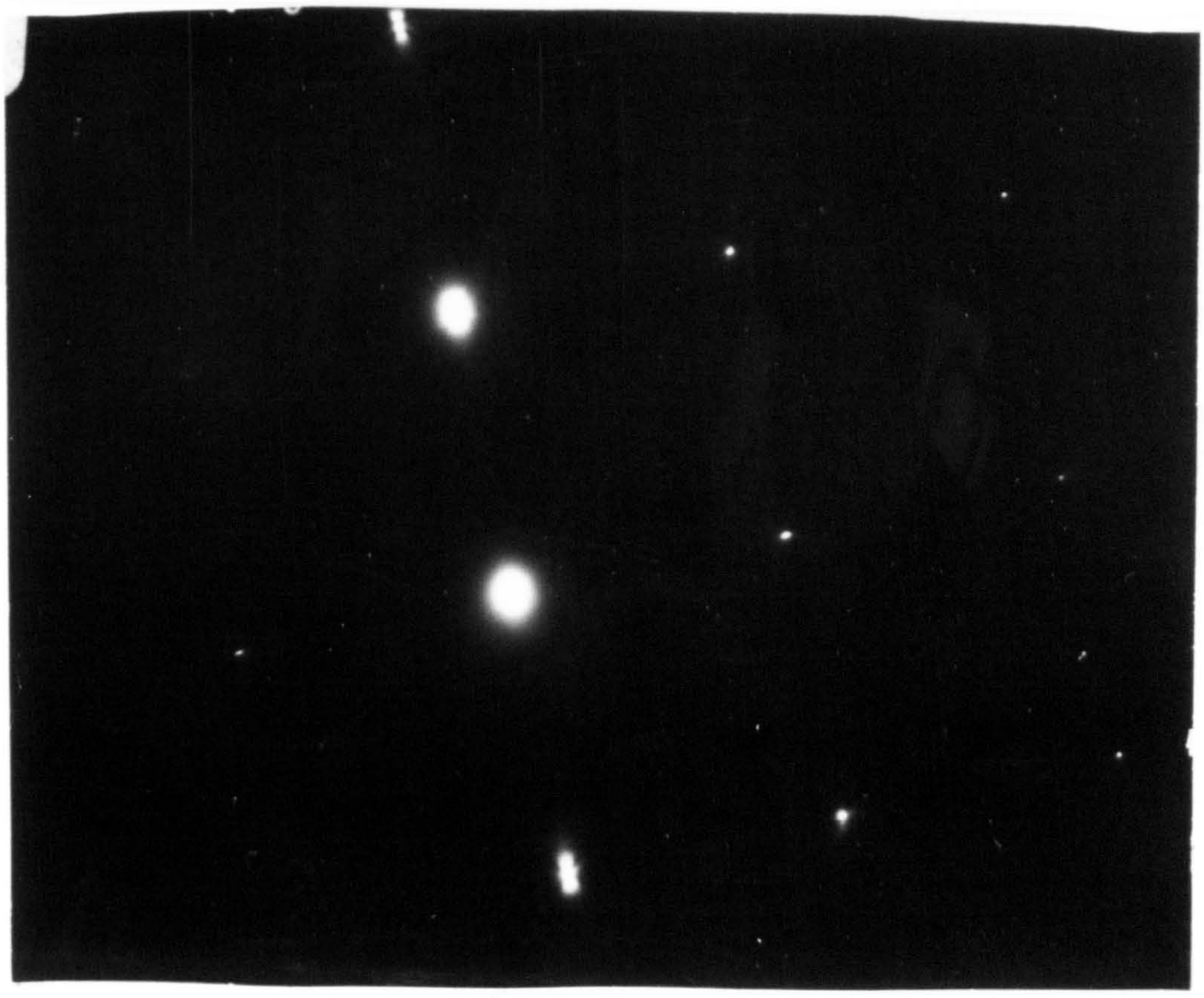

Fe:35Ni:1Nb nitrided for 333hrs 550°C in 30:70 NH_3:H_2

ELECTRON DIFFRACTION PATTERNS OF THE MODULATED STRUCTURE FORMED IN NITRIDED Fe:35Ni:Nb ALLOYS

where h is the highest order index of the diffracting hkl plane;

a is the unit-cell dimension

θ is the Bragg angle

$d\theta$ (in radians) is the separation from the main peak due to periodicity.

The mean modulation wavelength $\bar{\lambda}$ determined from side band spacing measurements and electron micrographs is found to increase with nitriding time, to decrease with increasing niobium concentration and appears to be independent of the nitriding potential (see Table IV.1). The coarsening rate of the mean modulation wavelength with nitriding time t can be described by a modification (Butler and Thomas, 1970) of the equation derived by Wagner (1961) for particle coarsening by a volume diffusion controlled mechanism where:

$$\bar{\lambda}^3 - \bar{\lambda}_o^3 = kt \qquad \ldots\ldots \text{IV.2}$$

where $\bar{\lambda}_o$ is the initial mean modulation wavelength at the onset of coarsening;

and k is the rate constant.

Plots of $\bar{\lambda}^3$ against t gave a linear relationship for Fe:35Ni:2Nb alloy nitrided in an equivalent constant nitrogen potential of 1.6×10^4 atmospheres at 550-750°C (Figures IV.9 and IV.10). The slopes of these plots

Table IV.1

Modulation wavelength of nitrided Fe:35Ni:1 and 2Nb alloys

Alloy	Time	$NH_3:H_2$	Temp.	$\bar{\lambda}$ in Å	a in Å	$\bar{\lambda}_o$ in Å
Fe:35Ni:2Nb	14h	21:89	550°C	33.55	3.6120	
	30h			36.22	3.6196	
	67.5h			40.63	3.6274	
	125h			43.12	3.6271	
	235h			46.52	3.6263	29.24
Fe:35Ni:1Nb	67.5h	21.89	550°C	38.23	3.6133	
	125h			48.65	3.6130	
	235h			52.20	3.6134	28.24
Fe:35Ni:2Nb	7h	5:95	600°C	47.95	3.6090	
	17h			51.13	3.6186	
	63.6h			60.68	3.6176	
	119h			65.11	3.6138	
	206h			67.56	3.6176	46.73
Fe:35Ni:1Nb	7h	5:95	600°C	51.25	3.6048	
	17h			56.77	3.6048	
	63.6h			61.38	3.6055	
	119h			63.28	3.6078	
	206h			71.38	3.6078	56.00
Fe:35Ni:2Nb	0.5h	10:90	600°C	37.69	3.6180	
	2h			39.90	3.6220	
	4h			40.60	3.6240	
	6.05h			43.40	3.6240	
	10.45h			52.60	3.6245	
	15h			54.75	3.6245	
	73h			71.09	3.6255	
	102h				3.6246	
	160h			78.87	3.6080	32.70

Alloy	Time	$NH_3:H_2$	Temp.	$\bar{\lambda}$ in Å	a in Å	$\bar{\lambda}_o$ in Å
Fe:35Ni:2Nb	2.1h	15:85	600°C	50.67	3.6250	
	13.5h			56.09	3.6248	
	41h			64.29	3.6160	
	92h			69.57	3.6176	
	133h			73.65	3.6118	46.73
Fe:35Ni:1Nb	2.1h	15:85	600°C	55.02	3.6048	
	13.5h			59.34	3.6152	
	27h			67.29	3.6142	
	41h			71.51	3.6109	
	92h			80.70	3.6122	
	133h			78.23	3.6133	49.32
Fe:35Ni:2Nb	5.5h	20:80	600°C	55.10	3.6206	
	16.5h			69.00	3.6192	
	24h			55.65	3.6282	
	96h			93.00	3.6205	
Fe:35Ni:2Nb	0.5h	11:99	650°C	54.07	3.6294	
	1.0h			62.68	3.6274	
	1.5h			69.10	3.6253	
	2h			74.58	3.6228	
	4h			73.28	3.6277	
	5h			95.04	3.6143	
	41h			105.98	3.6144	
	63h			103.39	3.6128	
	84h			131.71	3.6126	49.32
Fe:35Ni:1Nb	0.5h	11:89	650°C	55.05	3.6238	
	1.5h			71.88	3.6139	
	63h			113.85	3.6112	
Fe:35Ni:2Nb	7min	7:93	700°C	60.44	3.6282	
	15min			67.44	3.6262	
	30min			73.77	3.6213	
	45min			86.65	3.6258	

Alloy	Time	$NH_3:H_2$	Temp.	$\bar{\lambda}$ in Å	a in Å	$\bar{\lambda}_o$ in Å
Fe:35Ni:2Nb	61min	7:93	700°C	83.38	3.6254	
	120min			85.57	3.6207	
	421min			116.06	3.6123	
	96h			116.37	3.6095	54.83
Fe:35Ni:2Nb	3min	3.75:96.25	750°C	64.09	3.6258	
	4.3min			72.09	3.6236	
	5.7min			75.83	3.6236	
	7min			89.09	3.6222	
	2h			108.61	3.6044	
	15h			114.24	3.6061	

Fig. IV.9

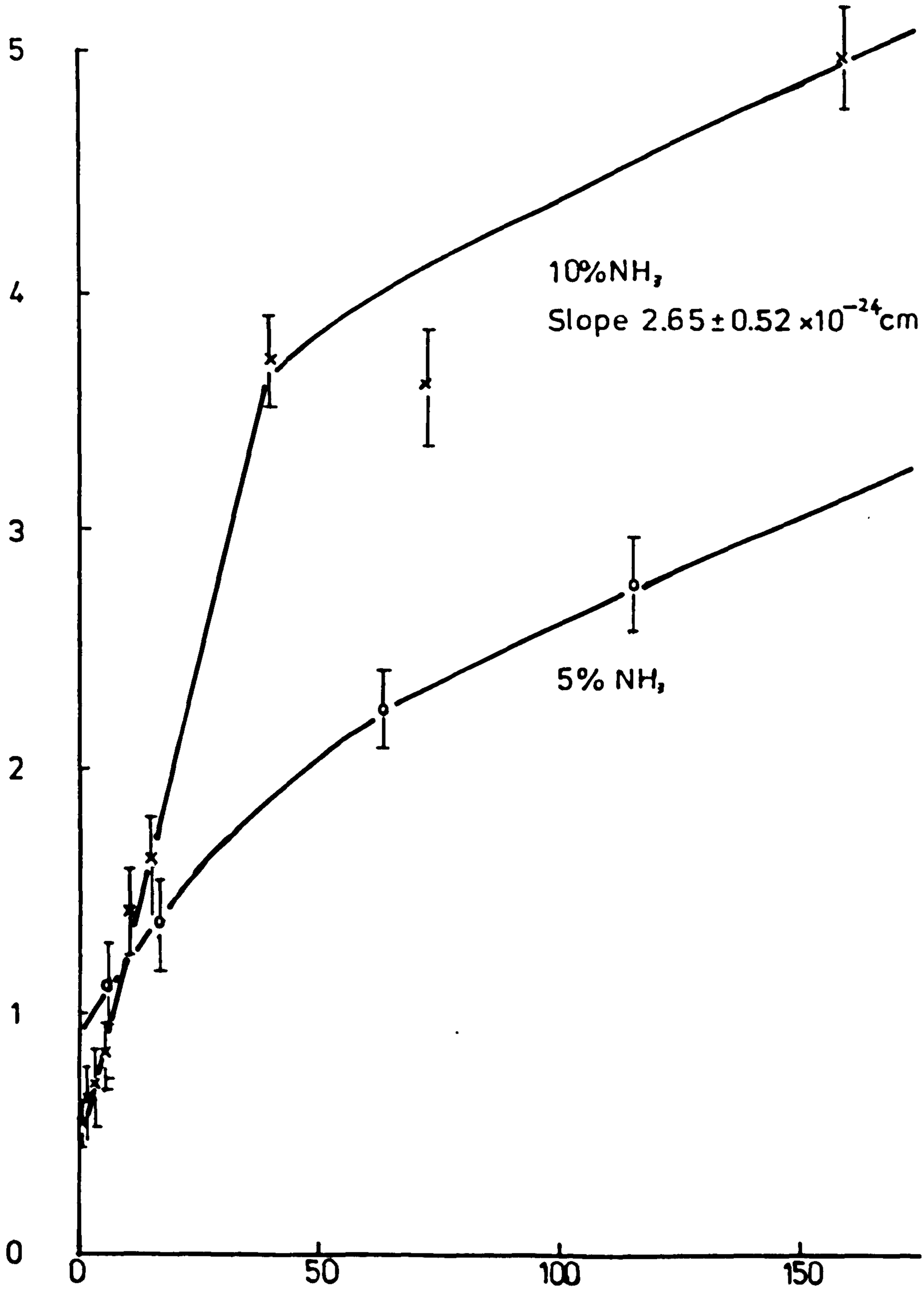

VARIATION IN MEAN MODULATION WAVELENGTH CUBED $\bar{\lambda}^3$ OF Fe:35Ni:2Nb NITRIDED IN 5:95 &10:90 NH_3:H_2 AT 600°C

Fig. IV. 10

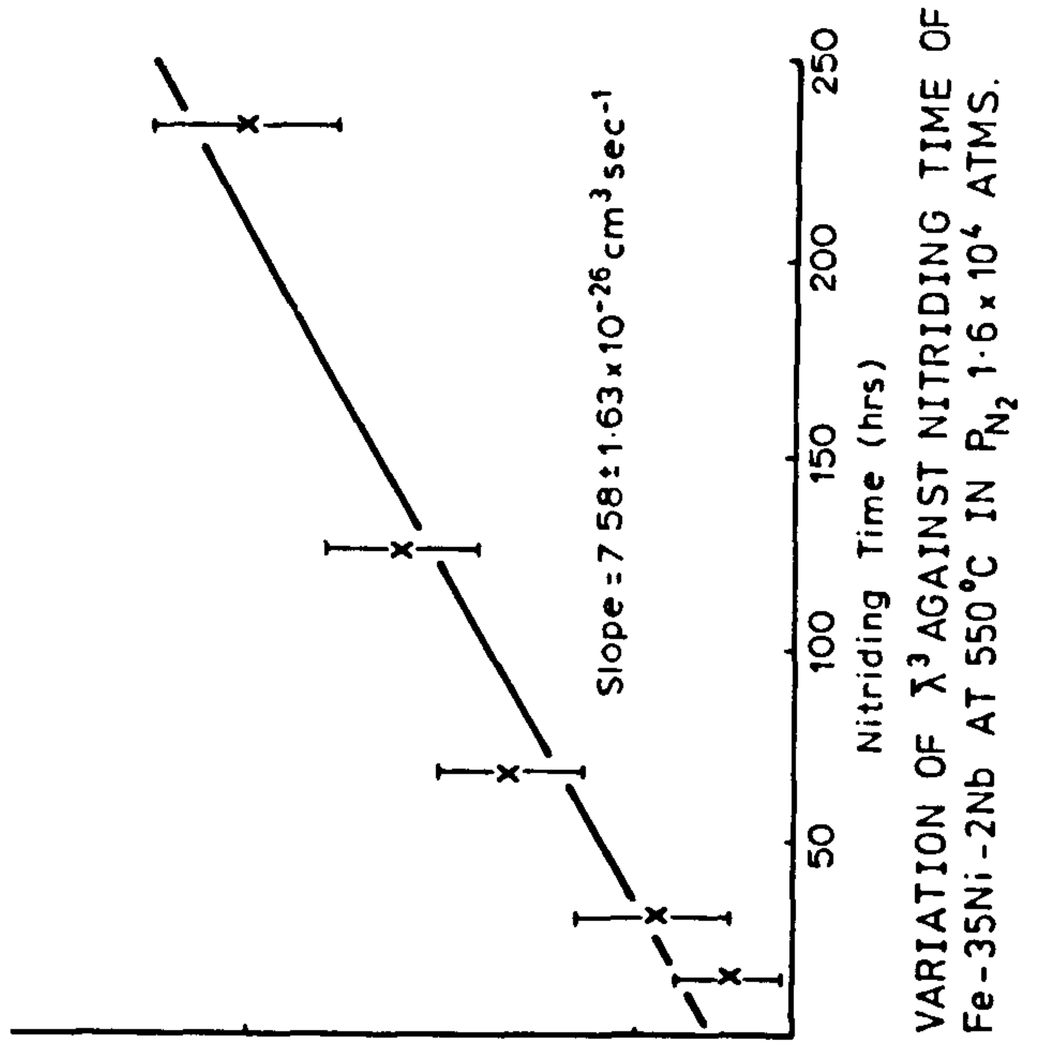

VARIATION OF λ^3 AGAINST NITRIDING TIME OF Fe-35Ni-2Nb AT 550 °C IN P_{N_2} 1·6 × 10^4 ATMS.

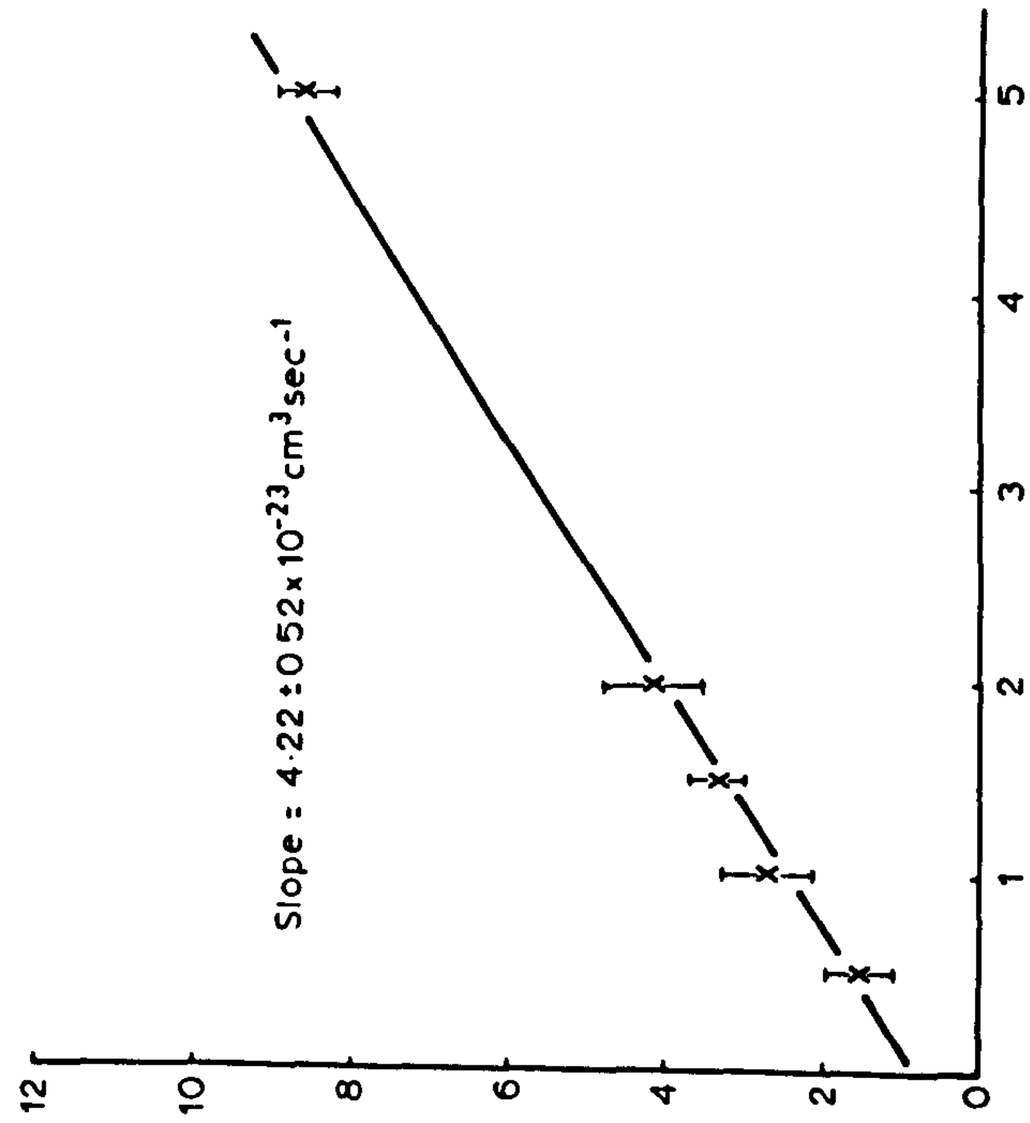

VARIATION OF λ^3 AGAINST NITRIDING TIME OF Fe-35Ni-2Nb AT 650 °C IN P_{N_2} 1·6 × 10^4 ATMS.

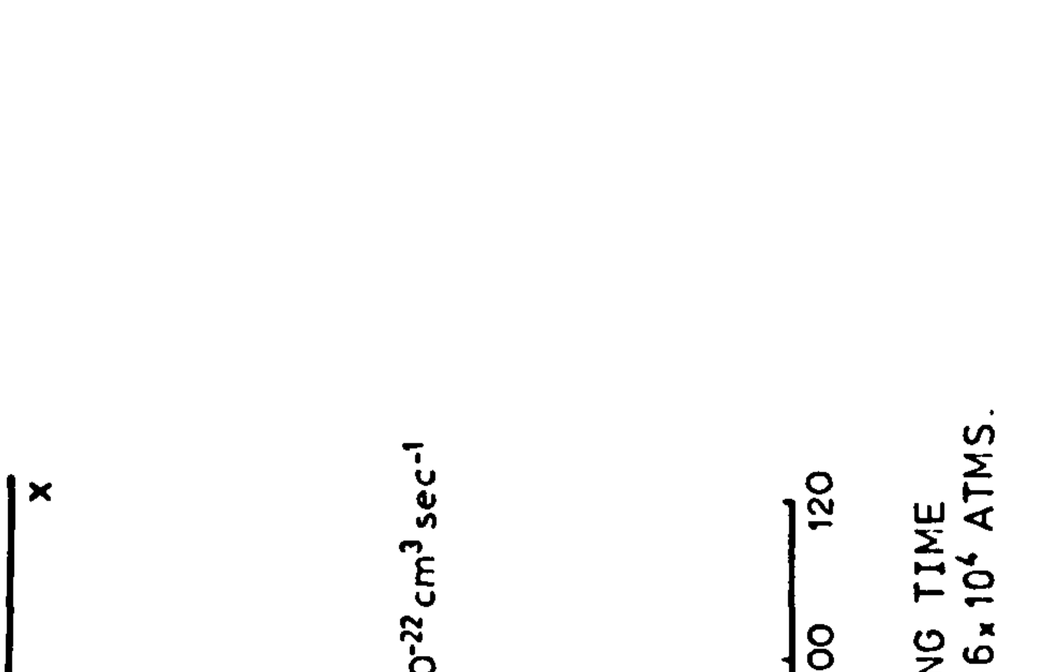

VARIATION OF λ^3 AGAINST NITRIDING TIME OF Fe-35Ni-2Nb AT 700 °C IN P_{N_2} 1·6 × 10^4 ATMS.

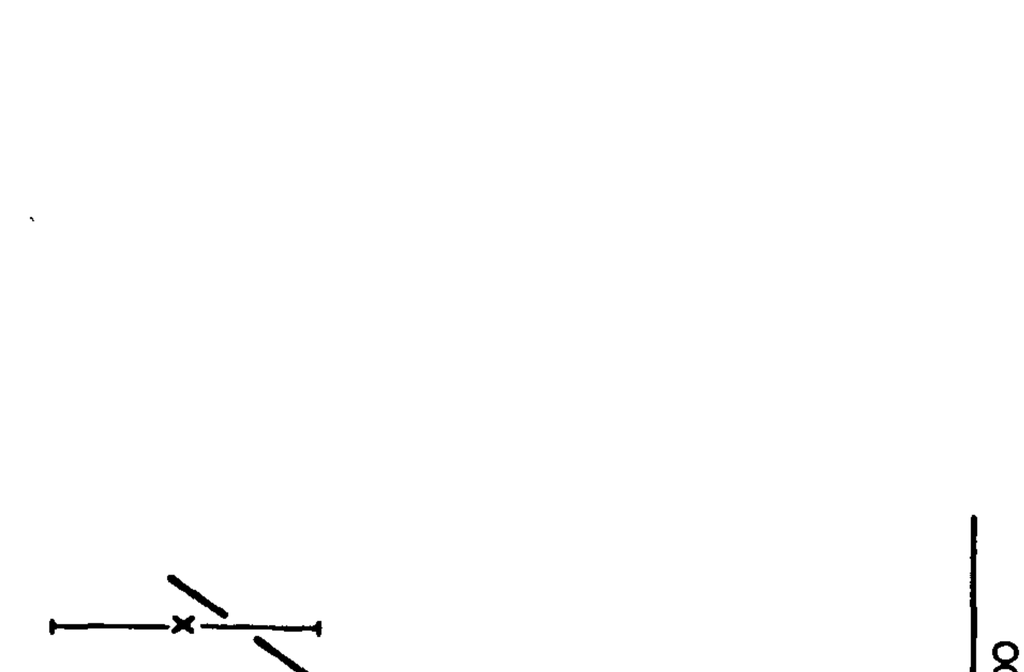

VARIATION OF λ^3 AGAINST NITRIDING TIME OF Fe-35Ni-2Nb AT 750 °C IN P_{N_2} 1·6 × 10^4 ATMS.

were calculated by a linear regression analysis and the errors quoted are the mean deviation. A further plot of log k against the reciprocal of the nitriding temperature, 1/T (see Figure IV.11a) gives an activation energy for modulation coarsening of 340 ± 23 kJmol^{-1} (81.3 ± 0.5 Kcal mol^{-1}) which is in good agreement with the value obtained by Sparke, James and Leak (1965) of 344 ± 21 kJ mol^{-1} (82.3 ± 0.5 Kcal mol^{-1}) for Nb diffusion in austenitic Fe-Nb alloys. Cahn (1968) has also shown that a plot of the nitriding temperature T against $1/\lambda_o^2$ (the initial modulation wavelength) should be linear and the intercept on the temperature axis is the coherent spinodal temperature above which the modulated structure is not formed. A plot of T against $1/\bar{\lambda}_o^2$ as shown in Figure IV.11b for Fe:35Ni:2Nb alloy nitrided in p_{N_2} of 1.6×10^4 atmospheres is linear and gives a modulation solvus temperature of 746 ± 14^{o}C.

Daniel and Lipson (1943) predicted that the number of side bands in reciprocal space for a periodic lattice parameter variation depends upon the non zero integers of the diffracting (hkl) plane. Hence for the (200) reflections the diffraction pattern will show two side bands, and for the (220) reflections four side bands as shown in Figure IV.8. The side band intensities of the modulated structure formed in Fe:35Ni:1 and 2Nb alloys

Fig. IV.11

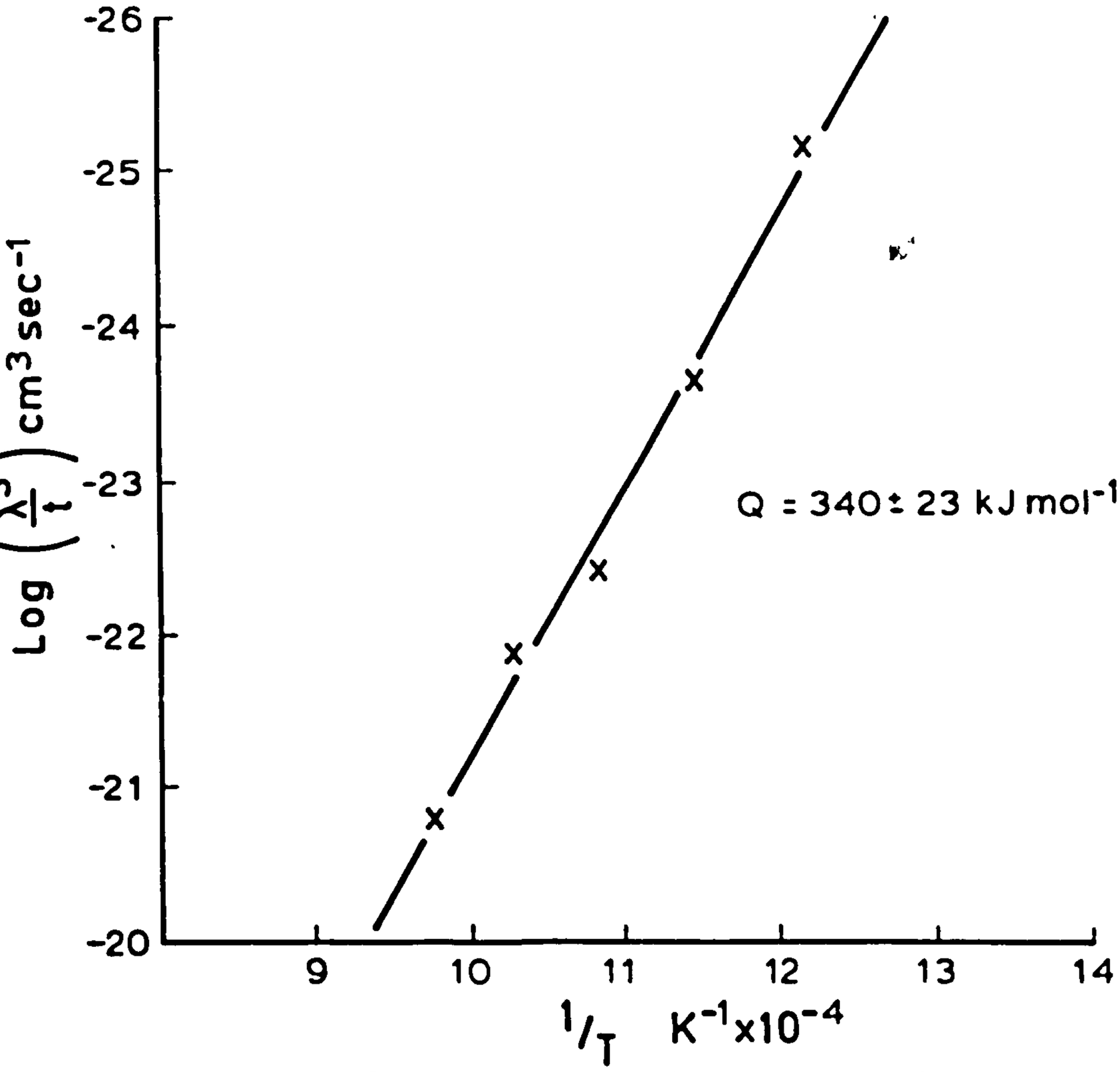

ARRHENIUS PLOT OF LOG k vs 1/T FOR THE COARSENING OF MODULATED STRUCTURES IN NITRIDED Fe-35Ni-2Nb

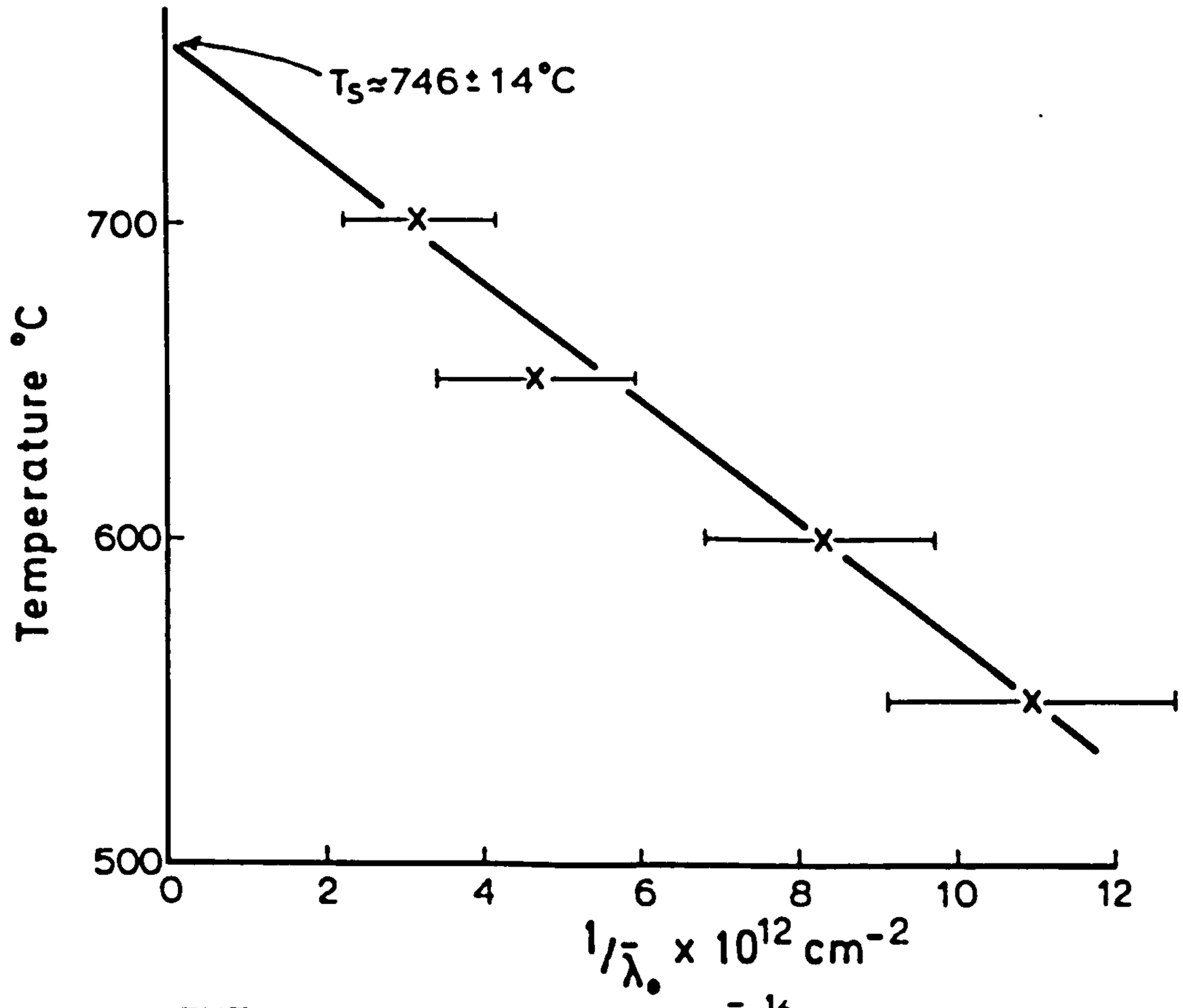

THE INITIAL WAVELENGTH $\bar{\lambda}_\bullet^{-1/2}$ vs TEMPERATURE FOR Fe-35Ni-2Nb ALLOYS NITRIDED AT $P_{N_2} \approx$ 1·6 x 10^4 atm.

during nitriding at 500-750°C are asymmetric (see X-ray photographs Figures IV.4 to IV.7) with an approximate ratio of 1:2.5 for the low angle to the high angle side-band intensity. The side-band intensity of the modulated structure of Fe:35Ni:2Nb nitrided in 11:89 NH_3:H_2 also increases with nitriding time as shown by X-ray photographs (Figure IV.6) and intensity measurements were made from the X-ray photographs (by a Joyce-Loeble microdensitometer adjusted for a constant background intensity and sensitivity); see Figure IV.12.

The unit cell dimension of the modulated structure formed in Fe:35Ni:Nb alloys is found to be equivalent to a solid solution of niobium and nitrogen in Fe:35Ni (Table IV.2) given by:

$$a_m = a + a_N wt\%N + a_{Nb} wt\%Nb \quad \ldots\ldots \text{IV.3}$$

where a is the lattice parameter of Fe:35Ni (3.5919 ± 0.0005 Å)

and a_N and a_{Nb} are the increases in the unit-cell dimension of Fe:35Ni produced by one wt% of nitrogen and niobium in solution respectively. Values of a_N and a_{Nb} can be determined from plot of the unit-cell dimension of Fe:35Ni:N and Fe:35Ni:Nb alloys against the nitrogen and niobium contents (Figure IV.13a)

Fig. IV.12

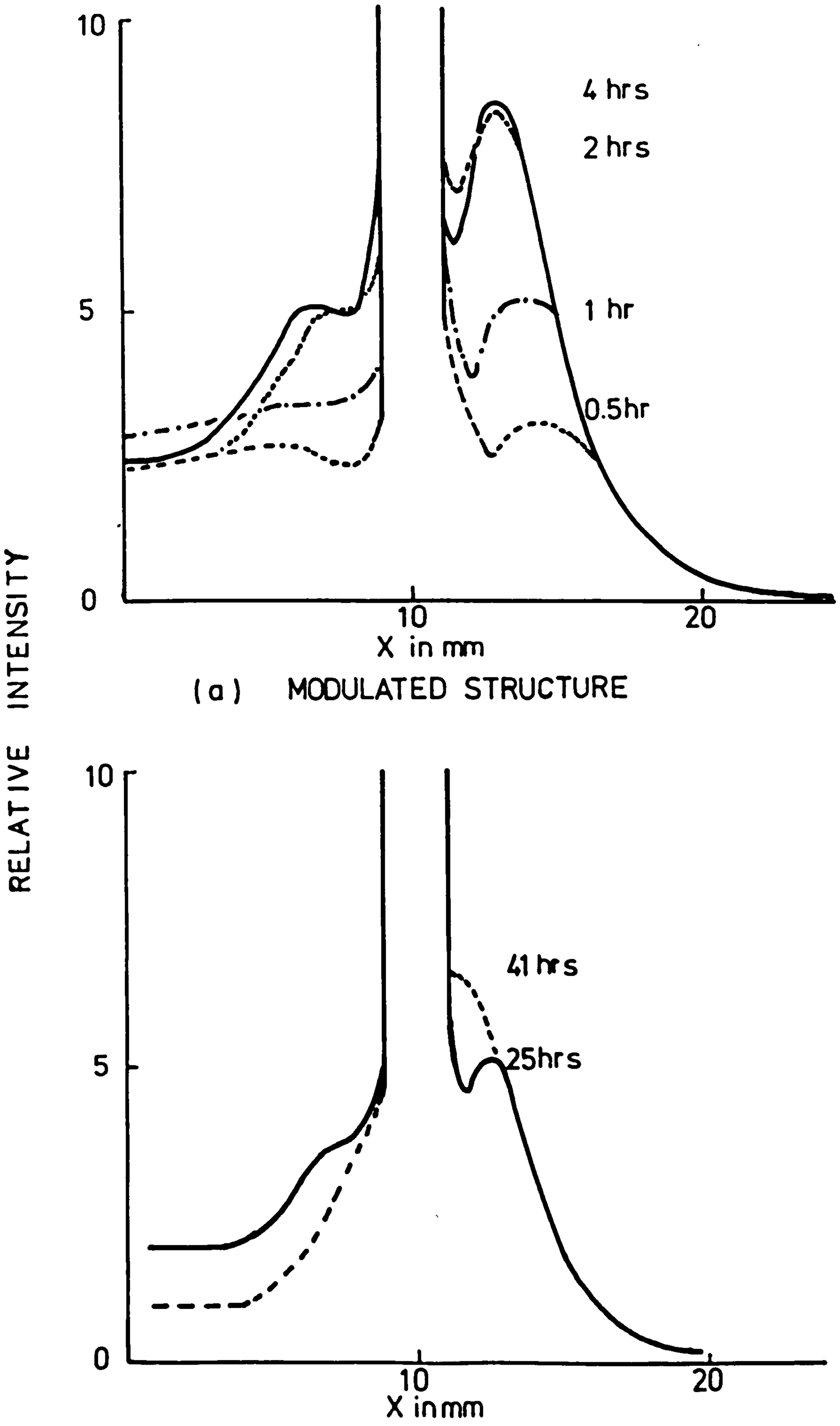

MICRODENSITOMETER TRACES OF {200} REFLECTIONS FROM X-RAY PHOTOGRAPHS OF NITRIDED Fe:35Ni:2Nb AT 650°C IN 11:89 NH_3:H_2 USING A JOYCE LOBEL MICRODENSITOMETER (constant background and sensitity)

Table IV.2

The lattice parameter of the modulated structure at 550-750°C

Alloy	$NH_3:H_2$	Temp.	$\bar{\lambda}_o$	wt%N	a in Å	a calc in Å
Fe:35Ni:2Nb	21:89	550°C	29.24	0.815	3.6274	3.6269
	5:95	600°C		0.502	3.6176	3.6154
	10:90	600°C	32.70	0.787	3.6255	3.6259
	11:99	650°C	49.32	0.903	3.6282	3.6310
	7:93	700°C	54.05	0.689	3.6254	3.6223
	3.75:96.25	750°C		0.747	3.6234	3.6244
Fe:35Ni:1Nb	21:89	550°C		0.650	3.6152	3.6180
	5:95	600°C		0.459	3.6078	3.6109
	10:90	600°C		0.570	3.6134	3.6150
Fe:35Ni:½Nb	10:90	600°C		0.480	3.6070	3.6106

Overaged modulated structure

Fe:35Ni:2Nb	10:90	600°C		0.787	3.6080	3.6090
	11:89	650°C		0.833	3.6126	3.6118
	7:93	700°C		0.689	3.6095	3.6062
	3.75:96.25	750°C		0.747	3.6052	3.6083

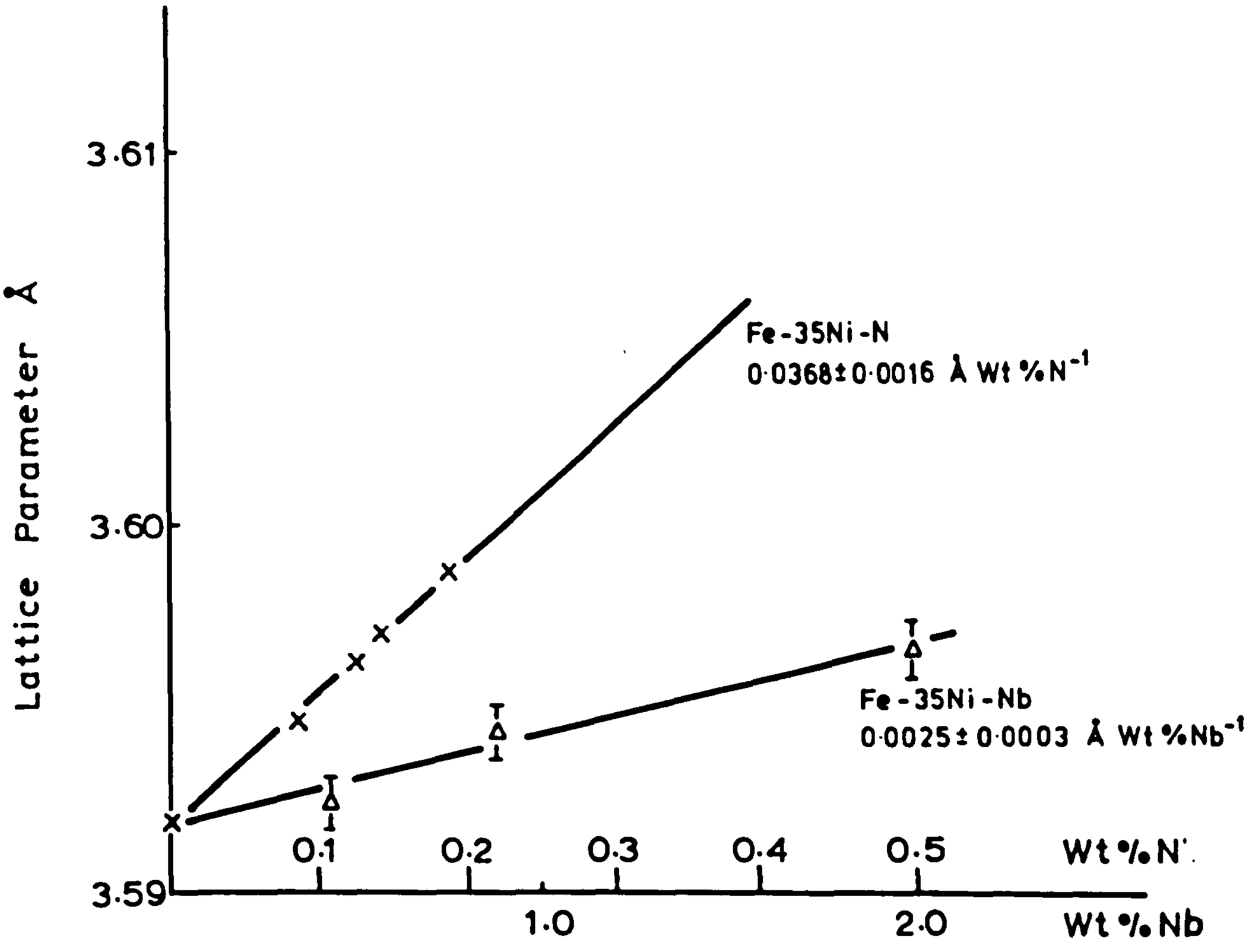

VARIATION OF LATTICE PARAMETER OF Fe-35Ni-Nb & N ALLOYS.

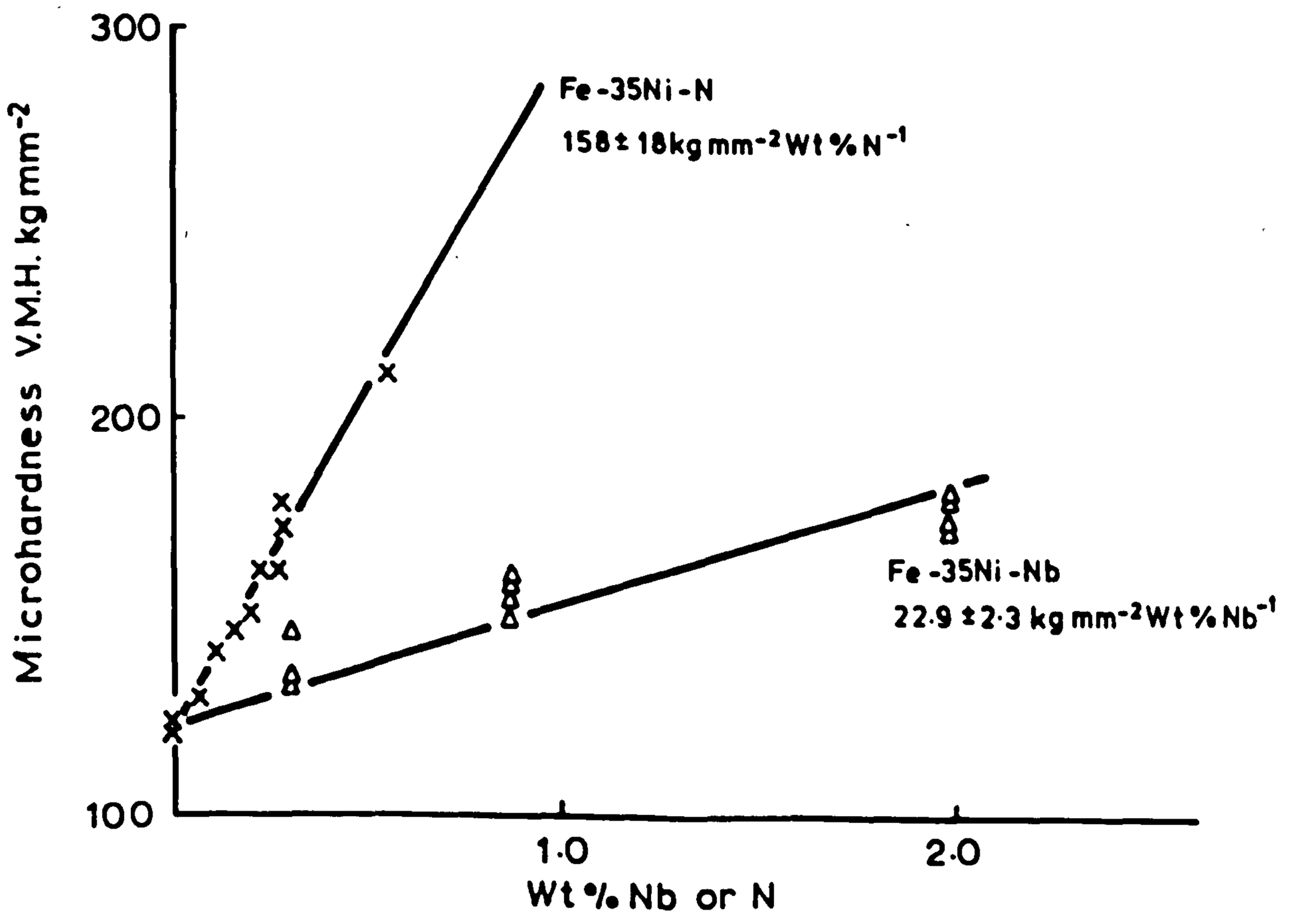

VARIATION OF MICROHARDNESS WITH SOLUTE CONCENTRATION OF Fe-35Ni-Nb & N ALLOYS.

respectively and are found to be:

$$a_N = 0.0368 \pm 0.0016 \text{ Å/wt\%N} \quad \ldots\ldots \text{IV.4}$$

$$a_{Nb} = 0.0025 \pm 0.0003 \text{ Å/wt\%Nb} \quad \ldots\ldots \text{IV.5}$$

The value of a_N of 0.0368 Å is slightly larger than that found by Jack (1951) for nitrogen in austenitic Fe-N alloys of 0.0334 ± 0.0034 Å. The value of a_{Nb} of 0.0025 is similar to that found for niobium in solution in austenitic Fe:30Ni:Nb alloys by Leith and Chaturvedi (1971). The variation of lattice parameter of Fe:35Ni:2Nb alloy with nitriding time in 10:90 NH_3:H_2 at 600°C is given by Figure IV.14a and shows an initial increase which is due to the increase of nitrogen concentration in the X-rayed layer. The lattice parameter remains constant during coarsening of the modulated structure and decreases as the modulated structure overages to form a fine dispersion of γ-NbN. The variation of microhardness with nitriding time for Fe:35Ni:2Nb in 10NH_3:90H_2 at 600°C is shown in Figure IV.14b. The increase in the microhardness is $\approx$ 100kg mm^{-2} in excess of that due to solid solution hardening by nitrogen and niobium contents in Fe:35Ni:2Nb nitrided at 600°C (that predicted from a plot of hardness against the nitrogen and niobium concentration in Fe:35Ni as shown in Figure IV.13b) and is an indication of the considerable

Fig. IV.14

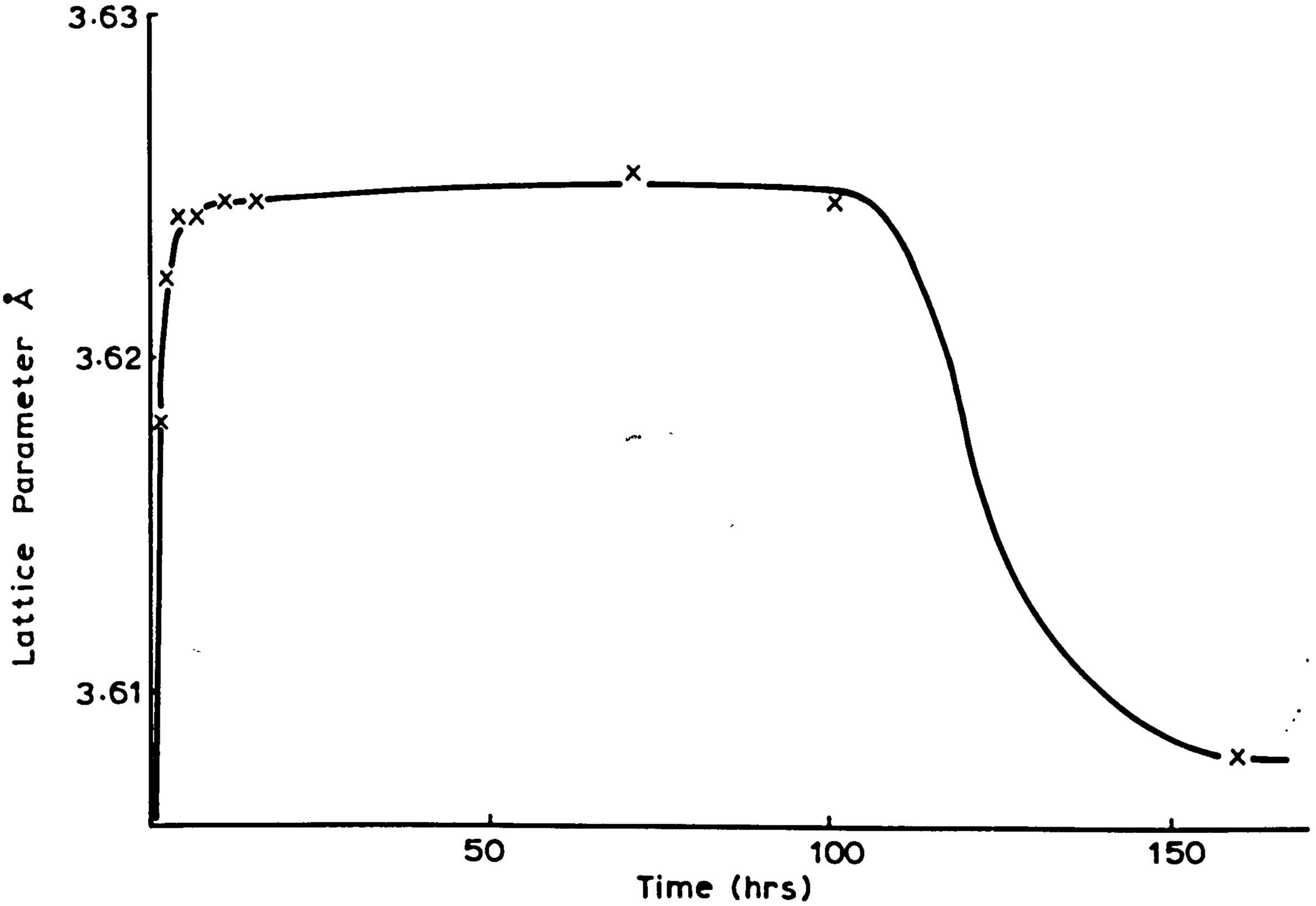

VARIATION OF LATTICE PARAMETER OF Fe-35Ni-2Nb ALLOY WITH NITRIDING TIME IN $10NH_3:90H_2$ AT 600 °C (Wt%N 0·76).

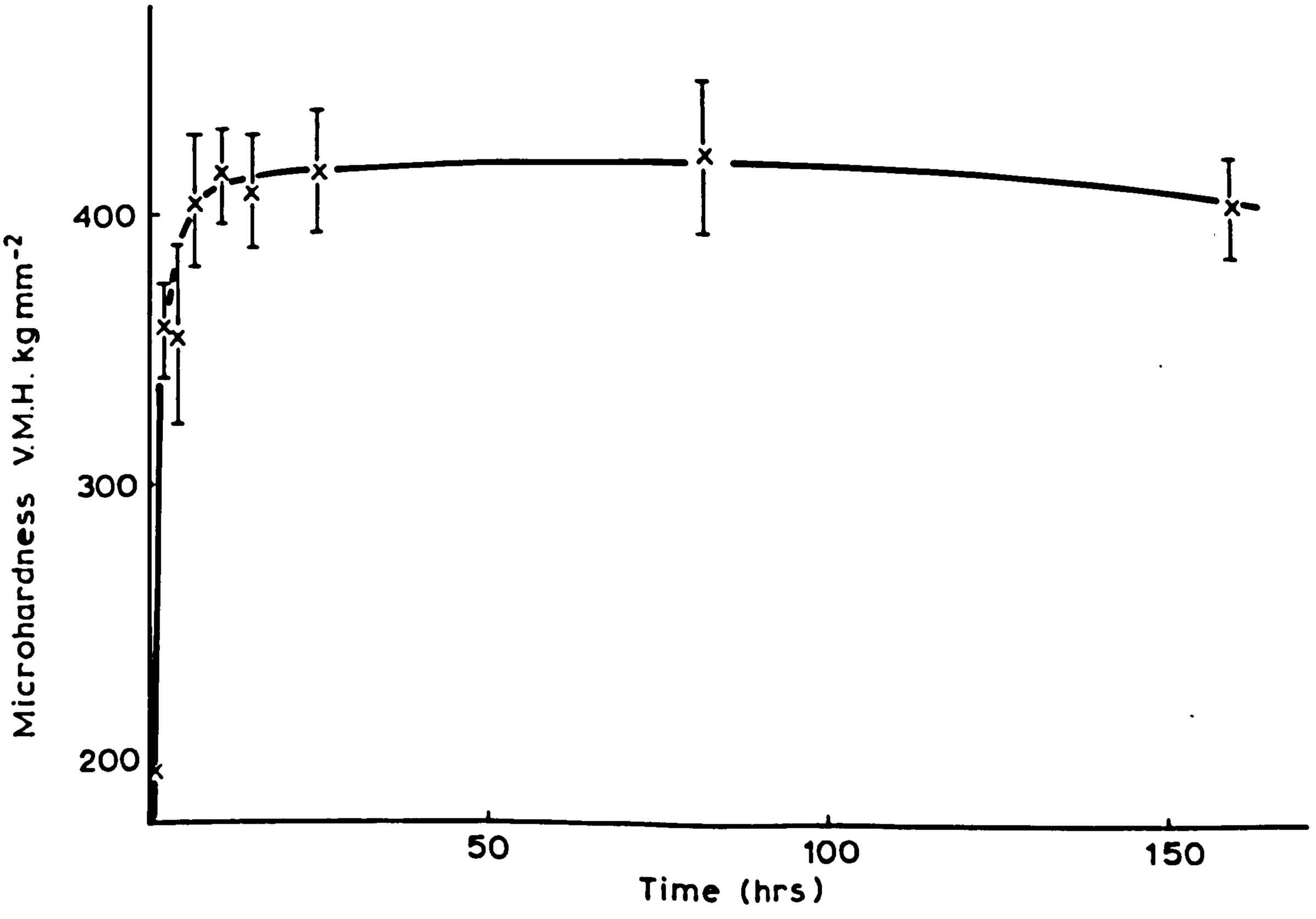

VARIATION OF THE MICROHARDNESS OF NITRIDED Fe-35Ni-2Nb WITH TIME IN $10NH_3:90H_2$ AT 600 °C (Wt%N 0·76).

elastic strain associated with the formation of interstitial-substitutional solute-atom clusters.

As the modulated structure overages at 550 and 600°C in $NH_3:H_2$ a precipitate free zone is formed at the grain boundaries and is associated with grain boundary precipitation of γ-NbN. After prolonged nitriding or hydrogen reduction at 550 and 600°C the modulated structure transforms into a fine dispersion of homogeneous γ-NbN (Figure IV.15). Side-bands persist long after the lattice parameter has decreased to level equivalent to that of the excess nitrogen in solution and may be due either to the slow transformation of clusters to γ-NbN, or to a periodic distribution of γ-NbN (Figure IV.5 and VI.6 and Table IV.1). The electron microstructure of Fe:35Ni:2Nb nitrided in 11:89 NH_3H_2 at 650°C is a fine dispersion of γ-NbN although side-bands of the modulated structure are observed at the surface of X-ray specimens (Figures IV.6 and IV.16). Homogeneous precipitation of γ-NbN occurs as the modulated structure overages and is associated with:

(i) a change in the modulation coarsening rate (Figure IV.9.and IV.10 and Table IV.1);

(ii) a decrease in the lattice parameter to a level equivalent to the excess nitrogen content after the precipitation of γ-NbN (Figure IV.14a and Table IV.2);

Fig. IV. 15

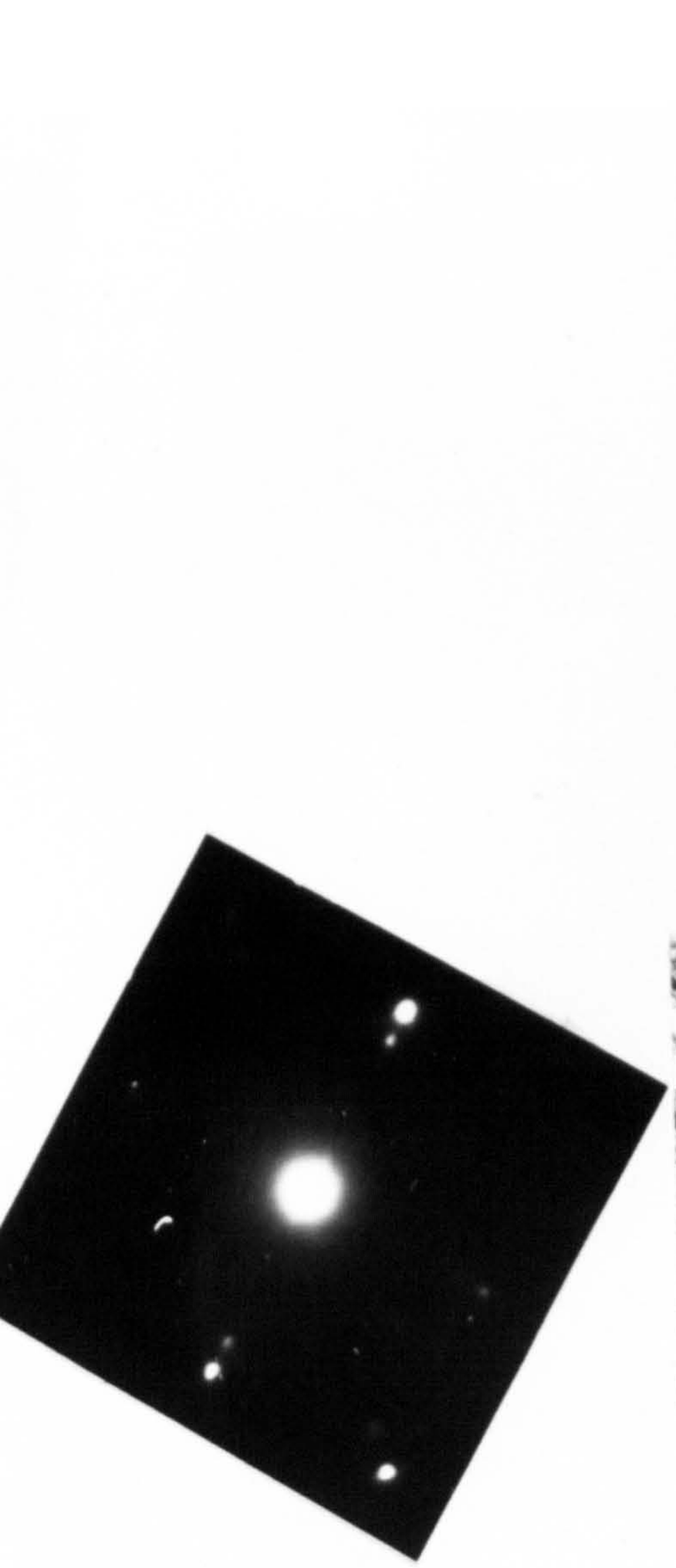

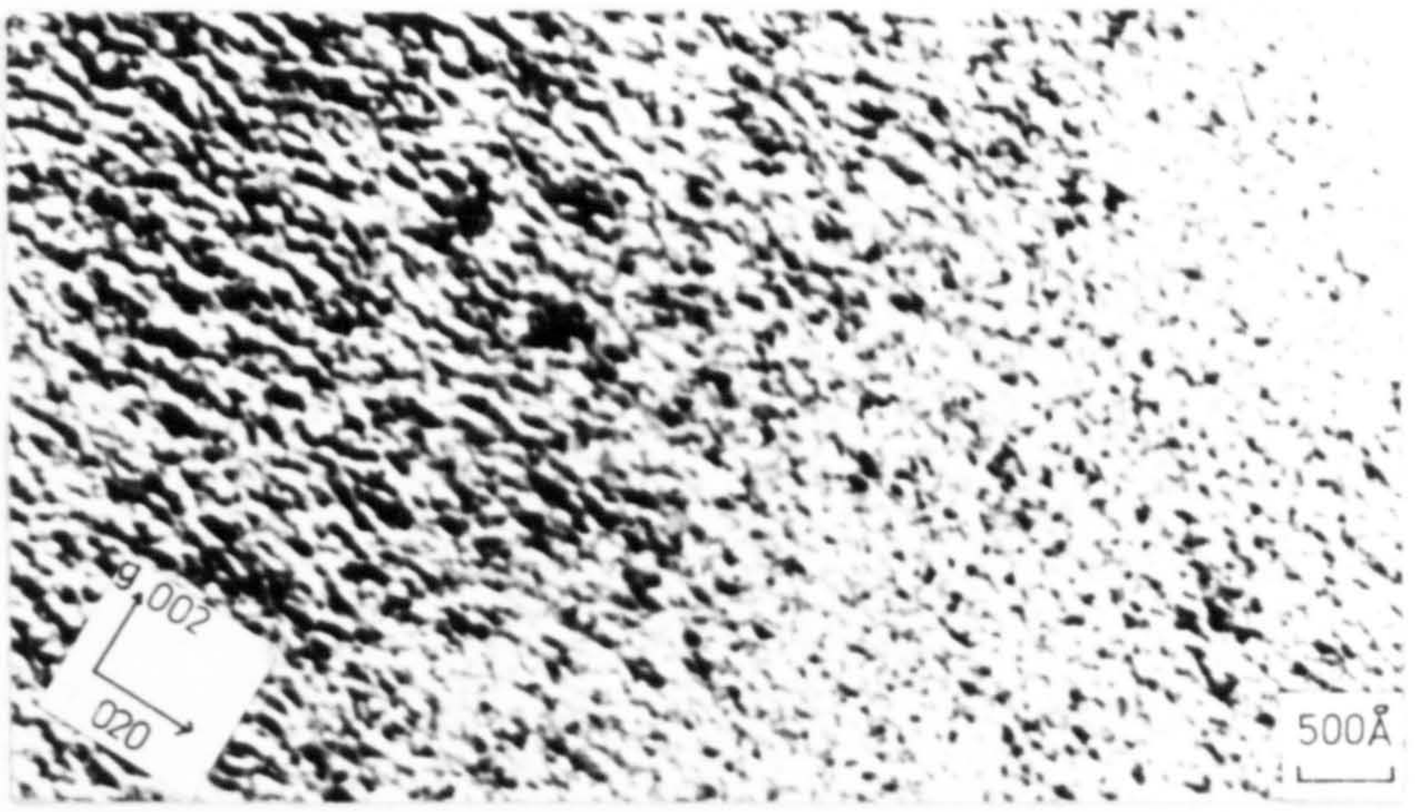

Fe : 35Ni : 0·5Nb

Fe : 35Ni : 1·0Nb

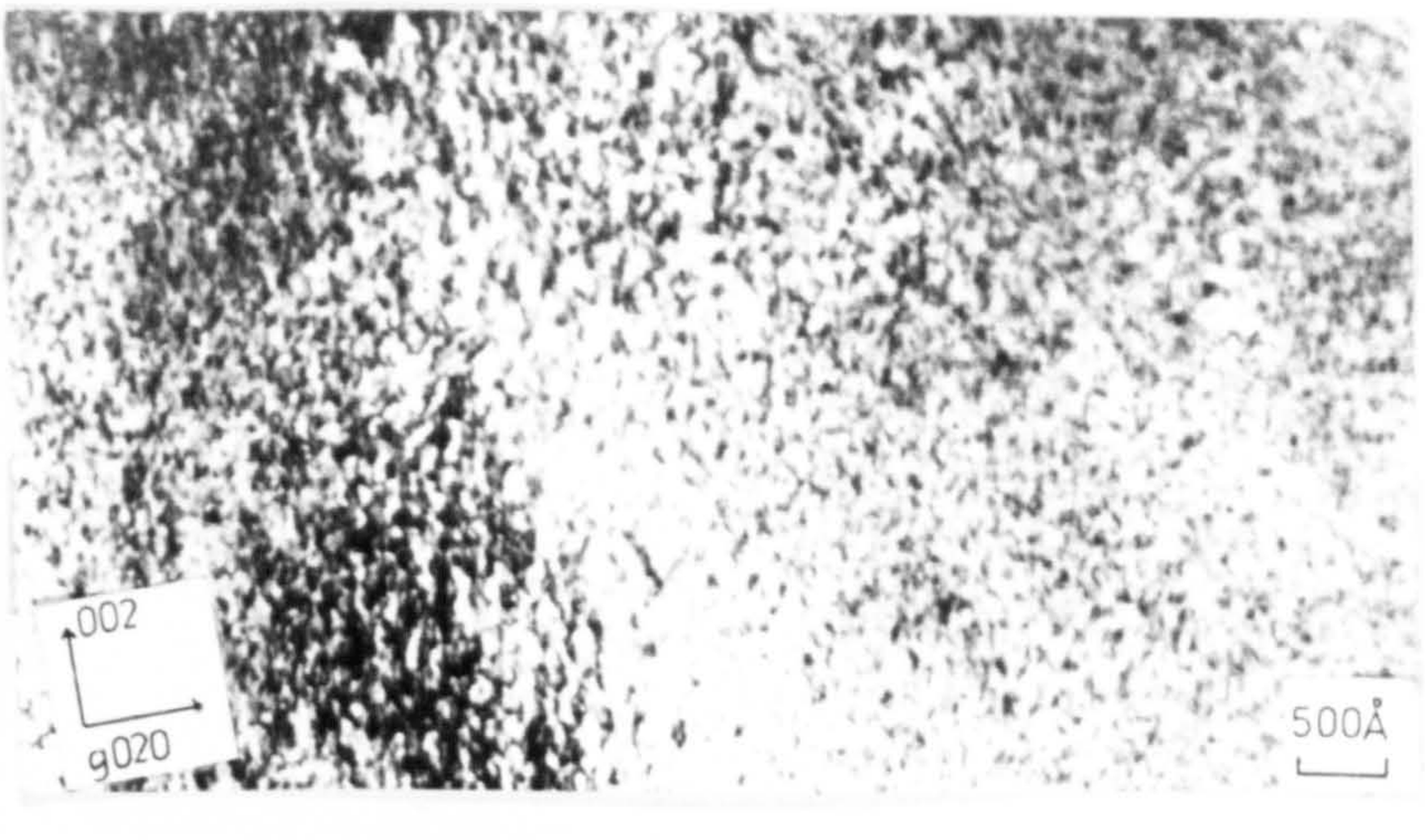

Fe : 35Ni : 2·0Nb

ELECTRON MICROSTRUCTURES OF Fe:35Ni:Nb ALLOYS NITRIDED 259hrs 600°C IN 10:90 NH_3 H_2 84 hrs H_2 REDUCTION

Fig. IV.16

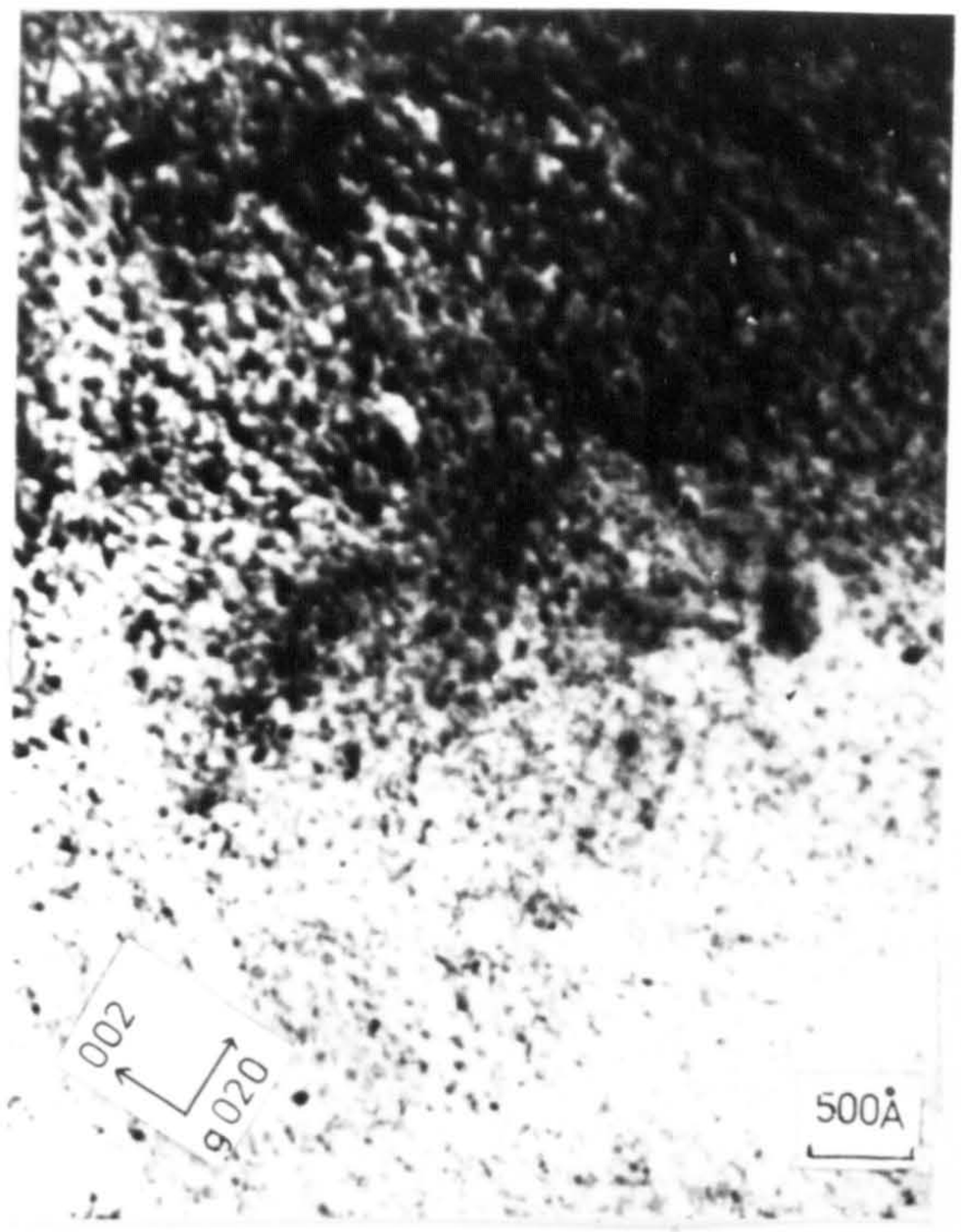

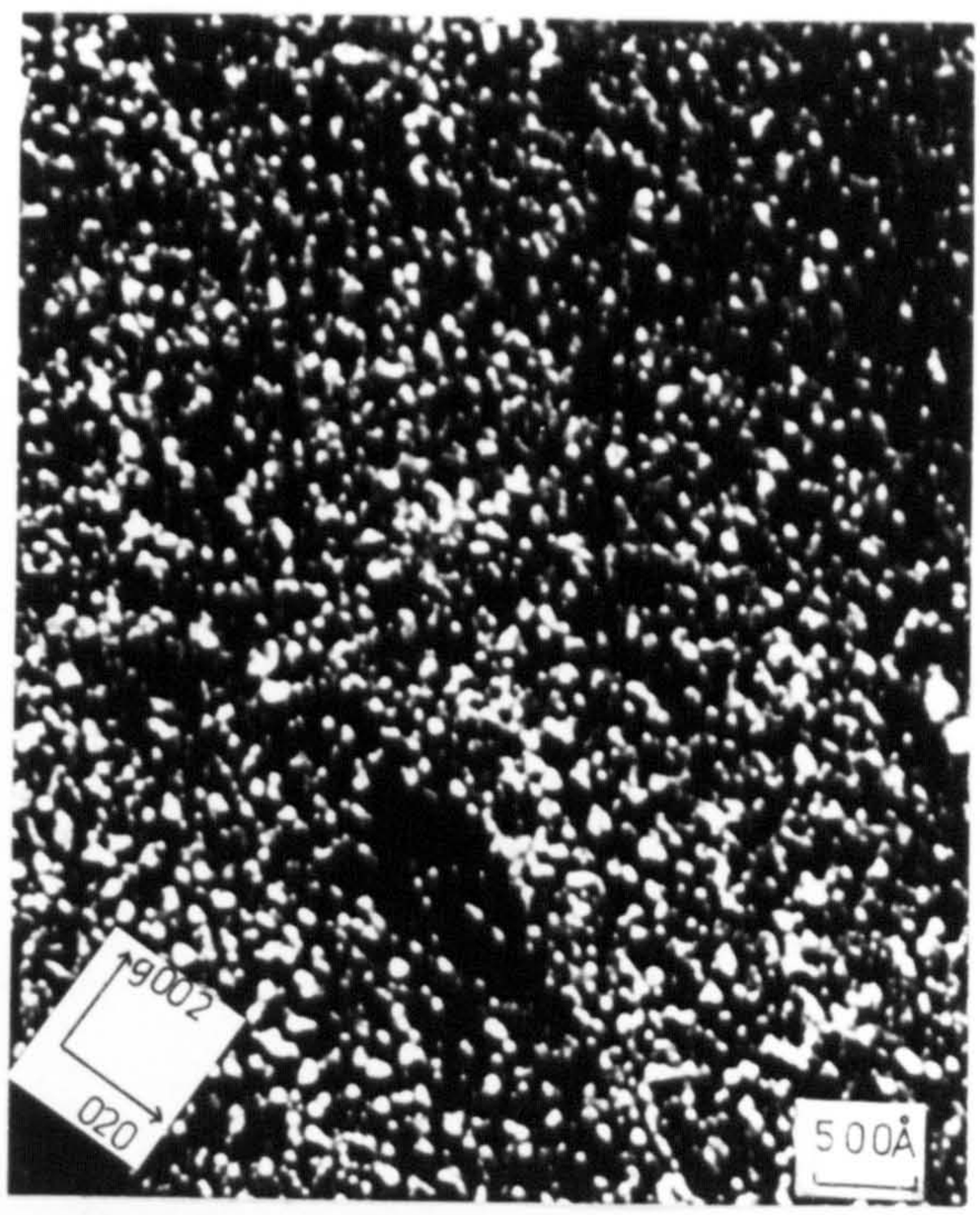

5 hrs

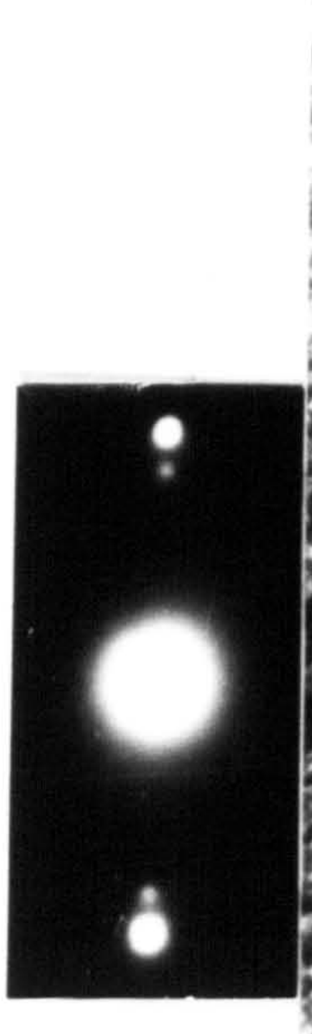

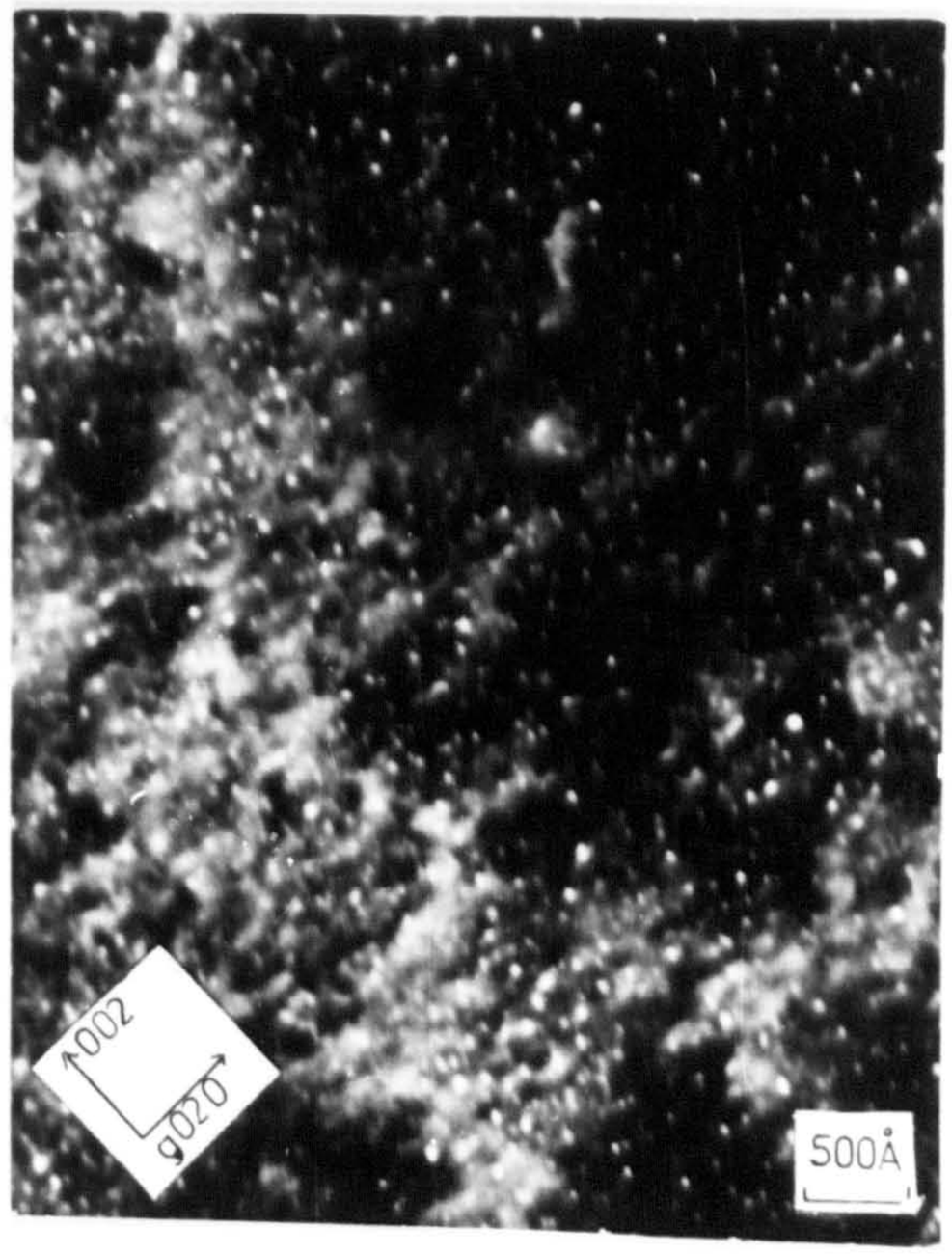

22hrs

ELECTRON MICROGRAPHS OF Fe:35Ni:2Nb

NITRIDED AT 650°C IN 11:89NH_3:H_2

(iii) a decrease in the side-band intensity (Figure IV.12);

and

(iv) a small decrease in the microhardness (Figure IV.14b).

Fe:35Ni:Nb alloys nitrided in nitrogen potentials of $5NH_3:95H_2$ at 600^oC show modulated structures simultaneously with γ-NbN with no corresponding increase in the lattice parameter (Figure IV.3 and Table IV.1). Fe:35Ni:0.5Nb nitrided in $20:80NH_3H_2$ at 550^oC gives a fine dispersion of γ-NbN and other results obtained at 600^oC suggest that this alloy does not form a modulated structure in $NH_3:H_2$ at these temperatures (Figure IV.2).

IV.3.2 Homogeneous precipitation of γ-NbN.

Electron microscopic examination of Fe:35Ni:Nb nitrided in $NH_3:H_2$ (1 to 20%NH_3) at 800^oC showed homogeneous precipitation of γ-NbN in the matrix. The major features of homogeneous precipitation of γ-NbN in these alloys are:

(i) the orientation relationship of γ-NbN precipitates with the austenite matrix is $(100)_{NbN}$ // $(100)_\gamma$ and $[100]_{NbN}$ // $[100]_\gamma$ (Figure IV.17);

(ii) the precipitate size at the centre of similarly nitrided Fe:35Ni:2Nb specimens increases with increasing thickness (Figure IV.18);

Fig. IV.17

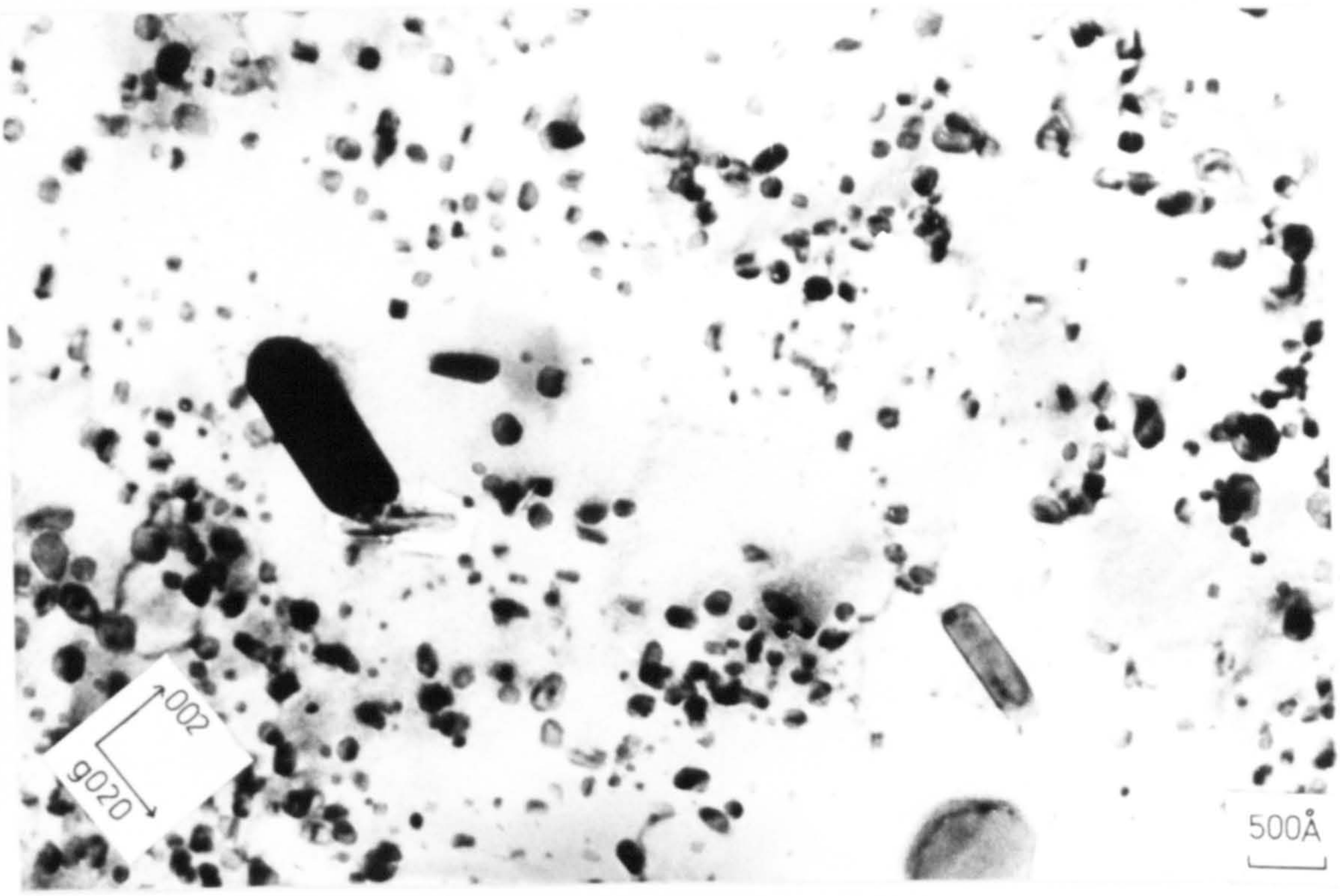

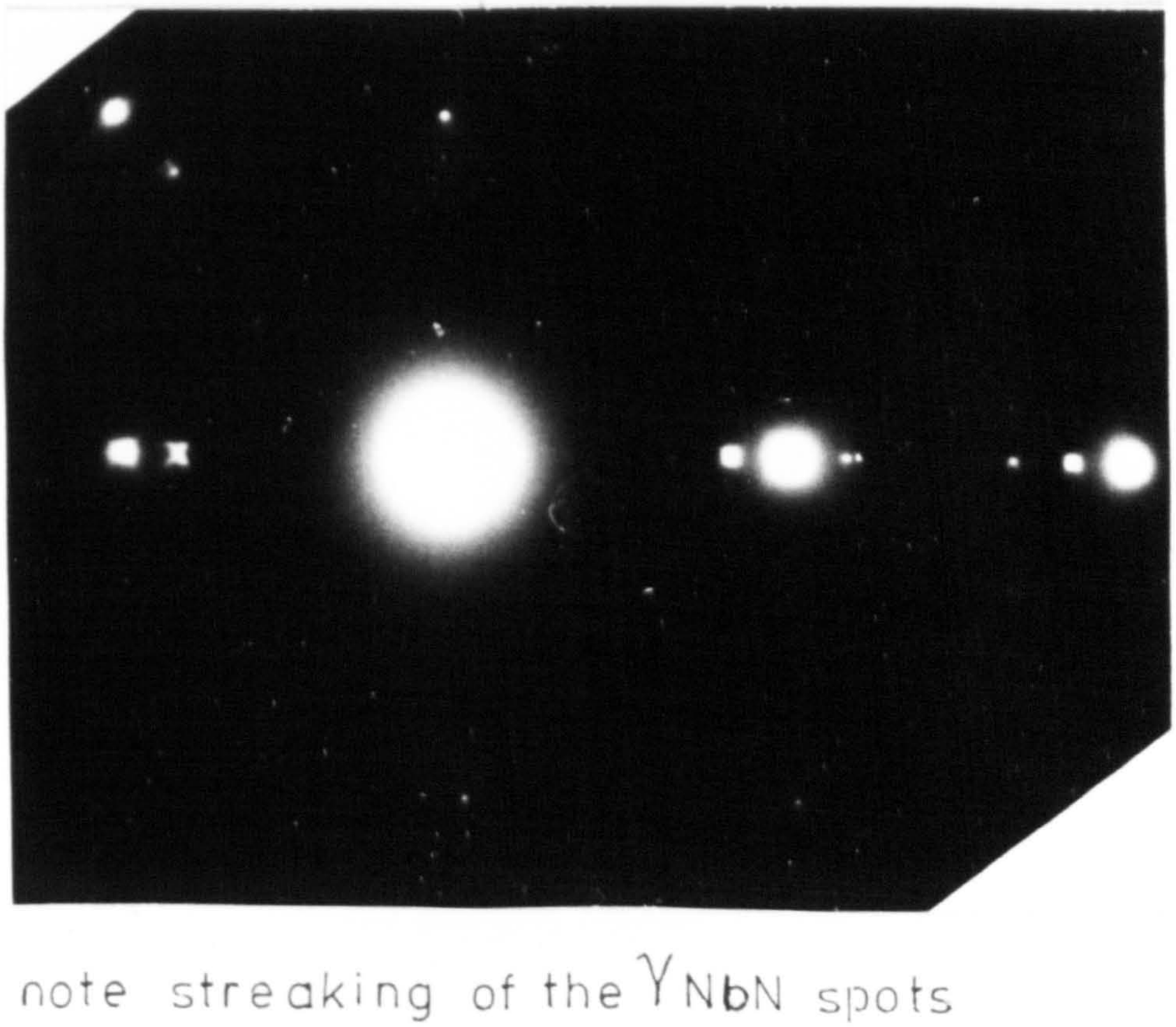

note streaking of the γ NbN spots

ELECTRON MICROSTRUCTURE AND DIFFRACTION PATTERN OF Fe:35Ni:2Nb NITRIDED IN 1:99 NH_3:H_2 FOR 428hrs AT 800°C

Fig. IV. 18

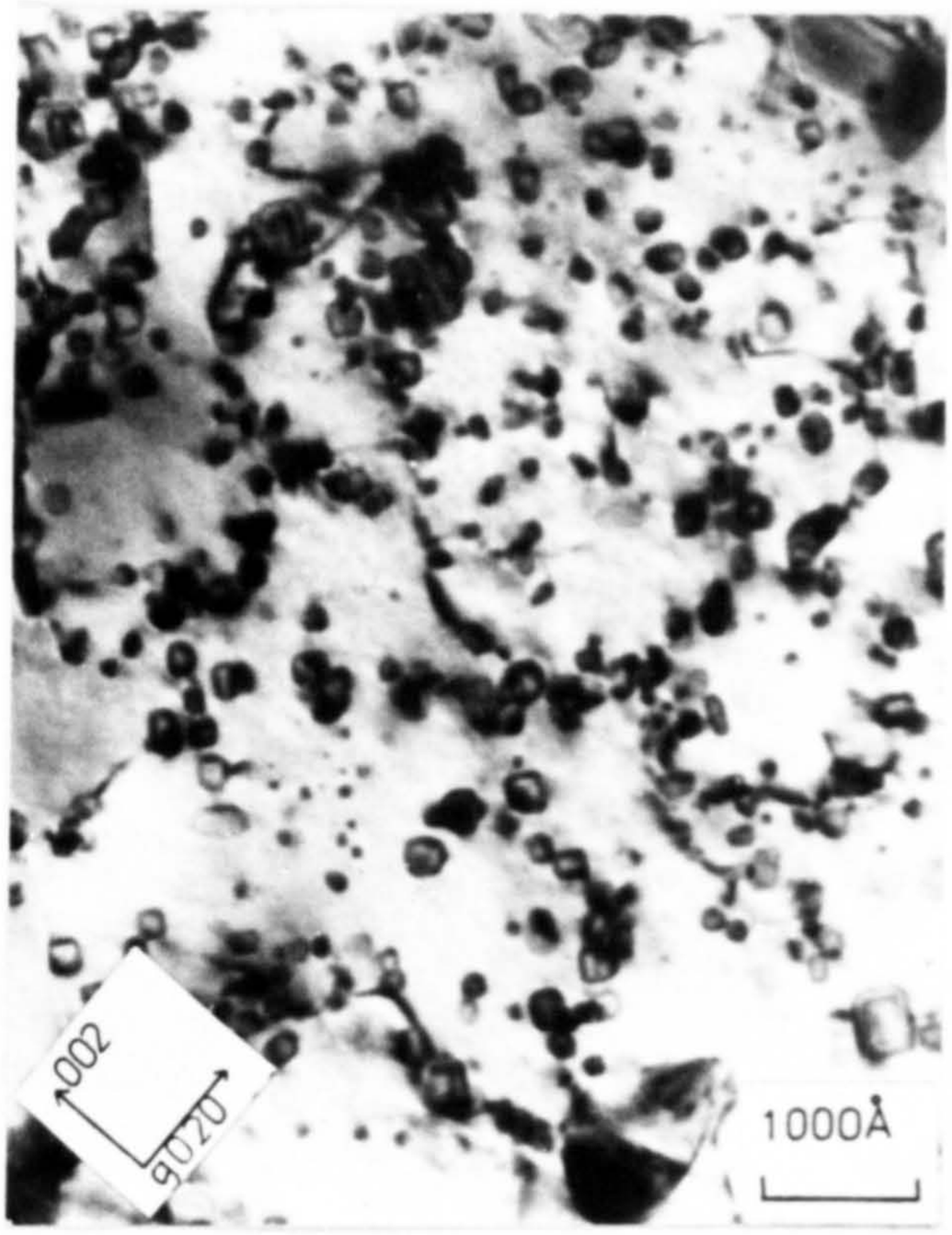

(a) 0·13 mm

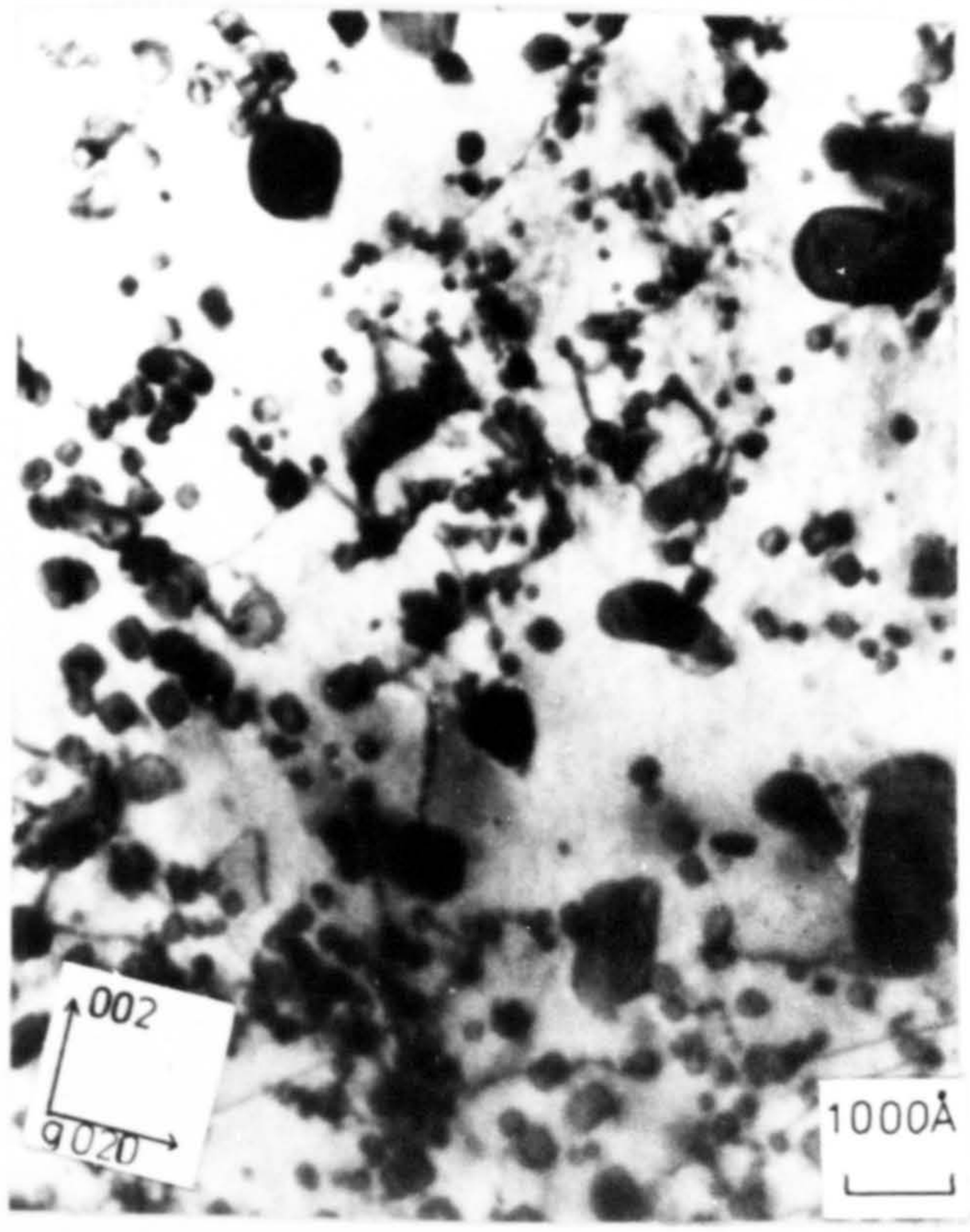

(b) 0·25 mm

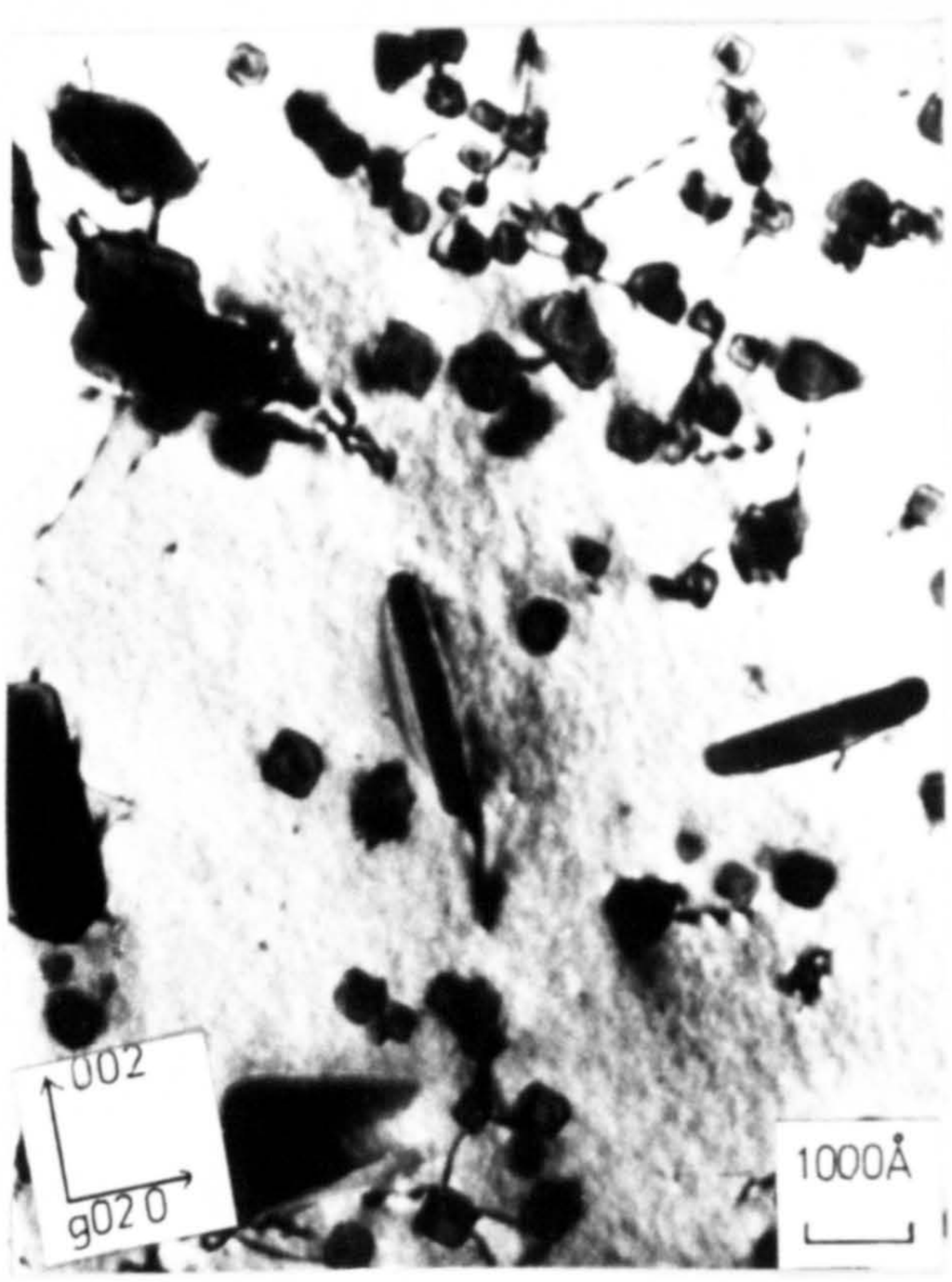

(c) 0·52 mm

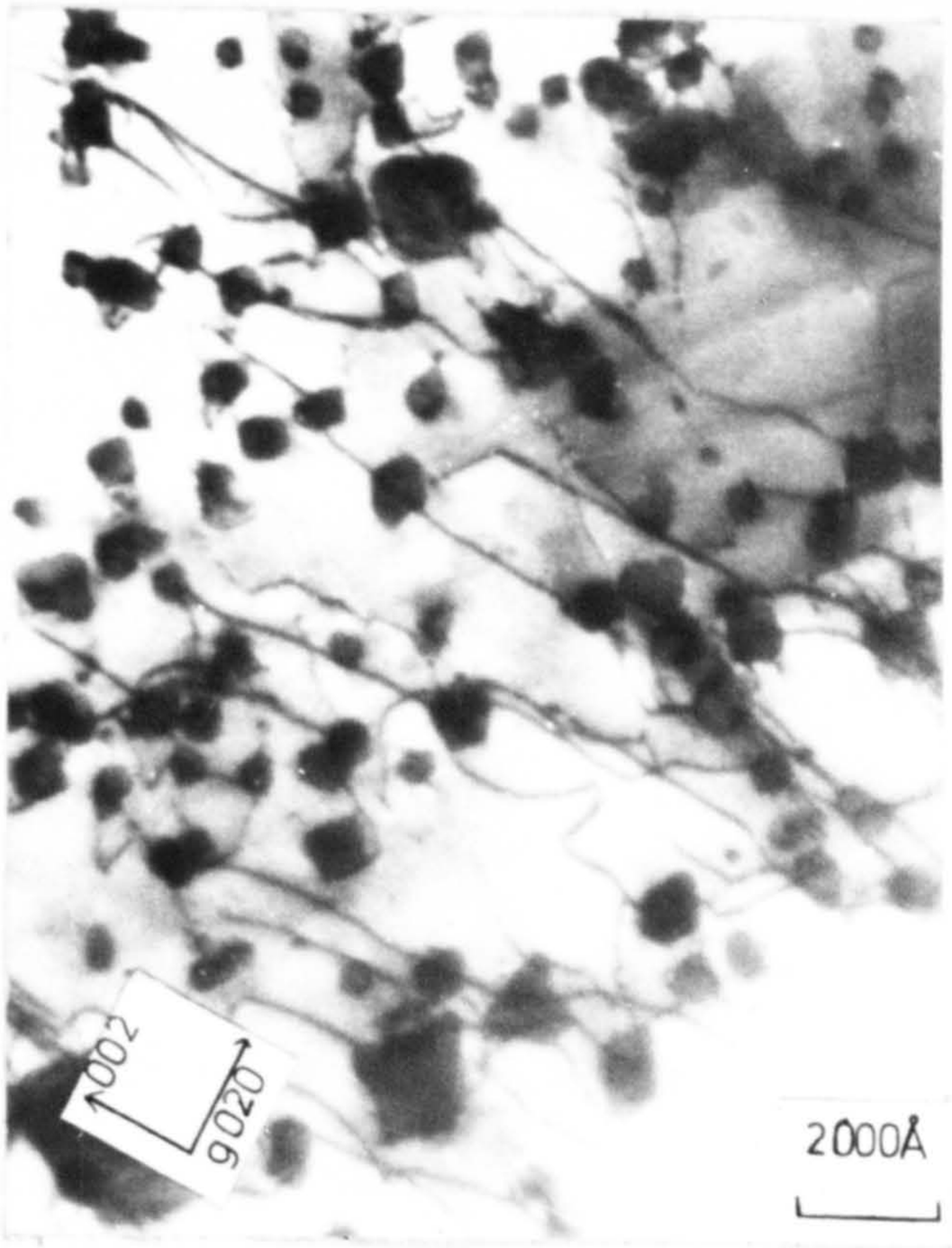

(d) 1·32 mm

ELECTRON MICROGRAPHS TAKEN FROM THE CENTRE OF (a) 0·13; (b) 0·25; (c) 0·52; & (d) 1·32 mm THICK SPECIMENS OF Fe : 35Ni : 2Nb NITRIDED FOR 428 hrs AT 800°C IN 1:99 NH_3:H_2

(iii) the coarsening rates of γ-NbN in Fe:35Ni:1 and 2Nb in 1:99 $NH_3:H_2$ are low compared with those in Fe:35Ni:0.5Nb and give a linear relationship between the cube of the precipitate radius and the nitriding time (Figure IV.19);

(iv) the initial spheroidal precipitates of γ-NbN overage at 800°C to form approximate octahedra with faces // to the {111} matrix planes and give rise to some small diffuse streaking of the γ-NbN precipitate reflections in the ⟨111⟩ directions in electron diffraction patterns (Figures IV.20 and IV.17). On further ageing the octahedra transform to platelets of γ-NbN (Figures IV.18 and IV.21) parallel to {100} matrix planes;

(v) the density of the grain boundary precipitation of γ-NbN at 800°C increases with the nitriding potential and is associated with a wide precipitate-free zone (Figure IV.1);

(vi) γ-NbN is identified from X-ray photographs taken from the centre of Fe:35Ni:2Nb specimens (Figure IV.22) after nitriding at 700 and 800°C in $NH_3:H_2$. The lattice parameter of these precipitates are respectively 4.36 and 4.37 Å which is in reasonable agreement with the values of 4.388-4.389 Å obtained by Roberts (1970) in nitrided Fe-Nb alloys and with 4.38 Å obtained by Brauer and Jander (1952)

Fig. IV. 19

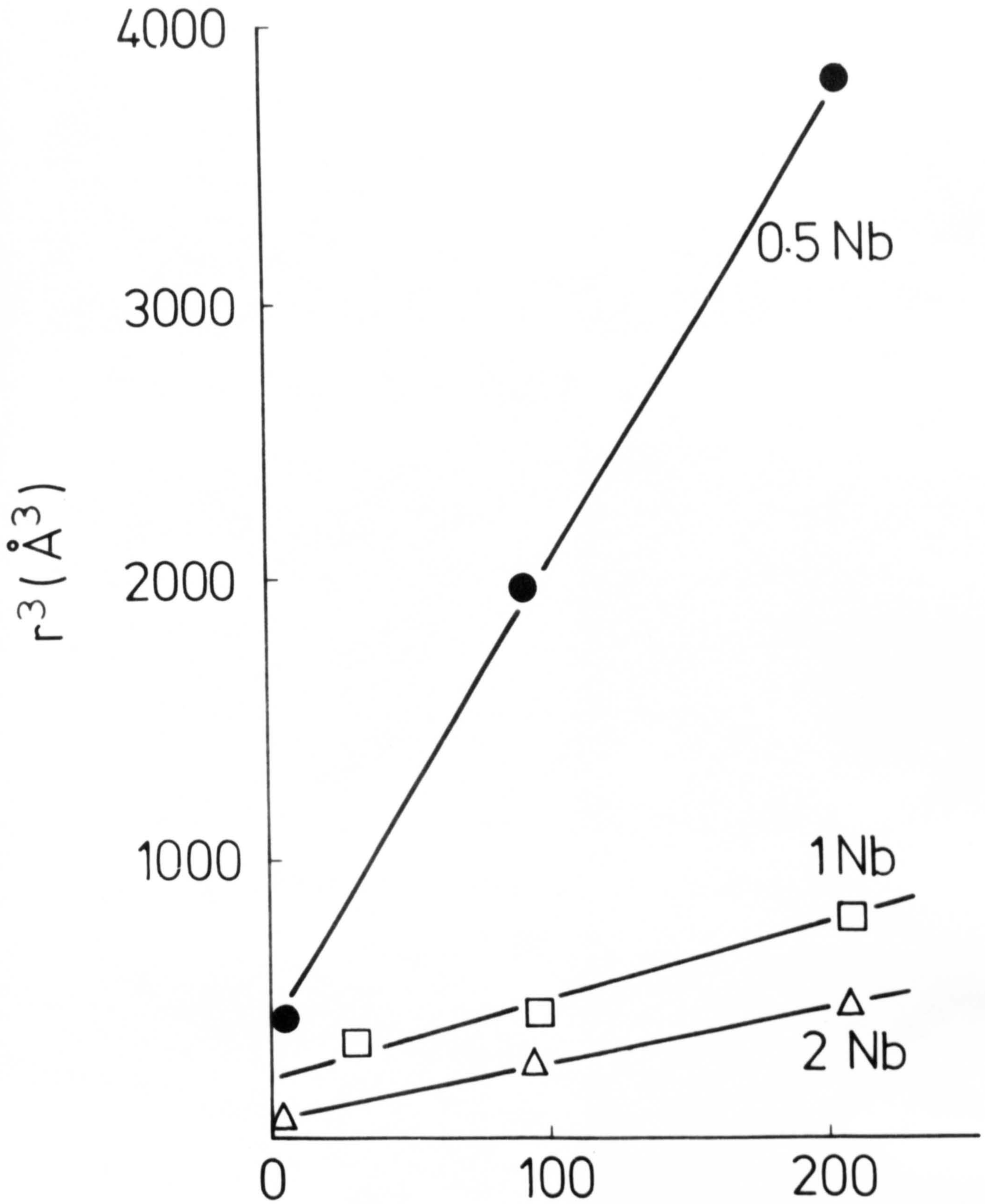

COARSENING RATE r^3 AGAINST TIME OF γNbN IN Fe-35Ni-Nb ALLOYS NITRIDED IN 1:99 NH_3:H_2 AT 800 °C.

Fig. IV.20

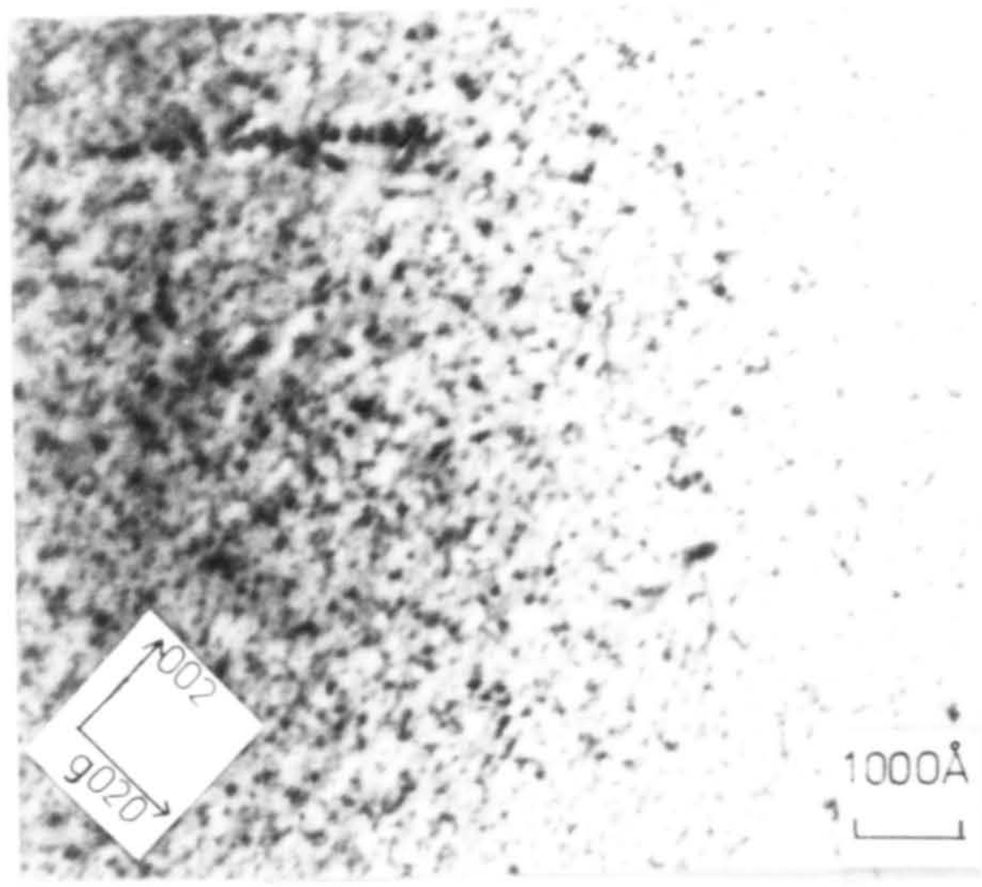

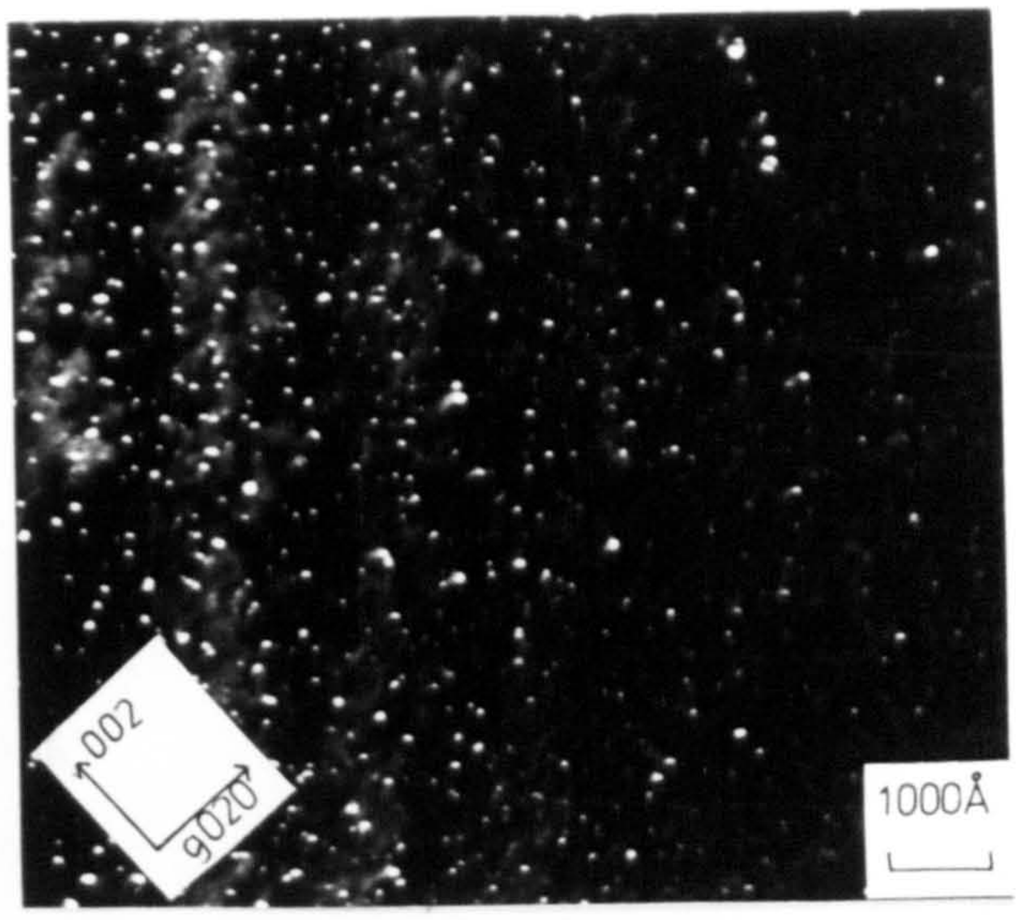

Fe:35Ni:0·5Nb 29hrs 800°C 5:95 NH_3:H_2 thickness 0·15mm

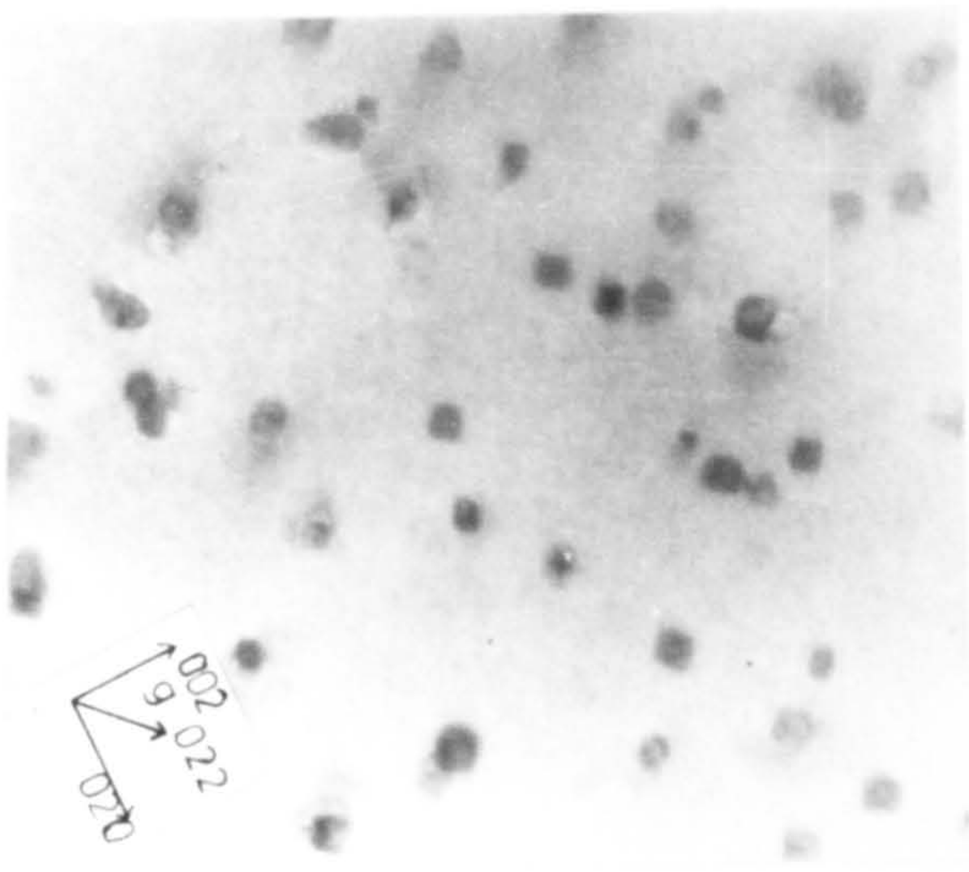

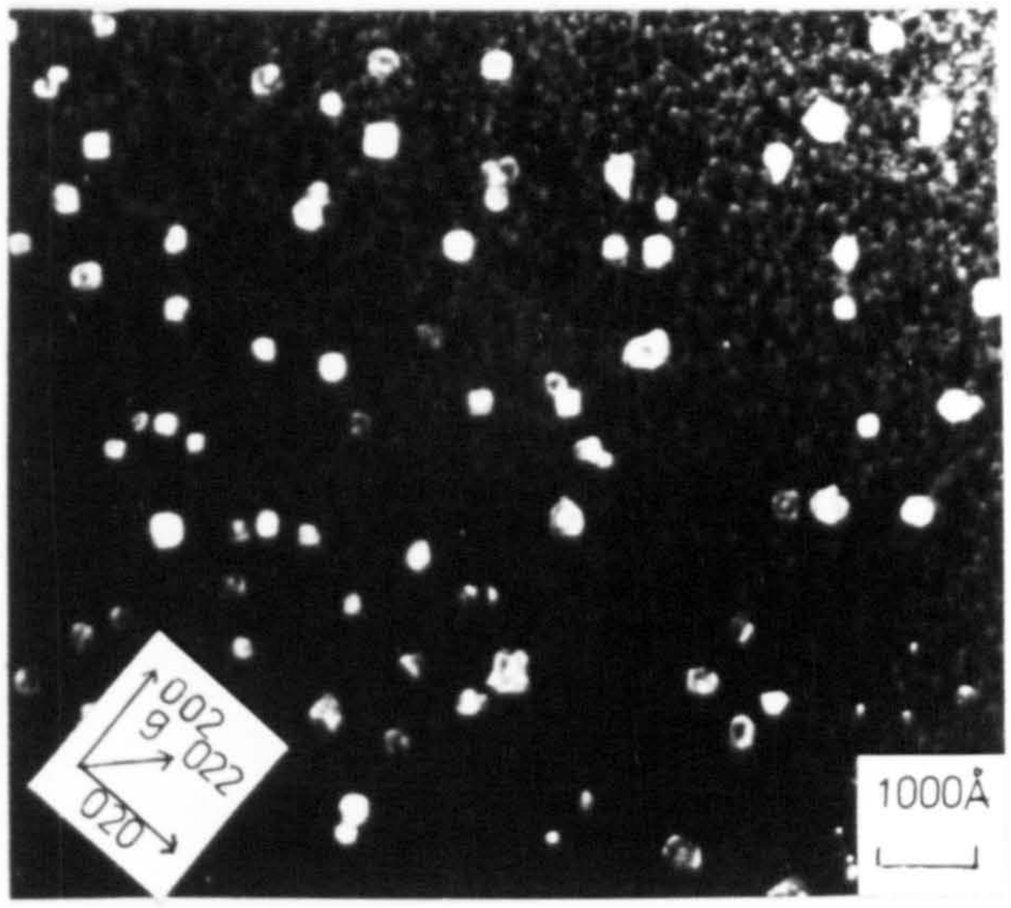

Fe:35Ni:0·5Nb 29hrs 800°C 5:95 NH_3:H_2 thickness 0·30 mm

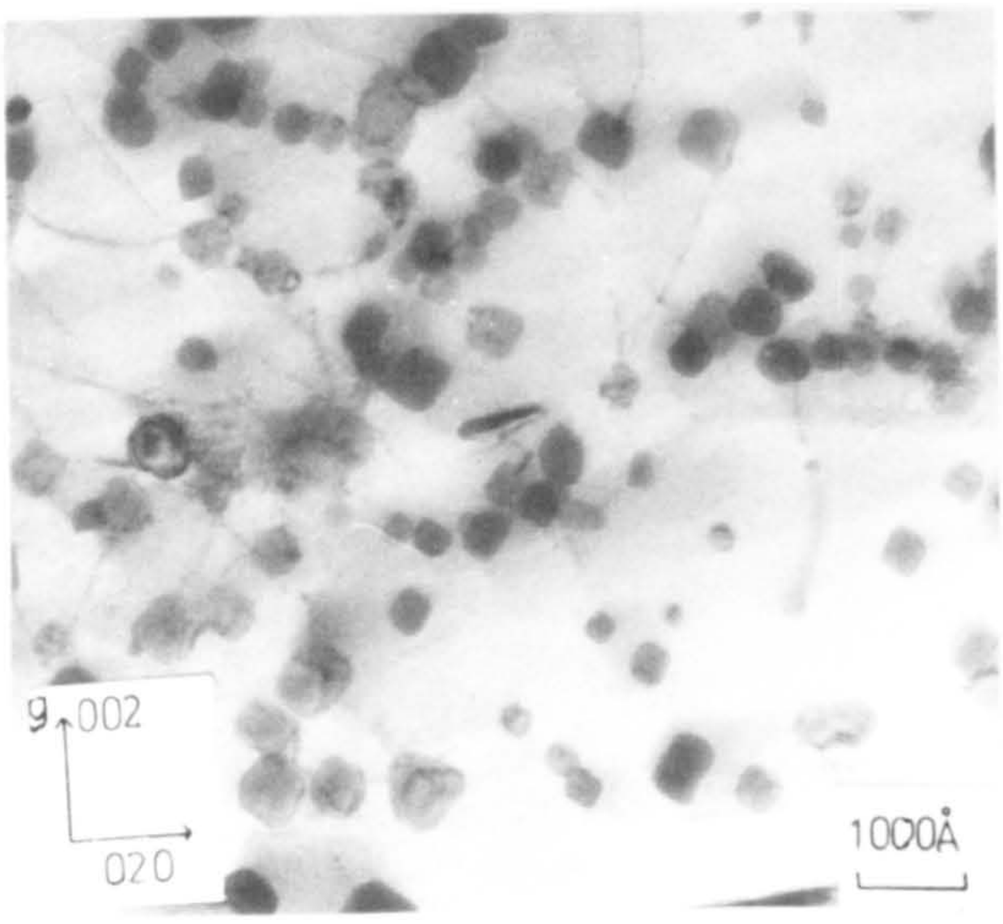

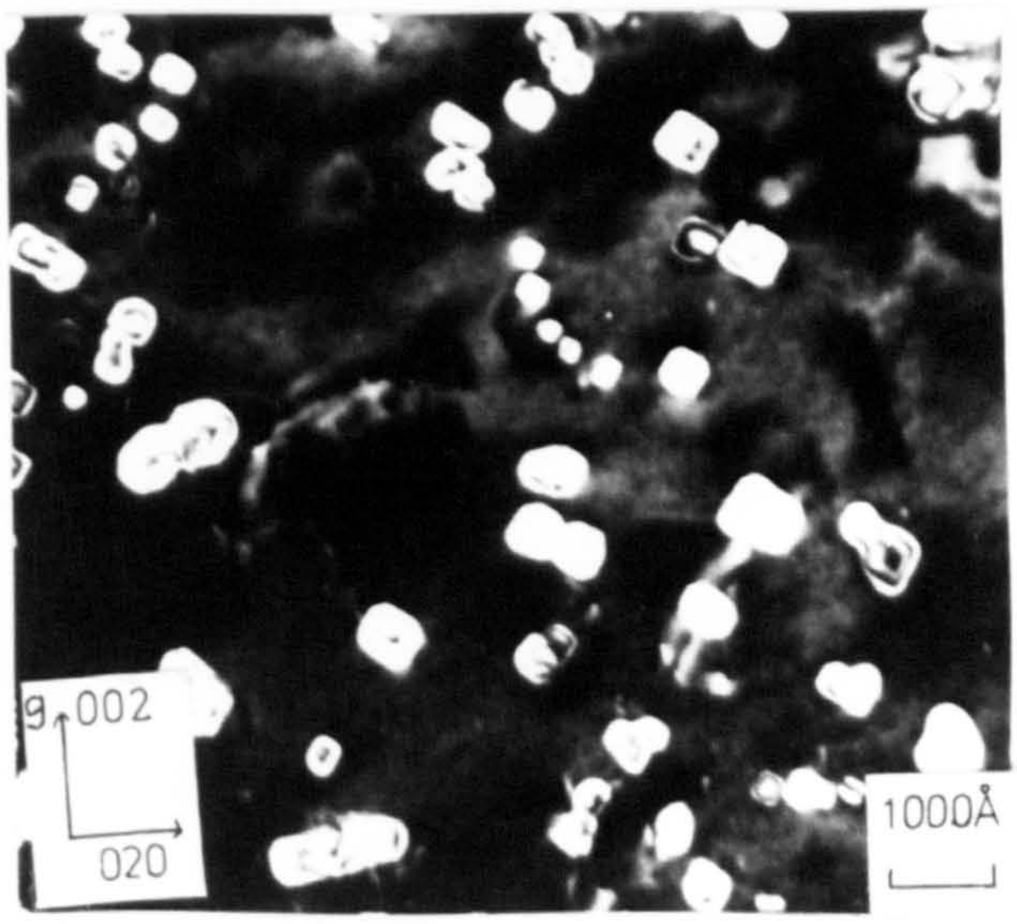

Fe:35Ni:2·0Nb 428hrs 800°C 1:99 NH_3:H_2 thickness 0·52mm

ELECTRON MICROGRAPHS SHOWING A RANGE OF γ NbN PRECIPITATE SIZES IN NITRIDED Fe:35Ni:Nb ALLOYS AT 800°C IN NH_3 H_2

Fig. IV.21

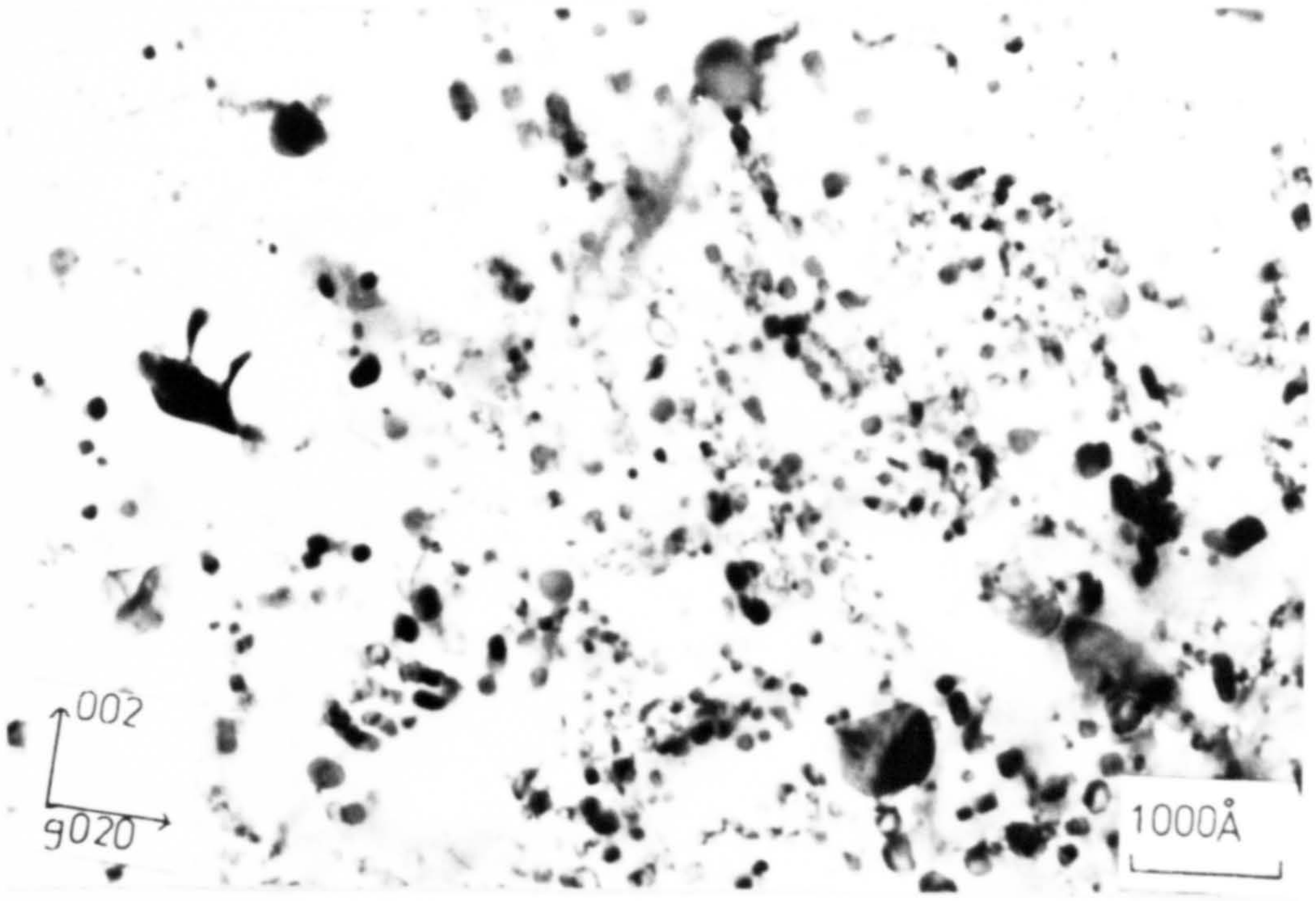

5 hrs

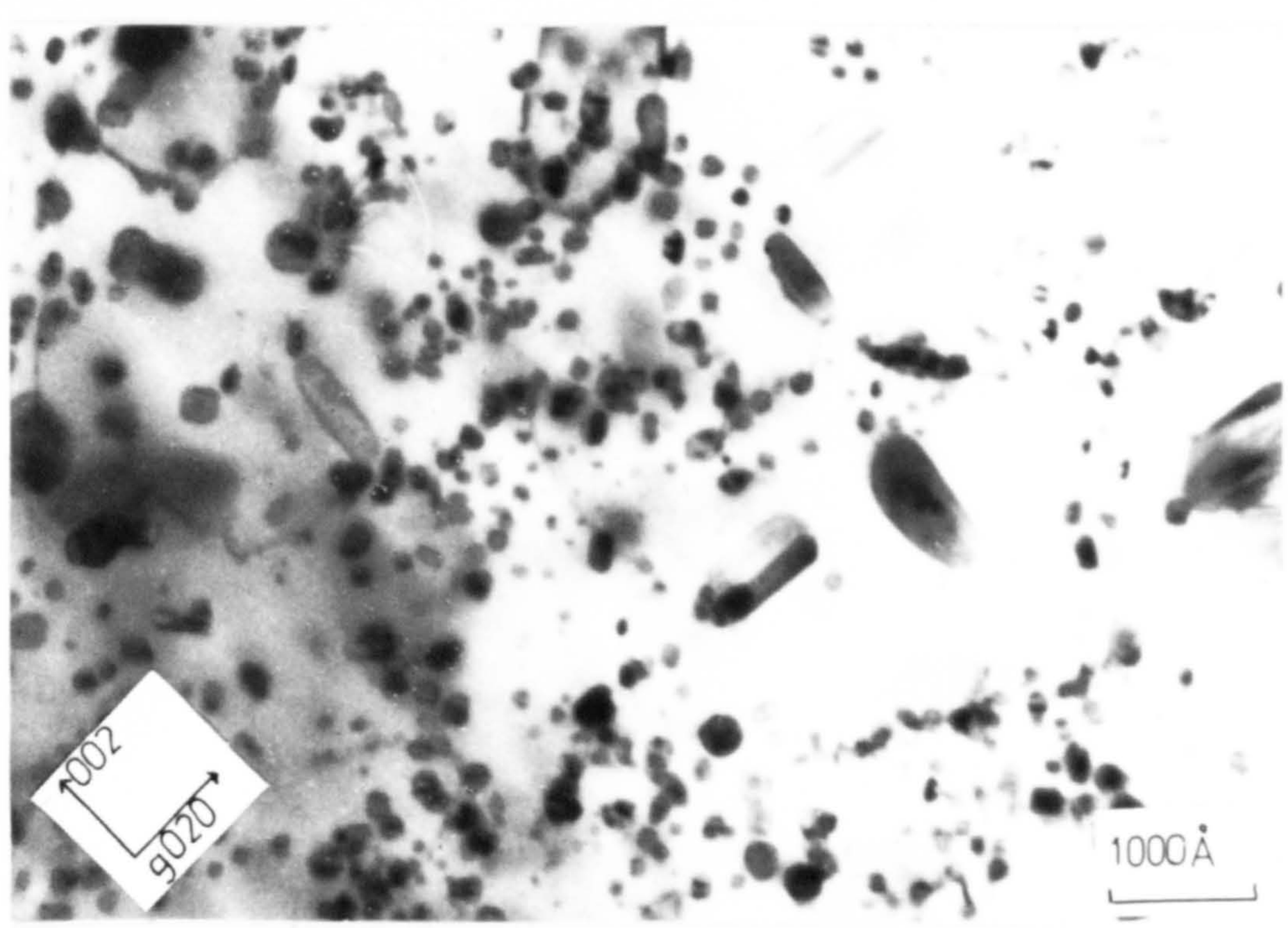

209 hrs

ELECTRON MICROSTRUCTURES OF Fe:35Ni:2Nb NITRIDED IN 1:99 NH_3 H_2 AT 800°C

Fig. IV.22

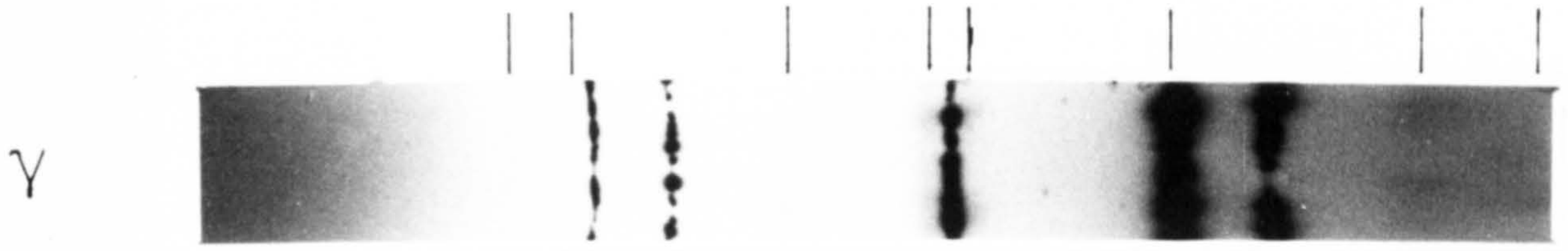

NIOBIUM NITRIDES PRECIPITATED IN Fe:35Ni:2Nb ALLOY BY CONSTANT ACTIVITY AGEING IN $NH_3:H_2$ AT 700 AND 800°C

in nitrided niobium. After prolonged ageing or hydrogen reduction at 800°C of nitrided Fe:35Ni:2Nb traces of δ-NbN(O) and ϵ-NbN(O) were also identified.

IV.3.3 Stacking fault precipitation of γ-NbN.

Stacking fault precipitation of γ-NbN is observed in advance of the homogeneous precipitated layer in Fe:35Ni:Nb alloys nitrided in $0.02NH_3:99.98H_2$ - $20NH_3:80H_2$ at 700°C and after prolonged nitriding in low NH_3 - containing gas mixture at 550 and 600°C (Figure IV.23). Stacking fault precipitation of γ-NbN occurs as discs on {111} planes, and these are similar to those observed in quench-aged Fe:Cr:Ni:Nb:N alloys (Borland and Honeycombe, 1970). The stacking faults formed in nitrided Fe:35Ni:Nb alloyd are not so clearly defined as those in Fe:Cr:Ni:Nb:N perhaps because they are unable to grow before the onset of homogeneous precipitation, or because the stacking fault energy in Fe:35Ni:Nb alloys is considerably higher.

IV.4 Discussion of results

IV.4.1 Modulated structures.

The modulated structures formed in nitrided Fe:35Ni:Nb alloys at 550 and 600°C are microstructurally

Fig. IV.23

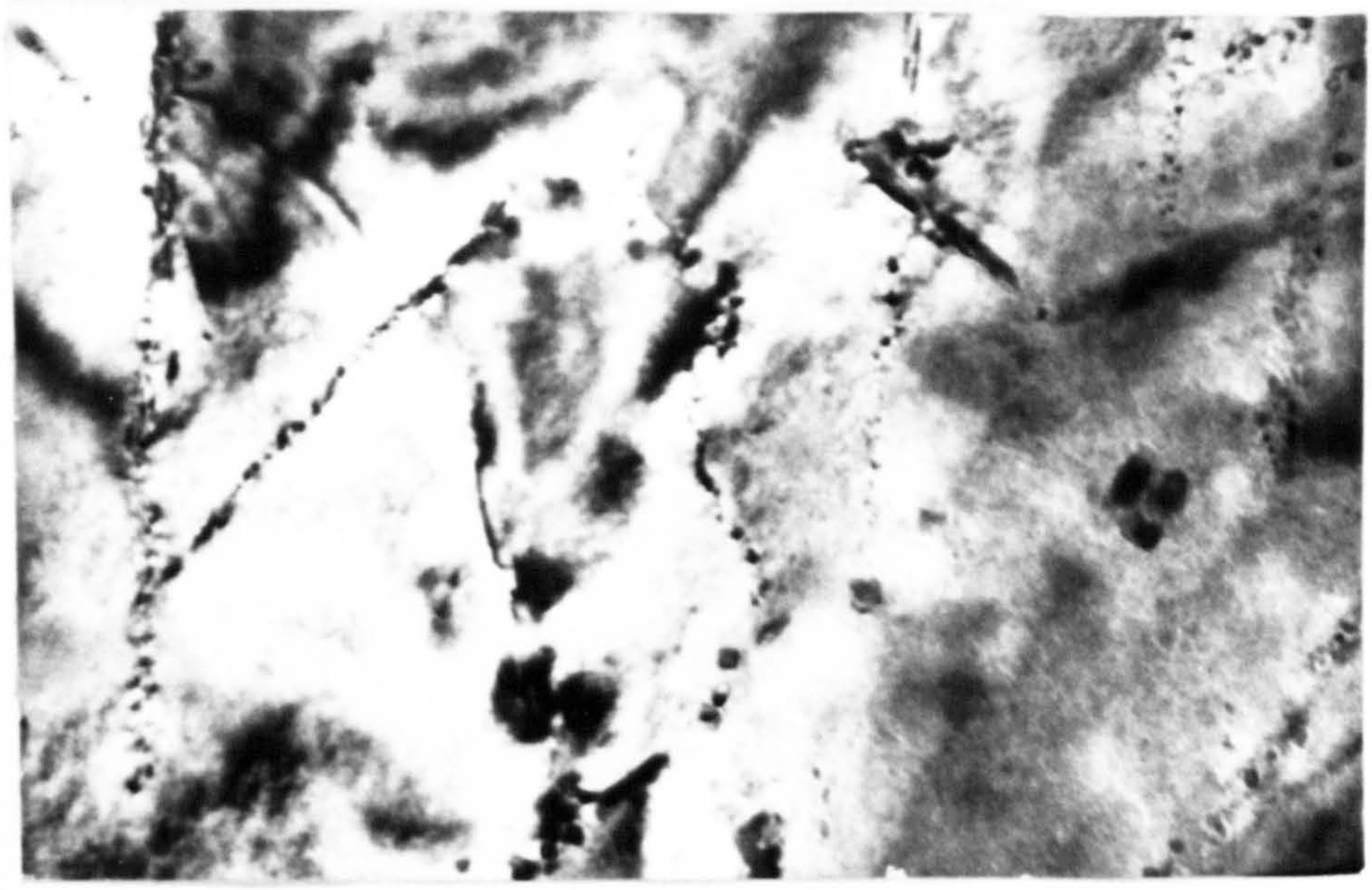

Stacking fault precipitation formed in Fe:35Ni:2Nb nitrided for 2hrs at 750°C in 5:95 $NH_3:H_2$

Stacking fault and homogenous precipitation formed in Fe:35Ni:2Nb nitrided for 17hrs at 700°C in 02:99.8 $NH_3:H_2$

Stacking fault and homogenous precipitation formed in Fe:35Ni:2Nb nitrided for 17hrs at 700°C in 02:99.8 $NH_3:H_2$

STACKING FAULT & HOMOGENOUS PRECIPITATION OF γ NbN AT 700 & 750°C IN NITRIDED Fe:35Ni:2Nb

similar to those found in Cu:Ni:Fe alloys during spinodal decomposition (Butler and Thomas, 1970). In both cases the modulated structure is associated with the absence of precipitate-free zones at the grain boundaries and with the presence of side-bands in electron and X-ray diffraction patterns. Similar observations have been made in Cu:Ti alloys (Cornie, Datta and Softa, 1972), and in nitrided Fe:35Ni:V alloys (Driver, Handley and Jack, 1972; Driver, Sinclair and Jack, 1974). The modulated structure is a result of the formation of interstitial-substitutional solute-atom clusters with a periodic distribution in the $\langle 100 \rangle$ directions and is also associated with:

(i) a high nitrogen to niobium atom ratio ($\approx$ 4:1. see Table IV.2);

(ii) a lattice parameter which is equivalent to a solid solution of niobium and nitrogen (see Table IV.2);

(iii) nitriding kinetics which are independent of niobium content. This suggests that the diffusivity of niobium is too slow to prevent rapid diffusion of nitrogen through the specimen, and so allows the nitrogen concentration to exceed the modulated structure solvus before the occurrence of γ-NbN precipitates (see Chapter V); and

(iv) a niobium concentration greater than 0.5Nb and at 600°C a nitriding potential greater than $5NH_3:95H_2$.

This implies the existence of a modulated structure solvus. Recent work by Driver et al (1974) has shown that a modulated structure solvus exists in nitrided Fe:35Ni:V alloys at 600-780°C depending on nitrogen potential and vanadium content.

These observations are similar in many ways to clustering in nitrided Fe;Nb alloys (Roberts, 1969) apart from the presence of side-bands.

After the modulated structure has been formed, subsequent nitriding causes rapid coarsening (Figures IV.9 and IV.10) at a rate dependent upon niobium diffusion but independent of nitrogen concentration (Table IV.1) at 600°C.

The side-band intensities of X-ray photographs of the Fe:35Ni:2Nb alloy nitrided in $11NH_3:89H_2$ at 650°C (Figures IV.6 and IV.12) and in 10:90 $NH_3:H_2$ at 600°C increased with nitriding time and are asymmetric where the degree of asymmetry at 650°C for the high angle to low angle intensity ratio increased from 2:1 at 1h to 3.5:1 at 4hrs. Similar observations on side-band asymmetry have been made in nitrided Fe:35Ni:V alloys by Driver et al (1974), and were attributed to the change in the wave form of the modulation. Preliminary work by Westin (1973) on the X-ray intensity of diffuse scattering of nitrided Fe:35Ni:1Nb and 2V alloys has shown that

the periodic structure is essentially a result of lattice parameter modulation due to nitrogen-atom clustering and the change in the side-band asymmetry is attributed to changes in both the modulation amplitude and wave form.

Several theories have been developed to explain the mechanism of spinodal decomposition in binary and ternary alloys as reviewed by Cahn (1968) and Hilliard (1970). Spinodal decomposition occurs in systems which exhibit a negative second derivative of the free energy and composition (d^2f/dc^2) which promotes uphill diffusion of the clustering solute atoms. Cahn also predicted that for alloys which spinodally decompose, a linear plot of $1/\bar{\lambda}_o^2$ against T would extrapolate to give a coherent spinodal temperature on the temperature axis. A similar plot for Fe:35Ni:2Nb nitrided at a constant nitrogen potential (1.6×10^4 atms) is linear and gave a spinodal temperature of $750^{\circ}C$. This temperature coincides with an upper temperature for the modulated structure formation as seen in X-ray photographs. Similar observations have been made by Driver et al (1974) who noted a sharp transition from the modulated structure to a fine dispersion of VN at about $780^{\circ}C$ in nitrided Fe:35Ni:V alloys.

The coherent spinodal temperature in Au:Ni alloys

is depressed several hundred degrees below the chemical spinodal temperature and moved to lower nickel contents (Golding and Moss, 1967) due to the large coherency strains associated with the modulated structure. Similar considerations may apply to the modulated structure formed in nitrided Fe:35Ni:Nb alloys. The solvus temperature is $\approx$ 1500°C below the solution treatment temperature (after Smith, 1962); the critical nitrogen to niobium atom ratio is moved from 1:1 to $>$ 2:1; and there are large coherency strains due to the mismatch parameter of γ-NbN and the matrix which is $\approx$ 21%.

The hardness increase due to the modulated structure is $\approx$ 100 VMH in excess of that predicted for a Fe:35Ni:2Nb:N solid solution (Figure IV.14b) and is an indication of the considerable elastic strain associated with the formation of clusters during nitriding.

No attempt was made to determine thermodynamic data from low angle scattering by modulations in these alloys (see Hilliard, 1970). It is also impossible to test the reversibility of interstitial-substitutional solute-atom clusters formed in Fe:35Ni:Nb solid solutions.,

In the absence of these thermodynamic data it is impossible to state the exact mechanism by which the modulated structure is formed. The results obtained by the present investigation, by Driver et al (1974) in

nitrided Fe:35Ni:V alloys, and by Westin (1973) indicate that the modulations are due to a periodic lattice parameter variation produced by interstitial-substitutional solute-atom clusters and not to fine scale precipitation of γ-NbN.

Khachaturyan (1969) has shown that fine scale precipitation may occur in a periodic array to minimise the bulk strain energy of alloy systems where the precipitate exhibits a large misfit parameter. This type of precipitation can produce similar microstructures to those observed in alloys during spinodal decomposition, and may explain the existence of periodic structures outside the modulated structure solvus. Krawitz and Sinclair (1974) have shown however that lattice parameter measurements can be used to determine unequivocally the difference between a solid-random or non-random solution (interstitial-substitutional solute-atom clusters) - and fine scale precipitation. The lattice parameter of the matrix decreases during fine scale precipitation due to solute depletion whilst no change occurs during clustering. A review of a large number of systems shows that the invariance of the lattice parameter occurs during clustering in both G.P. zone formation and spinodal decomposition. The lattice parameter of the modulated structure in Fe:35Ni:Nb alloys is equal to that of a non-random solid solution of the same niobium

and nitrogen concentrations (Table IV.2) and remains constant during modulation coarsening (Table IV.1 and Figure IV.14a). Where no marked increase in the lattice parameter occurs after nitriding, the subsequent electron microscopic examination shows precipitation of γ-NbN. Therefore the modulated structure is formed by clusters and not a fine dispersion of γ-NbN, and the results suggest that the modulated structure may be formed by spinodal decomposition.

As the modulated structure overages, Fe, Ni and excess N atoms are probably rejected in favour of Nb atoms until the nitrogen-niobium atom ratio is appropriate to form discrete particles of γ-NbN. Preliminary results of weight gain observations at 650°C on thin specimens show that the weight decreases from 0.90wt%N after 5hrs to 0.83 at 24.5hrs. At lower temperatures there is insufficient time for "through"-nitriding before the modulated structure starts to overage and so the resulting weight gain appears to remain constant. Driver et al (1974) has suggested that the excess nitrogen which is rejected from the modulations in nitrided Fe:35Ni:V alloys might be retained at the interface of the VN precipitate. This may explain the observed behaviour at 600°C in nitrided Fe:35Ni:Nb alloys where the weight remains constant after the modulated structure decomposes. At higher temperature the

modulations overage more rapidly and nitrogen probably diffuses more readily out of the specimen. γ-NbN then occurs as discrete particles of 30-35 Å in diameter.

The presence of fine scale precipitations of γ-NbN and side-bands in diffraction patterns after prolonged ageing at 550 and 600°C of nitrided Fe:35Ni:Nb alloys, after hydrogen reduction at 600°C (Figure IV.15), and also after nitriding at potentials insufficient to exceed the modulation solvus are similar to the observations made by Driver et al (1974) in nitrided Fe:35 Ni:V alloys. These observations of a fine scale precipitation of γ-NbN and side-bands in X-ray diffraction patterns are also similar to those made by Hillert, Cohen and Averbach (1961) in Cu:Ni:Fe alloys outside the spinodal.

This suggests that at some critical stage of the coarsening process, one observes, on an electron diffraction pattern the replacement of side-bands by diffuse γ-NbN spots which evolve towards sharp characteristics γ-NbN spots as the precipitates lose their coherency. During this transition stage separating full coherency from complete loss of coherency the following process may take place in a manner suggested by De Fontaine (1969): the selective growth and dissolution of coherent particles of γ-NbN and loss of coherency of the largest

particles. Since these mechanisms may operate simultaneously at different rates this may result in a very irregular structure containing clusters, coherent and incoherent precipitates of γ-NbN and may probably explain persistence of side-bands after the modulated structure has decomposed and the presence of side-bands outside the modulated structure solvus.

At temperatures above $600^{o}C$ the modulated structure is formed near the surface and, due to the slow build up of the nitrogen, stacking-fault and homogeneous precipitation of γ-NbN is observed (Figure IV.16) in the centre of the specimen.

IV.4.2 Homogeneous precipitation of γ-NbN.

Homogeneous precipitation of γ-NbN occurs in Fe:35Ni:Nb alloys during nitriding at $800^{o}C$, as the modulated structure overages, and at nitrogen potentials outside the modulated structure solvus at temperatures $750^{o}C$ in $NH_3:H_2$ gas mixtures.

Electron microscopic examination of Fe:35Ni:0.5, 1, and 2Nb alloys nitrided at $800^{o}C$ in 1:99 $NH_3:H_2$ show coarsening rates for γ-NbN precipitates of 49.89, 8.61 and 5.65×10^{-25} cm^3/sec respectively (Figure IV.19).

The coarsening rates of γ-NbN precipitates in Fe:35Ni:1 and 2Nb alloys nitrided in 1:99 $NH_3:H_2$ at 800°C increased to 3.46 and 2.89 x 10^{-22} cm^3/sec during hydrogen reduction after removal of the excess nitrogen. The particle size distribution of γ-NbN during coarsening is found to exist over a narrow range where the ratio of the precipitate radius over the mean particle radius varied between 0.25 and 2 with a maximum close to the mean radius.

Lifshitz and Slyozov (1961) and Wagner (1961) explained the time dependence of particle size coarsening by a diffusion controlled mechanism by assuming a narrow Gaussian distribution of size for the initial spherical particles and that the volume fraction of precipitate remained constant during coarsening. For coarsening times greater than that taken for the initial distribution to reach a steady state the approximate variation in mean particle radius r at any time t is given (Wagner 1961) as:

$$r^3 - r_o^3 = kt \qquad \text{.... IV.6}$$

$$k = \frac{8\ 6\ C_o\ Vm^2\ D}{9RT} \qquad \text{.... IV.7}$$

where r_o is the initial mean particle radius at the onset of coarsening:

δ, the matrix-particle interfacial energy;

C_o, the equilibrium molar concentration of solute in the matrix in mol/cm^3 ; $C_o = \frac{C_o wt\% \times 8.2707}{92.906}$;

T, the temperature ^oK;

Vm, the molar volume of γ-NbN (25.167 mol/cm^3) ;

and R, the gas constant.

The observed particle size distribution does not obey the Lifshitz-Slyozov distribution exactly but is similar to those observed experimentally by Jack (1969). A plot of r^3 against t (Figure IV.19) obeys the Wagner relationship for particle coarsening.

The equilibrium value of niobium solubility in Fe:35Ni:1 and 2Nb alloys nitrided in $1NH_3:99H_2$ at 800^oC is determined as 2.1 and 3.9 x 10^{-3} wt%Nb respectively (by equating the coarsening rates of γ-NbN k_1, and k_2 before and after hydrogen reduction, and assuming that γ-NbN redissolves after prolonged hydrogen reduction) from:

$$C_i = \frac{k_i C_2}{k_2} \quad \ldots\ldots \text{IV.8}$$

where C_i is the concentration of niobium in equilibrium with nitrided Fe:35Ni:Nb;

and C_2 is the concentration of niobium in solution after hydrogen reduction.

Using these values of niobium solubility and the nitrogen solubility in Fe:35Ni, a solubility product of γ-NbN at 800°C in Fe:35Ni:1 and 2Nb alloys is determined as 0.945, and 1.68×10^{-4} which is much larger than the predicted value of 3.16×10^{-6} for NbN in austenitic Fe:Nb:N alloys (Smith, 1966; Mori et al, 1964).

The value of the matrix-γ-NbN particle interfacial energy σ_1 can be derived from the grain boundary interfacial energy σ_2 and the dihedral angles (θ_1 and θ_2) made at the grain boundaries between γ-NbN and austenite (θ_2) and γ-NbN (θ_1) (after Smith 1948) where:

$$\sigma_1 = \frac{\sigma_2 \sin\theta_2}{\sin\theta_1} \quad \ldots\ldots \text{IV.9}$$

The dihedral angles θ_2 and θ_1 were determined from 50 particles as $134.9 \pm 8.2°$ and γ-NbN as $90.2 \pm 8°$. Using a value of the grain boundary surface energy in austenite of 850 ergs/cm^2 (Vlack, 1951) the matrix-γ-NbN interfacial energy is found to be 600 ± 90 ergs/cm^2. Herring (1951) found that grain boundary precipitates in solids are subjected to angular forces which attempt to turn the grain boundaries into crystallographic orientations which have a lower strain energy. After prolonged

ageing the platelets of γ-NbN re-align at an angle to the grain boundary in order to minimise their elastic strain energy. Since the error involved in determining the dihedral angle is large, any correction for the re-alignment of γ-NbN can be ignored.

Using the values of 6 the interfacial energy and the niobium solubility in nitrided Fe:35Ni:1 and 2Nb the effective diffusion coefficient is determined as 7.9 and 4.3 x $10^{-14}cm^2$/sec. which are an order of magnitude larger than the value of 4.3 x $10^{-15}cm^2$/sec. (Spark , James and Leak, 1965).

The interfacial energy of γ-NbN is the sum of the chemical energy due to mismatch of bonds across the boundary and the geometric energy due to the dislocation structure of the boundary (Swalin, 1962). The chemical strain energy of {111} planes in face centred cubic materials is less than that for {100} planes (Swalin, 1962). This may explain the formation of approximate octahedra γ-NbN with faces parallel to {111} planes during the early stages of ageing Fe:35Ni:Nb in $NH_3:H_2$ at 800°C. As the γ-NbN precipitates lose coherency with the matrix the geometric strain energy may become significant (because of the large mismatch between γ-NbN and Fe:35Ni of 22%) and hence cause the octahedra to transform to platelets parallel on the softer {100} planes.

The variation in particle size at the centre of specimens of different thicknesses did not obey the relationships determined by Kahlweit (1965). The variation in particle size with specimen thicknesses is similar to internal oxidation of Cu:Al alloys (Wood, 1959) where the deviation from the theory is most marked for higher alloy contents.

The modulated structure overages more rapidly to a fine dispersion of γ-NbN in nitrided Fe:35Ni:Nb alloys in ammonia-hydrogen gas mixtures with a small oxygen potential. This effect is more marked as the modulated structure approaches its solvus temperature. The modulated structures formed in Fe:35Ni:Nb alloys nitrided at 600°C in 10:90 $NH_3:H_2$ are less stable in specimens pre-annealed for 0.5h at 1200°C in an evacuated silica capsule than similar treated specimens in an aluminium capsule. Even though the oxygen content of the nitriding gases is maintained at a low level the affinity of niobium for oxygen in Fe:35Ni:Nb alloys is such that traces of δ-NbN(O) are formed after prolonged nitriding and δ-NbN(O) and ϵ-NbN(O) are formed after hydrogen reduction.

IV.4.3 Stacking fault precipitation of γ-NbN.

Stacking fault precipitation of γ-NbN occurs at the

nitriding interface of Fe:35Ni:Nb alloys nitrided at 650 to 750°C, and in nitrogen potentials from 0.02 : 99.98 - 20:80 NH_3:H_2 at 700°C. The precipitates occur as discs on {111} planes, and are similar to those observed in quenched aged Fe:Cr:Ni:Nb:N alloys (Borland and Honeycombe, 1970). There is some evidence to suggest that the stacking fault density is reduced as the nitrogen potential increases, and increases with nitriding time. This is indicated by the hardness profiles (see Chapter V) and electron microspecimens. In very low nitrogen potentials 0.02 NH_3:99.98H_2 in thin microspecimens the density of precipitates is reduced. Borland (1969) found that stacking fault precipitation of γ-NbN in quenched aged Fe:Cr:Ni:Nb:N alloys had an incubation period of $\approx$ 20hrs and a growth period of $\approx$ 200hrs at 700°C. The effect of increasing the nitriding potential may reduce the incubation time for stacking fault precipitation, and at higher nitriding potentials the onset of homogeneous precipitation of γ-NbN may occur earlier due to the more rapid increase in nitrogen concentration. This may explain the observed decrease in stacking fault density at high and very low nitrogen potentials since in both cases there may be insufficient time for nucleation and growth before the onset of homogeneous precipitation. Preliminary calculations of the nitriding kinetics at 700°C in 10NH_3:90H_2 in Fe:35Ni:2Nb show that the onset of homogeneous precipitation

of γ-NbN occurs at 0.11wt%N, and from electron micrographs about 9% of the available niobium is then precipitated at stacking faults (Chapter V). This suggests that stacking fault precipitation occurs in Fe:35Ni:Nb alloys only when the niobium concentration exceeds the nitrogen concentration, and that homogeneous precipitation occurs at nitrogen potentials lower than 0.02 NH_3:99.98 H_2 at 700°C.

IV.5 Conclusions

Three structures are formed in nitrided Fe:35Ni:Nb alloys in NH_3:H_2 at 500-800°C:

(i) a modulated structure;

(ii) homogeneous precipitation of γ-NbN;

and

(iii) stacking fault precipitation of γ-NbN.

The modulated structure is formed by interstitial-substitutional solute-atom clusters formed periodically as rods in $\langle 100 \rangle$ directions on $\{100\}$ planes. The modulated structure is obtained when: the niobium concentration exceeds 0.5wt%; and at 600°C in ammonia: hydrogen mixtures where the NH_3/H_2 ratio is $>5/95$; when the niobium to nitrogen atom ratio is $<1:2$; and at temperatures $\doteq 750$°C. The modulated structure is associated with:

(i) side bands in electron and X-ray diffraction patterns;

(ii) a lattice parameter which is equivalent to a solid solution of niobium and nitrogen in Fe:35Ni; and

(iii) a lattice parameter which remains constant during modulation coarsening. The modulation coarsening rate is dependent upon niobium atom diffusion where the activation energy is 340 kJ/mol^{-1} (81 $Kcal/mol^{-1}$).

The morphology of the modulated structure is similar to that found by Driver et al (1974) in nitrided Fe:35Ni:V alloys and to the modulated structure formed in Cu:Ni:Fe alloys during spinodal decomposition (Butler and Thomas, 1970).

Homogeneous precipitation of γ-NbN occurred in all $NH_3:H_2$ mixtures at 800°C, also as a periodic array when the modulated structure overages, and at nitriding potentials or niobium contents outside the modulated structure solvus.

The orientation relationship of γ-NbN matrix are

$$(100)\ NbN\ //\ (100)_\gamma \quad \text{and} \quad [100]\ NbN\ //\ [100]_\gamma$$

The initial spheroidal precipitates of γ-NbN overage at 800°C to form approximate octahedra with faces parallel to {111} matrix planes and these octahedra overage to

form platelets of γ-NbN parallel to the {100} matrix planes. Homogeneous precipitation of γ-NbN is associated with a wide precipitate free zone at the grain boundaries, and the initial octahedra in the grain boundaries overage to form platelets of γ-NbN at an angle to the grain boundary in order to minimise their strain energy. The elastic strain energy of the γ-NbN-matrix interface is found to be approximately 600ergs/cm^2. The coarsening rate of γ-NbN at 800^{o}C obeys the Wagner relationship for particle coarsening where the effective diffusion coefficient of 4×10^{-14}cm^2/sec.

The solubility product of γ-NbN is found to be $\approx 1.3 \times 10^{-4}$ which is about two orders of magnitude larger than extrapolated form of values obtained by Smith (1962) and by Mori et al (1964). The particle size of γ-NbN increases with nitriding depth.

Stacking fault precipitation of γ-NbN occurs as discs on {111} planes, and are similar to those observed in quenched aged Fe:Cr:Ni:Nb:N alloys (Borland and Honeycombe, 1970). These precipitates are formed when the niobium concentration exceeds the nitrogen concentration (i.e. at the nitriding interface) at temperatures of 650-750^{o}C.

Chapter V

THE NITRIDING KINETICS OF Fe:35Ni AND Fe:35Ni:Nb ALLOYS

V.1 Introduction

Previous work by Mortimer (1971) on the nitriding of ferritic Fe:Cr alloys and Pope (1972) on ferritic Fe:V alloys has shown that with binary ferrite alloys containing strong nitride forming elements nitriding in NH_3:H_2 gas mixtures proceeds by the formation of a hard subscale which advances progressively into the material. In both cases the rate controlling step during constant activity ageing at 400 to 600°C is by nitrogen diffusion through the matrix. Similarly the rate controlling step in nitriding pure α-iron (Darken, 1958) and γ-iron (Grieveson and Turkdogan, 1964a) is nitrogen diffusion through the matrix.

V.2 Experimental

Fe:35Ni:0.0, 0.5, 1.0, and 2.0 wt%Nb alloys were prepared as 0.5 and 1.25mm thick strip and annealed for 2hrs at 1200°C. The rate of nitriding was followed by two methods:

(a) by nitriding separate specimens for different times;

(b) by nitriding, weighing, sectioning, and re-nitriding the same specimens for different time intervals.

After each interruption a small sample was cut from the 1.25mm strip to measure the case depth and hardness profile.

V.3 Results

Typical hardness profiles and optical micrographs of Fe:35Ni and Fe:35Ni:Nb alloys nitrided in NH_3:H_2 gas mixtures at 600 to 800°C are shown in Figures V.1 to V.3.

At 600 and 800°C a single case is observed to advance at a parabolic rate into the specimen as shown in Figures V.4 and V.5.

However, at 650 to 750°C a double subscale is developed as shown by the hardness profiles and optical micrograph of Figure V.2 and V.6. From the optical microstructure a "tweed pattern" subsequently identified as due to stacking fault precipitation of γ-NbN (see Chapter IV) and corresponding to a lower hardness level can be seen in advance of the normal case. Similar parabolic nitriding rates were found for both subscales of the alloys nitrided

Fig. V. 1

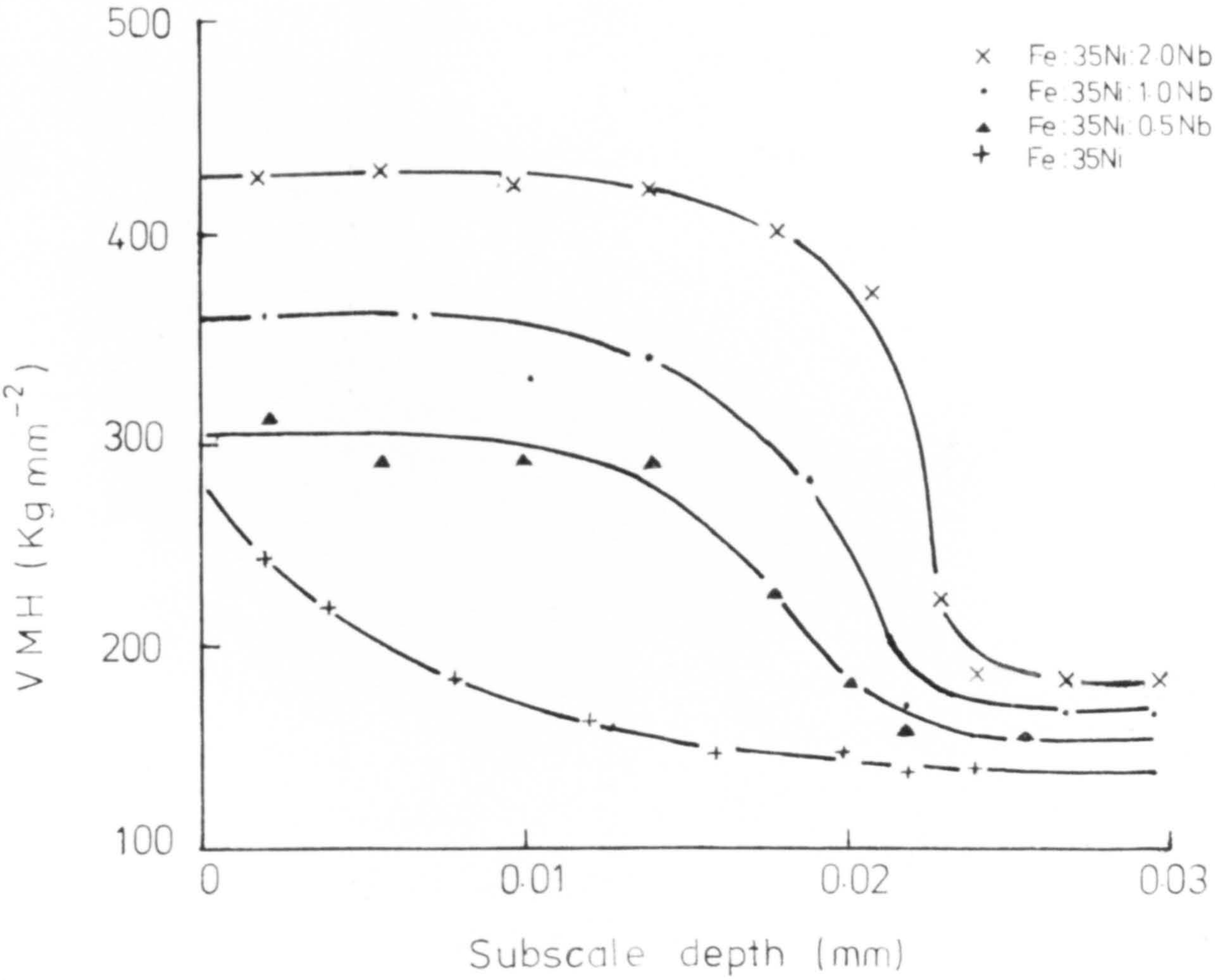

HARDNESS PROFILES OF Fe : 35Ni : 0 - 2·0Nb ALLOYS NITRIDED FOR 98hrs AT 600°C IN 20 : 80 $NH_3 : H_2$

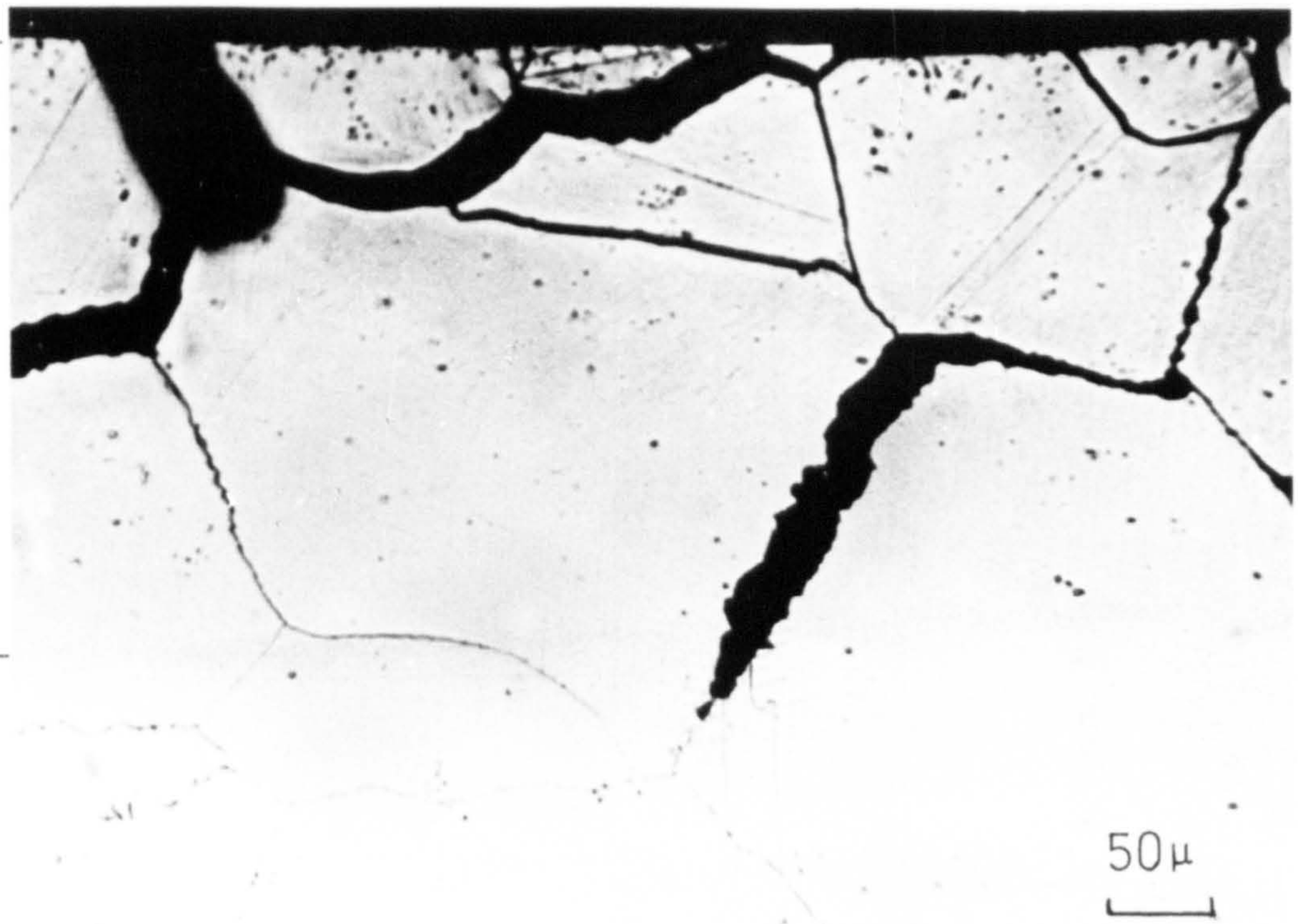

OPTICAL MICROGRAPH OF THE SUBSCALE IN Fe : 35Ni : 2Nb NITRIDED FOR 98hrs AT 600°C IN 20 : 80 $NH_3 : H_2$

Fig. V.2

Hardness profile produced by nitriding Fe-35Ni-2Nb at 700°C in 10%•NH_3:H_2 80hrs.

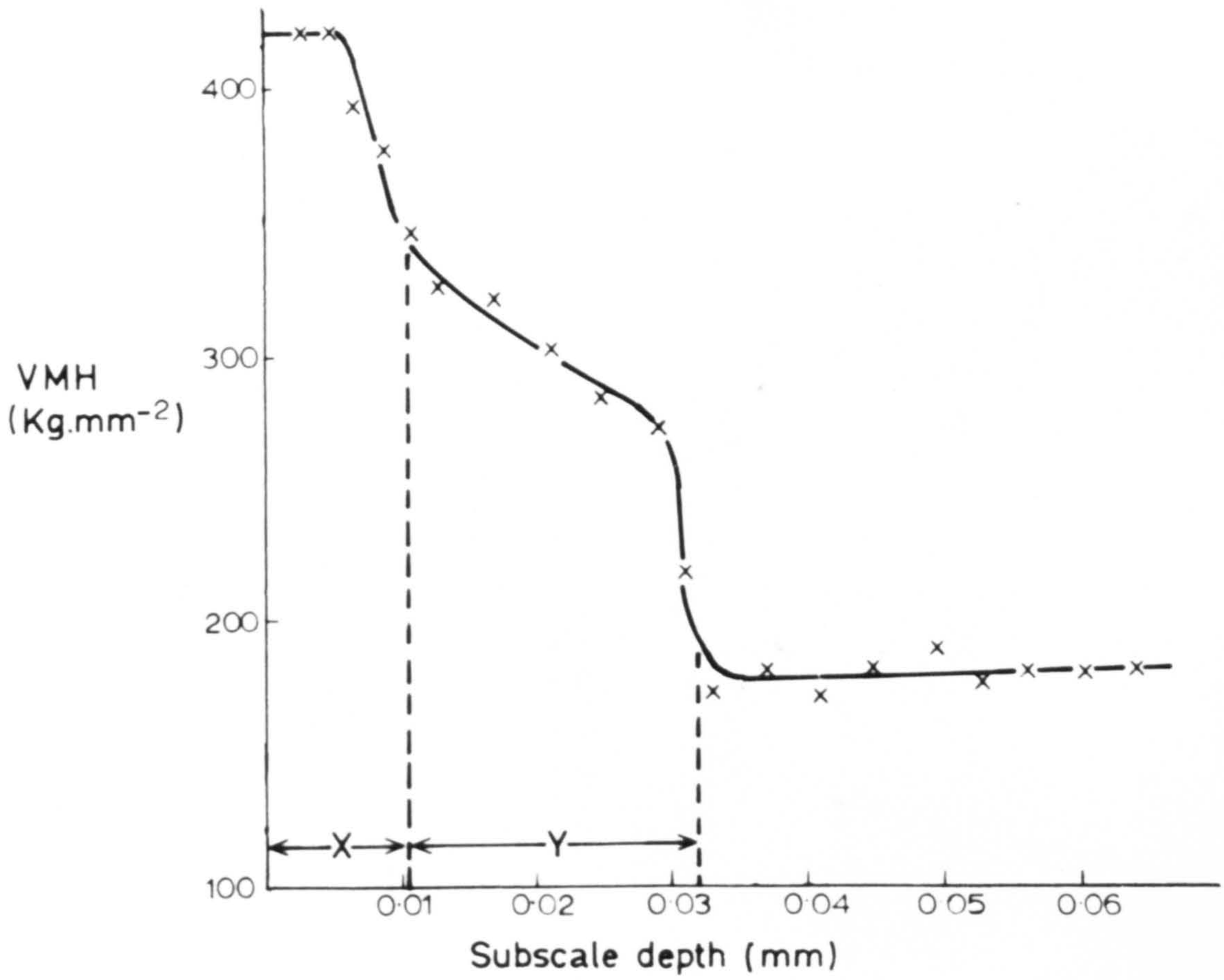

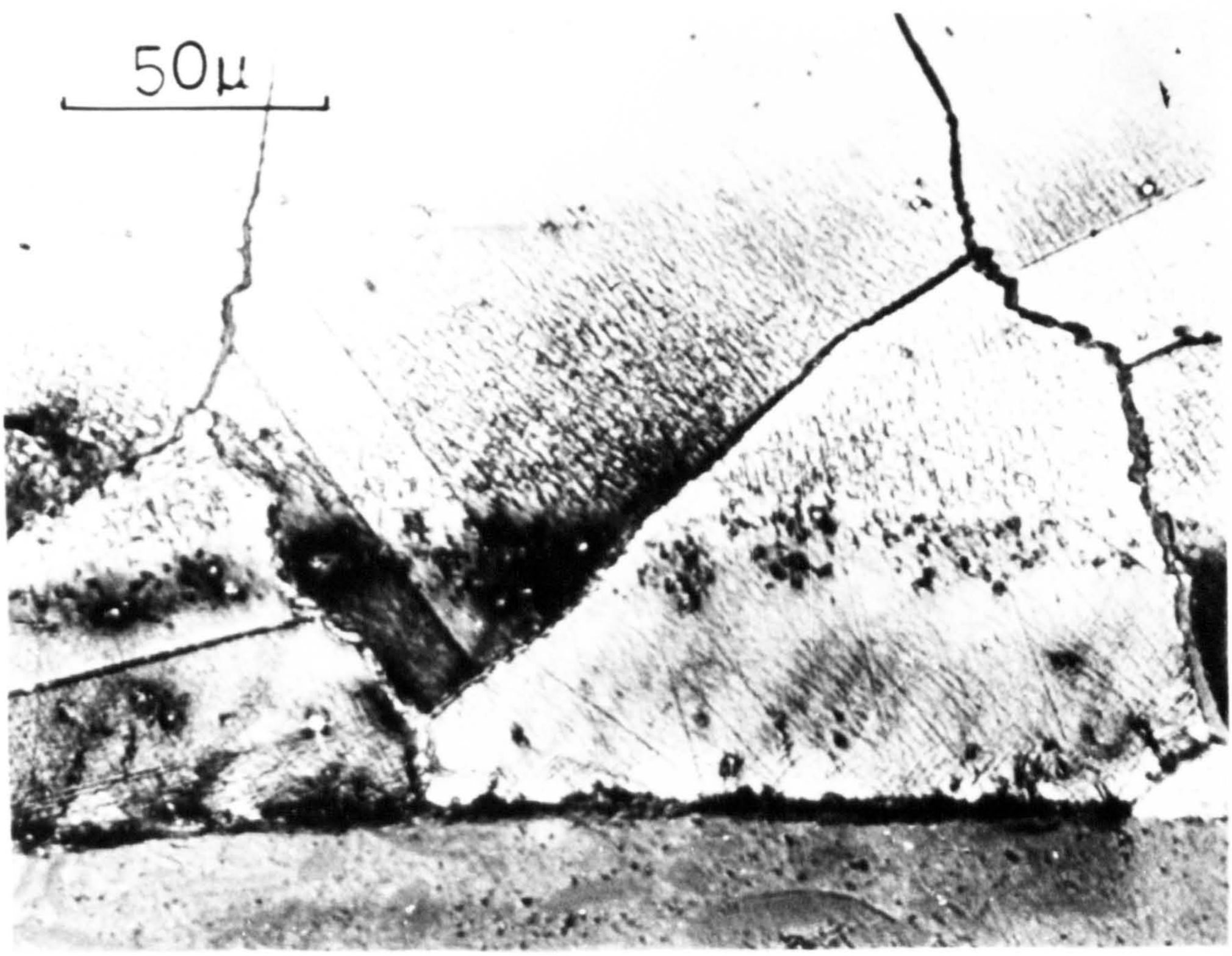

OPTICAL MICROGRAPH OF DOUBLE SUBSCALE IN Fe-35Ni-2Nb NITRIDED IN 10:90 NH_3:H_2 700°C 15 hrs.

Fig. V. 3

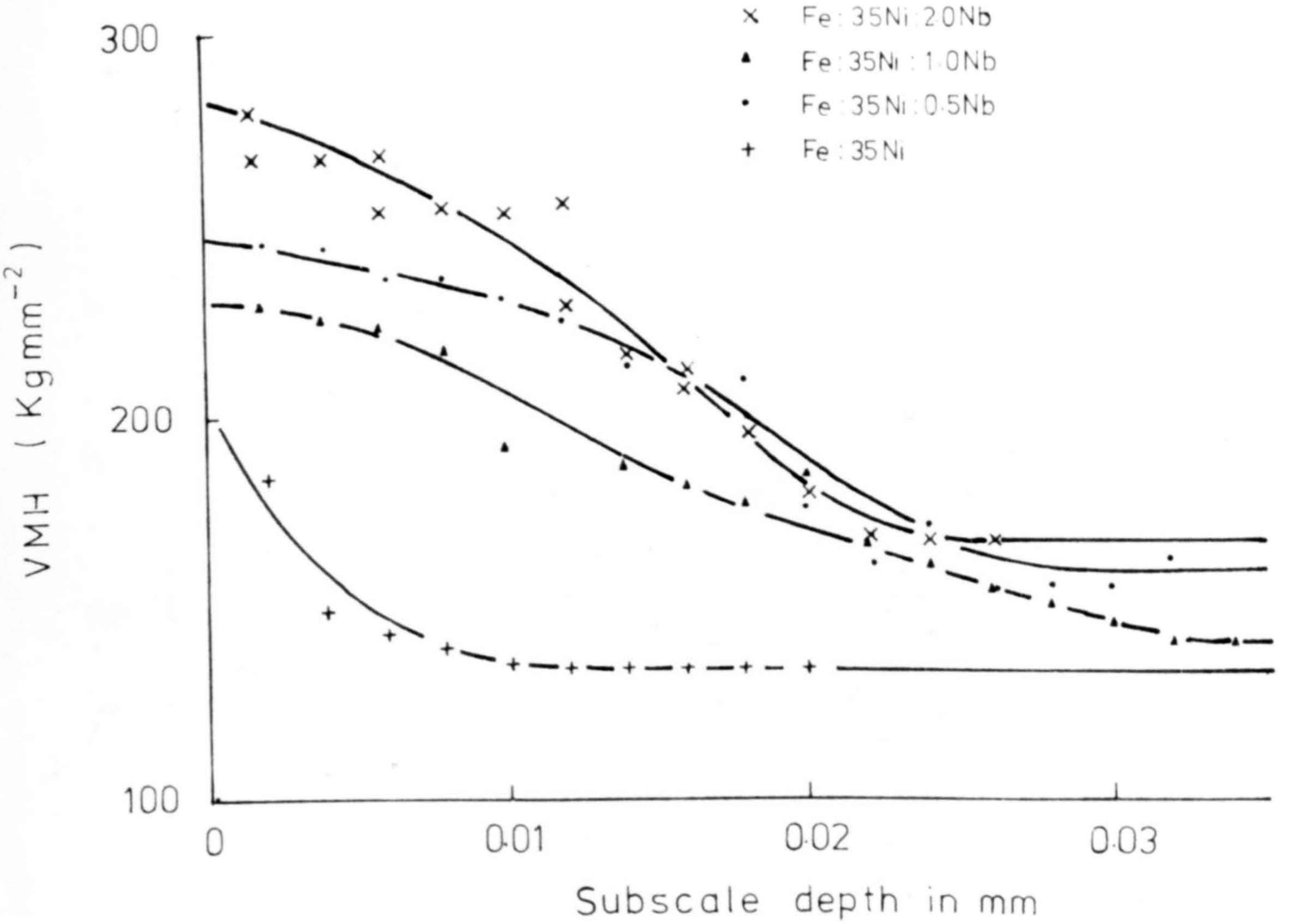

HARDNESS PROFILES OF Fe:35Ni:0-2·0Nb ALLOYS NITRIDED FOR 7hrs AT 800°C IN 7·8 : 92·8 NH_3:H_2

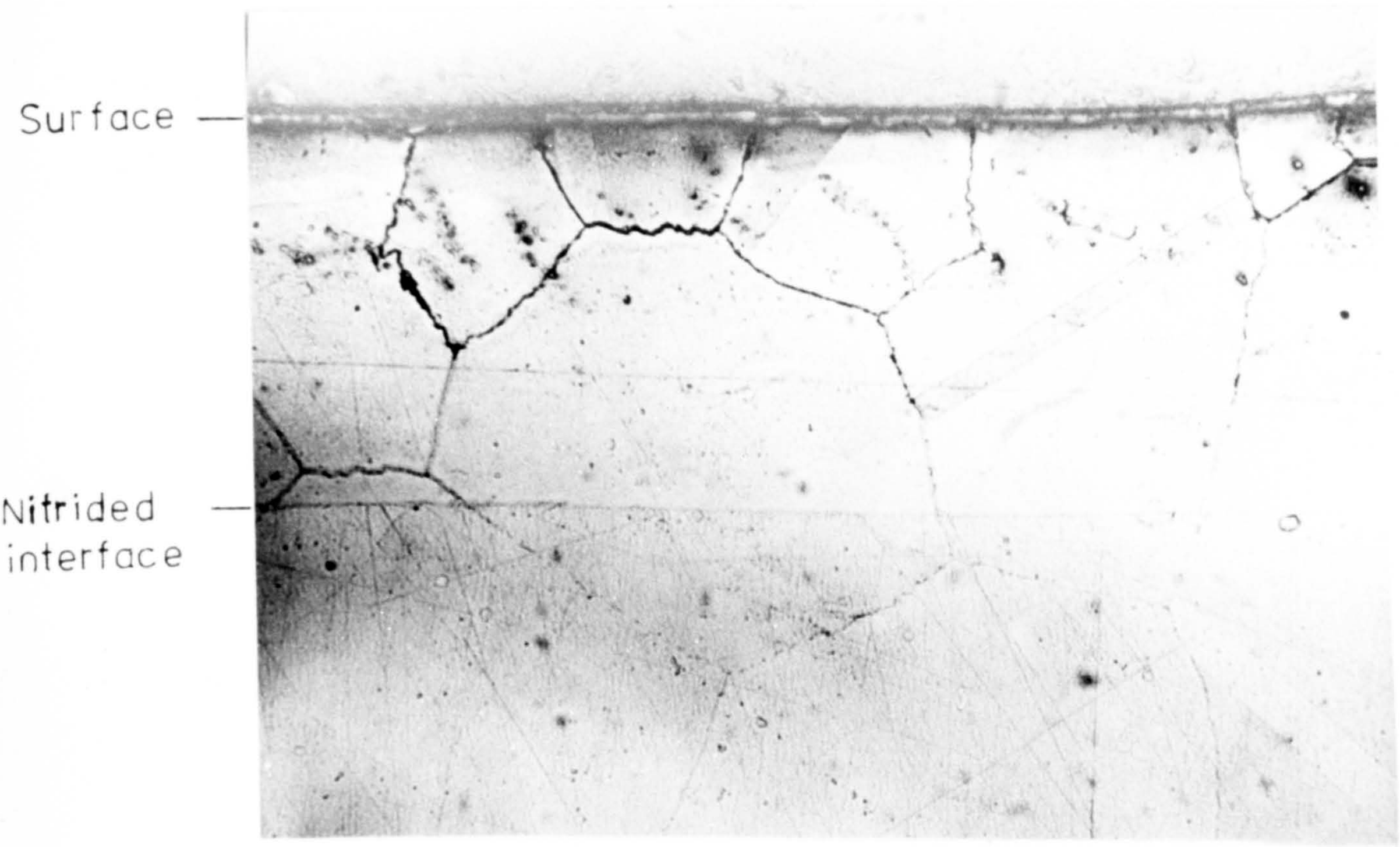

OPTICAL MICROGRAPH OF THE SUBSCALE IN Fe:35Ni:2Nb NITRIDED FOR 7hrs AT 800°C IN 7·2 92·8 NH_3:H_2

Fig. V. 4

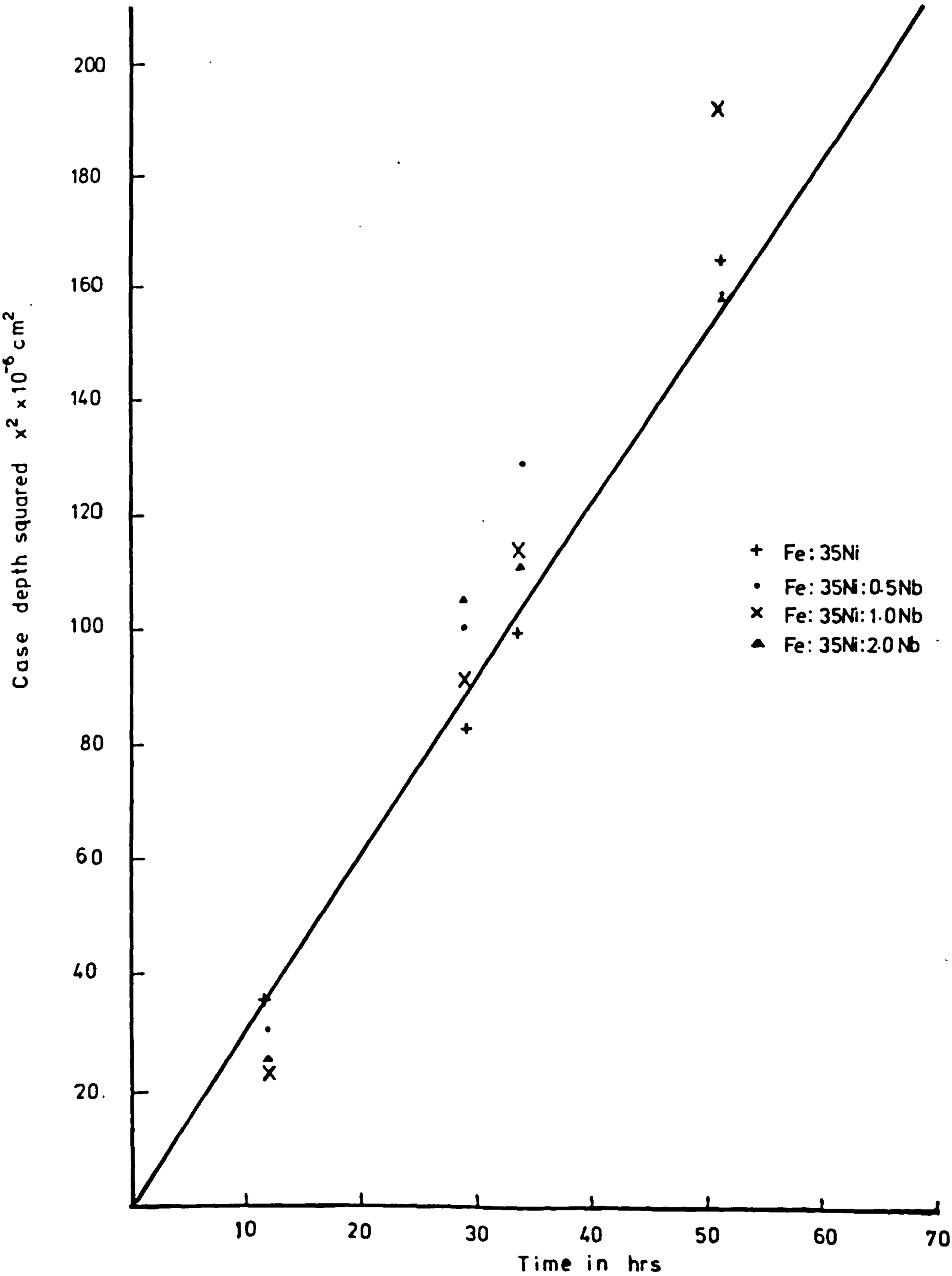

NITRIDING KINETICS OF Fe:35Ni:Nb ALLOYS IN 15:85 NH_3:H_2 AT 600°C

Fig. V.5

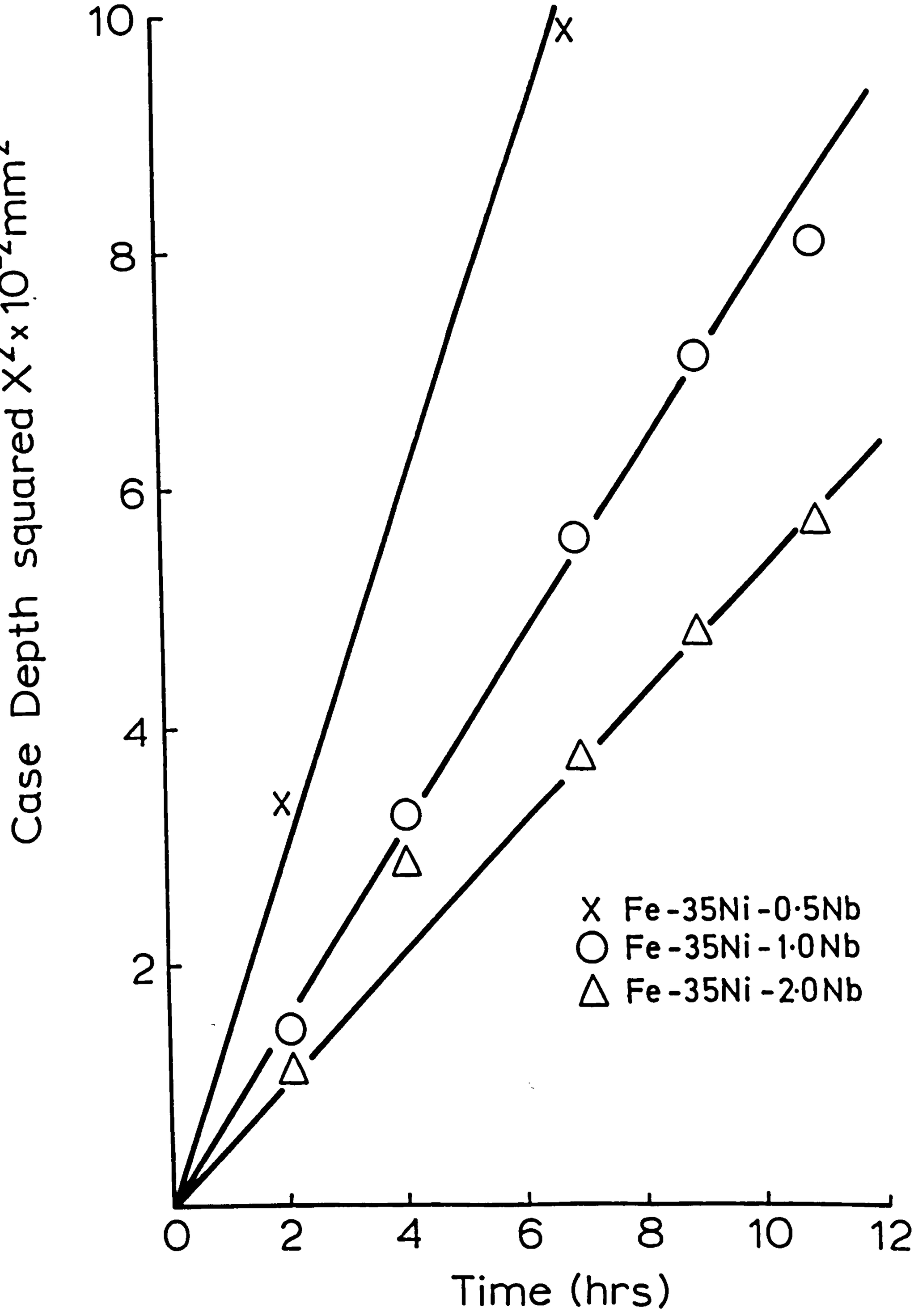

NITRIDING KINETICS OF Fe-35Ni-Nb ALLOYS
NITRIDED IN 8:92 NH_3:H_2 AT 800°C

Fig. V.6

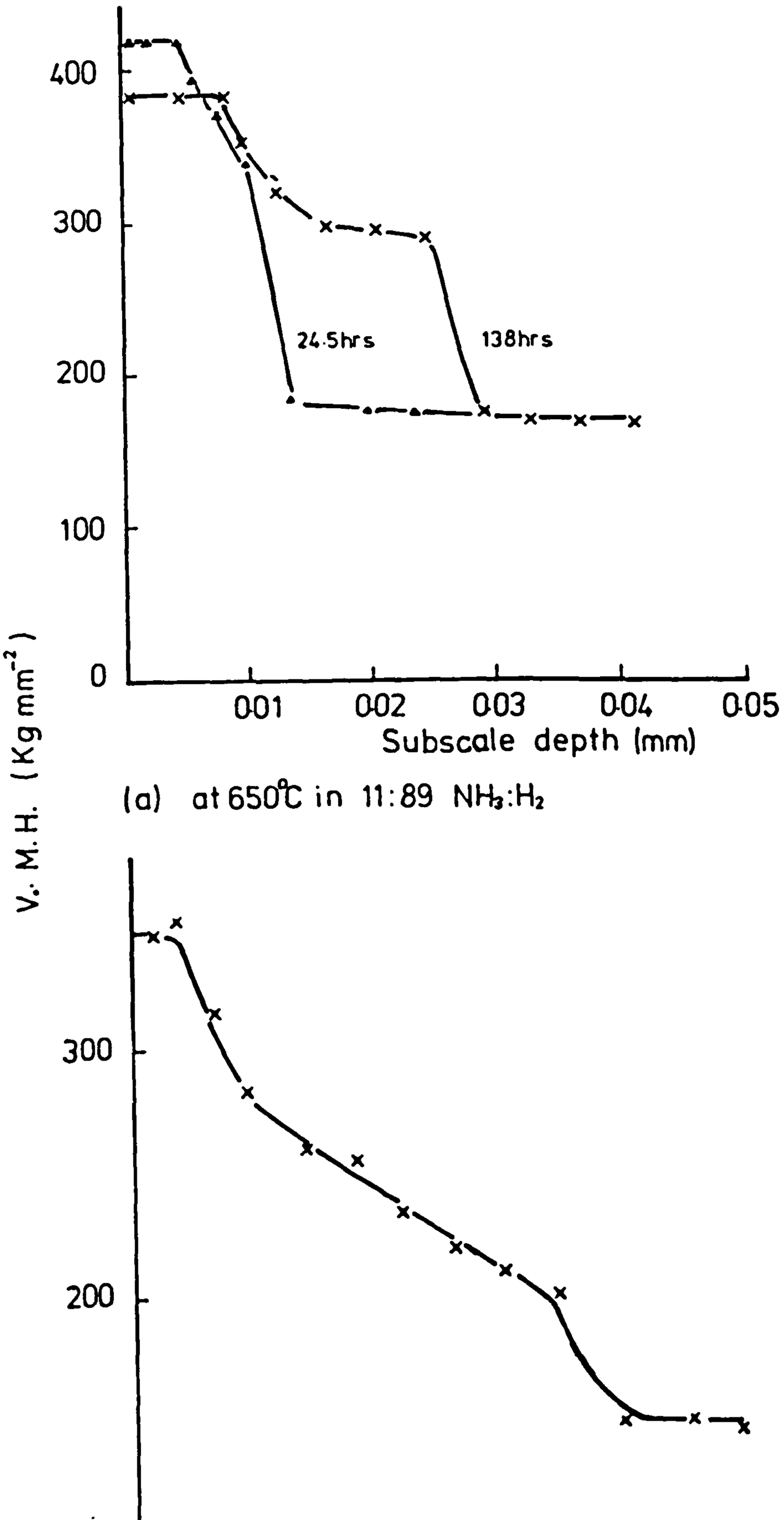

(a) at 650°C in 11:89 $NH_3:H_2$

(b) 17hrs at 750°C in 5:95 $NH_3:H_2$

HARDNESS PROFILES PRODUCED BY NITRIDING Fe:35Ni:2Nb AT (a)650°C AND (b) 750°C

at 700°C (Figures V.7a and b and 8). These results also demonstrate that by increasing the nitrogen potential the rate of nitriding of both subscales increases.

Alloys nitrided at 650°C and above showed a decrease in nitriding rate with increasing niobium content (Figures V.5, V.7 and V.8). However, at 500 to 600°C the case depth of the nitrided alloys appeared to be independent of niobium content and is similar to the depth of nitrogen in pure Fe:35Ni nitrided under similar conditions (Figures V.3 and V.4).

V.4 Discussion of results

V.4.a Nitriding kinetics of Fe:35Ni:Nb alloys at 800°C.

The nitriding kinetics of Fe:35Ni:Nb alloys at 800°C can be analysed by using an equation derived by Wagner (1959) and applied by Hepworth et al (1966) for the internal oxidation of a Fe:0.1wt%Al alloy in H_2:H_2O gas mixtures. Hepworth et al (1966) made the following assumptions which may be applied to nitriding kinetics:

(i) the nitrogen concentration decreases linearly from the surface to the interface between the nitrided and unnitrided zones;

(ii) the nitrogen concentration at the surface is in equilibrium with the gas phase;

Fig. V.7

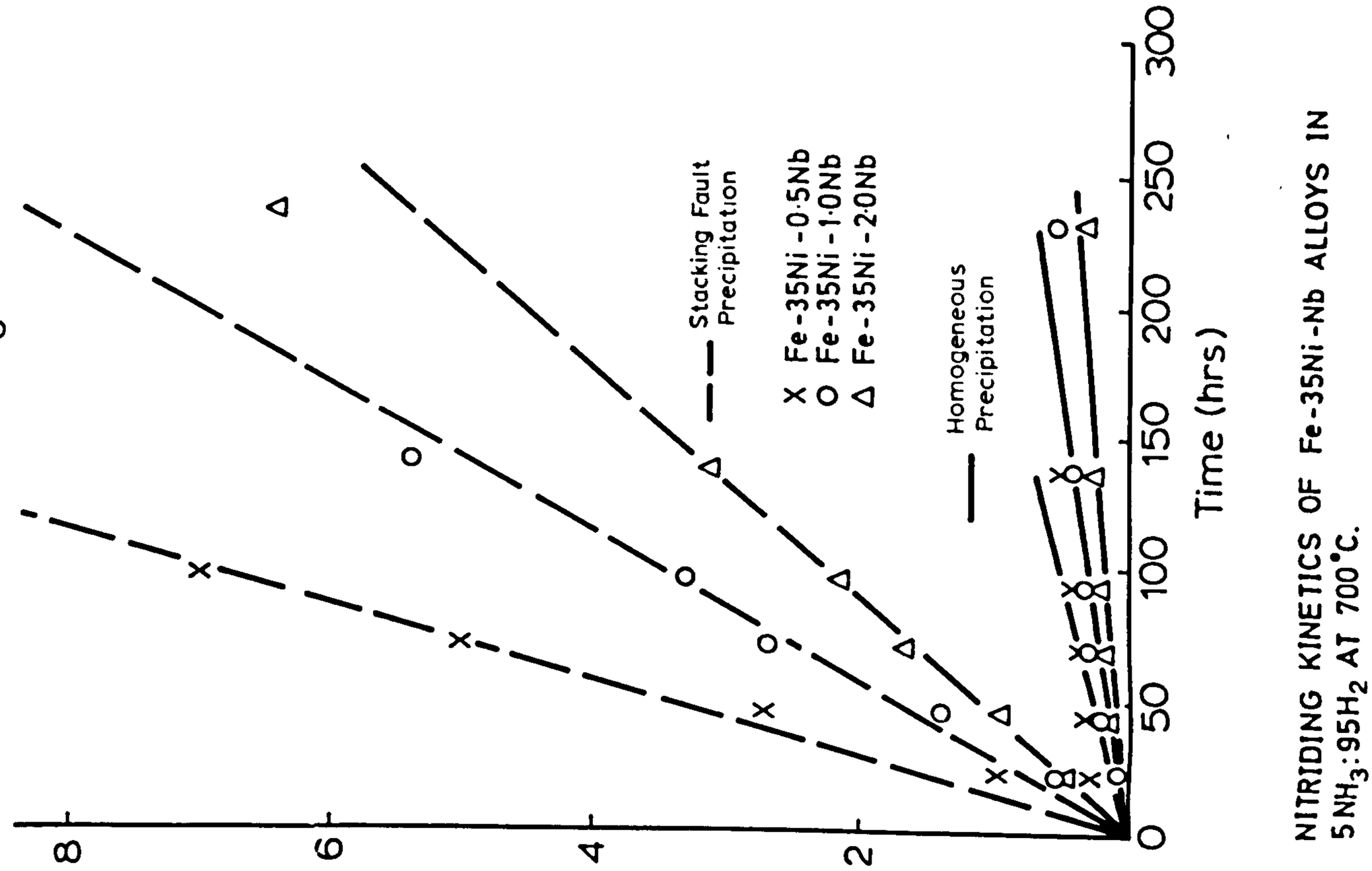

NITRIDING KINETICS OF Fe-35Ni-Nb ALLOYS IN $5NH_3:95H_2$ AT 700°C.

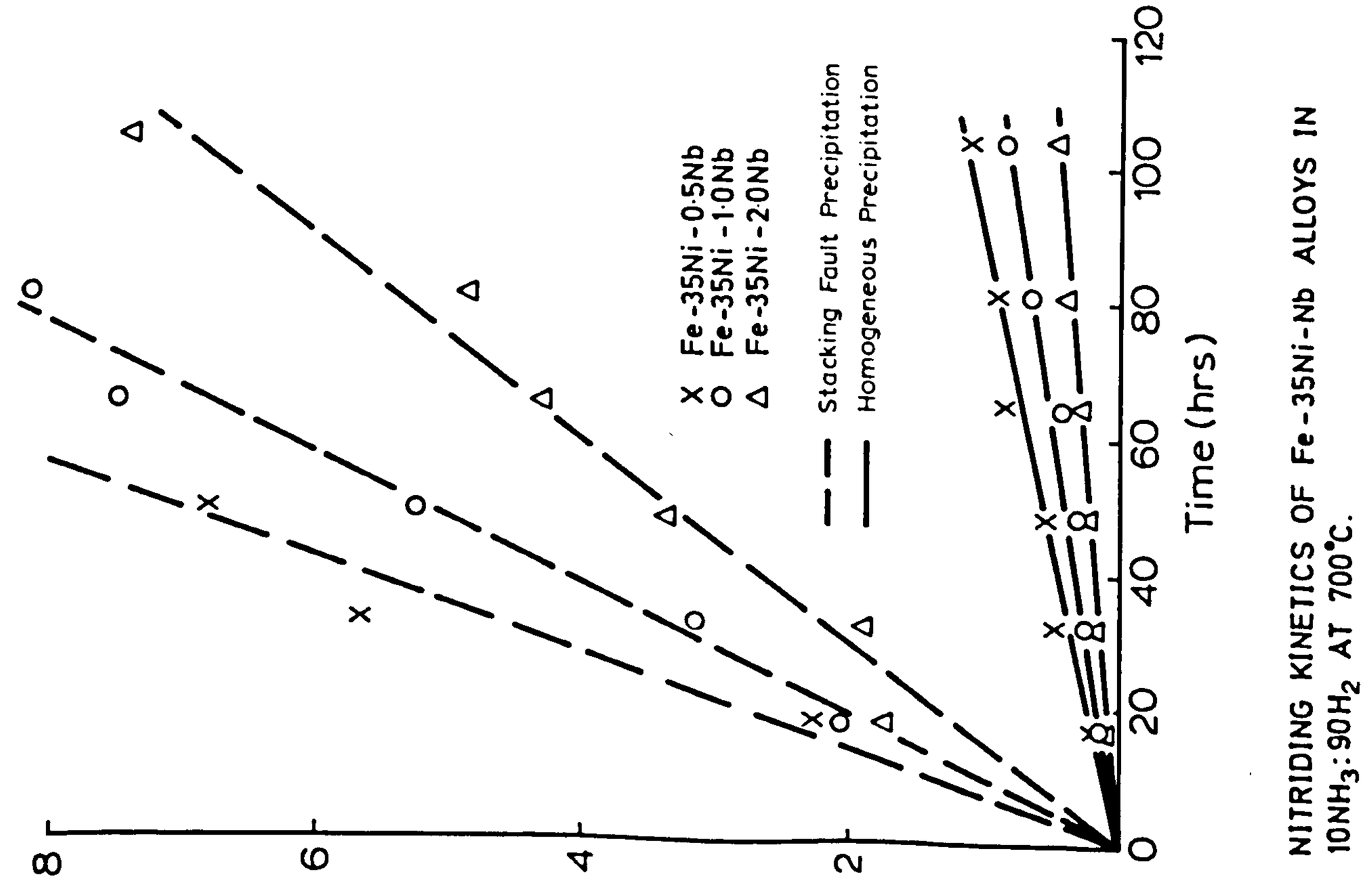

NITRIDING KINETICS OF Fe-35Ni-Nb ALLOYS IN $10NH_3:90H_2$ AT 700°C.

Fig. V. 8

Nitriding Kinetics of subscale advance of Fe-35 Ni-2Nb in NH_3:H_2 gas mixtures at 700°C.

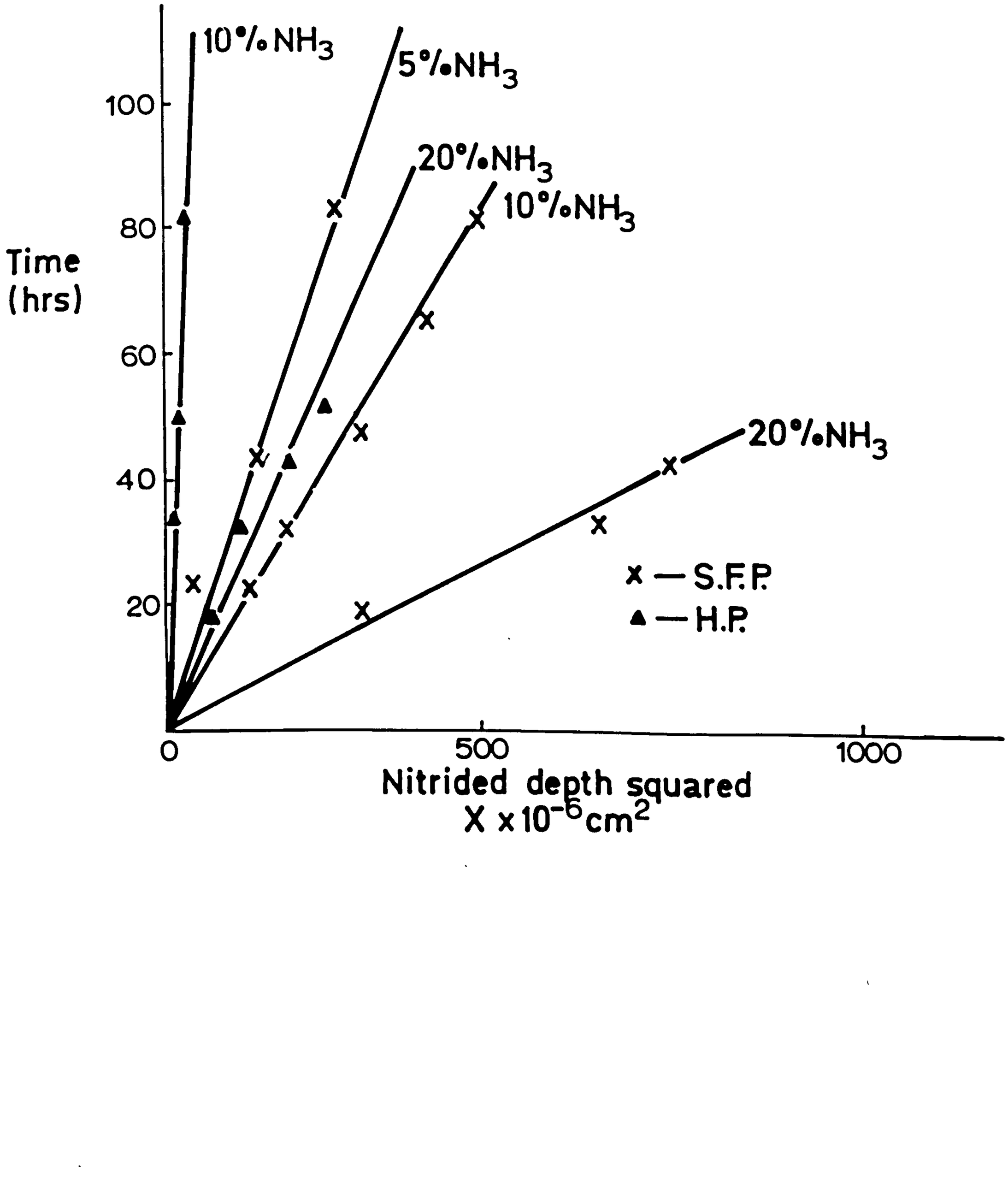

(iii) the niobium concentration and diffusivity in the alloy are such that counterdiffusion of niobium can be neglected;

(iv) the niobium and nitrogen concentrations are in equilibrium with γ-NbN at the interface of the case and the unnitrided core.

For the above conditions, and applying Fick's First Law, the kinetics of internal nitriding are given by:

$$\frac{dn}{dt} = \frac{c - c_1}{x} D \qquad \ldots\ldots \text{V.1}$$

where $\frac{dn}{dt}$ is the instantaneous flux of nitrogen into the specimen in gm atoms/cm^2 sec;

x is the instantaneous thickness of the nitrided layer;

c is the nitrogen concentration at the surface in equilibrium with the gas phase;

c_1 is the nitrogen concentration in Fe:35Ni:Nb alloys at the metal subscale interface in equilibrium with γ-NbN;

D is the diffusion coefficient of nitrogen in Fe:35Ni;

c_1 for γ-NbN at 800°C is $\approx 10^{-5}$ (Smith 1962) and hence can be ignored. The amount of nitrogen transported across unit area of the specimen is given by the mass

balance equation:

$$n = \frac{\rho}{zr} \ (wt\%Nb.10^{-2})x \qquad \ldots\ V.2$$

where ρ is the density of Fe:35Ni;

z is the atomic weight of niobium (92.8);

(wt%Nb) is the niobium concentration in the original material;

r is the nitrogen-niobium atom ratio in the nitrided layer.

By combining equations V.1 and V.2 and converting the nitrogen content to wt%,

$$\frac{dx}{dt} = \frac{92.8}{14\ r} \cdot \frac{(wt\%N)}{(wt\%Nb)} D \qquad \ldots\ V.3$$

and upon integrating:

$$\frac{x^2}{t} = \frac{92.8}{7\ r} \cdot \frac{(wt\%N)}{(wt\%Nb)} D \qquad \ldots\ V.4$$

The diffusion coefficients for nitrogen in Fe:35Ni: 0.5, 1.0, and 2.0Nb alloys at 800°C derived from the slopes of x^2 against t (Figure V.5) and equation V.4 are 5.6, 4.1 and 3.7 x 10^{-9} cm^2/sec respectively which compared favourably with the value of 5.7 x 10^{-9} cm^2/sec extrapolated from data of Grieveson and Turkdogan (1964a).

The rate of advance of subscale for other nitrogen potentials at 800°C can be determined from a plot of the outlet ammonia concentration against nitrogen solubility in Fe:35Ni and Fe:35Ni:Nb alloys as shown in Figure V.9.

V.4.b Nitriding kinetics of Fe:35Ni:Nb alloys at 650-750°C.

Under conditions for which a double subscale is formed the interpretation of results is more complex. Kindleman and Ansell (1970a) have studied in detail the nitriding kinetics of the double subscale formed by TiN precipitation in advance of chromium nitrides in nitrided austenitic Fe:Cr:Ni:Ti alloys. However, a simplified approach using a modified version of equation V.4 has been found adequate to analyse the present results if the nitrogen concentration varies linearly across the two subscales. The following symbols are defined:

C_3 is the surface concentration in equilibrium with the gas mixture;

C_2 is the nitrogen concentration at the primary-secondary interface;

and C_1 is the nitrogen concentration at the primary subscale-metal interface.

C_2 is thus the nitrogen concentration required to form homogeneous precipitates of γ-NbN; C_1 is the nitrogen concentration required to form stacking fault precipitation

Fig. V. 9

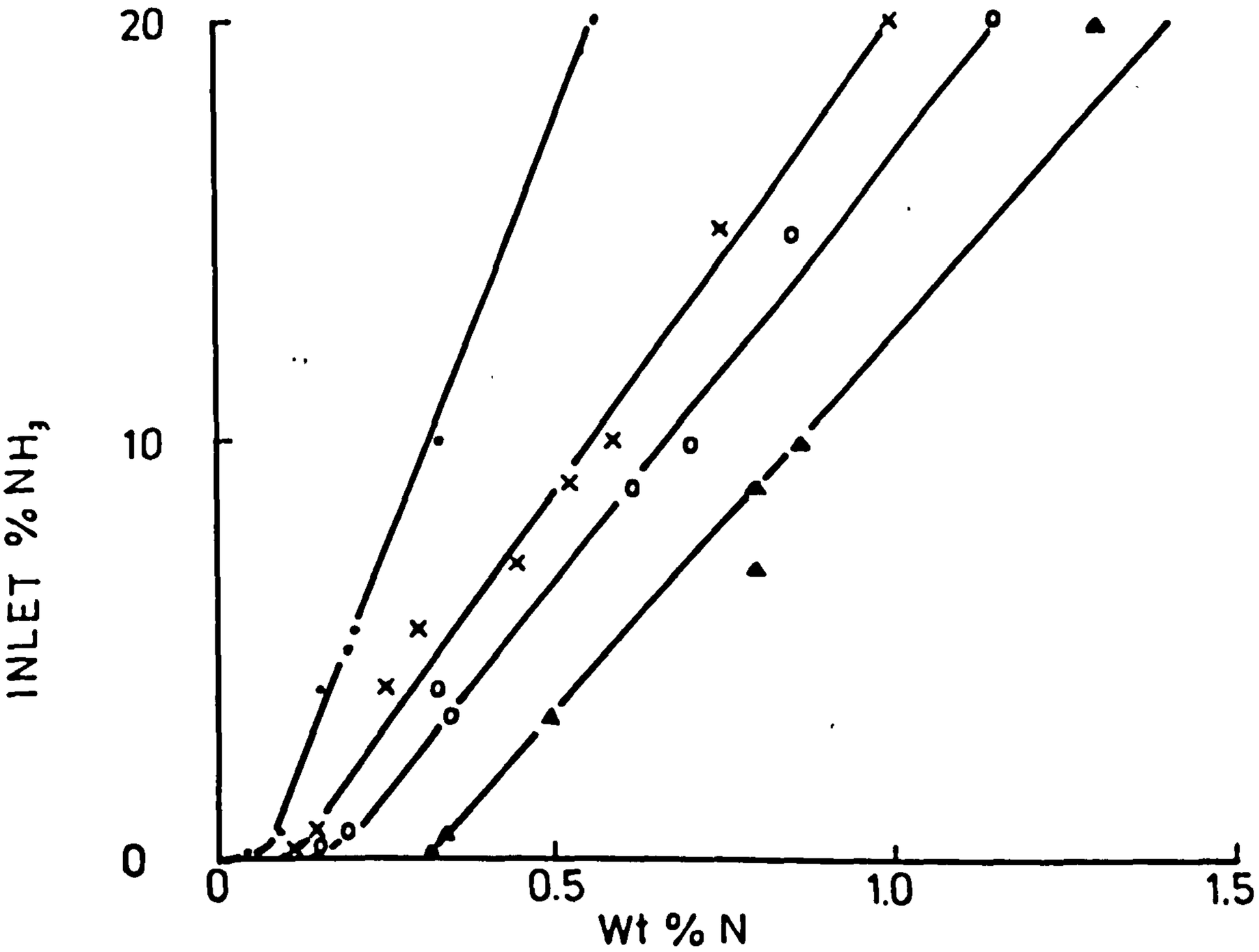

(a) ≃ 200hrs at 700°C

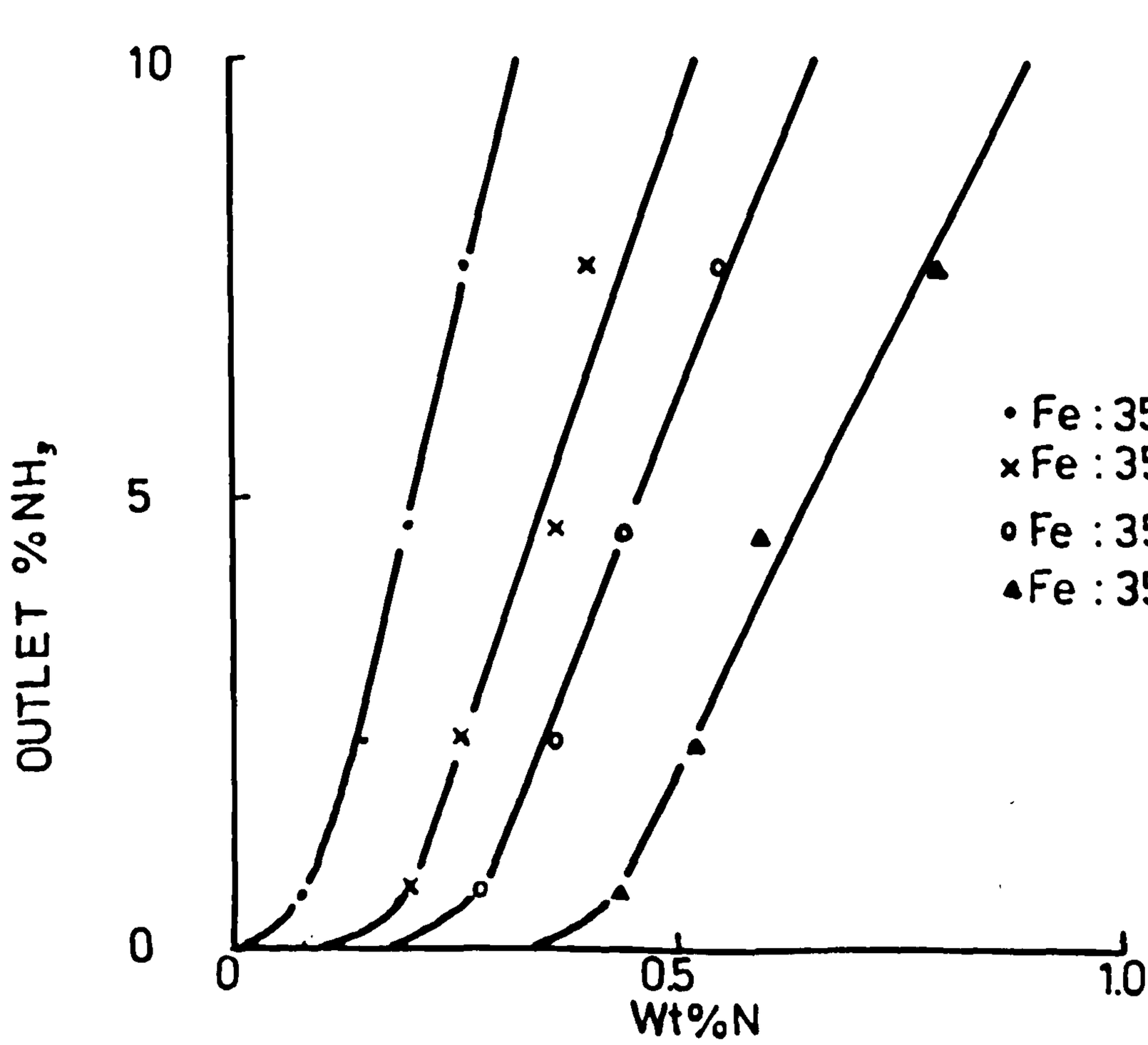

(b) ≃ 60hrs at 800°C

NITROGEN CONTENT OF Fe:35Ni:0-2Nb ALLOYS NITRIDED IN NH_3:H AT 700 & 800°C

of γ-NbN and is effectively zero since the solubility product of Nb and N is $\approx 10^{-6}$ at 700°C (Smith 1962). X is the thickness of the secondary (homogeneous γ-NbN) subscale and Y the thickness of the primary (stacking fault γ-NbN) subscale (Figure V.2).

Assuming that a fraction f of the niobium precipitates as γ-NbN in the stacking fault layer then the remaining fraction (1 - f) will precipitate homogeneously as γ-NbN in the secondary layer. The equation for internal nitriding when homogeneous precipitation occurs can therefore be written as

$$\frac{x^2}{t} = \frac{92.8}{7r_h(1-f)} \cdot \frac{C_3 - C_2}{wt\%Nb} D \quad \ldots\ V.5$$

where r_h is the nitrogen to niobium atom ratio in the homogeneous layer, and can be determined for different nitrogen potentials from a plot of the saturation nitrogen content in Fe:35Ni:Nb alloys against inlet ammonia concentration (see Figure V.9).

Similarly for the stacking fault precipitate layer the equation can be written as

$$\frac{Y^2}{t} = \frac{92.8}{7r_s f} \cdot \frac{C_2 - C_1}{wt\%Nb} D \quad \ldots\ V.6$$

where r_s is the nitrogen to niobium atom ratio in the stacking fault layer.

The nitriding rate of the primary stacking fault layer is higher than that of the secondary homogeneous case (Figures V.7 and V.8) as would be expected if f is relatively small and $(C_2 - C_1)$ is not too large. A typical value of f (the fraction of Nb precipitated as stacking fault precipitation of γ-NbN) derived from electron micrographs of Fe:35Ni:2Nb nitrided in 10 NH_3:90H_2 at 700°C is 0.09. From equations V.5 and V.6 the value of C_2 is calculated to be 0.11 wt%N where C_3 under these conditions is 0.32 wt%N. The diffusivity D of nitrogen in austenite at 700°C is calculated as $2.25 \times 10^{-10} cm^2/sec$ in Fe:35Ni:2Nb alloy nitrided in 10 NH_3:90H_2 compared with the value of $8.3 \times 10^{-10} cm^2/sec$ extrapolated from data by Grieveson and Turkdogan (1964a).

If there is a critical supersaturation C_2 for homogeneous precipitation of γ-NbN then C_2 is expected to be approximately constant at a constant Nb concentration for different nitriding potentials. However, for the Fe:35Ni:2Nb alloy nitrided in 20 NH_3:80 H_2 the value of C_2 is half that obtained for the same alloy nitrided in 10 NH_3:90H_2 assuming f remains constant. This simplified assumption of constant f for these fast

nitriding rates is therefore erroneous. This is reasonable since the nucleation and growth of stacking fault precipitation is a relatively slow process in niobium containing austenites. For example, Borland (1969) found that stacking fault precipitation of γ-NbN in Fe:Cr:Ni:Nb:N alloys had an incubation period of $\approx$20h and a growth period of $\approx$200h at 700°C. Hence at higher nitriding potentials the amount of stacking fault precipitation will be reduced since there is insufficient time for nucleation and growth before the onset of homogeneous precipitation. Some evidence for this suggestion is provided by the hardness profiles of the stacking fault precipitate layer. The hardness decreases with increasing depth within the specimen which indicates a variation in the stacking fault precipitate density throughout the primary layer.

V.4.c The nitriding kinetics of Fe:35Ni:Nb alloys at 500-600°C.

From Figure V.3 the rate of advance of the interface of the single case in Fe:35Ni:Nb alloys nitrided at 500-600°C is independent of niobium concentration, and is similar to the rate of penetration of Fe:35Ni. Lattice parameter measurements of these alloys nitrided at 600°C show that the modulated structure behaves as a clustered solid solution (Chapter IV). This unusual kinetic behaviour may possibly be explained by a variation of

effective surface nitrogen concentration with niobium concentration. For example, the wt%N term in equation V.4 is no longer the wt%N in equilibrium with Fe:35Ni but the wt%N in equilibrium with the Fe:35Ni:Nb solid solution. Thus since r the overall N:Nb atom ratio in the nitriding layer = wt%N 92.8 / wt%Nb14 both the (wt%N) and the (wt%Nb) terms in equation V.4 cancel out and hence:

$$\frac{X^2}{t} = 2D \qquad \text{.... V.7}$$

The diffusion coefficient of $5.3 \times 10^{-10} cm^2/sec$ for nitrogen diffusion in Fe:35Ni:Nb alloys nitrided in $15NH_3:85H_2$ and $20NH_3:80H_2$ is determined from the slope of the graph of case depth squared against nitriding time (Figure V.4) and equation V.11. This value is slightly higher than that obtained by Grieveson and Turkdogan (1964a) i.e. $7.6 \times 10^{-11} cm^2/sec$, but since the diffusivity of nitrogen in austenitic iron reported by other workers differs by an order of magnitude from that given by Grieveson and Turkdogan (see review by Grozier, Paxton and Mullins, 1965) the present value seems reasonable.

V.4.d The nitriding kinetics of Fe:35Ni.

Fe:35Ni specimens were nitrided at 500, 600, 700, and

800°C in $NH_3:H_2$ gas mixtures to give approximate constant surface nitrogen concentrations of 0.30 wt%N. At temperatures below 800°C the hardness profiles (Figure V.10) are similar to those observed in nitrided iron (Grieveson and Turkdogan, 1964a). Assuming that the nitrogen concentration is proportional to the hardness, the hardness profiles at 700 and 600°C could be analysed by an equation derived by Williamson and Adams (1919) for the heating up of a solid slab:

$$\frac{C_s - C_x}{C_s - C_o} = ht - \frac{h}{2D}\left(ax - \frac{x^2}{2}\right) \quad \ldots\ldots \text{V.8}$$

where C_s, C_x and C_o are the concentration of nitrogen at the surface, at x, and at the centre of the specimen respectively,

h, the nitrogen flux passing through unit surface area

D, the diffusion coefficient

a, the half specimen thickness

and x, the thickness of the nitrided layer.

The values of D calculated from Figure V.10 at 600 and 700°C are approximately 1.05×10^{-9} and 1.1×10^{-8} cm^2/sec respectively which are an order of magnitude larger than the values of 7.6×10^{-11} and 8.3×10^{-10} cm^2/sec extrapolated from Grieveson and Turkdogan (1964a). At 800°C the hardness profile appeared to be too insensitive

Fig. V.10

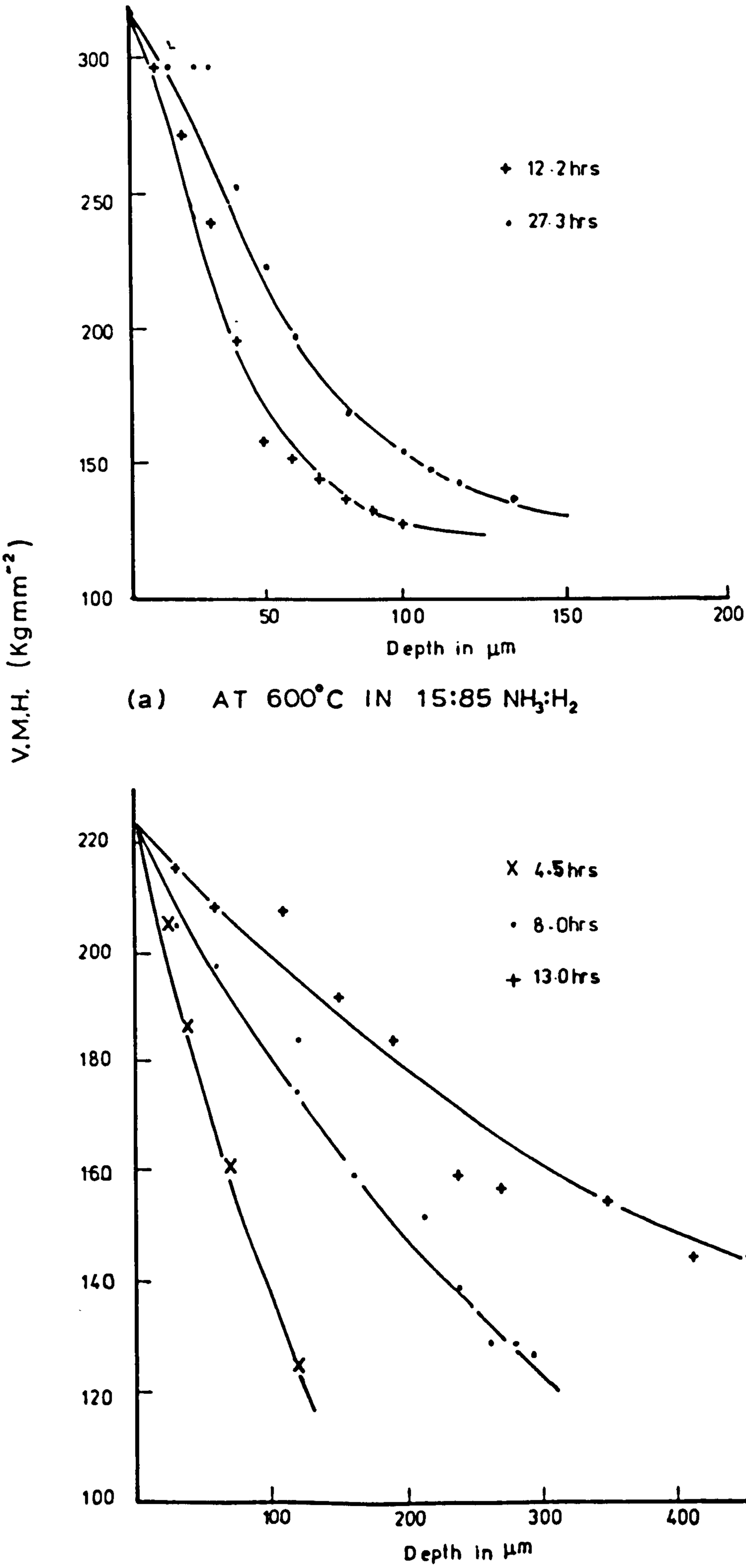

(a) AT 600°C IN 15:85 NH_3:H_2

(b) AT 700°C IN 20:80 NH_3:H_2

HARDNESS PROFILES OF Fe:35Ni NITRIDED AT a 600 AND b 700°C

to the nitrogen concentration to be analysed by equation V.8.

A plot of $\log \frac{x^2}{t}$ (the slope of case depth squared against the nitriding time) against the reciprocal of the nitriding temperature T is shown in Figure V.11. The activation energy derived from the slope of this plot is 176.4 $\pm$ 8.2 kJ/mol (41.7 Kcals/mol) which is in good agreement with the value of 168.44 kJ/mol (40.3 Kcal/mol) found by Grieveson and Turkdogan (1964a) for nitrogen diffusion in pure iron austenite.

V.5 Conclusions

(a) The nitriding kinetics at 800°C of austenitic Fe:35Ni:Nb alloys in which homogeneous NbN precipitation occurs are similar to the nitriding kinetics of ferritic alloys where the square of the subscale depth is:

(i) proportional to the nitriding time;

(ii) proportional to the surface nitrogen concentration; and

(iii) inversely proportional to the alloying element concentration.

(b) The above relationships hold for Fe:35Ni:Nb alloys

Fig. V. 11

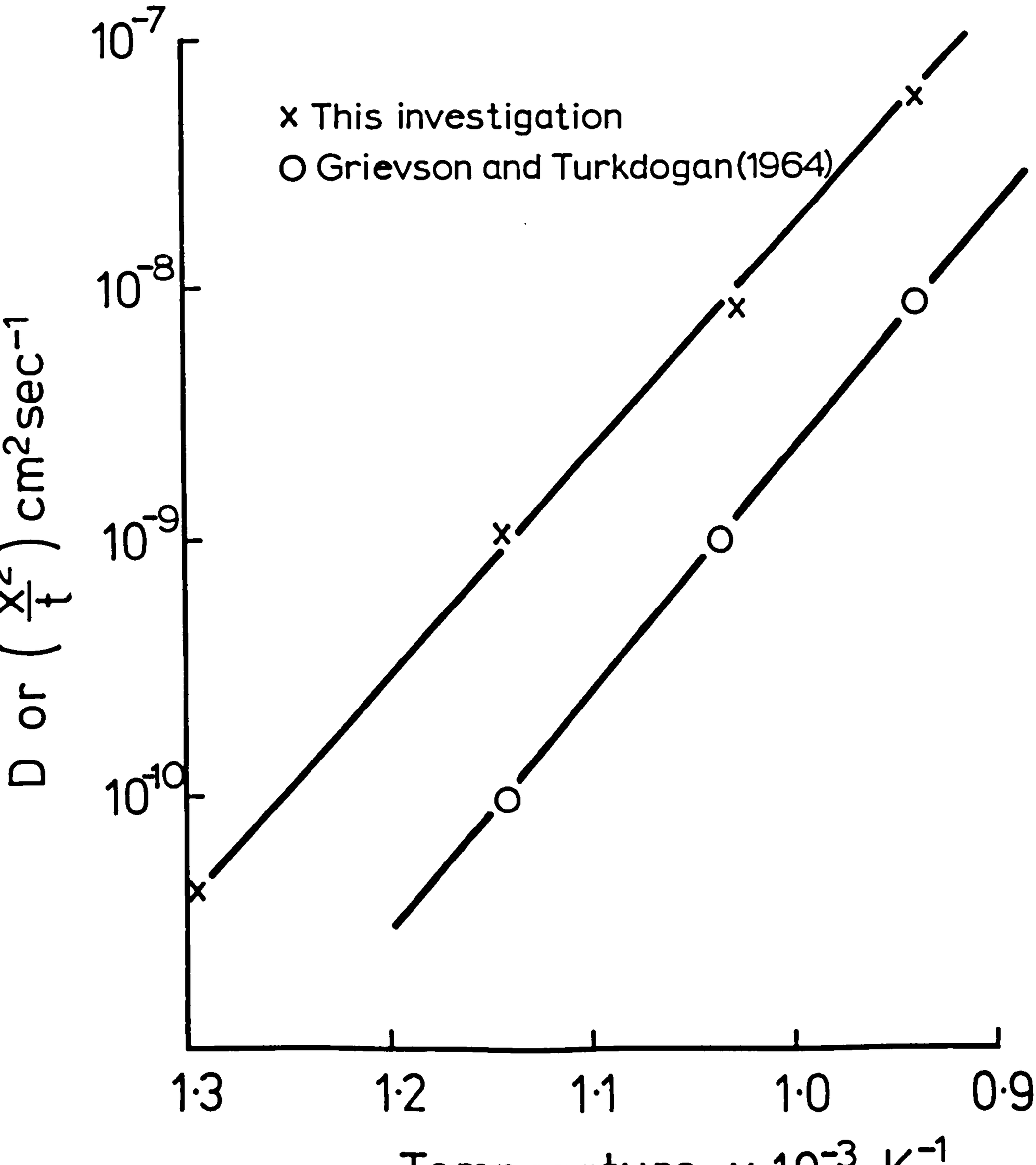

ARRHENIUS PLOT OF LOG (x^2/t) AGAINST 1/T FOR NITRIDED Fe-35Ni FOR A SURFACE CONCENTRATION OF NITROGEN (0·300 wt %N)

nitrided at 650 to 750°C where a double subscale is formed. The kinetics of the double subscale can be analysed by a modification of the usual equation for internal nitriding.

(c) The nitriding kinetics of the subscale advance at temperatures of 600°C and below, where a modulated structure is formed, is independent of the solute-atom concentration.

(d) The activation energy for nitrogen diffusion in nitrided Fe:35Ni of 176.4 kJol/mol (41.7 Kcal/mol) is in good agreement with that found by Grieveson (1964a) and Turkdogan in pure iron-nitrogen austenite.

Chapter VI

MECHANICAL PROPERTIES OF NITRIDED Fe:35Ni:Nb ALLOYS

VI.1 Introduction

Previous work by Roberts (1970) has shown that a high hardness and yield stress are developed by the G.P. zone structure in nitrided Fe-Nb alloys. These properties persist even after several hours overageing at temperatures approaching 700°C. However, the hardness and yield stress decreases rapidly after ageing at 800°C with the formation of the $Fe_{16}N_2$-type precipitate, and decrease still further with the formation of γ-NbN (Figure VI.1).

Kindleman and Ansell (1970b) have shown that the yield stress and tensile stress of nitrided austenitic Fe:18Cr:Ni:Ti alloys:

(i) increased with Ti content;

(ii) decreased with increasing specimen thickness due to a variation in the interparticle spacing and particle size with depth;

and

(iii) decreased with increasing test temperature.

Fig. V I.1

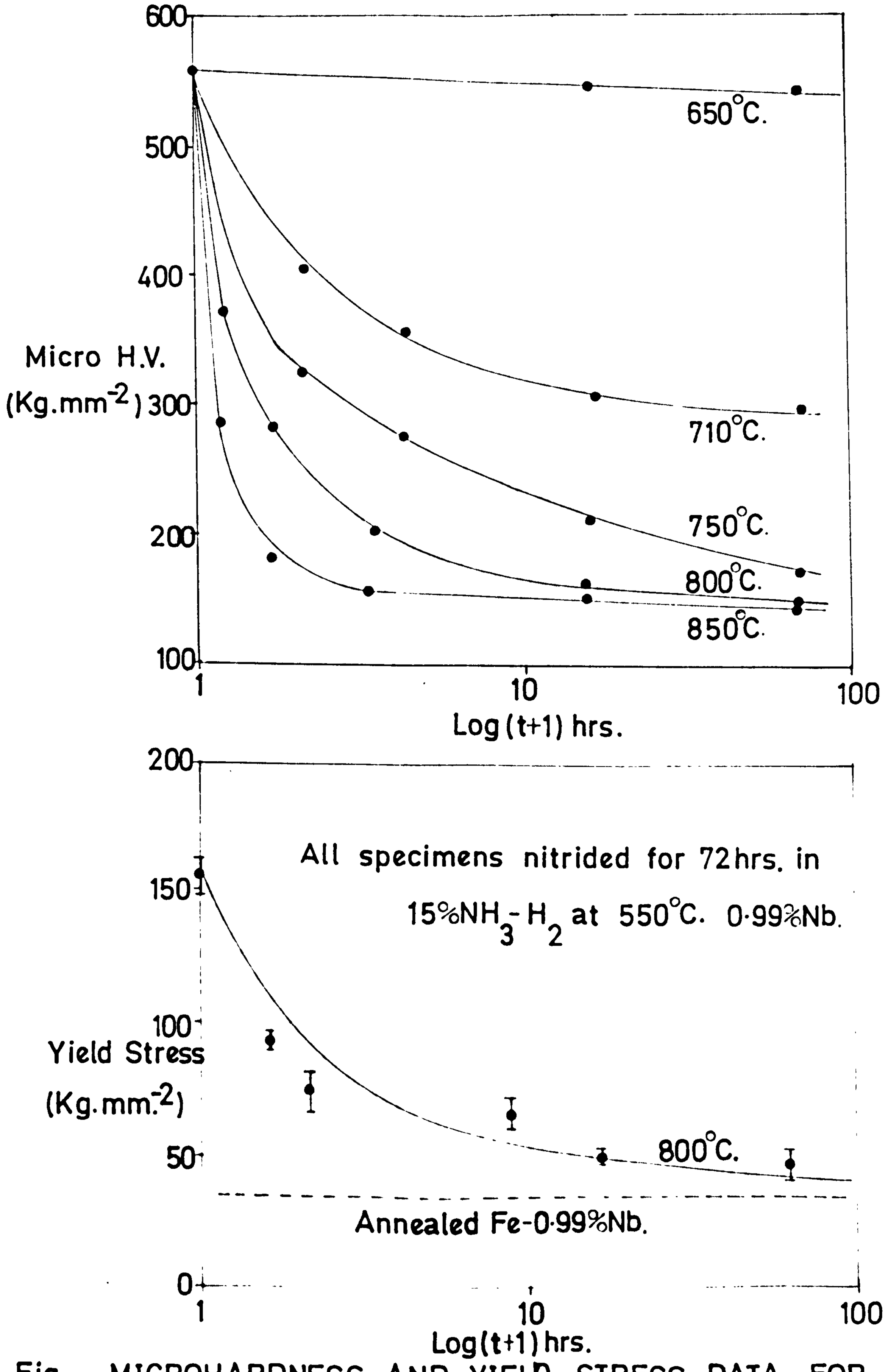

Fig. MICROHARDNESS AND YIELD STRESS DATA FOR OVERAGEING OF PEAK HARDNESS Fe-Nb-N ALLOYS.

Kindleman and Ansell (1970b) also noted that grain boundary precipitation of CrN in the nitrided layer led to porosity and embrittlement after hydrogen reduction.

VI.2 Experimental

Tensile specimens of Fe:35Ni and Fe:35Ni:0.5, 1.0 and 2.0Nb alloys were prepared with gauge lengths of 10 and 25mm, thicknesses of 0.15, 0.30. 0.50 and 1.25mm and widths of 5 and 12.5mm and were annealed for 0.5h at 950, 1050, 1150 and 1200°C respectively. Further specimens of Fe:35Ni:0-2Nb alloys were annealed for different times and temperatures to give a range of grain sizes. The grain size was determined by a linear intercept method and the resulting value multiplied by a factor of 1.65 (after Lements et al, 1954).

The mechanical properties of nitrided Fe:35Ni:0-2Nb alloys were determined after nitriding for different times in: $1NH_3:99H_2$ and $5NH_3:95H_2$ at 800°C; $10NH_3:90H_2$ at 600°C; and after hydrogen reduction of specimens nitrided for 5 and 16hrs at 800°C in $1NH_3:99H_2$.

The effect of test temperature upon the mechanical properties was determined for Fe:35Ni:2Nb nitrided for 95hrs at 800°C in $1NH_3:99H_2$.

The mechanical properties are also determined for Fe:35Ni:Nb alloys nitrided in $10NH_3:90H_2$ at 600^oC after 95% prior deformation.

VI.3 Results

Figure VI.2 shows typical stress strain curves for annealed Fe:35Ni and nitrided Fe:35Ni:0.0 and 0.5Nb alloys. In all cases the stress-strain curves exhibit no yield point. After an initial rapid rate of work hardening the flow stress of Fe:35Ni and Fe:35:Ni:N levels off, and there is no significant difference between their initial rate of work hardening (7.5 MNm^{-2} for 0.05-0.2, 15 and 19 MNm^{-2} for 0.1-0.5 and 40 and 46 MNm^{-2} for 1.0-5.0 elongation respectively for similarly annealed specimens) and the difference in flow stress is attributed to the friction stress of nitrogen. The nitrided Fe:35Ni:0.5 Nb alloy at 800^oC shows an increase in both the flow stress and the rate of work hardening compared with Fe:35Ni.

The variation in the 0.2% proof stress 6_f at 298^oK with grain size d in Fe:35Ni is shown in Figure VI.2b and obeys the Hall-Petch relationship (Hall, 1951; Petch, 1953); equation VI.1:

$$6_f = 6_o + k_y d^{-\frac{1}{2}} \quad \ldots\ldots \text{VI.1}$$

where the flow stress σ_o is determined as 191 ± 8 MNm^{-2} and k_y, a constant, as 0.44 ± 0.10 $d^{-\frac{1}{2}}$ $MNm^{-\frac{3}{2}}$.

The friction stress determined from the 0.2% proof stress for interstitial solid solution hardening of nitrogen in austenitic Fe:35Ni increased with decreasing grain size (Figure VI.3a) from 336 ± 44 to 462 ± 38 MNm^{-2} $wt\%N^{-1}$ for grain sizes of 0.082 to 0.052mm.

The variation in the 0.2% proof stress of Fe:35Ni:Nb with niobium content is 33 ± 4 $MNm^{-2}wt\%Nb^{-1}$ and is similar to the value of 40 $MNm^{-2}wt\%Nb^{-1}$ reported by Irvine et al (1969) in austenitic stainless steels (Figure VI.3b).

Similar observations are made in nitrided Fe:35Ni:Nb alloys to those made by Kindleman and Ansell (1970b) in nitrided Fe:18Cr:Ni:Ti alloys where the 0.2% proof stress decreases with increasing specimen thickness due to a variation in particle size with depth (Figure VI.4).

Figures VI.5 and Vi.6b show a decrease in the 0.2% proof stress and an increase in the ductility with nitriding time for Fe:35Ni:Nb alloys at $800^{o}C$ in $1NH_3:99H_2$ and $5NH_3:95H_2$ respectively due to particle coarsening.

Fig. VI.2

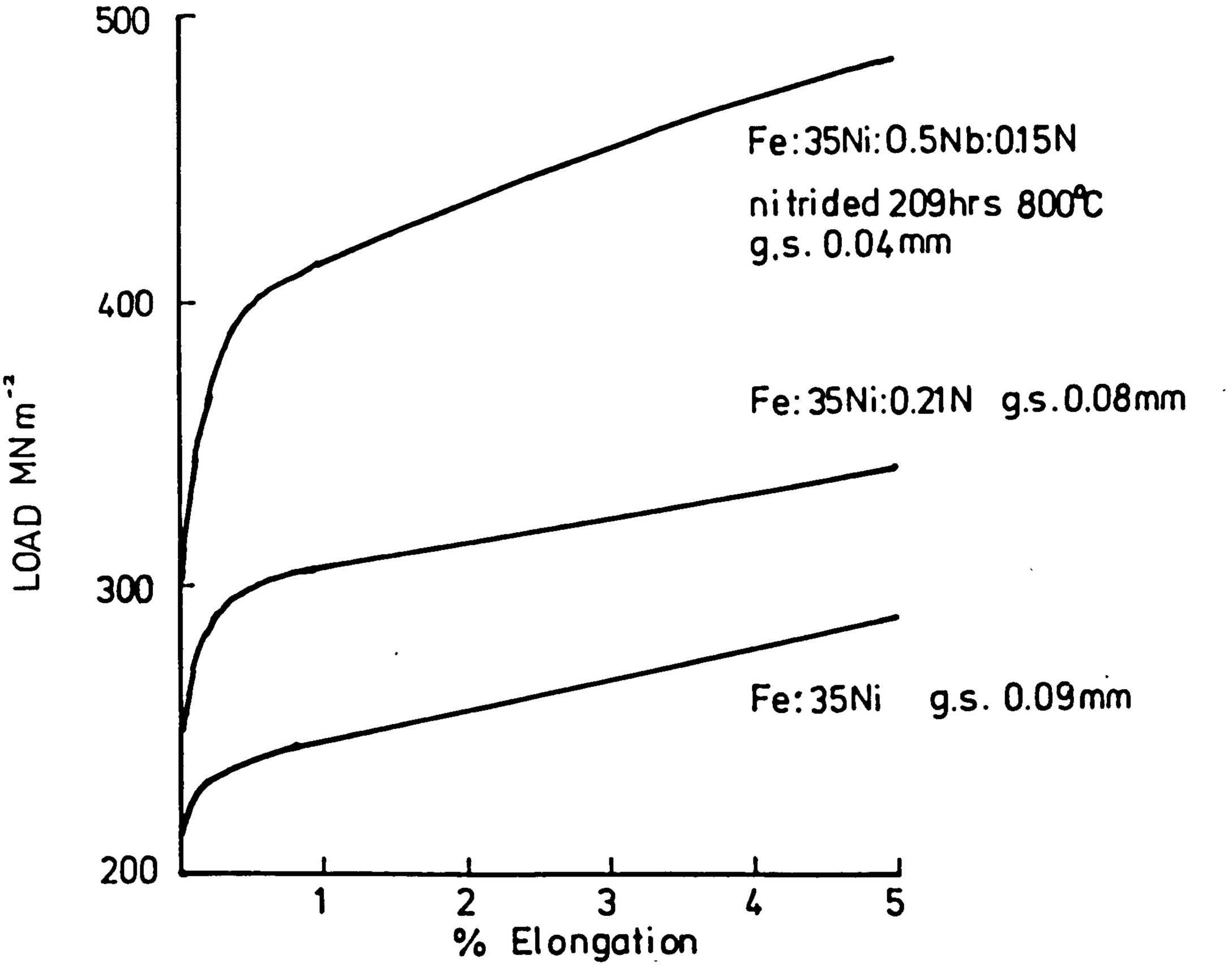

STRESS STRAIN CURVES OF Fe:35Ni AND NITRIDED Fe:35Ni:0 & 0.5 Nb ALLOYS

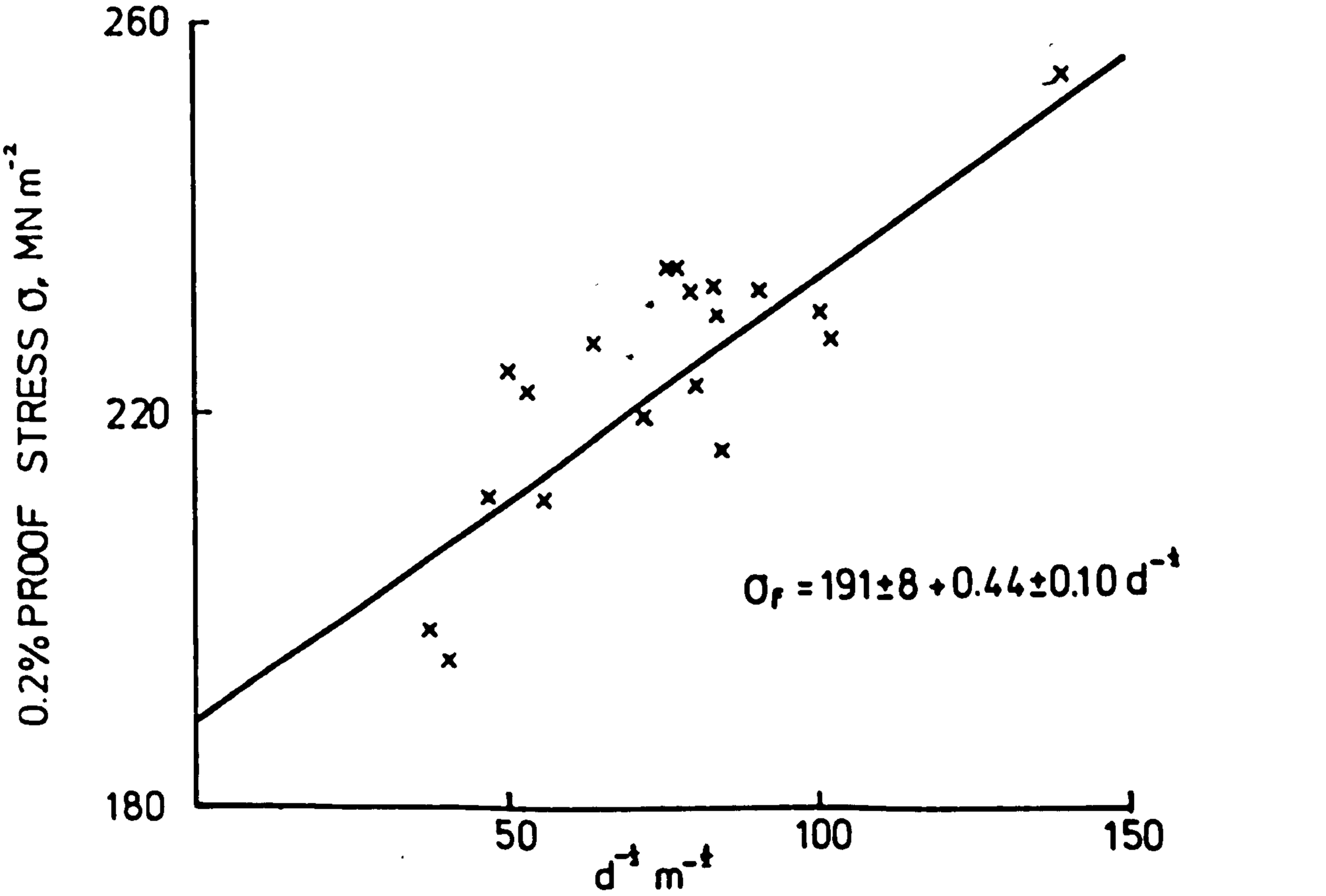

VARIATION IN 0.2% PROOF STRESS σ_f OF Fe:35Ni WITH GRAIN SIZE (Specimen thickness 0.52mm)

Fig. VI.3

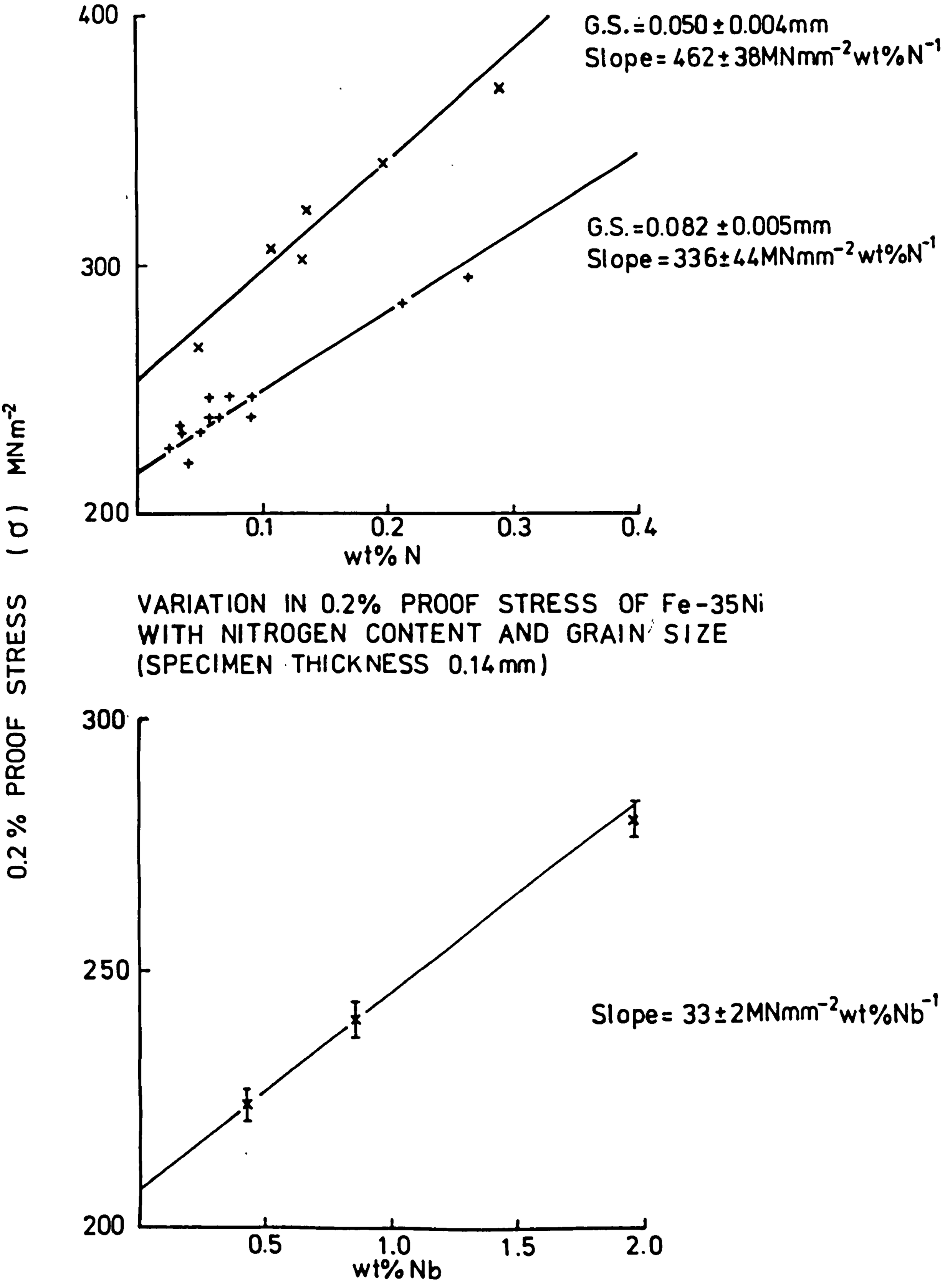

VARIATION IN 0.2% PROOF STRESS OF Fe-35Ni WITH NITROGEN CONTENT AND GRAIN SIZE (SPECIMEN THICKNESS 0.14mm)

VARIATION IN 0.2% PROOF STRESS OF Fe-35Ni WITH NIOBIUM CONTENT (SPECIMEN THICKNESS 0.52mm, GRAIN SIZE 0.413mm)

Fig. VI.4

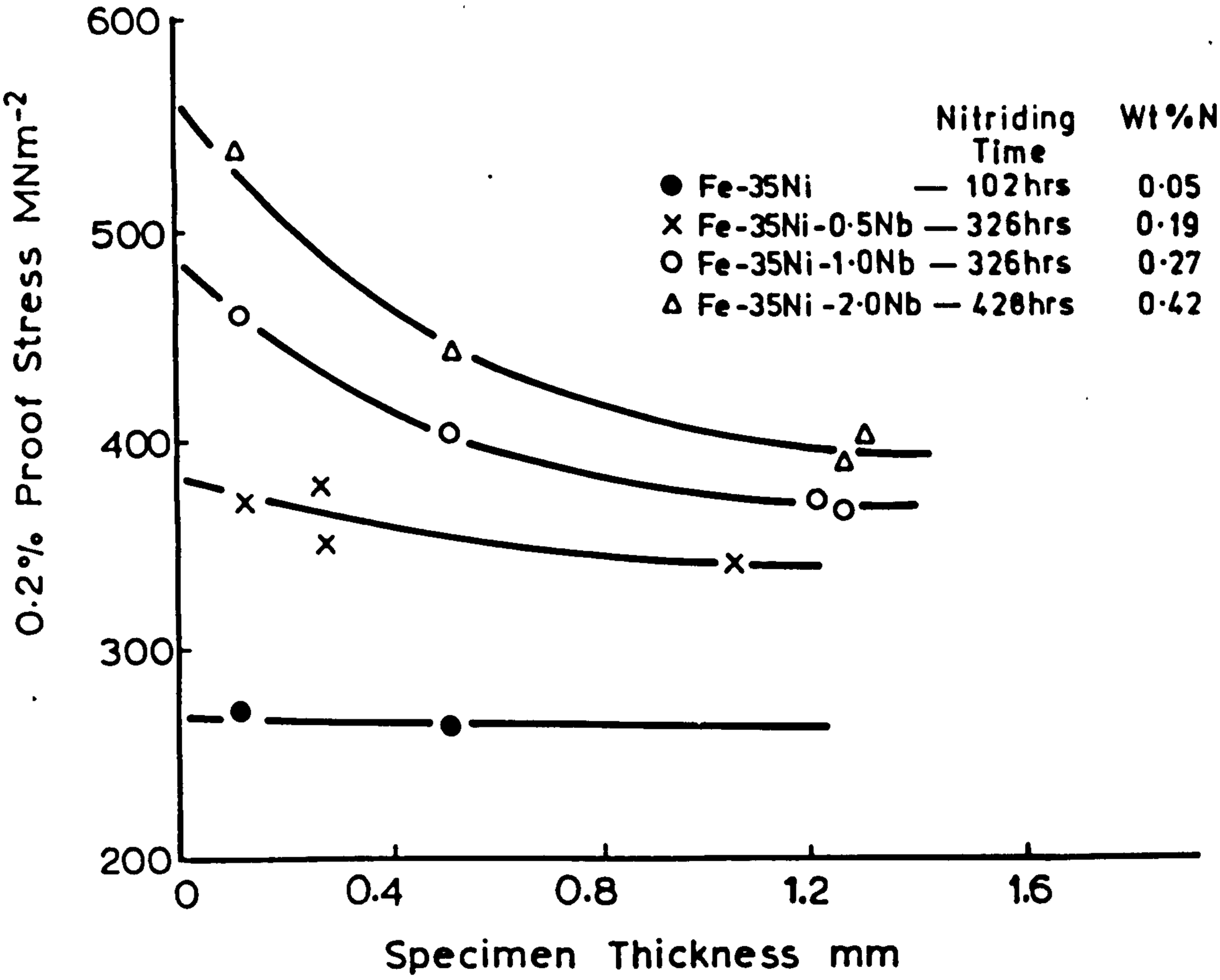

VARIATION OF 0·2% P.S. WITH SPECIMEN THICKNESS FOR ALLOYS NITRIDED IN $1NH_3:99H_2$ AT 800°C.

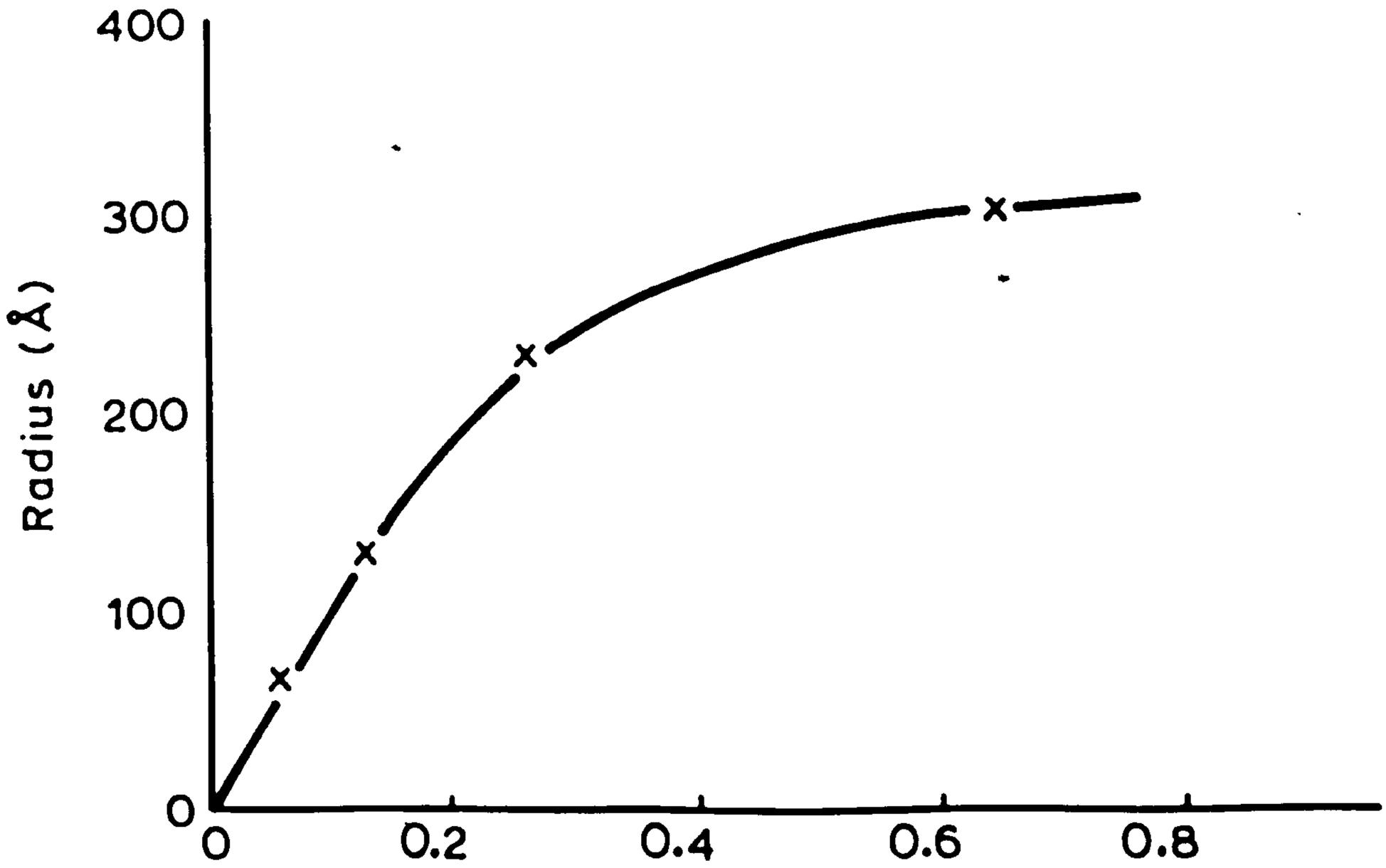

VARIATION OF MEAN PARTICLE RADIUS OF NbN AT THE CENTRE OF Fe-35Ni-2Nb ALLOYS NITRIDED FOR 428HRS AT 800°C (WT%N 0·42).

Fig. VI. 5

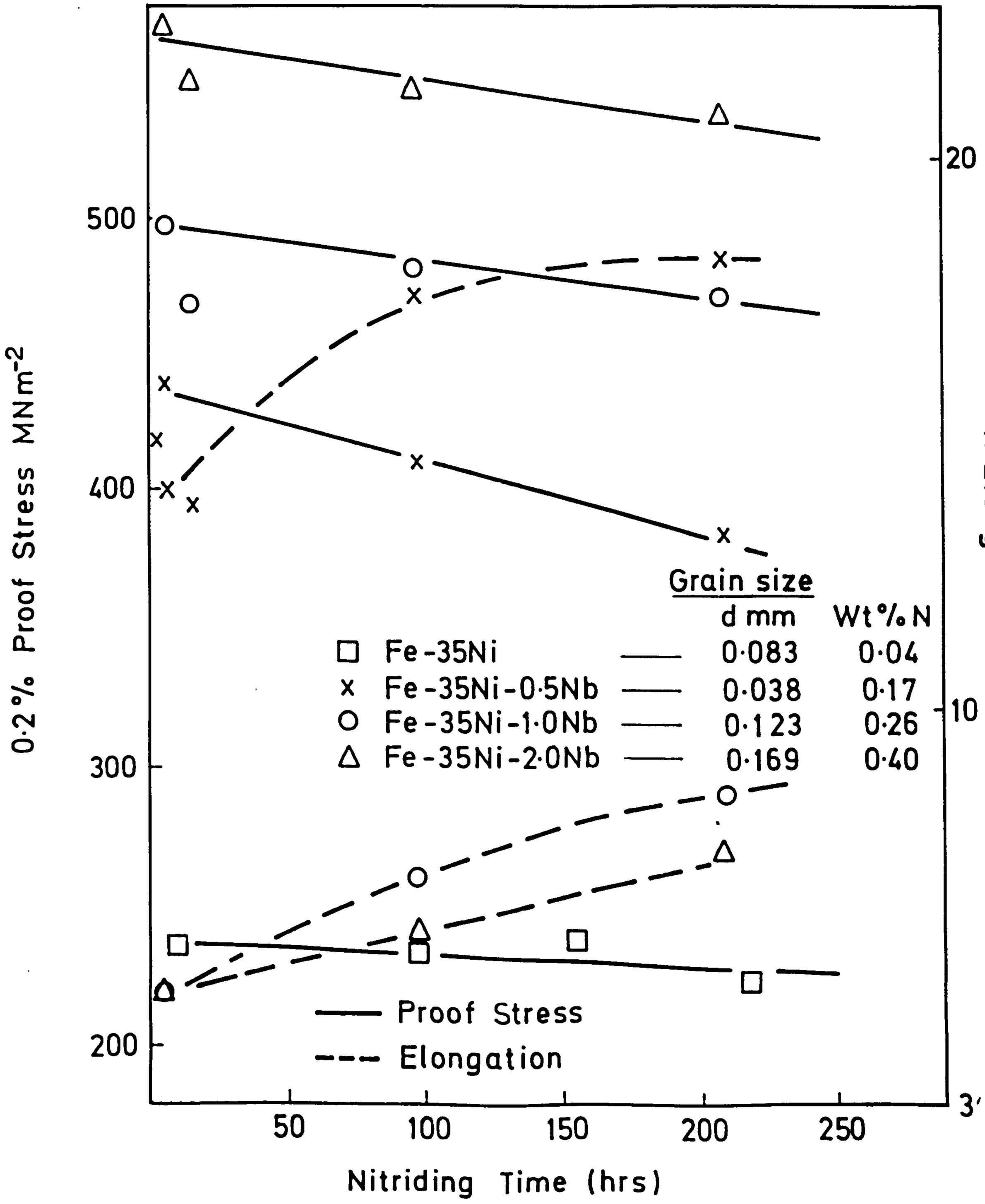

0·2% PROOF STRESS (≃0·13mm THICK SPECIMENS) OF Fe-35Ni-Nb ALLOYS NITRIDED IN $1NH_3:99H_2$ AT 800°C.

Fig. VI.6

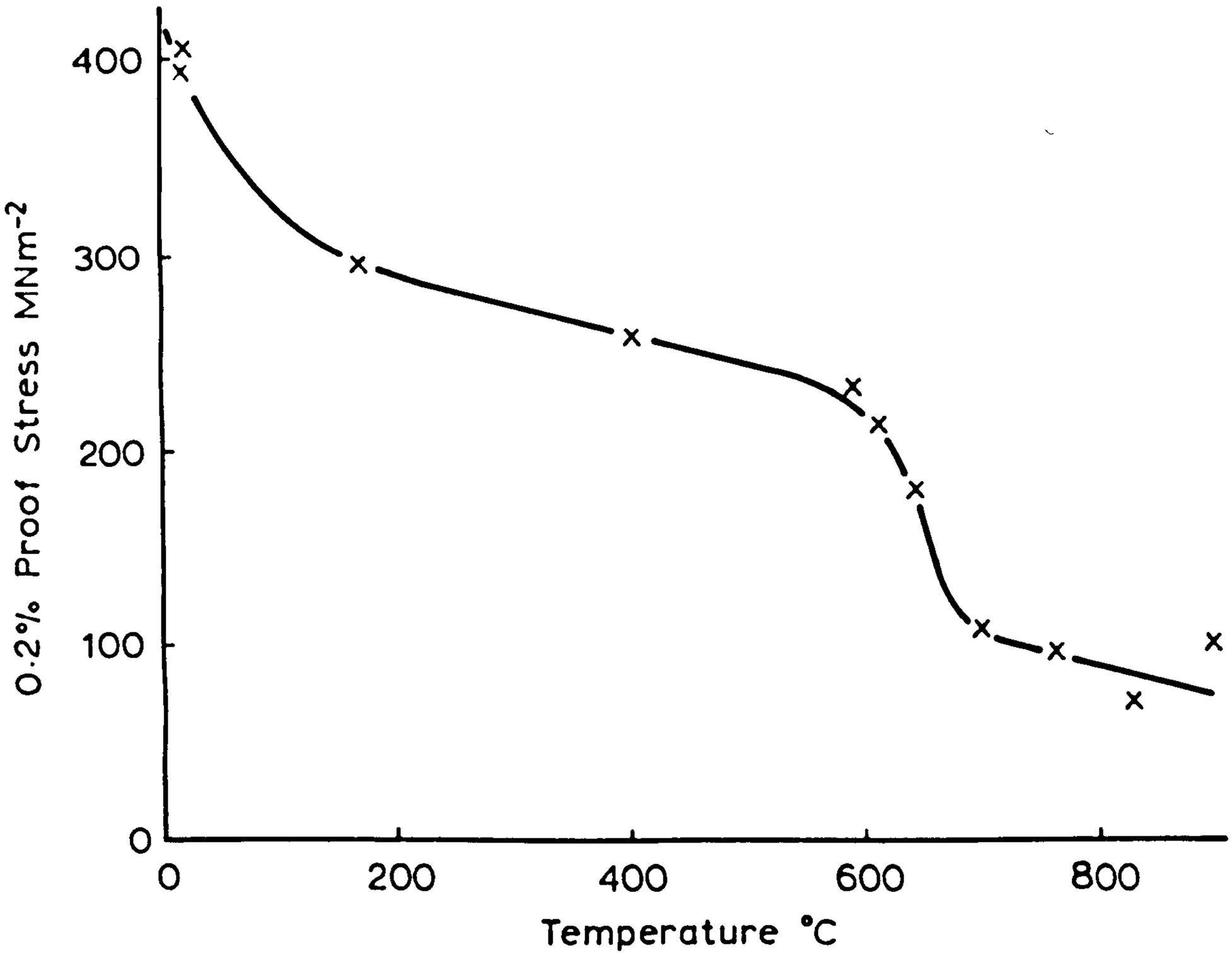

VARIATION OF 0·2% P.S. WITH TEMPERATURE FOR Fe-35Ni-2Nb NITRIDED FOR 95HRS, 800°C IN $1NH_3$: $99H_2$ (THICKNESS 0·53mm; GRAIN SIZE 0·165mm; WT%N 0·45).

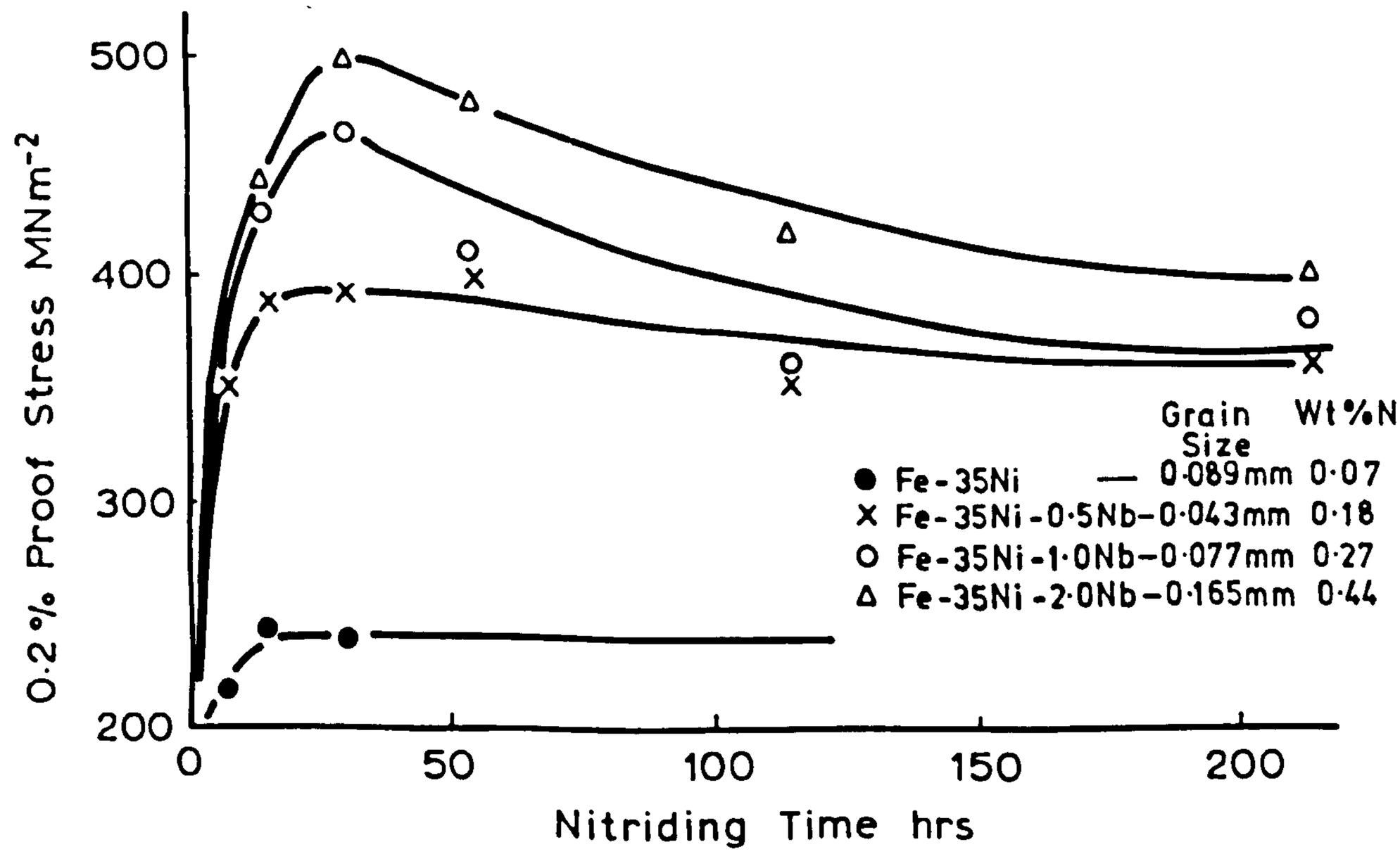

VARIATION OF 0·2% P.S. WITH NITRIDING TIME OF Fe-35Ni-Nb ALLOYS NITRIDED IN $5NH_3$:$95H_2$ AT 800°C (THICKNESS 0·55mm).

Figure VI.6a shows a decrease in the 0.2% proof stress with increasing test temperature of Fe:35Ni:2Nb alloy nitrided for 95hrs at 800°C in $1NH_3:99H_2$.

Figure VI.7 shows the 0.2% proof stress and the ductility of undeformed Fe:35Ni:0.0 and 0.5Nb alloys and Fe:35Ni:0-2Nb alloys after 95% prior deformation nitrided for various times at 600°C in $10NH_3:90H_2$.

VI.4 Discussion of results

The variation of the 0.2% proof stress σ_f of Fe:35Ni with grain size obeys the Hall-Petch relationship (equation VI.1) and from Figure VI.2 it follows that:

$$\sigma_f = 191 \pm 8 + 0.44 \pm 0.10 d^{-\frac{1}{2}} MNm^{-2} \quad .... \quad VI.2$$

The value of (k_y) in equation IV.2 of 0.44 $MNm^{-\frac{3}{2}}$ for Fe:35Ni:0.01C is similar to that found by Sonon and Smith (1965) at 304°K, i.e. 0.48 $MNm^{-\frac{3}{2}}$ in Fe:33Ni:15Cr: 0.07 (C + N) alloy, and the difference in the flow stress of 191 and 114 MNm^{-2} respectively is attributed to the chromium content of these workers' alloy.

Fig. VI. 7

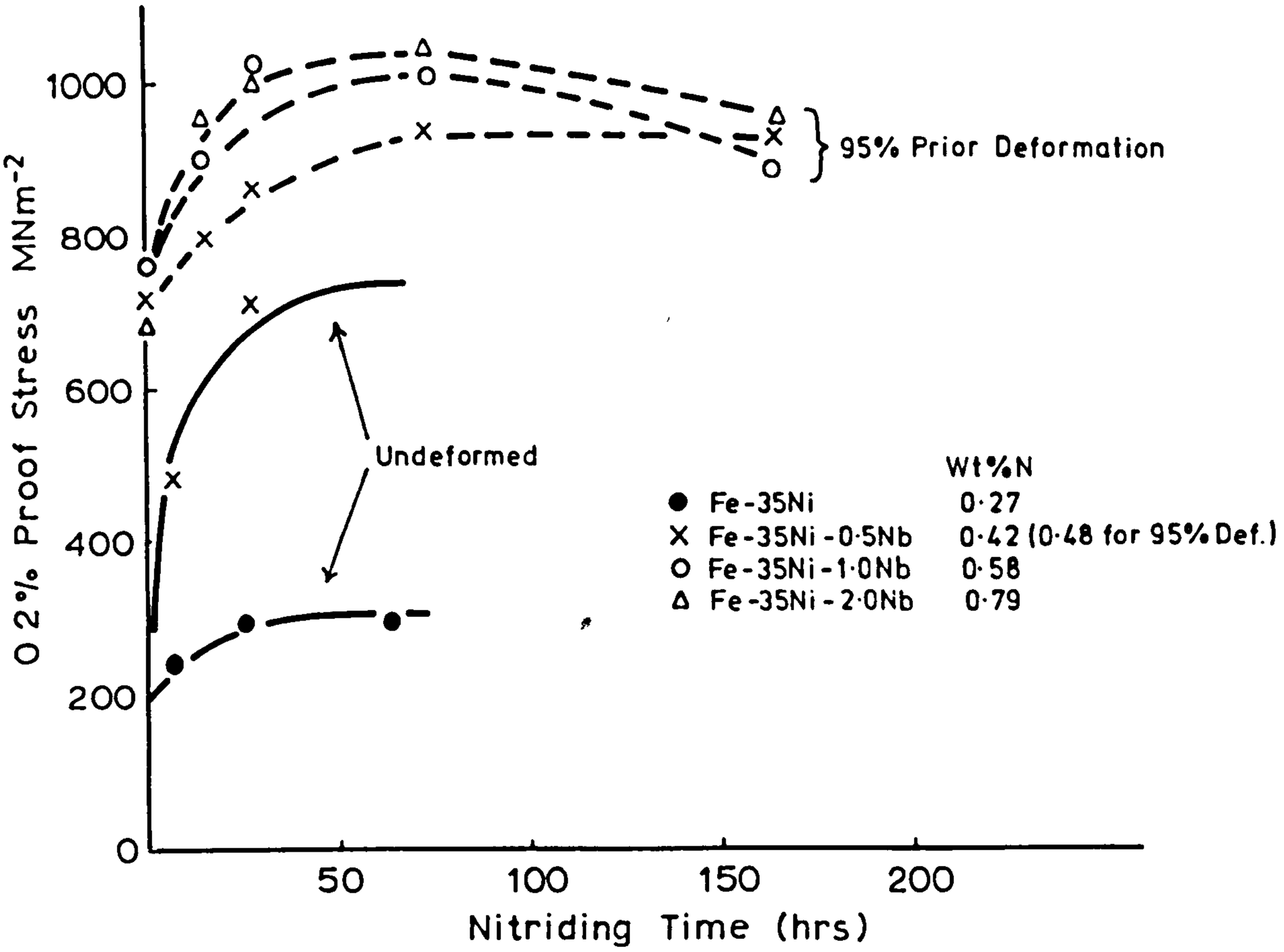

VARIATION OF 0·2% P.S. WITH NITRIDING TIME OF Fe-35Ni-Nb ALLOYS NITRIDED AT 600 °C IN $10NH_3:90H_2$ (THICKNESS 0·15 mm).

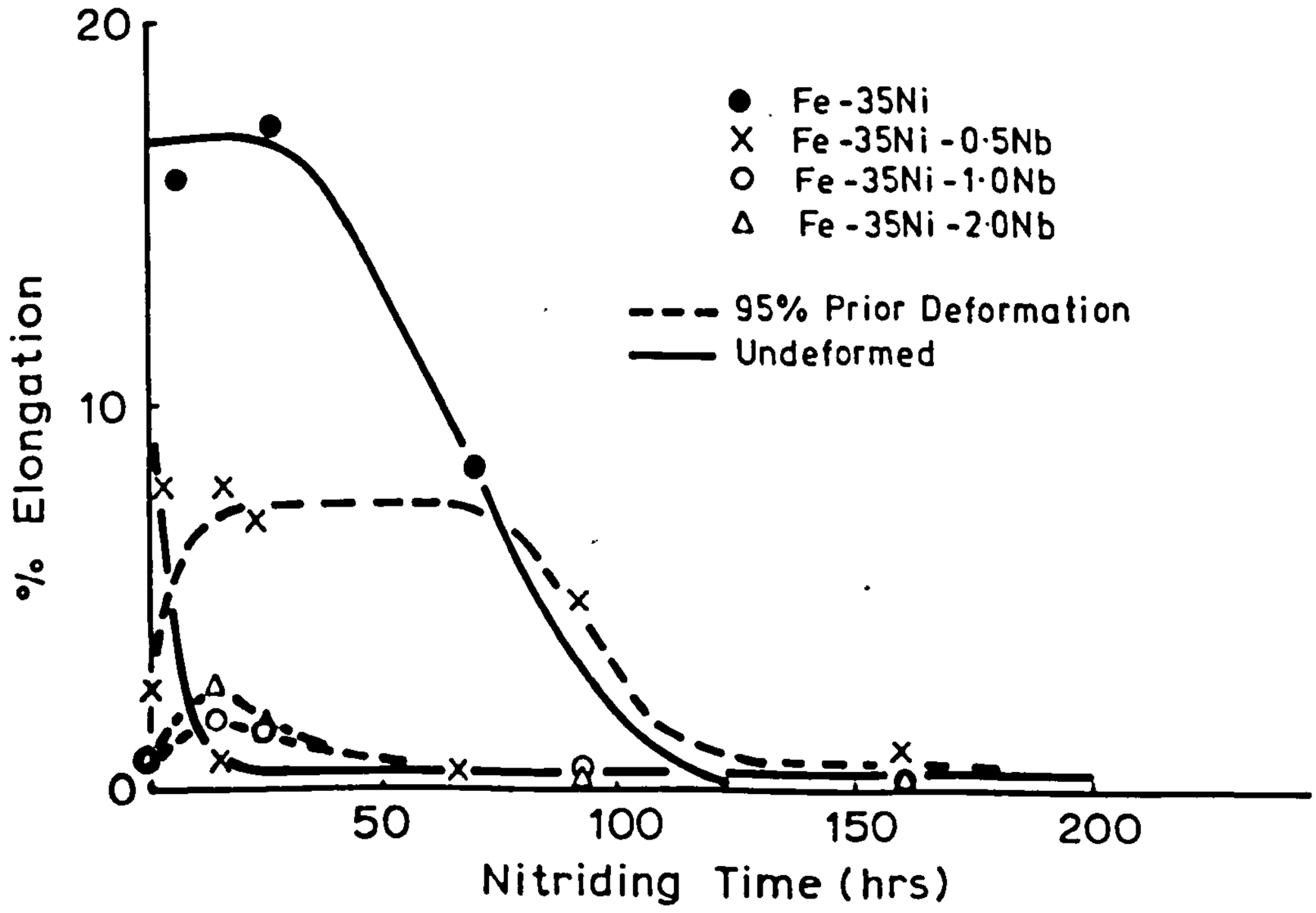

VARIATION OF ELONGATION OF Fe-35Ni-Nb ALLOYS WITH NITRIDING TIME AT 600 AND 800 °C.

The friction stress of nitrogen in nitrided Fe:35Ni determined from Figure V.3 increased from 336 to 462 MNm^{-2} with a decrease in the grain size from 0.082 to 0.050mm. The variation of the friction stress in Fe:35Ni with grain size is approximately $4.37 MNm^{-\frac{3}{2}}$ $wt\%N^{-1}$ which compares favourably with a value of $4.76\ MNm^{-\frac{3}{2}}\ wt\%\ (N + C)^{-1}$ for Fe:33Ni:14Cr alloys determined from Sonon and Smith (1965). The increase in k_y in nitrided Fe:35Ni may be due to:

(i) increased resistance to slip propagation at the grain boundaries into adjacent grains:

(ii) possible changes in the stacking fault energy which increase the stress required for cross-slip;

(iii) a change in the shear modulus.

Haush and Warlimont (1972) have shown that the shear modulus (G) of Fe:35Ni is a minimum and increases with small changes in the nickel content due to possible changes in the electronic structure. Work by Khomenko and Tseytlin (1969) has shown that additions of Si, Cr and Cu to Fe:35Ni increases the Young's modulus, and hence nitrogen may have a similar effect. However, the change in k_y of $4.37 MNm^{-\frac{3}{2}}$ due to nitrogen is much larger than that which can be attributed to any changes in the elastic and shear moduli of Fe:35Ni due to nitrogen (which may be a maximum of about $0.08 MNm^{-\frac{3}{2}}$).

Sonon & Smith(1965)attributed the increase in k_y in Fe:33Ni:15Cr alloys with the C and N content at low strains to an increased resistance to slip propagation occurring at the grain boundaries. They also found that this increase in k_y appeared to be independent of the test temperature below 155°C. Hence the increase in the friction stress in Fe:35Ni with grain size may be due to an increased resistance to slip propagation across the grain boundaries. The effect of any possible change in k_y due to a change in the stacking fault energy is probably small (Sonon and Smith, 1965).

The friction stress of nitrogen in austenitic Fe:17Cr:14Ni was found to be 316 $MNm^{-2}wt\%N^{-1}$ which is in good agreement with the value of 336 $MNm^{-2}wt\%N^{-1}$ in Fe:35Ni for grain sizes of 0.05 and 0.08mm respectively (Roberts and Bergström, 1965). The results of these workers are corrected for the nickel and chromium contents in Fe:17Cr:14Ni but they made no mention of any variation in the friction stress with grain size.

The variation in the 0.2% proof stress with the niobium content of 33$MNm^{-2}wt\%Nb^{-1}$ in Fe:35Ni is similar to the 40$MNm^{-2}wt\%Nb^{-1}$ found by Irvine et al (1969) in austenitic stainless steels. This variation is independent of the grain size.

The variation of the friction stress in austenitic Fe:35Ni with grain size with the nitrogen content is unusual in that this behaviour is not normally found in f.c.c. materials (Embury, 1971) and the behaviour of niobium is more normal.

The variation in the 0.2% proof stress of nitrided Fe:35Ni:Nb alloys with specimen thickness is similar to that observed by Kindleman and Ansell (1970) in nitrided Fe:Cr:Ni:Ti alloys and Woods (1969) in internally oxidised Cu:Al alloys. The decrease in the proof stress with specimen thickness is attributed to a variation in particle size with the nitriding depth (Figure VI.4). The use of thin specimens is preferred to electrothinned thick specimens in order to reduce the variation of particle size with specimen thickness. The latter is due to the difficulty of electrothinning Fe:35Ni:Nb alloys after nitriding.

The decrease in the 0.2% P.S. with nitriding time of Fe:35Ni:Nb alloys at 800°C in $1NH_3:99H_2$ (Figure VI.5)

is due to an increase in the particle size (Figure IV.17). The 0.2 P.S. also increases with the niobium content (Figure VI.5).

Various formulae were used in attempts to explain the dislocation particle-interaction in nitrided Fe:35Ni:Nb alloys (see Kelly, 1973; Brown and Ham, 1971). The theoretical and experimental flow stress increments $\Delta\sigma$ for a range of particle sizes of γ-NbN in nitrided and in hydrogen-reduced Fe:35Ni:Nb alloys are found to obey a relationship derived by Brown and Ham (1971) for Orowan looping (Figures VI.8 and Vi.9, and Table VI.1). The theoretical value is calculated from Brown and Ham's equation and multiplied by a Taylor factor of 2 (for polycrystalline materials) where:

$$\Delta\sigma = 2 \frac{0.4\ Gb\ \ln(2r_s/b)}{L\ (1-\nu)^{\frac{1}{2}}} \cos\left(\frac{\varphi}{2}\right) \quad \ldots\ \text{VI.3}$$

where G is the shear modulus of Fe:35Ni ($5.60 \times 10^4 MNm^{-2}$; Hausch and Warlimont, 1972);

b, the Burgers vector (2.55 Å);

φ, the cutoff angle where $\Delta\sigma$ is a maximum when $\varphi = 0^\circ$;

ν, Poisson's ratio (0.259; Kaye and Labye, 1968);

r_s, the effective particle radius (where $r_s = (\frac{2}{3})^{\frac{1}{2}} r$) ;

r, the particle radius;

Fig. VI.8

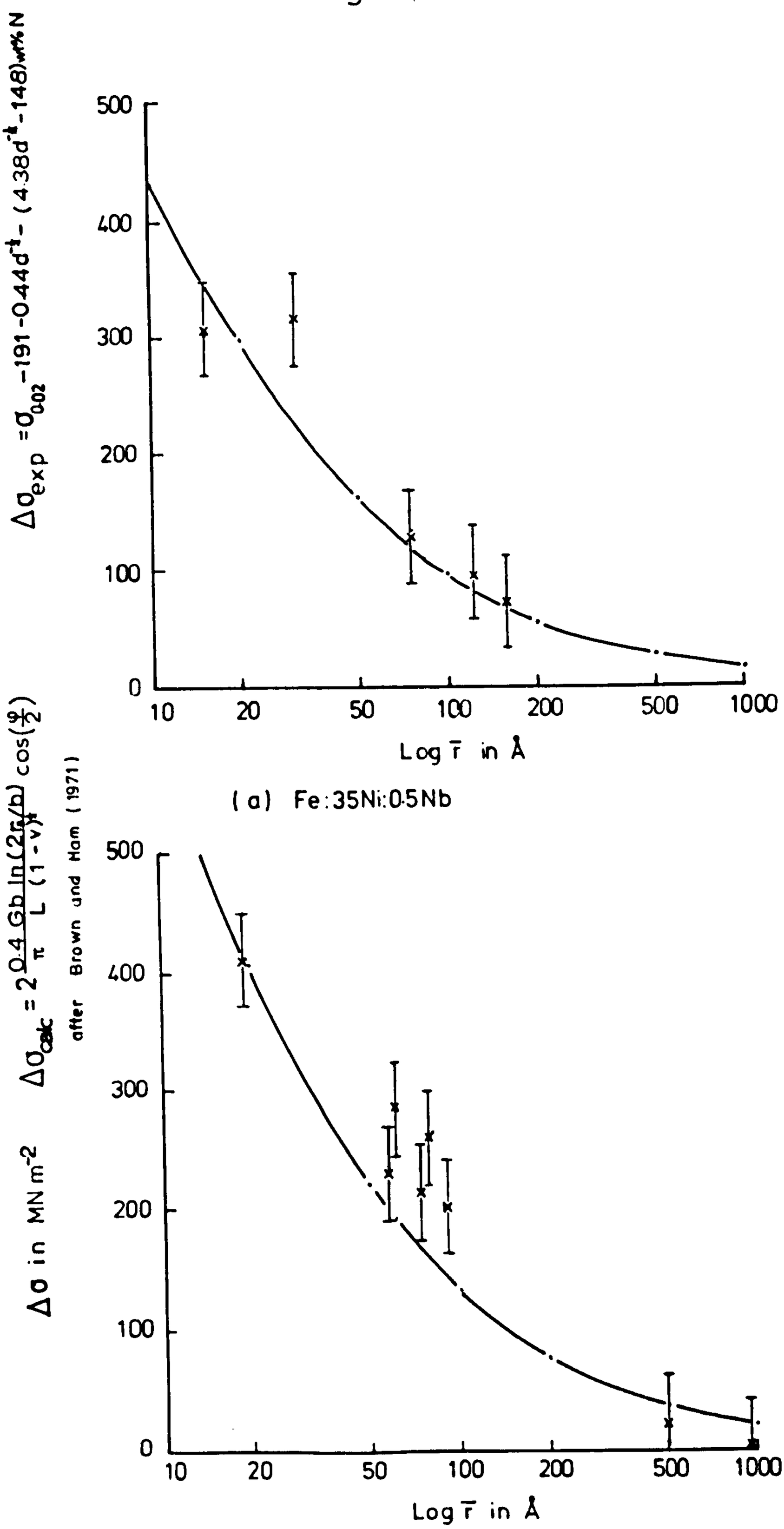

THEORETICAL AND EXPERIMENTAL FLOW STRESS INCREMENTS $\Delta\sigma$ FOR OROWAN LOOPING IN NITRIDED Fe:35Ni: (a) 0·5 & (b) 1·0 Nb ALLOYS

Fig. VI.9

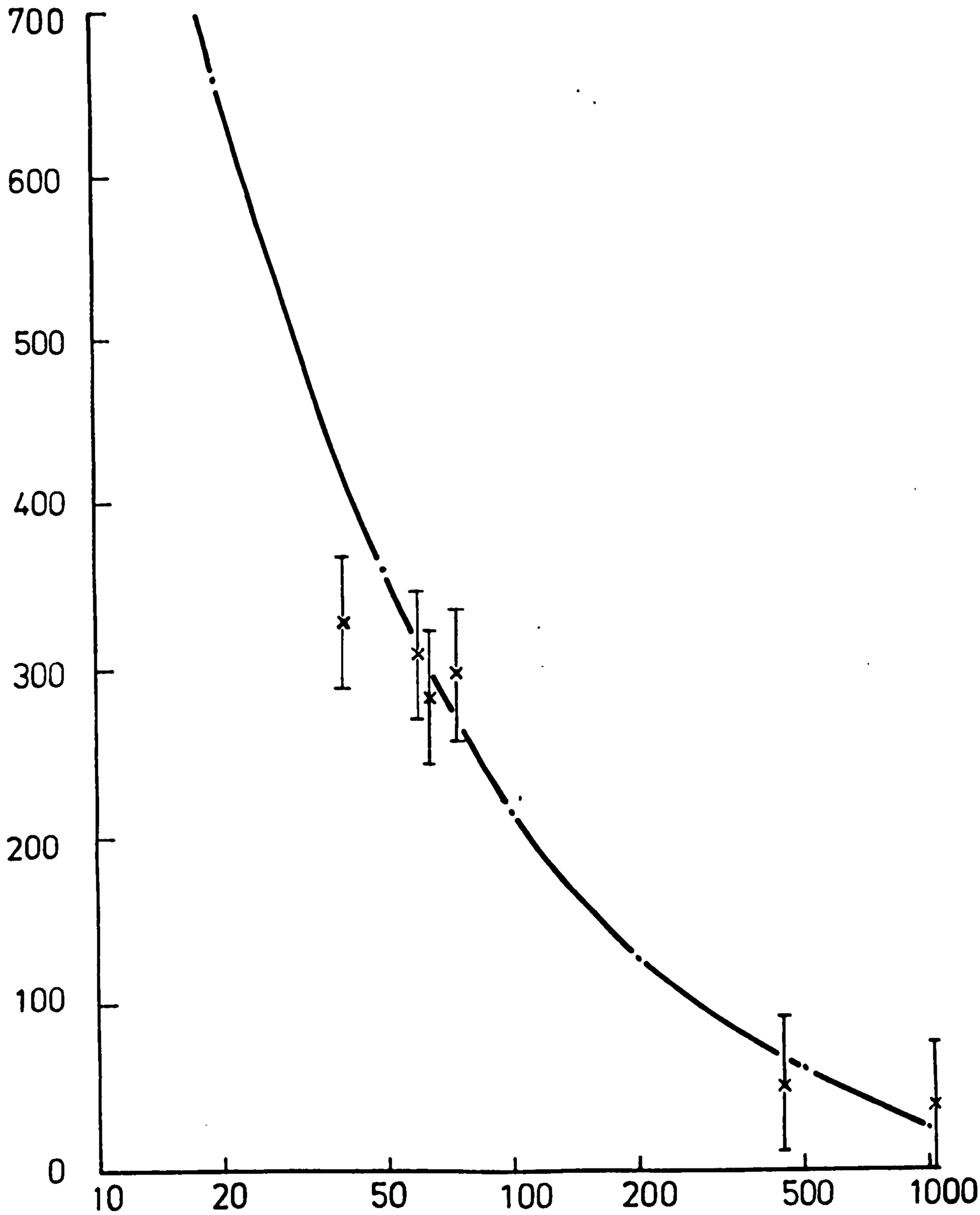

THEORETICAL AND EXPERIMENTAL FLOW STRESS INCREMENTS $\Delta\sigma$ FOR OROWAN LOOPING AROUND γ NbN PRECIPITATES IN NITRIDED Fe:35Ni:2·0Nb

Table VI.1

The variation of 0.2% P.S. $\Delta\sigma$ with precipitated radius r

Alloy	Grain Size mm	wt%N	ppt radius r Å	0.2% P.S. MNm^{-2}	Calc $\Delta\sigma$ in MNm^{-2}		
					-G.S.	-wt%N	$\Delta\sigma$ppt
Fe:35Ni:	0.041	.415	14.65	759	261	191	306
0.5Nb	"	.130	31.68	609	261	31	316
	"	.177	75.63	446	261	57	128
	"	.174	125.79	414	261	56	97
	"	.155	156.37	372	261	45	66
Fe:35Ni:	0.120	.174	18.99	651	231	11	409
1Nb	"	.265	59.30	497	231	34	232
	"	.279	75.09	483	231	37	214
	"	.229	97.72	462	231	25	209
	0.063	.129	497.50	265	246	0	19
	"	.129	920.00	246	246	0	0
Fe:35Ni:	0.168	.411	41.61	570	224	22	324
2Nb	"	.382	62.75	549	224	16	309
	0.113	.386	66.50	537	232	23	281
	0.168	.372	78.03	534	224	14	296
	0.113	.267	468.14	287	232	0	55
	"	.304	1062.50	270	232	1	37

Calculated from $\Delta\sigma = \sigma - 191 - 0.44d^{-\frac{1}{2}} - (4.38d^{-\frac{1}{2}} - 178)$ wt%N in solution

L, the interparticle spacing (where $L = \left[\left(\frac{\pi}{f}\right)^{\frac{1}{2}} - 2\right] r_s$);

and f the volume fraction of γ-NbN in the nitrided Fe:35Ni:0.5, 1 and 2Nb alloys (0.00565, 0.0113 and 0.0226 respectively).

The above relationship is applicable to the flow stress increment due to Orowan looping in elastic isotropic materials containing strong particles. This relationship may hold for nitrided Fe:35Ni:Nb alloys since any error due to the anisotropy will be corrected for by the values of G and ν, and γ-NbN will remain undeformed since its elastic modulus ($4.84 \times 10^{-5} MNm^{-2}$; Portnoi et al, 1968) is larger than that for austenite ($1.415 \times 10^{5} MNm^{-2}$; Hausch and Warlimont, 1972).

Electron micrographs taken from nitrided and deformed Fe:35Ni:Nb alloys showed dislocation looping around precipitates of γ-NbN (Figure VI.10) accompanied by a high rate of work hardening (Figure VI.2a) due to the increase in the dislocation density.

The mechanism of deformation in nitrided Fe:35Ni:Nb alloys containing small coherent particles of γ-NbN may occur by particle shear due to the lower interfacial energy. Preliminary calculations have shown that γ-NbN may lose its coherency during deformation for particle radii greater than 11 Å (from $r \approx b/\delta$ where δ is the linear fraction extension). This calculation does not account for the effect of interparticle spacing

Fig. VI.10

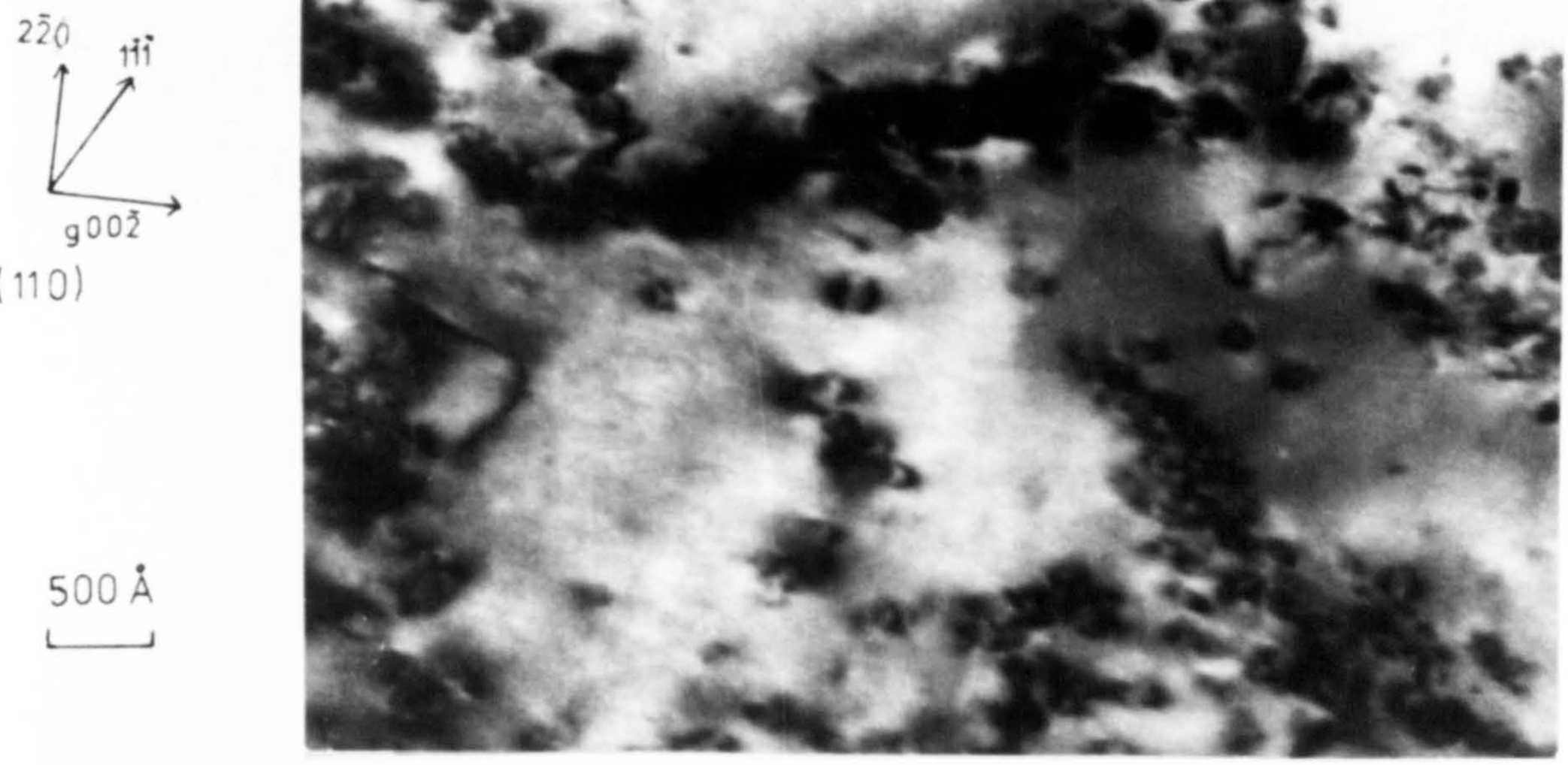

Dislocation loops in Fe:35Ni:0·5Nb nitrided for 13hrs at 800°C in 1:99 NH_3:H_2 after 1% strain

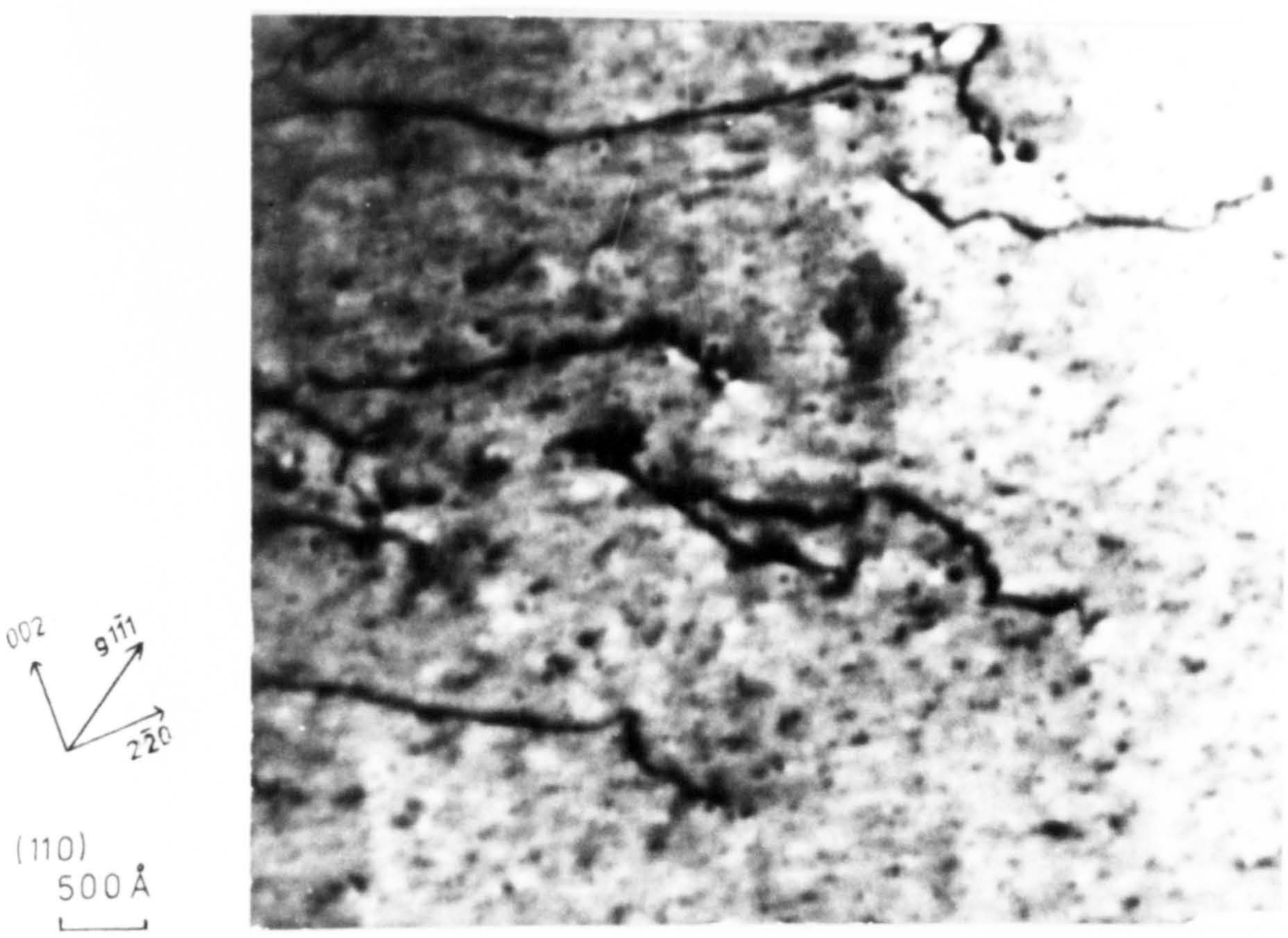

Dislocations in undeformed Fe:35Ni:2Nb nitrided for 16hrs at 800°C in 10:90 NH_3:H_2 and H_2 reduced for 24hrs at 800°C

since large volume fractions of precipitates will reduce the interparticle spacing and hence give a preferred shear deformation. However calculations of the shear stress due to coherency hardening or modulus hardening of nitrided Fe:35Ni:0.5, 1 and 2Nb alloys for a particle radius of 10 Å gave values (after Kelly, 1973) which are higher than those for Orowan looping.

The variation in the 0.2 proof stress of nitrided Fe:35Ni:2Nb with the test temperature (see Figure VI.6a) shows a marked decrease between 25 and 200°C, between 600 and 700°C and a smaller decrease at other temperatures. The smaller decrease in the proof stress with temperature between 200 and 600°C and above 700°C can be attributed to the temperature dependence of the shear modulus G, and is similar to that observed in nitrided Fe:Cr:Ni:Ti by Kindleman and Ansell (1970b). The initial decrease is similar to that observed by Harding and Honeycombe (1966) between 0 and 300°C in Fe:35Ni:1Ti:0.1C alloy. They also noticed a slight decrease in the proof stress above 600°C but they did not determine the extent of this decrease. However insufficient results have been obtained to analyse fully this effect.

The modulated structure formed in nitrided Fe:35Ni:Nb alloys at 600°C is very brittle due to the formation of a precipitate free zone at the grain boundaries.

Plewes (1973) has shown that the mechanical properties of the modulated structure formed in Cu:9Ni:6Sn alloys can be improved by prior deformation. Similar experiments carried out on Fe:35Ni:Nb alloys nitrided in 10:90 $NH_3:H_2$ at 600°C after 95% prior deformation (Figure VI.7) showed only a small improvement in the ductibility, and a proof stress of $\approx 1000 MNm^{-2}$. The electron microstructure of these alloys was highly dislocated with a cell size of ≈ 5000 Å and a fine dispersion of γ-NbN. The appearance of a cell structure might indicate that the Fe:35Ni:Nb alloys undergo recovery during nitriding at 600°C. Rosenbaum and Turnbull (1959) found that cold work prior to ageing Al:Si alloys promoted precipitation within the precipitate-free zone formed in the undeformed alloy. For this reason cold work may have reduced the precipitate-free zone in nitrided Fe:35Ni:Nb alloys.

The mechanical properties listed in Table VI.2 show the 0.2% proof stress, the tensile stress and elongation of nitrided Fe:35Ni:Nb alloys. The tensile stress increases with decreasing precipitate size and is often associated with a decrease in ductibility.

VI.5 Conclusions

Dislocation-particle interaction of γ-NbN in

Table VI.2

Mechanical properties of nitrided Fe:35Ni:Nb alloys

Alloy	%NH_3	Time hrs	Temp ^oC	0.2%P.S. MNm^{-2}	T.S. MNm^{-2}	Elong %	wt%N	G.S. mm	P.S. Å
Fe:35Ni		0.5	950	232	393	39.7	-	.12	
		2	1050	227	349	31.5		.25	
		2	1200	211	350	31.8		.43	
		150	539	306	313	0.8	.108	.05	
		150	600	341	377	4.0	.186	.05	
		150	650	321	374	8.8	.138	.05	
		150	700	301	337	5.7	.126	.05	
	10	160	600	373	388	3.0	.295	.05	
	1	5	800	234	342	18.0	.034	.08	
	1	95	800	267	313	7.5	.042	.08	
	1	209	800	225	343	18.6	.033	.08	
Fe:35Ni		2	1200	209	386	41.1		.56	
:0.5Nb		1.5	1150	236	401	39.5		.47	
	10	333	550	278	287	.3		.04	
	10	24	600	742	767	1.0	.277	.04	
	10	64.5	600	793	793	.25	.415	.04	
95%def	10	23	600	917	1038	5.9	.278		
"	10	73	600	950	1066	6.6	.412		
"	10	160	600	935	983	.9	.479		
	1	5	800	437	604	14.2	.167	.04	75
	1	95	800	414	588	17.0	.181	.04	125
	1	209	800	375	552	18.2	.155	.04	156
t=.15	1	326	800	367	367	.2	.181		
t=.25	1	326	800	348	376	1.8	.210		
t=.52	1	326	800	299	299.	.2	.180		
t=1.25	1	326	800	338	430	12.2	.180		

Alloy	%NH_3	Time hrs	Temp °C	0.2%P.S. MNm^{-2}	T.S. MNm^{-2}	Elong %	wt%N	G.S. mm	P.S. r in Å
Fe:35Ni		1.5	1100	241	418	32.0		.313	
:1Nb		2	1200	221	398	39.5		.595	
95%Def	10	15	600	988	1114	1.7	.208		
"	10	23	600	1036	1150	1.1	.420		
"	10	73	600	990	1070	0.5	.470		
"	10	160	600	887	887	0.2	.576		
84h H_2 reduced	10	326	600	651	651	0.2	.134	.063	19
	1	5	800	497	620	3.2	.265	.118	69
	1	97	800	481	577	5.3	.254	.118	75
	1	209	800	463	569	6.3	.229	.118	93
t=.52	1	326	800	405	414	1.1	.269		
t=1.32	1	326	800	371	403	3.3	.268		
Fe:35Ni		2	1200	263	483	26.2		.413	
:2Nb	1	5	800	570	718	7.4	.410	.169	41
	1	97	800	549	675	5.1	.382	.169	63
	1	209	800	534	692	7.3	.371	.169	78
102h H_2 reduced	1	16	800	287	391	5.8		.169	467
t=.15	1	428	800	537	592	2.4	.386	.113	66
t=.52	1	428	800	421	448	1.1	.425		
t=1.32	1	428	800	388	428	2.1	.426		
95%def	10	15	600	1017	1265	2.4	.372		
"	10	23	600	1036	1205	1.3	.380		
"	10	73	600	1115	1118	0.2	.645		
"	10	160	600	896	896	0.2	.787		
22°C	1	95	800	380	380	0.3			
193°C	1	95	800	288	329	0.8			
400°C	1	95	800	312	317	0.4			
590°C	1	95	800	248	248	0.3			
698°C	1	95	800	100	100	0.2			

nitrided Fe:35Ni:Nb alloys occurs by the Orowan mechanism.

The nitrided structure of Fe:35Ni:2Nb maintains a 0.2% proof stress greater than $200MNm^{-2}$ at temperatures up to $700^{o}C$.

Prior deformation marginally improves the mechanical properties of the modulated structure.

The mechanical properties are affected by the specimen thickness.

Chapter VII

SUMMARY OF EXPERIMENTAL RESULTS

The present investigation has shown that three structures are formed in nitrided austenitic Fe:35Ni:Nb alloys at 500-800°C in NH_3:H_2 gas mixtures:

(i) a modulated structure;

(ii) homogeneous precipitation of γ-NbN;

and

(iii) stacking fault precipitation of γ-NbN.

The modulated structure is formed by interstitial-substitutional solute-atom clusters in ⟨100⟩ matrix directions on {100} matrix planes in nitrided Fe:35Ni:1 and 2Nb alloys at nitrogen potentials which exceed the modulated structure solvus and below the maximum solvus temperature of 750°C. The morphology of the modulated structure is similar to that of spinodally decomposed Cu:Ni:Fe alloys (Daniel and Lipson, 1943; Butler and Thomas, 1970) and is associated with the presence of "side-bands" about the matrix reflections in X-ray and electron diffraction patterns. Since nitrogen atom diffusion in austenitic Fe:35Ni:Nb alloys is several orders of magnitude faster than the niobium atom diffusion,

the formation of clusters is probably controlled by the short-range atom diffusion of niobium. As the clusters overage, excess iron and nickel atoms are rejected in favour of niobium atoms until the niobium:nitrogen atom ratio in the clusters approaches 1:1. The coarsening rate of the modulated structure is controlled by niobium atom diffusion.

Outside the modulated structure solvus, or as the modulated structure overages in Fe:35Ni:Nb alloys nitrided at 550 to 750°C, homogeneous precipitation of γ-NbN occurs in a periodic array in order to minimise the bulk strain energy. The orientation of γ-NbN and the matrix shows a cube:cube relationship. The initial spheroidal precipitates of γ-NbN overage to form octahedra with their faces parallel to {111} matrix planes. The appearance of γ-NbN precipitates in bright field electron micrographs is accompanied by a decrease in the nitrogen content and the gradual disappearance of strain contrast in electron microstructures.

As the octahedra of γ-NbN overage they lose coherency and transform to platelets parallel to {100} matrix planes when the geometric interfacial energy becomes a significant factor. Calculation of the interfacial energy of γ-NbN gives an approximate value

of 600 ergs/cm^2.

It has also been shown that the precipitate size of γ-NbN formed at 800°C in nitrided Fe:35Ni:Nb alloys varies with specimen thickness. Also after prolonged ageing or hydrogen reduction of nitrided Fe:35Ni:Nb alloys the formation of oxynitrides occurs.

The present study is complicated by the formation of stacking fault precipitation of γ-NbN mainly at 650-750°C at the advancing nitriding interface in nitrided Fe:35Ni:Nb alloys. Stacking fault precipitation occurs when the niobium concentration exceeds the nitrogen concentration and is a relatively slow process. For this reason the density of stacking fault precipitates varies with the specimen thickness, with alloy content and with nitrogen potential. Due to the relatively slow increase in the nitrogen concentration at the centre of Fe:35Ni:Nb specimens, nitriding at 650-750°C gives both stacking fault and homogeneous precipitation of γ-NbN before the nitrogen concentration exceeds the modulated structure solvus. The present system is therefore not an ideal one in which to study modulated structures formed in nitrided austenitic Fe:Ni:X alloys.

The present investigation shows that the dislocation-particle interaction which occurs in nitrided Fe:35Ni:Nb

alloys is of an Orowan type. Further, the solution hardening which occurs is affected by the grain size. The 0.2% proof stress decreases with temperature and decreases with increasing specimen thickness due to a variation of particle size with depth. The mechanical properties of the modulated structure are marginally improved by prior deformation.

Because most of these studies were preliminary investigations, further work should be carried out to determine:

(i) the effect of a range of prior deformation on the properties of the modulated structure;

(ii) the high temperature properties of nitrided Fe:35Ni and Fe:35Ni:Nb alloys compared with unnitrided Fe:35Ni;
and

(iii) the variation in the 0.2% proof stress with nitrogen content of Fe:35Ni compared over a range of grain sizes.

The nitriding kinetics for all alloys are explained by a previously reported mechanism for internal oxidation and are controlled by nitrogen diffusion.

Appendix I

PRECIPITATION IN Fe:35Ni:Nb ALLOYS

I.1 Introduction

An investigation was carried out to determine whether the precipitation of any second phase occurred in Fe:35Ni:0.5-2Nb alloys during ageing at 700 and 800°C.

The effect of nickel additions to iron-niobium alloys is to increase the solubility of niobium in austenite (Leith and Chaturvedi, 1971) and promotes the formation of Ni_3Nb (Pread and Borland, 1969; Leith and Chaturvedi, 1971) at the expense of the Laves phase Fe_2Nb. Kirman (1968) has determined the effect of nickel content upon the precipitated phase Fe_2Nb and Ni_3Nb in Fe:15Cr:Ni:2.5 and 5Nb alloys (FigureAI.1). Since chromium promotes the formation of Fe_2Nb in Fe:Cr:Nb alloys (Voles and West, 1973) the exact location of the phase boundaries in Figure AI.1 may be moved to lower nickel contents in the absence of chromium.

The mode of precipitation of the second phase in austenitic Fe:Ni:Nb alloys may occur by a process of clustering (Ivanushkina and Livshitz, 1957; Manenc, 1969)

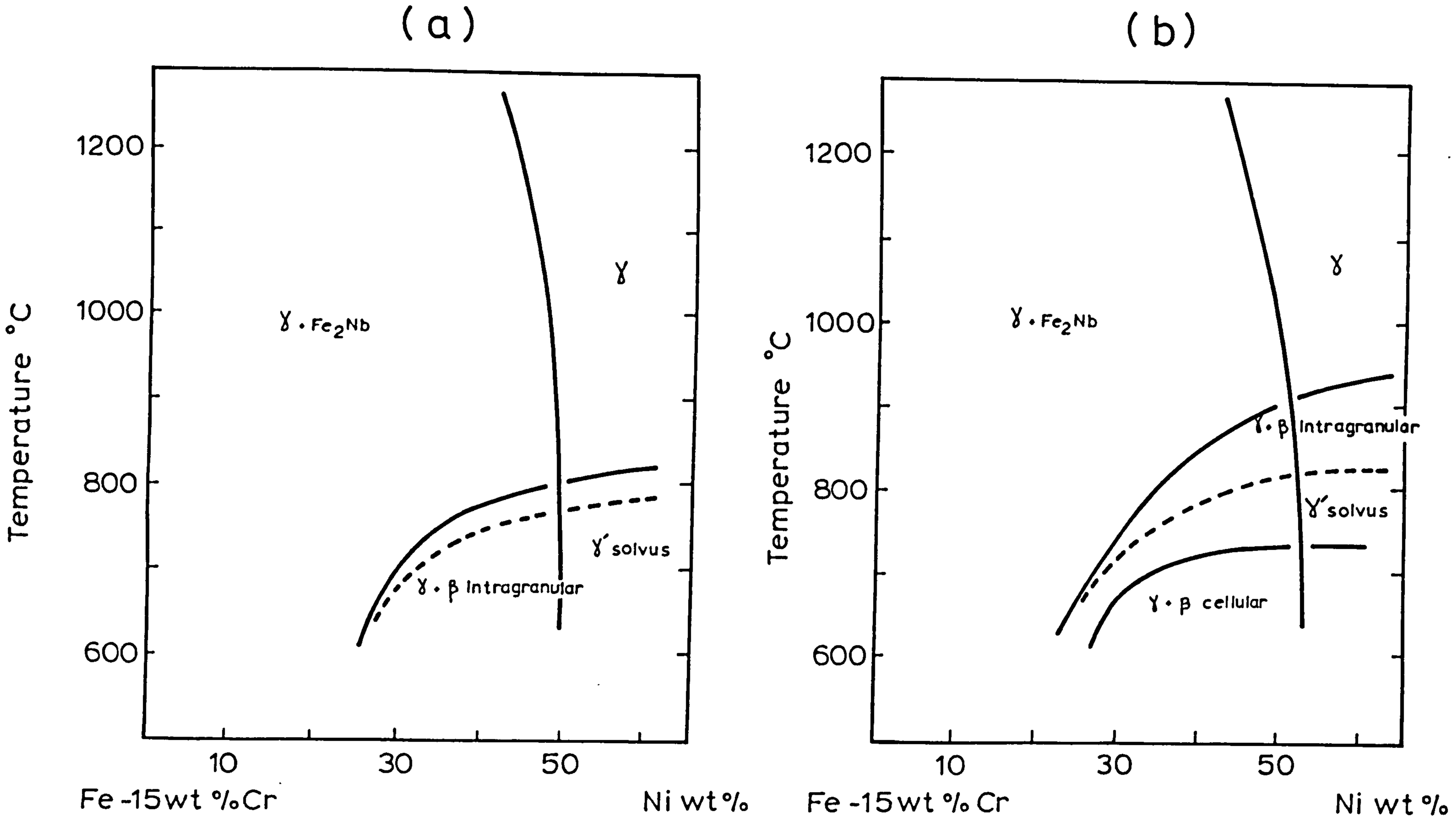

PSUEDO BINARY SECTIONS OF THE EOUILIBRIUM PHASES IN Fe-15Cr-Ni-Nb ALLOYS FOR (a) 2·5wt%Nb AND (b) 5wt%Nb ALLOYS AFTER KIRMAN (1968).

Fig. AI.1

and the formation of a metastable precipitate, either f.c.t. γ' (Manenc et al, 1968; Manenc, 1969; Faive, 1969) or b.c.t. γ^* (Pread and Borland, 1969) prior to the formation of the equilibrium precipitates of orthorhombic Ni_3Nb and hexagonal Fe_2Nb (Pread and Borland, 1969). Manenc (1969) found that the formation of clusters and is associated with a periodic structure, and side-bands in Fe:30Ni:5Nb alloy aged at 550°C and that this transformed to platelets of γ' parallel to {100} planes upon overageing at 650°C. Borland (1973) and Pread and Borland (1969) found that γ^* overaged to Ni_3Nb in the matrix of Fe:40Ni:6Nb at 775°C and to grain boundary precipitation of Fe_2Nb after prolonged ageing.

Leith and Chaturvedi (1971) identified a sequence of precipitation in Fe:30Ni:Nb alloys at 700 and 800°C similar to those observed by Pread and Borland (1969) in Fe:40Ni:6Nb alloys at 775°C. However, Leith and Chaturvedi (1971) determined the phases formed in Fe:30Ni:Nb alloys at 700 and 800°C from powders and electron microspecimens which had been annealed and aged in evacuated silica capsules. Work by Ramstead, Richardson and Bowles (1961) and Bell, Hetherington and Jack (1962) has shown that silica maintains an oxygen potential at temperatures of 700°C, and hence the discrepancy between the phases identified in the French

work and the others may be due to oxygen.

I.2 Experimental

Fe:12,18 and 25Ni:1 and 2Nb alloys were prepared from the master alloys by orgon-arc melting. The Fe:Ni:Nb alloys were solution treated in either evacuated silica capsules, or an evacuated alumina capsule with a zirconium getter and then aged at 700 and 800°C.

I.3 Results and discussion of results

X-ray examination of Fe:Ni:Nb alloys aged in silica capsules showed a face centred cubic phase of lattice parameter 4.46 Å (Figure AI.2). This phase is reported by Leith and Chaturvedi (1971) as Ni_3Nb and Fe_2Nb where the intensities of the reported lines are such that they cannot be attributed to either of these phases. X-ray investigation of Fe:Ni:Nb alloys annealed and aged in alumina capsules shows that the Laves phase Fe_2Nb is formed in Fe:12,18 and 25Ni:1 and 2Nb alloys where the intensities on X-ray diffraction patterns decreases with nickel content; traces of the Laves phase are seen in the aged Fe:35Ni:Nb alloys. X-ray photographs taken from Fe:35Ni:Nb alloys aged in hydrogen at 700

Fig. AI. 2

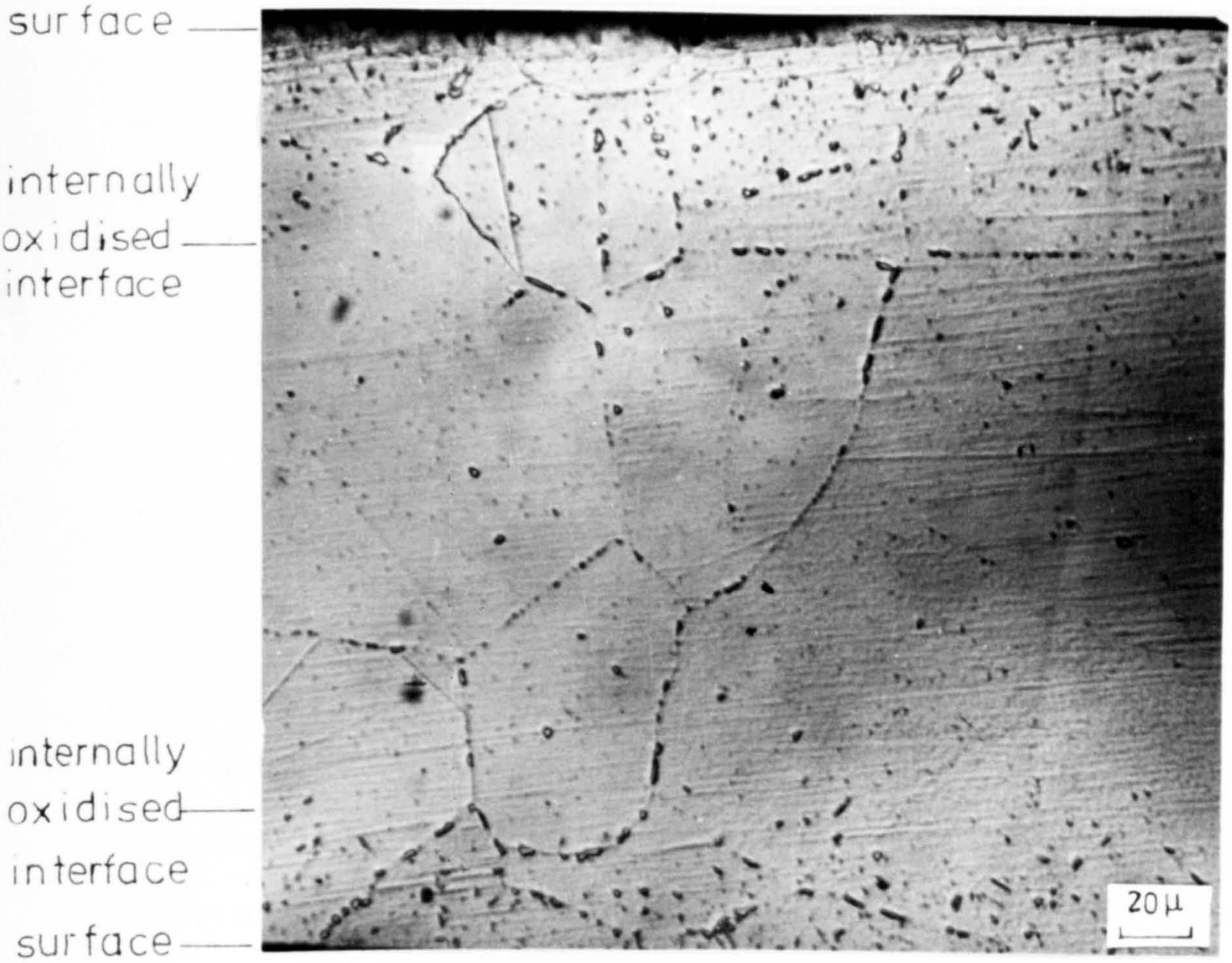

Optical micrograph of Fe:35Ni:2Nb aged for 160hrs in an evacuated silica capsule at 800°C

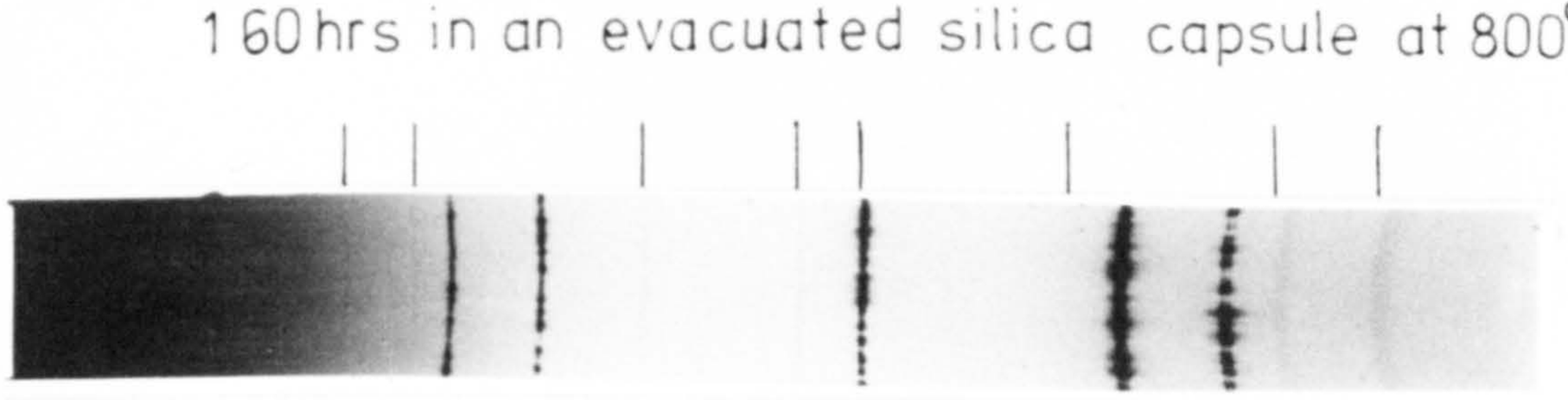

(a) eletropolished and aged in silca for 88hrs 800°C

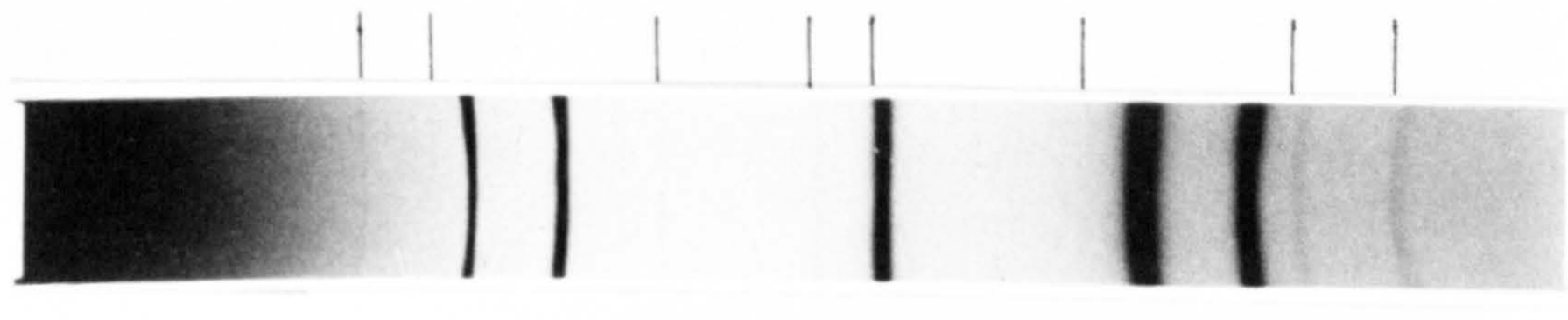

(b) annealed and aged in the same silca capsule for 160hrs at 800°C
___ NbO containing Ni

OPTICAL AND X-RAY PHOTOGRAPHS (FeKα; LiFmc.) OF Fe:35Ni:2Nb AGED FOR 88 & 160hrs AT 800°C IN AN EVACUATED SILICA CAPSULE

and 800°C showed the same f.c.c. phase which is found in Fe:Ni:Nb alloys aged in silica.

The f.c.c. phase occurs as coarse particles in the grain boundaries and in the grains of Fe:35Ni:2Nb aged for 160hrs in a silica-capsule at 800°C (Figure AI.2).

The electron microstructure of the centre of the same specimen is shown in Figure AI.3, and is similar to that observed by Manenc (1969) at 550°C in Fe:30Ni:5Nb alloy. The electron microstructure of Fe:35Ni:2Nb aged in alumina capsule for 88hrs at 800°C indicates no fine-scale precipitation in the matrix (Figure AI.3) but some coarse particles in the grain boundaries are attributed to the Laves phase Fe_2Nb.

Careful monitoring of the oxygen content of hydrogen by a zirconium getters placed before and after specimens in the nitriding apparatus has shown that the water vapour pressure varied between 0.1 and 10 p.p.m. From the standard free energy of formation of oxides as a function of temperature (Richardson and Jeffes, 1948) neither iron nor nickel oxides are stable at 700 and 800°C in water vapour pressures of 10 p.p.m. or less but niobium oxides are stable. No weight gain is recorded for Fe:35Ni:Nb alloys aged in alumina capsules but a weight gain of 0.06wt% is found in a large 0.15mm specimen of Fe:35Ni:2Nb aged in silica for 160hrs at 800°C where the

Fig. AI.3

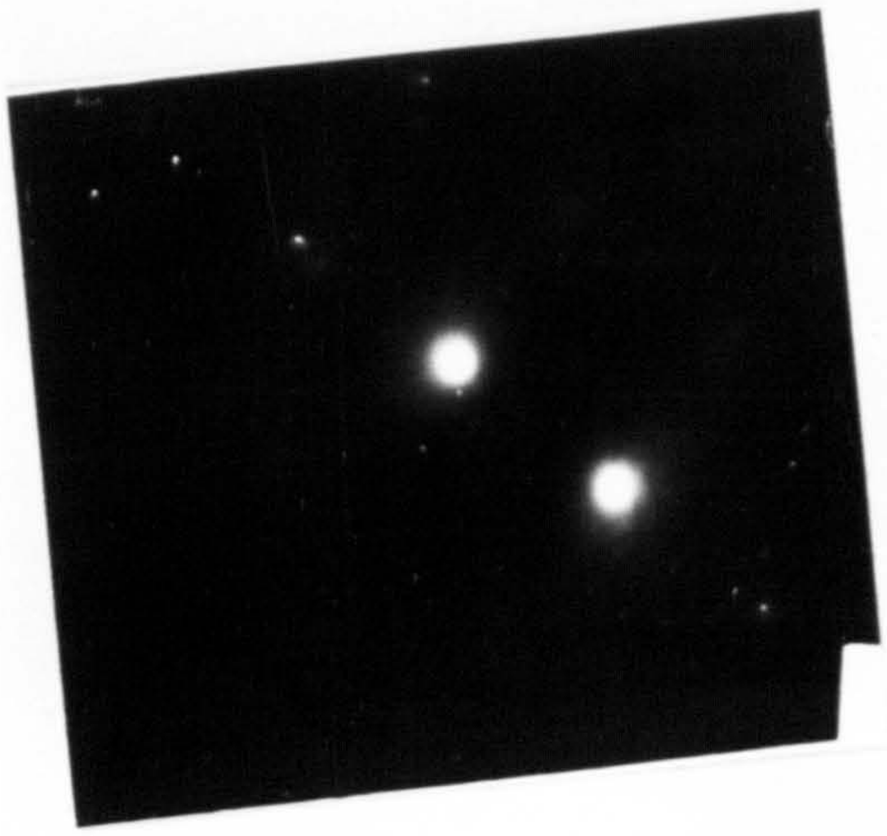

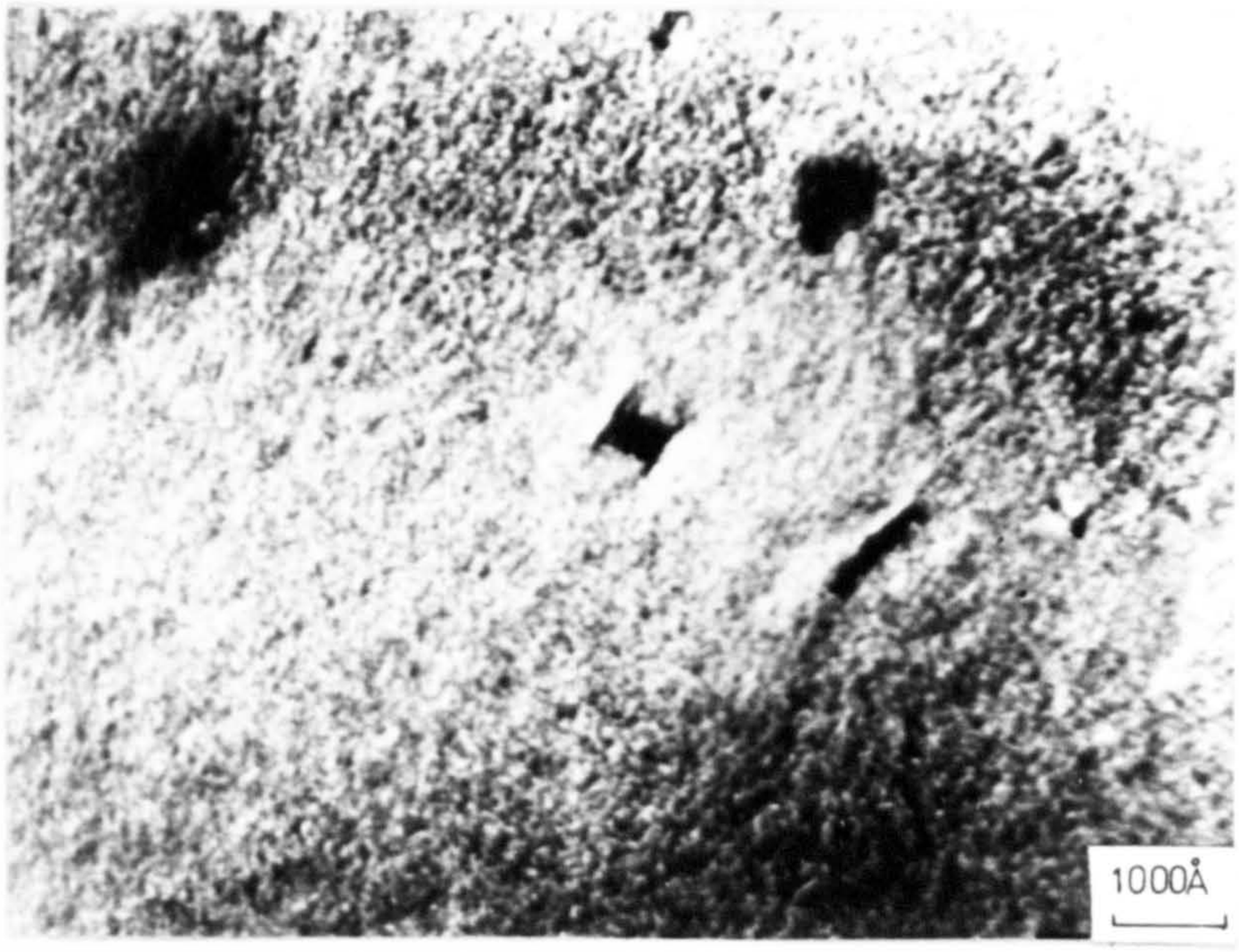

9 002
020

160hrs in silica

89 hrs in alumina

ELECTRON MICROSTRUCTURES OF Fe:35Ni:2Nb AGED IN ALUMINA AND SILICA CAPSULES AT 800°C

niobium to oxygen atom ratio in the oxidized layer is about 1:1. For these reasons the f.c.c. phase is assumed to be a f.c.c. niobium oxide most probably containing nickel i.e. (Nb,Ni)O.

Work by Turnock (1966) on Fe-Nb ocides at higher oxygen potentials found only higher niobium oxides and mixed Fe-Nb oxides. In the present investigation it is proposed that either NiO and NbO are completely miscible, or that some of the vacant sites in the defective NaCl structure of NbO reported by Brauer (1941) are filled with Ni and excess O in a random manner. This may then explain the difference in the lattice parameter from 4.20 Å for NbO to 4.46 Å and the change in the unit-cell symmetry from simple cubic to face-centred cubic.

I.4 Conclusions

(i) Only the Laves phase Fe_2Nb is precipitated in Fe:35Ni:N alloys at 700 and 800°C;

(ii) A f.c.c. phase is formed in Fe:Ni:Nb alloys aged at 700 and 800°C in a low oxygen potential in silica capsules and hydrogen;

(iii) The f.c.c. phase is probably a mixed oxide of NbO and NiO;

(iv) Previous work on the Fe:Ni:Nb system ignores the presence of oxygen and it seems possible that the reported phases and structures may be stabilized by oxygen.

Appendix II

NITRIDING OF Fe:Ni ALLOYS

II.1 Introduction

The effect of increasing nickel content in iron is to reduce the solubility of nitrogen in ferrite (Imai et al, 1966) and in austenite (Wriedt and Gonzalez, 1961; Heckler and Peterson, 1969; Atkinson and Bodsworth, 1970). Atkinson and Bodsworth (1970) have determined the following relationship for the variation of nitrogen content in nitrided Fe-Fe:15Ni alloys at 660 to 810°C:

$$\log a_N = \log \left(\frac{N_N}{1 - 5N_N} \right) - \frac{789}{T} + 3.615 + 2.422N_{Ni} \quad \ldots\ldots A\,II.1$$

where a_N is the activity of nitrogen in austenite

$(a_N = \sqrt{p_{N_2}})$

p_{N_2} is the effective partial pressure of nitrogen in ammonia-hydrogen gas mixtures

N_N is the atom fraction of nitrogen in nitrided Fe:Ni alloys;

N_{Ni} is the atom fraction of nickel in nitrided Fe:Ni alloys ;

and T is the nitriding temperature.

Log $(N_N / 1 - 5N_N)$ is used since a plot of log a_N against log N_N is non-linear. Where this term is based upon a geometric exclusion model on the premise that the strain field associated with each interstitial atom excludes from occupance a fixed number (4) of adjacent interstitial sites and only applies to nitrogen concentrations up to $\approx$ 2.5wt%.

However, this relationship may not apply to higher nickel contents since Wriedt and Gonzalez (1961) found that the heat of solution of nitrigen in austenite varies with the nickel content (from -3200cals/gm atom in pure iron to +3900 cals/gm atom in Fe:41Ni alloy). Further, Heckler and Peterson (1969) have shown that the activity coefficient of nickel in nitrided Fe:0-35Ni alloys a_N in equation II.1 varies with the nitriding temperature:

$$\log a_{Ni} = \left[\frac{32.4}{T} - 0.0056\right] \quad \ldots\ldots \text{AII.2}$$

For these reasons a limited study was made of nitrided Fe:Ni alloys and Fe:35Ni to determine the variation of nitrogen content with the nickel content and with the nitrogen potential at 600 to 800°C respectively.

Three phases have been found in nitrided Fe:Ni alloys: γ'-$(Fe,Ni)_4N$ (Arnott and Wold, 1960; Atkinson

and Bodsworth, 1970); hexagonal Ni_3N (Arnott and Wold, 1960); and ε-Fe_3N (Atkinson and Bodsworth, 1970). Arnott and Wold (1960) found that γ'-$(Fe,Ni)_4N$ formed in nitrided Fe:Ni alloys at 500°C has a wide range of nickel solubility (0-80at%Ni). Lehrer (1930) has shown that ε is formed in austenitic iron at temperatures above 650°C nitrided with NH_3:H_2 ratios greater than 10:90 (Figure II.1). Atkinson and Bodsworth (1970) found that ε-Fe_3N is formed in Fe:0-15Ni alloys nitrided in NH_3:H_2 at 660-810°C.

II.2 Experimental

Fe:8,12,18,25,40, and 47Ni were prepared by argon-arc melting pure iron and nickel with Fe:35Ni. Thin electron microspecimens of Fe:Ni were hydrogen annealed for 16hrs at 900°C and then the ammonia turned on and the specimen allowed to cool to the nitriding temperature. The Fe:Ni alloys were nitrided in this manner at 539, 600, 657, 700, 750, and 800°C and their nitrogen contents determined by weight gains and analysis. One of the difficulties involved in this study is the time required to "through"-nitride the higher nickel alloys at 600°C (at least 100hrs in $10NH_3$:$90H_2$). Fe:35Ni was nitrided in different NH_3:H_2 gas mixtures at 600, 700, 800°C and the nitrogen contents determined by weight gains. X-ray specimens of Fe-Ni were nitrided in higher nitrogen

potentials at 600, 700, and 800°C.

II.3 Results

The weight gains of Fe:35Ni nitrided at 700 and 800°C are shown in Figure V.9. At nitrogen potentials greater than $7NH_3:93H_2$ the nitrogen content of Fe:35Ni continued to increase with nitriding time, and the value shown in Figure V.9 is the amount of nitrogen in solution (determined by the initial decrease during hydrogen reduction). Electron microscopic examination of nitrided Fe:35Ni showed small amounts of grain boundary precipitation. At 800°C the weight gain of nitrided Fe:35Ni remained constant at nitrogen potentials greater than $15NH_3:85H_2$. This is attributed to the formation of a thin surface layer of a nitride which inhibits any further nitride formation. X-ray examination of Fe:Ni alloys nitrided at 800°C in $30NH_3:70H_2$ showed ε and γ' where the intensity of appropriate reflections in X-ray photographs decreased with increasing nickel content. The unit-cell dimension of γ' decreased with increasing nickel content but this phase might have been formed on cooling. Similar observations were made of a decrease in the unit-cell dimensions of ε with increasing nickel content. Furthermore, the X-ray reflections of ε disappeared in X-ray photographs taken from nitrided Fe:35Ni specimens

where the surface layer had been removed by electropolishing. At lower temperatures only γ' was identified in Fe:35Ni, and ε and γ' were identified in the lower nickel alloys.

II.4 Discussion of results

The solubility of nitrogen decreases with increasing nickel ocntent and the results are summarised in Table AII.1. Since a plot of log N against N_{Ni} is non-linear these results are analysed by a plot of log $(N/1 - 5N)$ against N_{Ni} (Figure AII.1) where the slopes of these plots at different temperatures are shown in Table AII.1 and the average value of the interaction parameter is -3.125. The variation in the interaction parameter is such that there appears to be no variation with the nitriding temperature within the limits of experimental error and is contrary to the observations of Heckler and Peterson (1969). The value of the interaction parameter is higher than the 2.422 obtained by Atkinson and Bodsworth (1970). The solubility of nitrogen in Fe:35Ni increases with the nitriding potential at 600, 700, and 800°C and a plot of log $\left(\frac{N}{1 - 5N}\right)$ against log $\sqrt{p_{N_2}}$ (Figure AII.2) is linear and the slopes at 700 and 800 were o.440, and 0.453 respectively. For this reason Henry's Law is not obeyed

Fig. A II. 1

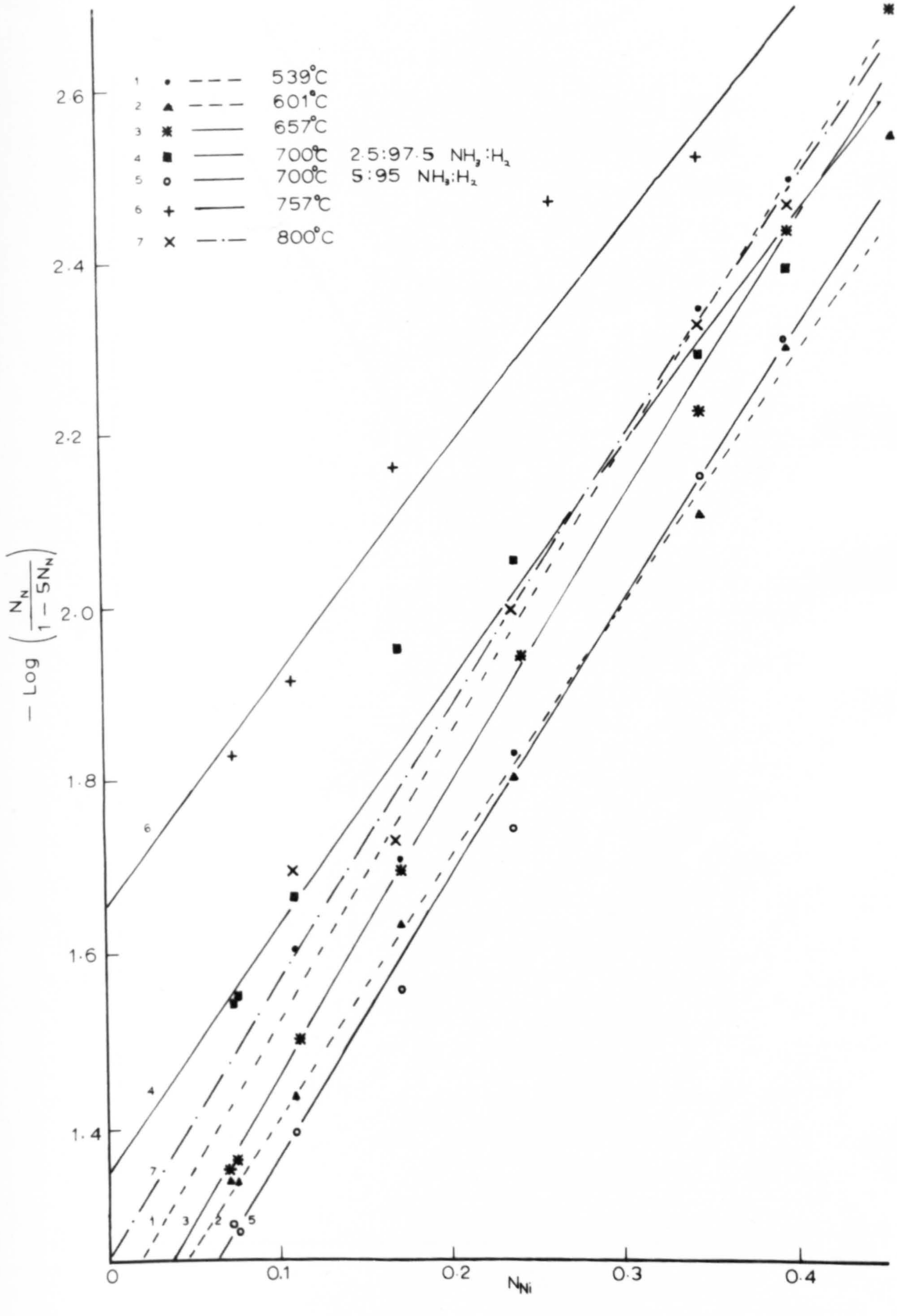

VARIATION IN $\mathrm{Log}\left(\frac{N_N}{1-5N_N}\right)$ WITH NICKEL CONTENT OF NITRIDED Fe:Ni ALLOYS AT 539 - 800°C

Fig. AII.2

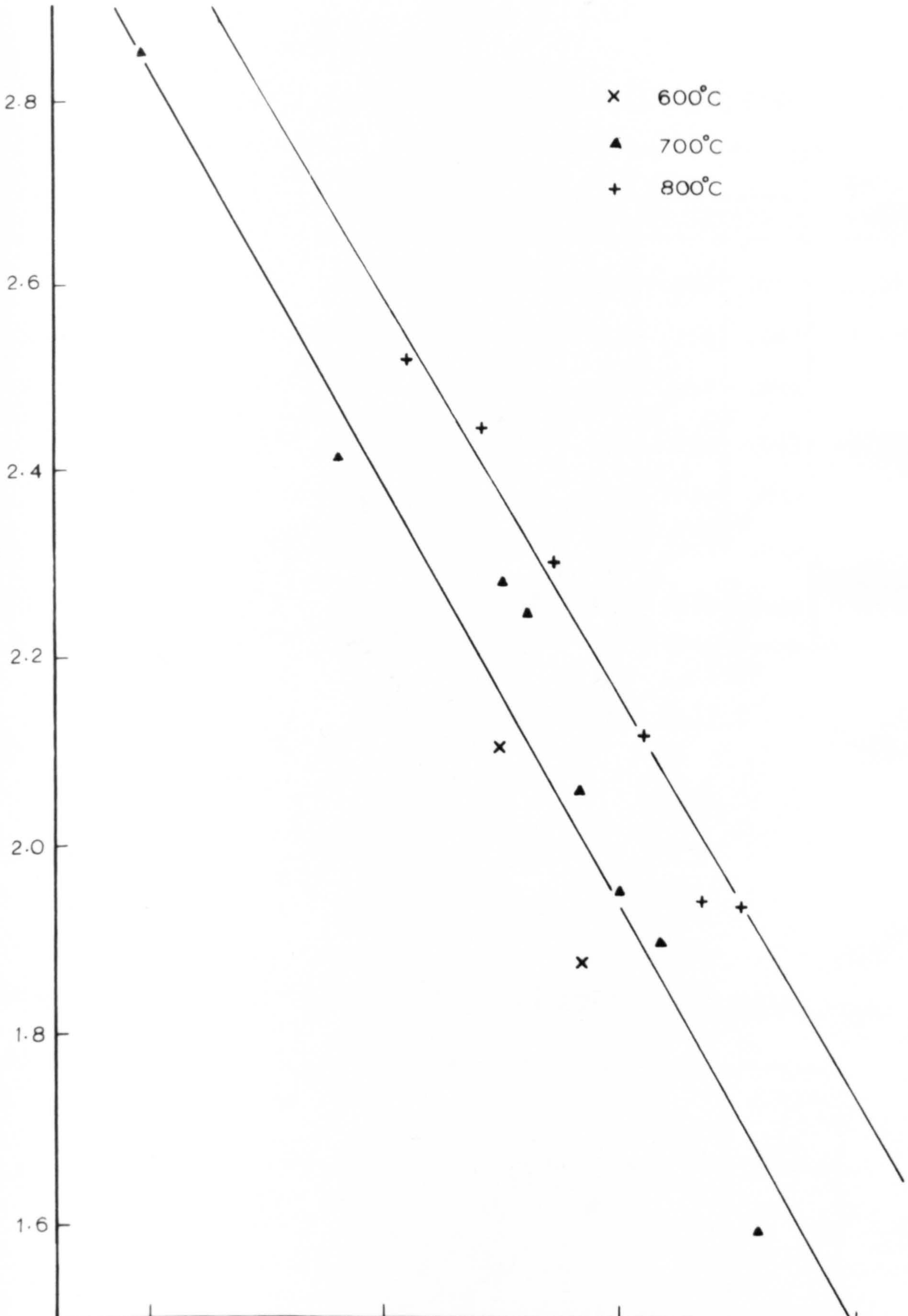

VARIATION IN $\text{Log}\left(\frac{N_N}{1 - 5N_N}\right)$ WITH $\text{Log}\sqrt{p_{N_2}}$ OF Fe:35Ni

NITRIDED AT 600 - 800°C

Table AII.1

(a) Nitrogen solubility in Fe:Ni alloys at different temperatures

%NH_3	P_{N_2}	Temp 0^oC	wt%N for Ne:Ni alloys								slope wt%Ni
			7.80	8.11	12.01	18.49	24.85	35.6	40.93	47.09	
7.5	812	539	.516	.493	.562	.448	.343	.108	.074	.016	-3.4257
5.0	1498	601	.949	.973	.791	.526	.365	.186	.114	.065	-3.1172
3.7	1692	657	.927	.915	.688	.461	.265	.138	.087	.039	-3.3554
2.5	1161	703	.632	.622	.491	.264	.212	.126	.094	.047	-2.7901
1.8	1120	749	.342		.349	.285	.163	.082	.072	.032	-2.9754
5.0	5628	700	1.057	1. 06	.863	.614	.418	.169	.117	.042	-3.2048
3.0	5781	800	.475	.588	.462	.434	.239	.113	.082	.052	-3.0052

where

$$\log\sqrt{p_{N_2}} = \log p_{NH_3} - \frac{3}{2}\log p_{H_2} - \frac{10400 - 7.1T \log T - 3.79\,T}{2.303\ RT} \quad .. \quad AII.4$$

(from Kubaschewski and Evans, 1958)

(b) Nitrogen solubility in Fe:35Ni at different nitriding potentials

Temp 0^oC										slope
600	%NH_3	,				5.0		10		
	wt%N					.143		.311		
700	%NH_3	0.07	0.5		2.5	5.5	7.0	10	20	0.4401
	wt%N	.035	.094		.126	.193	.262	.295	.567	
800	%NH_3		0.5	1.0	2.0	4.5		10		0.4528
	wt%N		.074	.087	.121	.143		.274		

and the average activity coefficient is 0.446. The temperature dependence of nitrogen solubility is determined from values of nitrogen solubility in nitrided Fe:35Ni at different temperatures and is expressed by:

$$\log\left(\frac{N}{1 - 5N}\right) = 0.446 \log \sqrt{p_{N_2}} + \frac{1652}{T} - 3.600 - 3.125\, N_{Ni} \quad ..AII.3$$

where the maximum deviation of the calculated value from the observed value differed by $\approx$ 0.05wt%N at low nickel contents. For this reason it appears that the heat of solution may change with the nickel content in accordance with the observations by Wriedt and Gonzalez (1961).

ε -Fe_3N is formed at the surface of Fe:35Ni nitrided at temperatures above 700°C, and γ'-Fe_4N is probably formed at the grain boundaries at 700°C and lower temperatures. The unit-cell dimensions of ε and γ' decrease with increasing nickel content and so also does the amount of nitride formed under similar conditions.

II.5 Conclusions

The nitrogen solubility of Fe:Ni alloys decreases with increasing nickel content. The relationship derived by Atkinson and Bodsworth could not be applied

to the higher nickel alloys and an approximate relationship is given to explain the variation of nitrogen content in Fe:8-47Ni alloys.

Both ε and γ' are formed in nitrided Fe:Ni alloys.

List of References

Ardell, A.J., (1968) Acta Met. 16, 511.

Arnott, R.J. and Wold, A., (1960) J. Phys. Chem. Solids. 15, 152.

Atkinson, D. and Bodsworth, C., (1970) J.I.S.I. 208, 587.

Bell, T., Heatherington, G. and Jack, K.H.,(1962) Phys. Chem. Glasses 3, 141.

Borland, D.W., (1969) Ph.D. thesis, Sheffield University.

Borland, D.W. and Honeycombe, R.W.K., (1970) Met. Sci. Journ. 4, 14.

Borland, D.W., (1973) private communication.

Brauer, G., (1941) Z. Anorg. Chem. 248, 1.

Brauer, G. and Esselborn, R., (1961) Z. Anorg. Chem. 309, 151.

Brauer, G. and Jander, J., (1952) Z. Anorg. Chem. 270, 161.

Brown, L.M. and Ham, R.K., (1971) Strengthening Methods in Crystals, Kelly, A. & Nicholson, R.B., Elsevier Pub. Co. 9.

Bucknall, E.H., (1957) Met. Prog. 72, 110.

Butler, E.D. and Thomas, G., (1970) Acta Met. 18, 847.

Cahn, J.W., (1968) Trans. A.I.M.E. 242, 166.

Coffman, A.W., (1930) Indust. Eng. Chem. 24, 151.

Corney, N.S. and Turkdogan, E.T., (1955) J.I.S.I. 180, 344.

Cornie, J.A., Datta, A. and Softa, W.A., (1972) Met. Trans. A.I.M.E. 4, 727.

Cost, J.R. and Wert, C.A., (1963) Acta Met. 11, 231.

Daniel, V. and Lipson, H., (1943) Proc. Roy. Soc. A182, 378.

Darken, L.S., (1958), N.P.L. Symposium No. 9.

Darken, L.S., Smith, R.P. and Filer, C.W., (1951)
Trans. A.I.M.E. 191, 117.

De Fontaine, D., (1969) Acta Met. 17, 477.

Driver, J.D., Handley, J.R. and Jack, K.H., (1972)
Scanda. Met. 1, 211.

Driver, J.D., Sinclair, R. and Jack, K.H., (1974) to be
published.

Duerden, I.J. and Hume-Rothery, W., (1966) J. Less C.
Metals 11, 381.

Elliot, R.P., (1965) Constitution of Binary Alloys
1st Supplement, Macgraw Hill.

Faive, G., (1969) Phys. State Sol. 35, 249.

Fast, J.D. and Verrijp, M.B., (1955) J.I.S.I. 180, 337.

Gerhardt, E., Fromm, E. and Jakob, D., (1964) Z. Metal. 55, 423.

Golding, B. and Moss, S.C., (1967) Acta Met. 15, 1239.

Grieveson, P. and Turkdogan, E.T., (1964a) Trans. A.I.M.E.
230, 407.

Grieveson, P. and Turkdogan, E.T., (1964b) Trans. A.I.M.E.
230, 1604.

Grozier, J.D., Paxton, H.W. and Mullins, W.W., (1965)
Trans. A.I.M.E. 233, 190.

Guard, R.W., Savage, J.W. and Swarthout, D.G., (1967)
Trans. A.I.M.E. 239, 643.

Hahn, H. and Muhlbergh, H., (1949) Z. Anorg. Chem. 258, 77.

Hall, E.O., (1951) Proc. Phys. Soc. 64.B, 547.

Hansen, M., (1958) Constitution of Binary Alloys. Macgraw Hill.

Harding, H.J. and Honeycombe, R.W.K., (1966) J.I.S.I. 204, 259.

Hausch, G. and Warlimont, H., (1972) Z. Metal. 63, 547.

Hausch, G. and Warlimont, H., (1973) Acta Met. 21, 401.

Hayes, P.C., (1972) M.Sc. thesis, Newcastle University.

Heckler, A.J. and Peterson, J.A., (1969) Trans. A.I.M.E. 246, 2537.

Hepworth, M.T., Smith, R.P. and Turkdogan, E.T., (1966) Trans. A.I.M.E. 236, 1278.

Hillert, M., Cohen, M. and Averbach, B.L., (1961) Acta Met. 9, 536.

Hilliard, J.E., (1970) Phase Transformations. American Soc. of Metals, Ohio. 497.

Imai, Y., Masumato, T. and Sakamato, M., (1968) J. Japan Inst. Met. 31, 1095.

Irvine, K.J., Gladman, T. and Pickering, F.B., (1969) 209, 1017.

Ivanuskina, A.Z. and Livshitz, B.G., (1957) Phys. Met. Metallog. 5, 527.

Jack, D.H., (1969) Ph.D. thesis, Cambridge University.

Jack, K.H., (1948) Proc. Roy. Soc. A205, 34.

Jack, K.H., (1951a) Proc. Roy. Soc. A208, 200.

Jack, K.H., (1951b) Proc. Roy. Soc. A208, 216.

Jack, K.H., (1972) Scanda Met. 1, 195.

Jack, K.H. and Jack, D.H., (1970) J.I.S.I. 210, 790.

Juza, R. and Sachsze, W., (1943) Z. Anorg. Chem. 251, 201.

Kahlweit, M., (1965) Prog. Solid State Chem. 2, 134.

Kaye, G.W.C. and Elaby, T.H., (1968) Tables of Physical and Chemical Constants. Longmans Green, 33.

Kelly, P.M., (1973) Int. Met. Rev. 18, 31.

Khachaturyan, A.G., (1969) Phys. State. Sol. 35, 119.

Khomenko, O.A. and Tseytlin, A.M., (1969) Phys. Met. Metallog. 28, 60.

Kindleman, L.E. and Ansell, G.S., (1970a) Met. Trans. A.I.M.E. 1, 163.

Kindleman, L.E. and Ansell, G.S., (1970b) Met. Trans. A.I.M.E. 1, 507.

Kirman, I., (1968) Ph.D. thesis Sheffield University.

Krawitz, A. and Sinclair, R., (1974) to be published.

Kubaschewski, O. and Evans, E. LL., (1958) Metallurgical Thermodynamics. Pergamon Press.

Leith, K. and Chaturvedi, M., (1971) Met. Trans. A.I.M.E. 2, 1407.

Lehrer, E., (1930) Z. Electrochem. 36, 460.

Lements, B.S., Averbach, B.L. and Cohen, M., (1954) Trans. A.S.M. 46, 851.

Li, C.Y. and Oriani, R., (1966) 2nd Bolton Landing Conf., Met. Soc. A.I.M.E. New York. 431.

Lifshitz, I.M. and Slyozov, V.V., (1961) J. Phys. Chem. Solids. 19, 35.

Manenc, J., (1969) Bul. Du Cercle d'Etude des Metaux, 11, 1.

Manenc,J., Bourgeot, J. and de Boer, H., (1968) Scripta Met. 2, 453.

Mori, M.T., Fujita, K., Tokizone, M. and Yamaguchi, K., (1964) Tetsa Tu Hugane 50, 911.

Mortimer, B., (1971) Ph.D. thesis Newcastle University.

Nelson, J.B. and Riley, D.P., (1945) Proc. Phys. Soc. 57, 160.

Paranjpe, V.G., Cohen, M., Bever, M.B. and Floe, L.F., (1950) Trans. A.I.M.E. 242, 673.

Pehlke, R.D. and Elliot, J.F., (1960) Trans. A.I.M.E. 242, 673.

Petch, N.J., (1953) J.I.S.I. 165, 25.

Peters, W. and Fisher, W.A., (1948) Arch. Eisen. 19, 161.

Plewes, J.T., (1973) 3rd. Int. Conf. on Strength of Metals and Alloys. Cambridge, 109.

Pope, M., (1972) Ph.D. thesis Newcastle University.

Portnoi, K.I., Mukaseev, A.A., Gribkov, V.N. Levinskii, Y.V. and Prokof'ev, S.A., (1968) Porosh. Met. 3, 32.

Pread, K.A. and Borland, D.W., (1969) Scripta Met. 3, 267.

Pylaeoa, E.N., Gladshevskii, E.I. and Kripyakevich, P.I., (1958) J. Inorg. Chem. U.S.S.R. 3, 206.

Ramstead, H.F., Richardson, F.D. and Bowles, P.J., (1961) Trans. A.I.M.E. 221, 1021.

Rienacher, R.G. and Hohl, K.H., (1960) Mon. Auet, Akad Weisen. 12, 201.

Richardson, F.P. and Jeffes, J.H.E., (1948) J.I.S.I. 160, 261.

Roberts, W., (1970) Ph.D. thesis Newcastle University.

Roberts, W. and Bergström, Y., (1972) Scanda Met. 1, 261.

Rosenbaum, H.S. and Turnball, D., (1959) Acta Met. 6, 664.

Schönberg, N., (1954) Acta Chem. Scanda. 8, 208.

Shunk, F.H., (1969) Constitution of Binary Alloys, 2nd Supplement. Macgraw Hill.

Sieverts, A., Zapf, G. and Maritz, H., (1938) Z. Phys. Chem. 183, 19.

Silcock, J.M. and Tunstall, W.J., (1964) Phil. Mag. 10, 361.

Smith, C.S., (1948) Trans. A.I.M.E. 175, 190.

Smith, R.P., (1962) Trans. A.I.M.E. 224, 15.

Sonon, D.E. and Smith, G.V., (1965) Trans. A.S.M. 58, 353.

Speich, G., (1962) Trans. A.I.M.E. 224, 850.

Spiers, D., (1969) Ph.D. thesis Newcastle University.

Spiers, D., Roberts, W., Grieveson, P. and Jack, K.H., (1970)
Proc. Int. Conf. on Strength of Metals and Alloys
2, 601. A.S.M.

Sparke, B., James, D.W. and Leak, G.M., (1965) J.I.S.I.
203, 152.

Stephenson, A., (1973) Ph.D. thesis Newcastle University.

Swalin, R.A., (1962) Thermodynamics of Solids. Wiley.

Swisher, J. and Turkdogan, E.T., (1967) Trans. A.I.M.E. 239, 426.

Taylor, T.A. and Doyle, N.J., (1966) J. Less C. Metals. 13, 399.

Turnock, A.E., (1966) J. Am. Cerm. Soc. 49, 117.

Vlack, V.L.A., (1951) J. of Metal. 3, 251.

Volwes, M.D.J. and West, R.D. (1973) J.I.S.I. 211, 147.

Wagner, C., (1959) Z. Electrochem. 63, 117.

Wagner, C., (1961) Z. Electrochem. 65, 1961.

Weiner, G.W. and Berger, J.A., (1955) J. of Metals. 5, 360.

Westin, L., (1973) internal report.

Wood, D.L., (1959) Trans. A.I.M.E. 215, 925.

Wriedt, H.A. and Gonzalez, O.D., (1961) Trans. A.I.M.E.
221, 532.

Wriedt, H.A. and Zwell, C., (1962) Trans. A.I.M.E. 224, 1242.

List of Figures

List Of Tables